Doctoral theses at NTNU, 2016:2016:244

Jørgen Larsen Sugar

Retrosplenial connectivity with the (para)hippocampal region

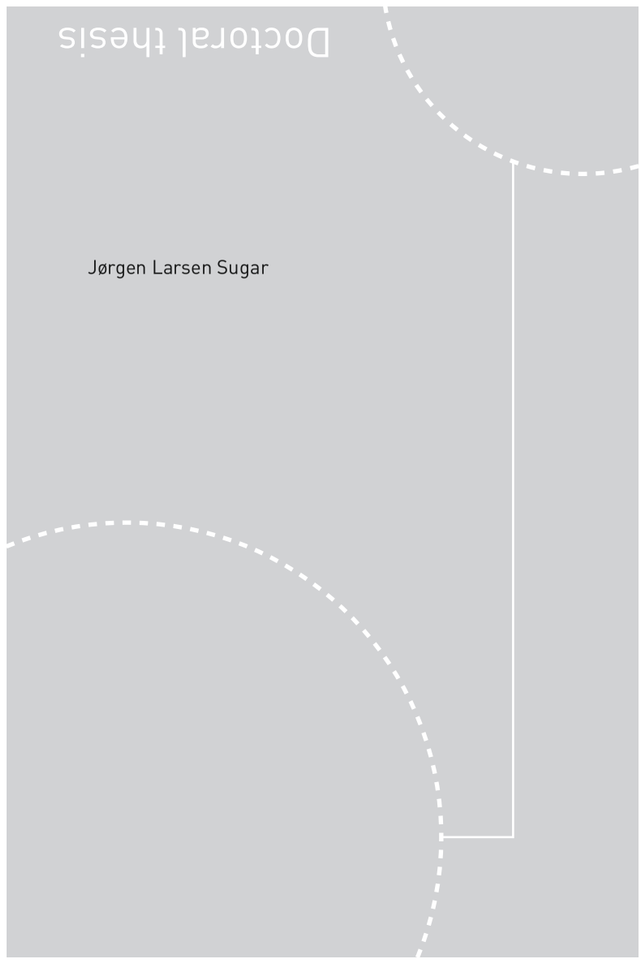

ISBN 978-82-326-1826-2 (printed ver.)
ISBN 978-82-326-1827-9 (electronic ver.)
ISSN 1503-8181

NTNU
Norwegian University of
Science and Technology

Doctoral theses at NTNU, 2016:2016:244

NTNU
Norwegian University of Science and Technology
Thesis for the Degree of
Philosophiae Doctor
Faculty of Medicine
Kavli Institute for Systems Neuroscience/
Centre for Neural Computation

NTNU
Norwegian University of
Science and Technology

Jørgen Larsen Sugar

Retrosplenial connectivity with the (para)hippocampal region

Thesis for the Degree of Philosophiae Doctor

Trondheim, September 2016

Norwegian University of Science and Technology
Faculty of Medicine
Kavli Institute for Systems Neuroscience/
Centre for Neural Computation

NTNU
Norwegian University of
Science and Technology

NTNU
Norwegian University of Science and Technology

Thesis for the Degree of Philosophiae Doctor

Faculty of Medicine
Kavli Institute for Systems Neuroscience/
Centre for Neural Computation

ISBN 978-82-326-1826-2 (printed ver.)
ISBN 978-82-326-1827-9 (electronic ver.)
ISSN 1503-8181

Doctoral theses at NTNU, 2016:244

Printed by NTNU Grafisk senter

Norges teknisk-naturvitenskapelige universitet

Det medisinske fakultet

Retrosplenial connectivity with the (para)hippocampal region

Den hippocampale- og parahippocampale regionen (HF-PHR) mottar input fra flere cortikale og subcortikale strukturer, og en av de cortikale strukturene som er sterkt koblet til HF-PHR er retrosplenial cortex (RSC; Wyss and Van Groen, 1992). Studier i gnagere og primater har vist at både RSC og HF-PHR er viktig for visuospatiell kognisjon og hukommelse (Vann et al., 2009; Ranganath and Ritchey, 2012). De lignende funksjonelle egenskapene til RSC og HF-PHR samt de sterke forbindelsene, indikerer at det er en funksjonell sammenheng mellom de to regionene. Men nøyaktig hvilke subregioner av HF-PHR som er koblet sammen med hvilke subregioner av RSC, topografiene til disse forbindelsen innenfor hver subregion og hvordan informasjon som bruker disse forbindelsene blir integrert i den mottakende region er hittil ukjent.

I denne avhandlingen ble de anatomiske forbindelsene mellom HF-PHR og RSC undersøkt på flere nivåer. I den første delen av avhandlingen re-analyserte jeg alle publiserte anatomiske tracerstudier som omhandler forbindelser mellom HF-PHR og RSC. Projeksjonene innenfor og mellom HF-PHR og RSC ble presentert i et interaktivt koblingskart.

I den andre delen av avhandlingen undersøkte jeg den synaptiske organiseringen til en av disse forbindelsene, nemlig forbindelsen fra RSC til medial entorhinal cortex (MEC), en subregion i PHR. Jeg viste at RSC sender sterke projeksjoner til lag V av MEC, i tillegg til noen få fibre til lag III av MEC. En ultrastrukturell undersøkelse av synapsene og optogenetisk stimulering av disse fibrene i *in vitro* hjerneskiver indikerte at den største andelen av RSC-synapser i lag V av MEC er eksitatoriske. Videre identifiserte jeg hvilke lag V nevroner som er postsynaptiske til disse synapsene. Data fra elektron mikroskopi viste at den største andelen av postsynaptiske mål er dendrittiske spina. Data fra konfokal mikroskopi og optogenetiske eksperimenter indikerer at blant de postsynaptiske målene finnes det pinsipalceller som har aksoner i superfisielle lag av MEC.

I den tredje og fjerde delen tok jeg en utviklingsmessig tilnærming for å studere hvordan forbindelsene mellom de to regionene utvikles. For å oppnå dette brukte jeg klassiske retro- og anterograde tracere som ble injisert i rotter med forskjellig alder. Utviklingen og den topografiske distribusjonen til de anatomiske forbindelsene fra postnatal dag (P)1 til P28 ble karakterisert. Jeg viste at de tidlig utviklede forbindelsene mellom RSC og HF-PHR er organisert på en topografisk måte, likt med hvordan forbindelsene er organisert hos voksne og denne organiseringen er tilstede allerede når de første aksonene ankommer sine terminalområder.

Jeg konkluderte derfor med at informasjon fra RSC kan nå frem til HF gjennom pyramidale nevroner i lag V av MEC som projiserer til superfisielle lag av MEC. Nevroner i de sistnevnte lag kan videresende denne informasjonen fra RSC til HF, fordi disse lagene inneholder nevroner som projiserer til HF. Alternative multisynaptiske ruter som kobler RSC til HF via PHR inkluderer projeksjoner fra RSC til henholdsvis postrhinal cortex og presubiculum. Begge strukturene mottar input fra RSC blant annet i de superfisielle lag som inneholder nevroner som projiserer til MEC. Den tidlige utviklingen av forbindelsene mellom RSC og HF-PHR allerede på et tidlig postnatalt stadium før nevronene er funksjonelt differensiert, tyder på at forbindelsene mellom RSC og HF-PHR blir organisert uavhengig av erfaring. Den tidlige utviklingen av topografisk organiserte koblinger mellom RSC og HF-PHR foreslår at RSC og HF-PHR er deler av ett funksjonelt system og at koblingene mellom RSC og HF-PHR er nødvendig for funksjonen av dette systemet.

Kandidat: Jørgen Sugar

Veileder: Professor Menno P. Witter

Insitutt: Kavli Insitute for Systems Neuroscience/Centre for Neural Computation

Finansiering: DMF NTNU, Forskningsrådet

Summary

The hippocampal formation and parahippocampal region (HF-PHR) receives input from a variety of cortical and subcortical structures, and one of the cortical regions which are heavily interconnected with HF-PHR is the retrosplenial cortex (RSC; Wyss and Van Groen, 1992). RSC is known to be important for a number of cognitive functions, and in both rodents and humans the RSC contribution to visuospatial cognition and memory has recently been reviewed in detail (Vann et al., 2009; Ranganath and Ritchey, 2012). The similar functional attributes of RSC and HF-PHR and the dense connections between the regions suggest a relationship. However exactly which HF-PHR subdivisions are connected with which part of RSC, the topographies of the connections within these subregions and how information carried by these connections are integrated in the receiving subregion is unknown.

In this thesis I explored anatomical connections between HF-PHR and RSC at several levels. In the first part of the thesis all published anatomical tract-tracing experiments which comprise HF-PHR – RSC connections were reanalyzed. All reported projections within and between HF-PHR and RSC were presented in an interactive connectome.

In the second part I explored the synaptic organization and postsynaptic targets of one of these connections namely the projection originating in RSC and terminating in medial entorhinal cortex (MEC), a subregion within PHR. I showed that RSC projects densely to layer V of MEC, with very few fibers targeting layer III. An ultrastructural assessment of the synaptic complexes and optogenetic stimulation of these fibers in an *in vitro* slice preparation indicated that the majority of RSC synapses in MEC layer V are excitatory. I further identified the layer V neurons postsynaptic to these synapses. The electron microscopical data show a striking dominance of spines of putative principal neurons as targets for RSC inputs. Confocal data and optogenetic data indicate that among the postsynaptic targets are spiny principal cells which project to superficial layers of MEC.

In the third and fourth part I took a developmental approach to study how the interconnections between the two regions develop. To this end I used classical retro- and anterograde tracers injected in differently aged rats. The development of the anatomical connections and the development of the topographical distribution of these connections from postnatal day (P)1 to approximately P28 were characterized. I showed that developing RSC – HF-PHR interconnections are organized in a topographical manner, similar to the adult situation and that this topographical organization is present already when the first axons arrive their termination site.

I thus concluded that information from RSC may reach HF through pyramidal neurons in layer V of MEC which issue projections to the superficial layers of MEC. Neurons in the latter layers may relay information from RSC to HF since these layers harbor neurons projecting to HF. Alternative multisynaptic pathways connecting RSC via PHR to HF likely include RSC projections to postrhinal cortex and presubiculum. Both structures receive RSC inputs among others in superficial layers, which

harbor neurons projecting to superficial layers of MEC. The early development of the reciprocal connections between RSC and HF-PHR, already at an early postnatal stage, before neurons are functionally differentiated, suggests that RSC-PHR interconnections are organized by experience-independent mechanisms. This experience independent topographic organization suggests that RSC and HF-PHR are parts of one tightly coupled functional system and that RSC – HF-PHR interaction is necessary for proper functioning of the two regions.

Acknowledgements

The present work was carried out at The Kavli Institute for Systems Neuroscience, Centre for Neural Computation. In 2007 I was granted a scholarship from the Medical Student Research Program at the Faculty of Medicine (DMF) at The Norwegian University of Science and Technology (NTNU). I want to thank the institute, DMF and NTNU for giving me the opportunity to conduct the research presented in this thesis.

I want to show my gratitude to my supervisor, Menno Witter for accepting me as a student and as a PhD candidate. I want to thank you for your guidance, sharing your knowledge, for your patience and always having your office door open.

Further, I want to thank the team at the Institute and all co-authors for interesting discussions, for your help and for your motivation. Especially I want to thank Ragnhild Gisetstad, Bruno Monterotti, Ellen Husby, Hanne Soligard, Grethe Olsen and Paulo Girão. Without your help the work in this thesis could not have been performed.

I also want to thank Natalie Cappaert, Niels van Strien and Ingrid Riphagen for guidance, help and good teamwork during the project which resulted in paper 1 in this thesis. Further the material presented in paper 2 of this thesis was partly processed at the Laboratory of Electron Microscopy at NTNU and St Olav's Hospital. I want to thank the laboratory for allowing me to use the facilities and Nan Skogaker, Linh Hoang and Gro Møkkelgjerd for suggestions, guidance and excellent teaching.

I want to thank Kamilla Haugland for fruitful cooperation during her master thesis work. Her hard work resulted in the data presented in paper 4.

Finally, I want to thank Siri, my family and my friends for your patience and encouraging and positive feedback.

Jørgen Sugar

Contents

Preface and overview of the thesis

How humans perceive, act, learn and remember has intrigued philosophers, scientists and lay people for ages. Today we know that the central nervous system is responsible for cognition, behavior and for a variety of processes throughout the body. However, to explain and understand these processes has proven to be a challenging task, as the central nervous system comprises an enormous amount of neurons and inconceivable amounts of connections between them.

Neurons are the elementary signaling and processing elements of the brain. They are commonly polarized, with receptive or afferent dendrites and efferent axons, and they are organized into networks. The cell membrane of neurons and complex molecular structures embedded in it create electrical currents which make it possible to convey and transfer electrical- and chemical signals between neurons in a network. An important aim for neuroscientists is to understand how neurons are organized into signaling pathways, and how inputs are transferred and integrated and thereafter processed into relevant outputs from the network. Such knowledge is pivotal for the understanding of both normal brain functioning and how diseases affect our brain.

The cerebral cortex covers the white matter of the cerebral hemispheres and constitutes the outer surface of the two hemispheres. The cerebral cortex has been subdivided in distinct areas, using either structural or functional criteria. One of the first who formally delineated the cerebral cortex based on morphological criteria was Brodmann (1909). He used distribution of cell bodies, the appearance of cortical layers, and particularly used cell types and specific arrangements of cells in clusters and/or columns as criteria. His division comprised about 50 different subdivisions, many of which have later been attributed with specific functional connotations. Modern electrophysiological- and imaging techniques reveal that different cortical areas perform different computations. These differences explain the particular symptoms observed after damage of specific brain areas. For instance damage of the dorsal precentral gyrus results in a selective impairment of muscles, while a lesion of the left superior temporal gyrus results in a receptive aphasia (Wernicke, 1874). These differences can be explained by the different afferents and efferents of each area. The primary motor cortex in the precentral gyrus is, through the spinal cord connected to peripheral muscles, while Wernicke's area, in the superior temporal gyrus is connected to auditory and visual cortices, areas elementary for the understanding of written- and spoken language (Demonet et al., 2005). Thus discrete inputs and the processing of these inputs within neural networks make complex functions possible.

To understand how the cerebral cortex and subcortical structures contribute to complex cognitive functions it is necessary to understand how different brain areas interact and how information are processed within a neuronal network. Information processing depends among others on the architectural composition- and termination of *afferents* in the network and the architectural composition and intrinsic connectivity *within* the network. Knowledge about structural organization and connectivity at several

levels is essential for the understanding of brain functioning. For instance, knowledge about the main interconnections between different brain areas can reveal or explain functional relationship of these areas. Second, knowledge about the interconnectivity between identified neuronal populations can reveal the mechanisms how specific cell groups contribute to distinct computations within the network. Third, knowledge about the interconnections between neurons at the synaptic level gives us information about how segments of dendrites can integrate inputs from single synapses used by the neuron to compute a useful output.

The complex architecture of neurons and their inconceivable amount of interconnections make the assessment of global network functioning a difficult task. It is therefore necessary to find models of cortical networks that can be evaluated at smaller and more comprehensible scales. Model systems are easier to assess and fundamental knowledge of elementary processes of these networks can hopefully be obtained relatively more easily. In our experiments we have chosen to focus on the (para)hippocampal region (HF-PHR) for two main reasons. First its contribution to declarative memory processes and spatial cognition is easily accessible for behavioral studies both in humans and other animals such as rodents and extensive data are available that provide insight in the functional contributions made by this domain and the subdivisions within (Eichenbaum et al., 2007). The fascinating findings of several different spatially modulated neurons within HF-PHR give us an excellent possibility to relate anatomical findings with functional attributes. In addition, this region has been extensively studied at the level of its intrinsic and extrinsic connectional architecture (Burwell et al., 2002). These features make HF-PHR well suited to be used as a model for investigation of neural networks.

HF-PHR receives input from a variety of cortical and subcortical structures, and one of the cortical regions which are heavily interconnected with HF-PHR is the retrosplenial cortex (RSC; Wyss and Van Groen, 1992). RSC is known to be important for a number of cognitive functions, and in both rodents and primates the contribution of RSC to visuospatial cognition and memory has been emphasized (Vann et al., 2009; Ranganath and Ritchey, 2012). The similar functional attributes of RSC and HF-PHR and the dense interconnections between the regions suggest a functional relationship. However exactly which PHR subdivisions are interconnected with which part of RSC, the topographies of the connections within these subregions and how the connections are integrated in the receiving subregion is unknown.

In this thesis anatomical connections between HF-PHR and RSC were analyzed. I have investigated the connections at several of the levels mentioned above. In the first part of the thesis all published anatomical tract-tracing experiments which comprise HF-PHR – RSC interconnections were reanalyzed. All reported projections within and between HF-PHR and RSC were presented in an interactive connectome.

In the second part I explored the synaptic organization and postsynaptic targets of one of these connections namely the projection originating in RSC and terminating in MEC, a subregion within PHR.

In the third and fourth part I took a developmental approach to study how the connections between the two regions develop. To this end classical retro- and anterograde tracers were injected in differently aged rats. The development of the anatomical connections and the development of the topographical distribution of these connections from postnatal day (P)1 to approximately P28 were characterized.

The new data on the organization of HF-PHR – RSC interconnectivity and on their postnatal development provide insight in how information originating from different regions of RSC is likely integrated in different parts of HF-PHR, leading to new hypotheses/inferences about the functional relevance of such integration.

List of Papers

Paper 1

The retrosplenial cortex: intrinsic connectivity and connections with the (para)hippocampal region in the rat. An interactive connectome.

Jørgen Sugar[1], Menno P. Witter[1], Niels M. van Strien[2] and Natalie L. M. Cappaert[3]*

[1] Kavli Institute for Systems Neuroscience, Centre for the Biology of Memory, Faculty of Medicine, Norwegian University of Science and Technology, Trondheim, Norway

[2] FMRI-group, Department of Circulation and Medical Imaging, Faculty of Medicine, Norwegian University of Science and Technology, Trondheim, Norway

[3] Center for NeuroScience, Swammerdam Institute for Life Science, University of Amsterdam, Netherlands

Frontiers in Neuroinformatics. 2011 Jul 27;5:7.

Paper 2

Superficially projecting principal neurons in layer V of medial entorhinal cortex in the rat receive excitatory retrosplenial input.

Rafał Czajkowski[12]*, **Jørgen Sugar**[1]*, Sheng-Jia Zhang[1], Jonathan J. Couey[1], Jing Ye[1], and Menno P. Witter[1]

[1]Kavli Institute for Systems Neuroscience, Centre for Neural Computation, Faculty of Medicine, Norwegian University of Science and Technology, 7491 Trondheim, Norway, and

[2]Neurobiology Center, Nencki Institute of Experimental Biology, 02-093 Warsaw, Poland

*R.C. and J.S. contributed equally to this study.

The Journal of Neuroscience. 2013 Oct 2;33(40):15779-92.

Paper 3

Development of projections from the retrosplenial cortex to the (para)hippocampal region in the rat.

Jørgen Sugar[1], Menno P. Witter[1]

[1]Kavli Institute for Systems Neuroscience, Centre for Neural Computation, Faculty of Medicine, Norwegian University of Science and Technology, Trondheim, Norway

Elife. 2016 Mar 23;5.

Paper 4

Development of projections from the (para)hippocampal region to the retrosplenial cortex in the rat.

Kamilla G. Haugland[1,2], **Jørgen Sugar**[1], Menno P. Witter[1]

[1]Kavli Institute for Systems Neuroscience, Centre for Neural Computation, Faculty of Medicine, Norwegian University of Science and Technology, Trondheim, Norway

[2]Currently at the Institute for Clinical Medicine, Faculty of Health Sciences, The Arctic University of Norway, Tromsø, Norway

Not yet submitted

Introduction and objectives

The rat hippocampal formation (HF) is a curved structure positioned posteriorly in the brain. Dorsally, HF is positioned close to the midline directly dorsal to the septal complex of the basal forebrain and the dorsal tip of HF is therefore often referred to as the septal tip of HF (Fig. 1A). The hippocampal formation extends over the diencephalon towards a more posterior and ventrolateral position and the ventral tip of HF, having a close association with the amygdala is often referred to as the temporal tip. The parahippocampal region (PHR) is situated on the brain surface posterior and ventral to HF. HF-PHR has attracted attention since the beginning of formal study of the nervous system. One of the reasons for this interest is the characteristic cytoarchitecture of the region (Fig. 2). HF differs from all other cortical areas since it is a three-layered cortex, comprising only one, very densely populated, principal cell layer. Most proximally situated is the dentate gyrus (DG) with a principal cell layer made up of granule cells. Distal to the DG is the Ammon's horn or Cornu Ammonis (CA fields, CA1, CA2, and CA3) and the subiculum (SUB) with a principal cell layer populated by pyramidal cells. PHR, which is extensively interconnected with HF, is positioned distally to HF and differs from the latter since it consists of multiple principle cell layers (Fig 2). It comprises the postrhinal cortex (POR), perirhinal cortex (PER), parasubiculum (PaS), presubiculum (PrS), lateral entorhinal cortex (LEC) and medial entorhinal cortex (MEC; (Witter and Amaral, 2004; Fig. 1).

Bilateral lesions of HF-PHR in humans and other animals have been associated with an inability to form episodic memories (Scoville and Milner, 1957; Jarrard, 1978). However, this form of amnesia is temporally graded, so that HF-PHR damaged patients and animals cannot encode new memories or recall recent memories, but are largely unimpaired in remembering events from the past. These observations lead researchers to hypothesize that episodic memories are formed and temporarily stored in HF-PHR and eventually consolidated in the neocortex where they are retained and from where they can be retrieved (Buzsaki, 1996). Others have suggested that the neocortex and HF-PHR serve different roles in formation of episodic memories, HF-PHR being necessary for rich and detailed recall of remote memories while the neocortex is necessary for more gist-like (semanticized) recall of remote memories (Moscovitch et al., 2016). Common for both views is that interaction between HF-PHR and neocortex is important for formation and recall of remote memories.

HF-PHR has for a long time been associated with the ability to recognize one's own self-location and the ability to navigate in space (Jarrard, 1978; Maguire et al., 2006). The contribution of individual subareas of HF-PHR to spatial cognition has been evaluated in animals such as the rat. Initial recordings of single neurons in HF-PHR lead to the discovery in CA1 of neurons which fire only when an animal is situated in a particular location in space (O'Keefe and Dostrovsky, 1971). The discovery of these 'place cells' lead to the theory that HF contained a cognitive map of an animal's local environment made from the overlapping fields of multiple place cells, potentially covering the whole environment (O'Keefe

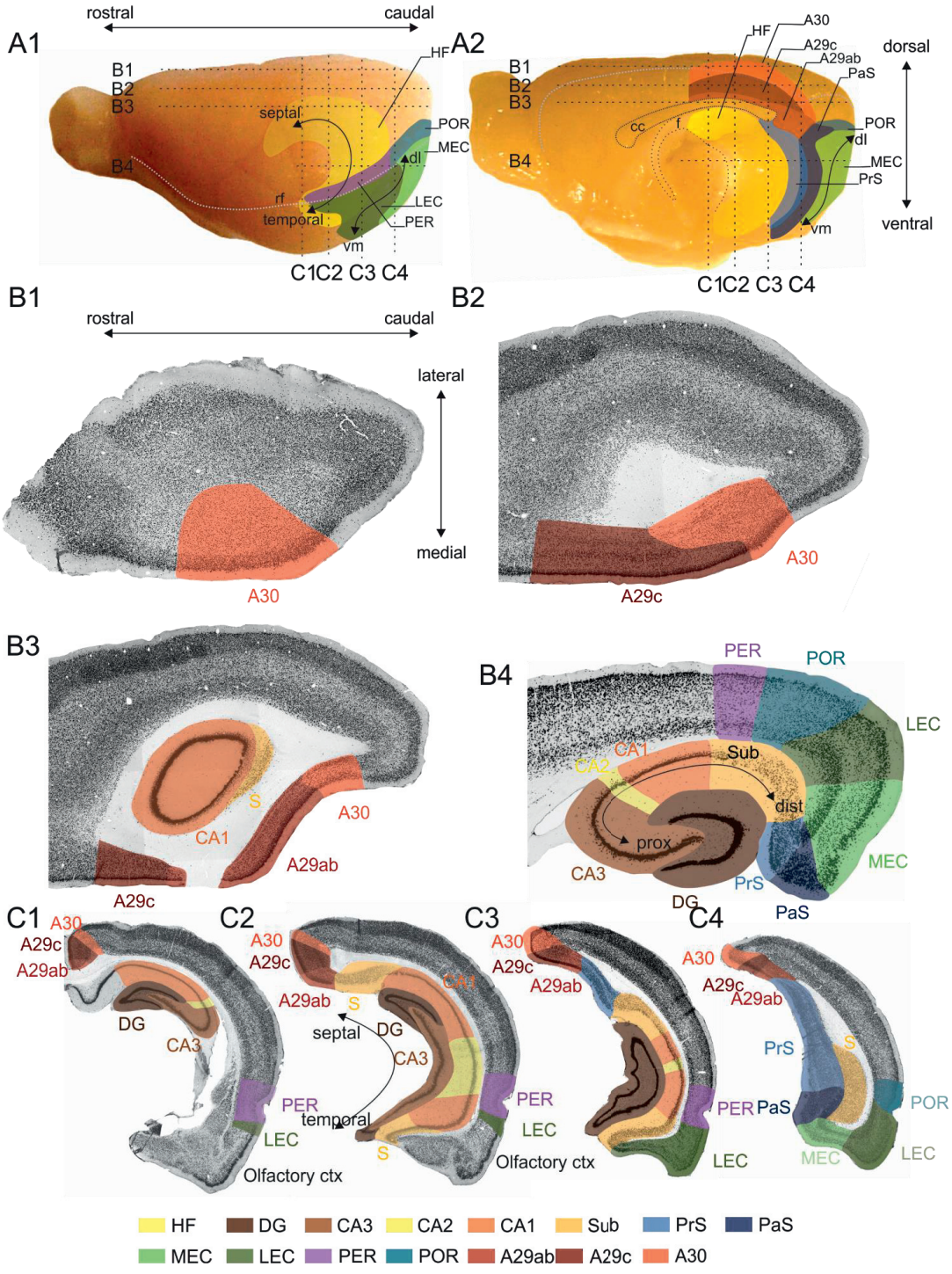
A1
rostral
caudal
B1
B2
B3
B4
HF
septal
POR
MEC
dl
rf
LEC
temporal
PER
vm
C1C2 C3 C4
A2
A30
HF
A29c
A29ab
PaS
dorsal
cc
f
POR
dl
MEC
PrS
ventral
vm
C1C2 C3 C4
B1
rostral
caudal
lateral
medial
A30
B2
A30
A29c
B3
S
A30
CA1
A29ab
A29c
B4
PER
POR
LEC
CA1
CA2
Sub
dist
prox
CA3
DG
PrS
MEC
PaS
C1
A30
A29c
A29ab
DG
CA3
PER
LEC
Olfactory ctx
C2
A30
A29c
A29ab
S
CA1
septal
DG
CA3
temporal
PER
LEC
S
C3
A30
A29c
A29ab
PER
LEC
Olfactory ctx
C4
A30
A29c
A29ab
PrS
S
PER
PaS
POR
LEC
MEC
LEC
HF
DG
CA3
CA2
CA1
Sub
PrS
PaS
MEC
LEC
PER
POR
A29ab
A29c
A30

Figure 1. Schematic representation of the position and cytoarchitectonic delineations of the retrosplenial cortex (RSC), hippocampal formation (HF) and the parahippocampal region (PHR) in the rat brain.

*Lateral **(A1)** and midsagital **(A2)** views of the rat brain. The RSC is subdivided into A29ab, A29c and A30. For orientation purposes, rostrocaudal, dorsoventral, lateromedial and septotemporal axes are indicated (A1, A2, B1, C2 respectively). The hippocampal formation consists of the dentate gyrus (DG), CA3, CA2, CA1 and the subiculum (SUB). The parahippocampal region is subdivided into the presubiculum (PrS), parasubiculum (PaS), the entorhinal cortex, which has a lateral (LEC) and a medial (MEC) subdivision, the perirhinal cortex (PER) and the postrhinal cortex (POR). For orientation in HF the long or septotemporal axis is used (C2). The main axis applied in case of PrS and PaS is also the septotemporal axis. Another commonly used axis is referred to as the proximodistal axis which indicates a position closer to DG or closer to PHR, respectively (B4). The dashed horizontal and vertical lines in panels A1 and A2 indicate the levels of four horizontal- and four coronal sections, which are shown in B1-4 and C1-C4. The gray stippled line in A1 represents the position of the rhinal fissure (rf) and in A2 it represents the global delineation of the dorsal surface of the brain with the midsagital and occipital surfaces.*

***(B)** Four horizontal sections of the rat brain; the levels of these sections are indicated in A1 and A2. The subfields of HF, PHR and RSC are color-coded, see color panel below C.*

***(C)** Four coronal sections of the rat brain; the levels of these sections are indicated in A1 and A2. The subfields of HF, PHR and RSC are color-coded, see color panel below C.*

and Nadel, 1978). However, the discovery of place cells lead to a discussion of where the origin of the spatial signal in HF was located. An obvious possibility was that the spatial signal was computed in HF itself. However, lesions of the upstream hippocampal fields, DG and CA3 do not change the firing pattern of place cells in CA1 (McNaughton et al., 1989; Brun et al., 2008). These findings implied that the spatial signal is either computed in CA1 itself or outside HF. Likely candidates for investigation were therefore LEC and MEC, situated not only one synapse upstream of both DG and CA3, but also one synapse upstream of the CA1 (Fig. 2). The first recordings were done in MEC since connectional studies indicated that MEC was the most likely candidate to represent spatial information (Witter et al., 1989). These recordings revealed that neurons in MEC represent multiple positions in space organized in a regularly patterned grid-like structure, universally covering all environments of a moving animal (Fyhn et al., 2004; Hafting et al., 2005). Neurons representing head-directionality (HD), borders of the environment, conjunctive grid and HD representations and the speed of the animals were also discovered in MEC, PrS and PaS (Taube et al., 1990; Sargolini et al., 2006; Boccara et al., 2010; Brandon et al., 2011; Burgalossi et al., 2011; Yartsev et al., 2011; Killian et al., 2012; Krupic et al., 2014; Carpenter et al., 2015; Hardcastle et al., 2015; Kropff et al., 2015). Further, if MEC is lesioned animals are impaired in a spatial memory task and display altered place cell firing in HF (Miller and Best, 1980; Parron et al., 2004; Steffenach et al., 2005; Van Cauter et al., 2008; Hales et al., 2014). These findings indicate that MEC, PrS and PaS are parts of a system which supports spatial cognition (McNaughton et al., 2006). On the other hand, LEC which is also directly connected to HF does not contain these spatially modulated cells, but contains cells which are tuned to objects and odors (Hargreaves et al., 2005; Deshmukh and Knierim, 2011; Tsao et al., 2013; Leitner et al., 2016). When LEC is lesioned, rats are impaired in tasks where processing of the contexts, objects or non-spatial cues are necessary (Hunsaker et al., 2013; Van Cauter et al., 2013; Wilson et al., 2013).

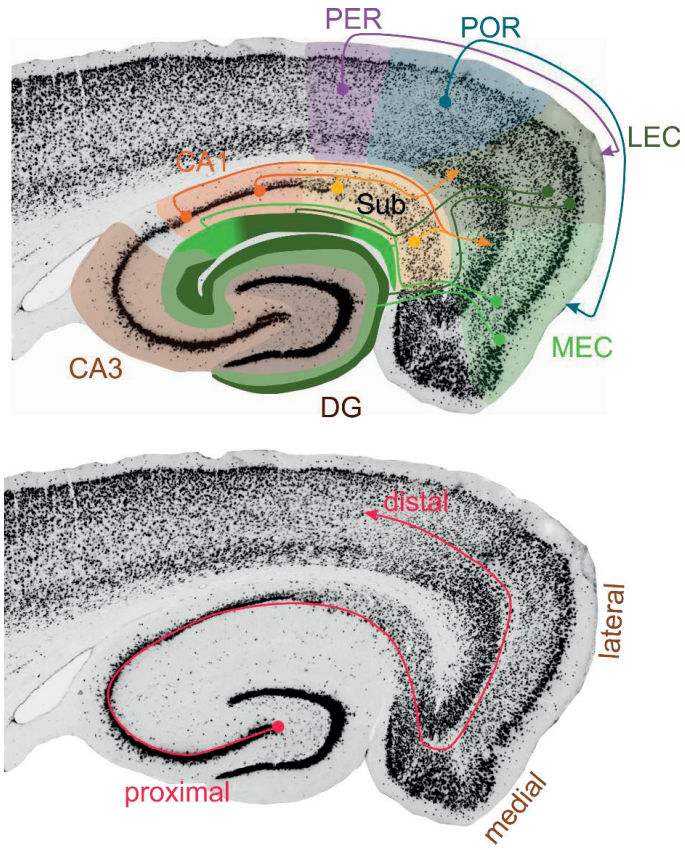

Figure 2. Schematic representation of the overall connectivity of the entorhinal cortex.

Horizontal section of HF-PHR. The medial entorhinal area (MEC) is targeted by inputs from the postrhinal cortex. The lateral entorhinal area (LEC) receives an input from the perirhinal cortex. Neurons in layer II of both subdivisions project to the dentate gyrus (DG) and CA3 and these projections are topographically organized so that afferents from LEC terminate in the superficial part of the molecular layer of DG and stratum lacunosum-moleculare of CA3, while the afferents from MEC terminate in deeper part of the same layers. Neurons in layer III of EC project to CA1 and the subiculum (SUB) and these projections are topographically organized in a columnar fashion where inputs from LEC terminate in the distal CA1 and the proximal SUB, while the terminals originating from MEC are present in the proximal CA1 and the distal SUB. A corresponding topography can also be observed in CA1 and SUB projections to the deep layers of EC projections. Neurons in the proximal CA1 and distal SUB target MEC, while neurons in the distal CA1 and proximal SUB target LEC.

Naturally, the same question originally posed for HF can now be posed for PHR; where is the origin of the spatial signal observed in PrS, PaS and MEC? Some important observations can provide the foundation for an educated guess. First of all, the appearance of the grid pattern is assumed to be dependent on several sensory inputs such as proprioception, vestibular information and optic flow

(McNaughton et al., 2006), suggesting that the grid pattern most likely is produced in a high-order multimodal cortex such as PHR. Second, the grid cell pattern is highly regular in *all* environments maintaining the spatial scaling, orientation and relative spatial phases between environments (Hafting et al., 2005), suggesting that a local connectivity similar to what can be found in MEC is important for the production of the grid pattern (Couey et al., 2013). Third, local network properties in conjunction with characteristic inputs of MEC are sufficient to create the characteristic structure of the grid pattern (Burgess et al., 2007; Hasselmo et al., 2007; Garden et al., 2008; Couey et al., 2013). Lastly, in none of the areas projecting to PrS, PaS and MEC, grid cell- or border cell representations have been observed. Therefore, it is believed that the regular hexagonal arrangement of grid fields across an environment is a result of computations within the networks of one or several of these areas. It is currently hypothesized that information about velocity-, direction and speed of the animal is integrated into one universal representation of current location, a process called path integration while allocentric sensory information anchor the grid pattern to the external environment and continuously update the positional firing of the spatially modulated cells in PHR (McNaughton et al., 2006; Hardcastle et al., 2015; Stensola et al., 2015). An important challenge is to understand how HF-PHR networks are capable of integrating afferent information and eventually use this to form a universal representation of space.

The presence of spatially modulated cells in one part of the HF-PHR circuit provides us with an excellent tool to relate these specific functional firing patterns to the underlying connectional architecture. One of several relevant cortical regions interconnected with PHR is RSC. This region is intriguing for a number of reasons. First of all RSC has consistently been shown to be important for tasks in which spatial navigation and (autobiographical) memory are necessary components (Maguire, 2001). Secondly, RSC is preferentially connected with the regions of PHR involved in visuospatial processing, namely POR, PrS, PaS and MEC (Wyss and Van Groen, 1992; Shibata, 1994; Jones and Witter, 2007). Finally the RSC projections to MEC and PaS differs from most other cortical inputs since it targets layer V and not the typical cortical input layers I-III of MEC and PaS (Jones and Witter, 2007). The overarching aim of this thesis is therefore to detail the connections between RSC and HF-PHR and how the information carried by these connections may interact with the various components of the local HF-PHR network.

Retrosplenial cortex

The RSC is the most caudal subdivision of the midline cortex which is generally referred to as the cingulate cortex. In primates, the cingulate cortex is subdivided in three or four regions along the rostrocaudal axis, The most caudoventral subdivision of the posterior cingulate which arches around the splenium of the corpus callosum, is referred to as RSC (Vogt, 2015). In primates, RSC is often considered a transitional cortex between the allocortex and the neocortex, with its poorly layered appearance caudally towards PrS and its six-layered appearance rostrally towards the posterior cingulate cortex (Kobayashi and Amaral, 2000). In primates, RSC is connected reciprocally with HF-PHR, anterior-, lateral dorsal- and lateral posterior nuclei of the thalamus, prefrontal cortex, dorsal superior

temporal sulcus, visual cortices V2 (afferent) and V4 (efferent) and cingulate areas 23, 24 and 31 (Morris et al., 1999; Kobayashi and Amaral, 2003, 2007).

In humans, RSC activity is modulated in different tasks ranging from speech production and comprehension, motivation, to pain (Small et al., 2001; Wik et al., 2006; Awad et al., 2007). However RSC is consistently responsive to tasks for which spatial navigation and (autobiographical) memory are necessary components (Maguire, 2001). Further, RSC is a component of the so-called default mode network. The default mode network is an interconnected system of brain regions, involving the lateral- and medial parietal areas, the medial frontal- and medial temporal lobe region and RSC (Buckner et al., 2008; Greicius et al., 2009). This network of brain regions is not only active during retrieval of autobiographical memories, but also when an individual is not focused on the outside world and instead is performing internal tasks such as daydreaming, envisioning the future, retrieving memories, or probing emotions and actions of others (Buckner et al., 2008). Although the function of the default mode network and the role of RSC within it remain elusive, it has been argued that RSC is not activated by spatial navigation *per se*, but serves a range of cognitive functions, some of which are crucial for spatial navigation and episodic memory.

In the rodent, RSC comprises the entire posterior cingulate cortex (Vogt et al., 1981). It extends over half the length of the cerebral hemispheres and is thereby one of the largest cortical regions in this group of animals. It is bordered rostrally by the anterior cingulate cortex/midcingulate cortex, caudoventrally by PHR and laterally by parietal and visual cortices. Based on cytoarchitectonic features, RSC can be divided into four subdivisions, area (A)29a, A29b, A29c and A30 (Fig. 1; (Vogt et al., 2004). A29a is the most ventral subdivision and it differs from the dorsally adjacent A29b since it lacks a fully differentiated layered structure. Cytoarchitectonically, A29a has a homogenous layer II/III, while in A29b this layer is divided into a thin superficial densely packed zone and a less dense deeper zone (Vogt et al., 1981). Area 29b is distinguished from A29c based on differences in AchE staining, in which layer IV is more densely labeled in A29c compared A29b (Jones and Witter, 2007). Cytoarchitectonically, A30 shows an abrupt widening and a less dense packing of layer II/III compared to A29b and A29c (Vogt et al., 1981; Sripanidkulchai and Wyss, 1987; van Groen and Wyss, 1992; Jones et al., 2005). Also, layer IV of A30 is wider than in A29b/A29c and in layer V neuron somata tend to be larger in A30 than in all subdivisions of A29 (Krieg, 1946; van Groen and Wyss, 1992). The rodent RSC is reciprocally connected to structures known to be involved in memory formation and in visuospatial processing such as visual A17 (caudal A30) and A18b (A30 and A29c), anterior and lateral dorsal nuclei of the thalamus, the mammillary bodies, posterior parietal cortex and the dorsolateral prefrontal cortex (van Groen and Wyss, 1990c; Reep et al., 1994; van Groen and Wyss, 2003). In addition RSC is densely connected to HF-PHR (Jones and Witter, 2007), and these connections are extensively reviewed in paper 1 (Sugar et al., 2011).

Functions of retrosplenial cortex

Based on the vast number of publications investigating the deficits in RSC lesioned rats and the activation pattern of RSC in humans, it is now commonly thought that RSC is a key player in processing of information important for spatial navigation and spatial cognition. There have been attempts to test whether RSC of humans and rats is involved in processing of specific classes of spatial information. Several studies have focused on the difference between allocentric (based on environmental cues such as landmarks) and egocentric navigational strategies (based on internal cues such as proprioception and vestibular information). RSC lesioned animals are impaired both in tasks depending on 'internally' generated cues (Cooper and Mizumori, 1999; Cooper et al., 2001; Whishaw et al., 2001; Elduayen and Save, 2014), and in tasks requiring 'external' sensory information (Whishaw et al., 2001; Vann and Aggleton, 2002, 2005; Pothuizen et al., 2008; Hindley et al., 2014a). This is also true for the human since activation patterns of RSC are sensitive to tasks where the subjects are depleted for distal cues and have to rely on internal path integration for successful navigation (Sherrill et al., 2013) and to tasks relaying on external visual cues (Auger et al., 2012; Auger and Maguire, 2013; Sulpizio et al., 2013; Marchette et al., 2014). With respect to the latter, RSC is more sensitive to permanent landmarks compared to less reliable cues, possibly reflecting that RSC is more interested in cues important for the calculation of a heading direction. These notions are also reflected in patients with lesions of RSC, who commonly show learning deficits, difficulties in remembering recent autobiographical events and topographical disorientation (Takahashi et al., 1997; Osawa et al., 2008). These patients can recognize familiar landmarks which are visually present, but cannot use these landmarks to produce a sense of direction or calculate the spatial relationship between familiar environments. In rats, there has been a systematic attempt to single out whether RSC is involved in the processing of a specific class of cues to produce an allocentric heading. When RSC lesioned rats are taught to alternate left/right in a cross-maze and are subsequently depleted for both visual extra-maze cues and intra-maze cues, they show a significant drop in performance compared to controls, suggesting that RSC lesioned animals are not able to keep track of the heading direction when there are no visual cues available (Pothuizen et al., 2008). These findings are supported by extra-cellular *in vivo* recordings, showing that in intermediate rostrocaudal RSC ~10% of the neurons in RSC are modulated by the heading direction (Chen et al., 1994; Cho and Sharp, 2001) and is in-line with the fact that RSC is interconnected with a series of brain regions containing HD cells, such as anterior nuclei of the thalamus and PHR (van Groen and Wyss, 1990c, 1992, 2003).

Several authors have tried to single out contributions from each of the subdivisions of RSC. First, lesions of A29c, but not A29ab disrupts performance during acquisition in the Morris water maze, while A30 lesions impair the use of visual allocentric cues in the radial-arm maze (van Groen et al., 2004; Vann and Aggleton, 2005). Second, rats with lesions of A29 are as impaired as rats with both A29 and A30 lesioned when the rats are tested in a radial arm task. In the same task increased expression of immediate

early genes (IEG) is detectable in A29 if the radial arm maze-task is performed either in the dark or in the light, while in A30 IEGs are only detected after performance in light (Pothuizen et al., 2009). Based on these studies it can be concluded that A30 seems to be more involved in processing of visual cues than A29. This observation is consistent with the anatomical connections of RSC in that the caudal A30 has more prominent connections with visual cortices compared to the subdivisions of A29. On the other hand, A29 seems to play a more general role during spatial working memory and memory acquisition, which is yet to be defined in more detail.

There are also functional differences between rostral and caudal RSC. In the Morris water maze, animals with lesions in only caudal parts of RSC are impaired, suggesting that at least the caudal RSC is important for the navigational attributes of RSC. If the same animals are tested in a 8-arm radial arm maze which is rotated halfway during foraging (and the remaining food was rebaited to the same extra-maze-position and to new intra-maze position), caudally lesioned animals were impaired suggesting that the integrity of caudal RSC is also important for the use of extra-maze cues (Vann et al., 2003). However, no experiments have directly compared the functional differences of rostral and caudal RSC.

The notion that RSC seems to be involved in several different navigational strategies has led to suggestions that RSC has an integrative role during navigation. This is of particular interest since RSC lesioned animals seems to be mostly impaired when distal environmental cues and internal information is put in conflict with each other, for instance if a maze is rotated during an experiment (Vann and Aggleton, 2002; Vann et al., 2003; Vann and Aggleton, 2004; Nelson et al., 2014). This hypothesis is supported by the anatomical connections of rat RSC with the parietal cortex, known to contain neurons representing spatial information in an egocentric reference frame and its connections to parahippocampal structures known to contain spatial neurons that represent information in an allocentric reference frame (Fyhn et al., 2004; Whitlock et al., 2012). In fact, neurons encoding space both in egocentric and allocentric reference frames have also been observed in RSC (Alexander and Nitz, 2015). Comparably, human RSC has also been found to integrate information from the parietal cortex and information from HF-PHR (Guterstam et al., 2015). The idea that the human RSC integrates spatial information from several reference frames is supported by the notion that RSC lesioned patients cannot use familiar landmarks to produce a sense of directionality (Takahashi et al., 1997; Hashimoto et al., 2010). Additionally several studies have revealed that RSC activity is increased not only during pure navigational tasks, but also during visual scene perception (Epstein and Higgins, 2007; Park and Chun, 2009), scene imagination (Hassabis and Maguire, 2007), and looking at images of permanent objects (Auger et al., 2012; Auger and Maguire, 2013). These observations do suggest that RSC is not specifically important during navigation and spatial cognition, but more likely is involved in more general information processing which is among others necessary for successful navigation and spatial cognition.

A second line of experiments has investigated whether RSC is important for processing of spatial contexts. If the rat RSC is lesioned, the animals cannot use the spatial context as a cue to guide a motor response (Nelson et al., 2014) or use context as a CS to elicit a fear response (Keene and Bucci, 2008a). Supporting these findings are reports that neuronal ensembles in RSC process contextual information in a fear conditional paradigm (Cowansage et al., 2014). In humans, RSC has also been shown to encode contextual information. If a subject is shown multiple different images from the same spatial context, RSC activity differentiates images from different- and similar contexts (Park and Chun, 2009). Several experiments have tried to reveal whether RSC encodes specific features of an event or context. To this end, animals and humans have been exposed to contexts and events where non-spatial cues are important. For instance, activity in RSC increases if subjects are exposed to non-spatial features of a context (Burgess et al., 2001; Bar and Aminoff, 2003). In rabbits, *in vivo* extra-cellular recordings revealed that RSC neurons are responsive to acoustic tones suggesting that RSC also plays a role in processing of non-spatial features of events or contexts (Gabriel et al., 1991; Smith et al., 2002). RSC lesioned animals are not able to use multimodal cues (such as a visual signal and a tone) either presented simultaneously or in series as a conditional stimulus for a food-reward or an electric shock (Keene and Bucci, 2008b; Robinson et al., 2011; Robinson et al., 2014). These results suggests that RSC plays a role in forming initial associations between multiple sensory stimuli. Possibly, RSC could use these associations to form a representation of an event. In support of this hypothesis are the results of a recent study in which rats were exposed to the same objects in light and dark (Hindley et al., 2014b). Importantly, in the light paradigm the animals were restricted from touching the objects leaving only visual information available, while in the dark only somatosensory information was available for the rats. This experiment revealed that RSC lesioned animals were able to recognize objects across sessions if the animals had access to the same sensory modality as they had during the first exposure. However if the animals were first presented with the object in the dark (only somatosensory information) and then in the light (only visual information) RSC lesioned animals treated the objects as if they were new, supporting the hypothesis that RSC is important to form initial associations between the sensory stimuli and suggesting that RSC is important for integrating multiple sensory representations. RSC lesioned animals are also impaired in experiments assessing more complex cognitive abilities where environmental information is not important. For instance RSC lesioned rats are unable to discriminate between temporal separable events suggesting that RSC is also involved in more complex sensory processing (Todd et al., 2015). All in all, these findings suggest that RSC is not only restricted to process pure spatial information, but has a general role in combining multimodal information, possibly necessary to encode single events.

Another line of experiments has focused on the role of RSC during memory encoding. RSC neurons play a role during spatial memory formation since single RSC neurons show increased activity during learning in a spatial memory task, and if these active neurons are inhibited or stimulated the performance

of the subjects decreases or increases respectively (Czajkowski et al., 2014). Additionally, neurons in rostral RSC have been reported to form place fields in parallel with improved performance in a navigational task, showing that single RSC neurons change their firing patterns in parallel with encoding (Smith et al., 2012). Importantly neural activity is not only limited to formation of spatial memory. In rabbits, *in vivo* extra-cellular recordings have revealed that RSC neurons are responsive to acoustic tones. Interestingly, the firing rate of the neurons increases if the tone is relevant for the animal, for instance if a tone is used as a conditional stimulus before a foot-shock or a reward (Gabriel et al., 1991; Smith et al., 2002). Conversely, if a tone is presented to the animal without being followed by a foot-shock, the responsive neurons will reduce their responsiveness to the stimuli. These findings suggest that neurons encode stimuli which predict an outcome. Interestingly, if SUB, the structure providing the main output from HF-PHR to RSC, is lesioned, the responsiveness of RSC neurons is attenuated suggesting that HF outputs are important for the RSC activity (Gabriel et al., 1987).

In the classical memory formation hypothesis, episodic memories are initially formed in HF and later consolidated in the neocortex, implying that recent memories are transiently stored in HF and later "moved" to the neocortex. There has been an increasing interest in the role of RSC during memory consolidation. The idea that RSC is one of the cortical areas important for consolidation of HF-dependent memories has recently been challenged. First, RSC is able to encode contextual memories also when HF is transiently silenced suggesting that RSC is able to encode memories independently of HF (Cowansage et al., 2014). Second, in contrast to other neocortical regions, metabolism in RSC (and HF-PHR) declines as a function of time since encoding, thereby suggesting that RSC is not important for memory consolidation (Bontempi et al., 1999). In addition, there are several studies which have tested the importance of RSC during recall of recent unconsolidated memories. Expression of recent memory depend on a functional RSC (Maviel et al., 2004; Corcoran et al., 2011; Katche et al., 2013a) and if protein synthesis in RSC is inhibited during memory encoding, long term memories are abolished (Katche et al., 2013a). Together these reports suggest that RSC is important for encoding of memories and thus questions whether consolidation of HF-dependent memories into RSC occur. During memory formation and consolidation, RSC seems to act more similar to HF-PHR and more different to other cortical areas.

The similar functional attributes of HF-PHR and RSC have motivated investigations of functional interactions between RSC and HF. In both humans and rodents, activity patterns in HF-PHR and RSC are correlated, suggestive of functional interactions between the two regions (Bontempi et al., 1999; Iaria et al., 2007). Additionally, the interaction between the regions has also been tested directly in the rodent. First, HF-neurons temporarily change the location of their place fields if RSC is temporarily inactivated (Cooper and Mizumori, 2001). Second, if HF is lesioned RSC neurons change their firing patterns (Gabriel et al., 1987). Third, if HF neurons which are active during a contextual fear conditioning task are silenced, the activity of RSC neurons which are targeted by these neurons is also

decreased (Tanaka et al., 2014). Fourth, if c-fos expression is blocked either in RSC or HF during a fear conditioning task, c-fos expression in the other region (HF or RSC respectively) is also decreased (Katche et al., 2013b). Finally, theta rhythmicity in RSC and HF is coherent during explorative behavior (Young and McNaughton, 2009). All in all, these findings support the notion that there is a functional overlap between RSC and HF-PHR and that these areas also are critically dependent on each other for proper functioning. The anatomical connections between RSC and HF-PHR ascertain that information transfer between the areas can occur. However, how neural signals from RSC are integrated in HF-PHR circuitry is still elusive. I therefore aimed to assess the anatomical substrate for interaction between these areas. In the next section, I give a brief overview of the interconnections of the HF-PHR regions which are connected with RSC, before I give an overview of the flow of information within the HF-PHR.

Subiculum

SUB is nearly devoid of cortical inputs except from the projections originating in EC and CA1. Entorhinal inputs originating in LEC target the proximal SUB while inputs originating in MEC target distal SUB (Honda and Ishizuka, 2015). In addition to the input from EC there are several subcortical inputs to SUB. There are dense inputs originating from the medial septum, diagonal band of Broca and supramamillary nucleus. Inputs also originate in amygdala and the midline nuclei of the thalamus including the nucleus reuniens. Modulatory inputs from locus coerulus, ventral tegmental area and raphe nuclei reach SUB as well (Cappaert et al., 2015).

SUB, in conjunction with CA1 is the main output structure of HF and projects to a number of cortical and subcortical brain regions. The connectivity patterns of SUB are organized along its proximodistal border where proximal and distal SUB seems to have clearly segregated connectivity patterns (Cappaert et al., 2015). The proximal SUB targets deep layers of LEC, infralimbic- and prelimbic cortex and PER. Subcortical projections from proximal SUB target nucleus accumbens, lateral septum and amygdala. On the other hand, distal SUB targets all layers of PrS, superficial layers of PaS, deep layers of MEC and RSC. The projection to PrS is also topographically organized such that within distal SUB, the most distally located neurons target distal PrS while more proximal neurons of SUB target proximal PrS (O'Reilly et al., 2013). Subcortically distal SUB projects to the ventromedial hypothalamus.

Presubiculum

Presubiculum is connected to several other PHR subdivisions. First of all, PrS is the 'defining' projection of MEC. The projection originates in layer II and III and terminates in layer I and III. It stops abruptly at the border between MEC and LEC. Even though the projection terminates mainly in superficial layers, neurons in deep layers V-VI have dendritic arborizations in superficial layers and receive PrS input (Canto et al., 2012). The PrS-MEC projection targets both spiny dendrites and smooth dendrites, presumably of principal neurons and interneurons respectively (van Haeften et al., 1997). Across the proximodistal axis there is a clear topography with respect to the location of terminal fibers in MEC;

neurons in distal PrS project to medial MEC while neurons in proximal PrS project to more lateral parts of MEC (Caballero-Bleda and Witter, 1994; Honda et al., 2011). Along the dorsoventral extend of PrS the projection to MEC changes; in the ventral two thirds PrS-MEC projections are excitatory, while in the dorsal third a large proportion of the ipsilateral projection is inhibitory (van Haeften et al., 1997).

PrS is devoid of neocortical inputs except for a weak neocortical input originating in the anterior midline cortex and in visual cortices (Vogt and Miller, 1983; Jones and Witter, 2007) and reciprocal connections with RSC. Single neurons in layer V issue collaterals to both SUB, RSC and short range axonal arbors locally in PrS (Honda et al., 2011). With respect to the RSC projection, both deep and superficial layer termination have been reported (van Groen and Wyss, 1990a; Honda et al., 2011). The RSC projection is topographically organized, such that dorsal PrS project to rostral RSC while ventral PrS project to caudal RSC (van Groen and Wyss, 1990b). PrS receives dense inputs from RSC layer V which terminates in both deep and superficial layers (Jones and Witter, 2007). The RSC projection target pyramidal neurons in layer III which project to superficial layers of MEC and thereby provide a second pathway from RSC to the superficial layers of MEC (Kononenko and Witter, 2012), in addition to the RSC to MEC layer V to MEC layer II pathway (Czajkowski et al., 2013).

PrS is reciprocally connected to the anterior nuclei of the thalamus and the medial septum (Cappaert et al., 2015).

Parasubiculum

The most dense output originating from PaS is the projection terminating in layer II of EC and the projection to PrS (van Groen and Wyss, 1990a; Caballero-Bleda and Witter, 1994). Similarly to PrS, PaS only receives a weak neocortical input originating in the midline cortex and in visual cortices. These projections target the deep layers of PaS (Vogt and Miller, 1983; Jones and Witter, 2007). There are also reciprocal connections between the deep layers of PaS and RSC.

Subcortical connections exist since PaS projects weakly connected to the anterior nuclei of the thalamus and the mammillary bodies and PaS receives a prominent input from amygdala (van Groen and Wyss, 1990a; Wright et al., 2010).

Entorhinal cortex

EC is commonly subdivided in a medial part and a lateral part. These two subdivisions can be easily separated based on cytoarchitectonic differences (Insausti et al., 1997). Neurons in layer II are generally clustered in diffuse islands in LEC while in MEC the layer II cells are homogeneously distributed and are slightly larger compared to the layer II cells of LEC. Additionally, the border between layer II and III is more clearly demarcated in MEC. In the deep layers, neurons in MEC tend to be arranged in ordered columns while there is no clear columnar arrangement of neurons in the deep layers of LEC.

LEC and MEC differ with respect to their connectivity with other parts of HF-PHR and with HF. Whereas MEC is primarily targeted by inputs from POR, LEC receives a major cortical input from PER (Burwell and Amaral, 1998). In addition, PrS projects exclusively to layer III of MEC while PaS projects to layer II of both MEC and LEC, although the projections to LEC are much weaker (Caballero-Bleda and Witter, 1994). In addition, they differ with respect to main cortical inputs. MEC and LEC are connected differentially to other cortical areas. In contrast to LEC, which target cortical areas such as piriform cortex, orbitofrontal cortex, ACC and insular cortex, MEC issues efferents to RSC, POR, parietal cortex and visual areas. Return projections from the midline cortex arise in prelimbic, infralimbic and orbitofrontal cortex and primary target LEC while neurons in layer V of RSC predominantly target MEC (Burwell and Amaral, 1998; Jones and Witter, 2007; Kerr et al., 2007). Layer II neurons of motor areas preliminary innervate MEC and avoid LEC (Burwell and Amaral, 1998).

It should be noted that the dorsomedial part of MEC differs from the remainder of MEC in a number of inputs. Olfactory inputs avoid dorsomedial MEC and target more lateral and ventral parts of MEC and LEC. Similarly, amygdalar inputs target mainly layers III and V of LEC and ventromedial MEC and avoid dorsomedial MEC (Pitkanen et al., 2000). In contrast inputs originating in supramamillary nucleus and tuberomamillary nucleus target mostly the dorsomedial MEC and avoid the rest of EC (Haglund et al., 1984; Saper, 1985).

Postrhinal cortex

Another region involved in spatial information processing is POR. POR issues projections to subiculum, mainly to its distal parts (Naber et al., 2001). POR is also projecting to superficial layers of MEC, most densely to dorsomedial MEC and the projection is excitatory (Koganezawa et al., 2009). The main HF-inputs to POR arise in CA1, while PaS and MEC provide the most substantial parahippocampal input to POR (Furtak et al., 2007).

With respect to extra-HF-PHR connections, POR is reciprocally connected to dorsal RSC, parietal cortex and visual cortices and auditory cortices (Wyss and Van Groen, 1992; Furtak et al., 2007; Agster and Burwell, 2009). A minority of the inputs is subcortical and arise mainly in dorsal thalamic nuclei (Furtak et al., 2007).

Segregated and converging information streams within HF-PHR

PHR is the main gateway between the cortex and HF. In the classical model of HF-PHR connectivity, sensory inputs converge on superficial layers of EC, either directly or indirectly through other parahippocampal cortices. Neurons in the same layers are the origins of the perforant path, the largest cortical input to HF (Fig. 2; Witter et al., 2000). Axons of neurons in layer II of EC terminate in DG and CA3, while layer III neurons project to CA1 and SUB. In HF there is more or less a unidirected information flow where DG and CA3 are situated upstream of CA1 and SUB. Output from HF originates in CA1 and SUB and targets the deep layers of EC, which are generally accepted to be the main origin

of projections to the neocortex. However exceptions to these patterns are evident as olfactory projections from EC originate from layer II and III, the cingulate cortex targets deep layers of EC and a weak projection from the deep EC layers to HF is evident (Insausti et al., 1997; Gloveli et al., 2001; Jones and Witter, 2007).

A number of experiments have suggested that different modalities of information is processed in distinct parts of PHR. As reviewed in the section above, LEC and MEC differ from each other with respect to their overall connectivity (Fig. 2). PrS, PaS, MEC and POR mainly receive inputs from areas known to be important for visuospatial processing, such as RSC, parietal cortex and visual cortex. On the other hand, LEC and PER are targeted by insular and olfactory cortices as well as the amygdala, areas known to be important for context, odor-processing and emotions (Burwell and Amaral, 1998; Kerr et al., 2007). These differences are concurrent with the single cell recordings and imaging in rats and primates since there is spatially modulated activity in PrS, PaS and MEC, while in LEC and PER there is activity related to processing of objects, contexts and odors (Fahy et al., 1993; Suzuki et al., 1997; Fyhn et al., 2004; Hargreaves et al., 2005; Deshmukh and Knierim, 2011; Naya and Suzuki, 2011; Killian et al., 2012; Ranganath and Ritchey, 2012; Tsao et al., 2013; Warburton and Brown, 2015; Leitner et al., 2016).

The spatial- vs non-spatial input streams through MEC and LEC, respectively, converge in DG and CA3 since projections from LEC terminate superficially in the molecular layer of DG and stratum lacunosum-moleculare of CA3, while the afferents from MEC terminate in deeper parts of the same layers (Witter et al., 1989). It is thus possible that the two information streams target different segments of the same granule- and pyramidal cell dendrites and information conveyed by MEC and LEC could possibly be integrated within DG and CA3.

On the other hand, the entorhinal inputs to CA1 and SUB are topographically organized in a columnar fashion where inputs from LEC and MEC terminate in different parts of CA1 and SUB. Inputs originating in LEC terminate in distal CA1 and proximal SUB, while the terminals originating from MEC are present in proximal CA1 and distal SUB (Naber et al., 2001). A corresponding topography along the transverse axis can also be observed in the CA1 to SUB projections and in CA1/SUB to EC projections (Fig. 2). Neurons in the proximal CA1 target the distal SUB and neurons in both proximal CA1 and distal SUB project to deep layers of MEC. On the other hand, neurons in the distal CA1 target the proximal SUB and neurons in both distal CA1 and proximal SUB project to deep layers of LEC (Tamamaki and Nojyo, 1995; Naber et al., 2001). Recordings from CA1 and SUB support these findings by reporting that spatial representation is organized along the transverse axis of CA1 and SUB with the strongest spatial representation in the proximal CA1 and distal SUB (Sharp and Green, 1994; Henriksen et al., 2010).

It is therefore generally thought that there are two pathways of information flow through the HF-PHR. One concerned with visuospatial information mainly involving the POR, PrS, PaS, MEC, proximal CA1

and distal SUB. The other concerns non-spatial information mainly involving PER, LEC distal CA1 and proximal SUB (Witter et al., 2000; Eichenbaum et al., 2007; Ranganath and Ritchey, 2012). Interestingly RSC is mainly interconnected with the HF-PHR areas involved in visuospatial information.

Objective I

I have argued above that the similar attributes of RSC and HF–PHR strongly suggest that the two regions are functionally related. However, how neural signals from the RSC are integrated in the HF-PHR circuitry is still elusive. Details about the anatomical connectivity provide a solid basis to functionally assess such integration and in the first two papers, I therefore aimed to assess the anatomical substrate for interaction between these areas.

To investigate the anatomical substrate for RSC – HF-PHR interactions we first aimed to review all written reports assessing anatomical connections between the rat RSC and the HF-PHR. An interactive connectome integrated with a previously published connectome on rat HF-PHR connections was presented in paper 1 (van Strien et al., 2009).

In paper 2, I aimed to investigate one of the most prominent connections between the RSC and the HF-PHR, namely the projection from the RSC to MEC. Details about the synaptic organization of the RSC projections to MEC are unknown, and most importantly it is currently not known how RSC inputs reach HF. Direct projections from RSC to HF do not exist, suggesting that alternative pathways must exist for RSC to communicate with HF. One possibility is that RSC inputs reach superficial layers of MEC indirectly through layer V of MEC. Layer II/III of MEC harbor neurons projecting to HF and could thereby mediate RSC inputs to HF. Our first aim was therefore to characterize the RSC to layer V projection at the synaptic level. Secondly, I asked whether its postsynaptic target cells include superficially projecting pyramidal neurons in layer V. To this end, neuroanatomical and optogenetic *in vitro* electrophysiological experiments were combined.

Development of HF-PHR and RSC

HF-PHR develops from distinct proliferative zones in the neuropeithelium. The HF and PrS/PaS/MEC are derived from two anatomically distinct primordia (Bayer, 1990a; Abellan et al., 2014). The two primordia are located close to each other in the medial pallium, adjacent to the cortical hem and have similar gene expression patterns during early embryological development in both the chicken and in the mouse (Abellan et al., 2014). Morphologically they can be identified and separated from the neocortex in the rat from around E15-16 (Bayer, 1980b). The primordium of RSC is located in the dorsal pallium directly dorsal to the medial pallium. However the RSC primordium shares most of the gene expression patterns of the medial pallium (Abellan et al., 2014) which might be taken as an indication that (part of) RSC actually originates from of the medial pallium. Directly ventral and posterior to the medial pallium sits the dorsolateral caudal pallium which is the origin of the mouse LEC. Compared to the medial pallium, the dorsolateral caudal pallium expresses a different set of transcription factors during early

embryological development and has therefore been suggested to be distinct from the medial pallium (Abellan et al., 2014). At early stages the ventricular wall is occupied by radial glial cells which undergo asymmetrical cell division to form the principal cells of the HF-PHR and RSC. The cortical layers of the rat HF-PHR form from E17 and there are two main gradients with respect to the corticogenesis in HF-PHR. First, as in the rest of the cortex, neurons destined for deep layers are produced earlier than superficially destined neurons. Second, there is a gradient along the transverse plane in HF-PHR so that lateral parts of PHR form before medial parts and distal parts of HF-PHR form before proximal parts (Fig 2). For instance, the cortical plate of LEC can be identified from E17, and the neuroepithelium deep to EC disappears around E22 (Bayer, 1980b). On the other hand the principal cell layer in HF can be identified from E19 and the HF neuroepithelium does not disappear until P1. There are exceptions from these rules as neurons in layer III of EC appear *after* layer II neurons and the superficial layers of PrS and PaS, even though located distally to HF, are organized *after* HF (as late as E22; Bayer, 1980a, b). Neurogenesis of the rat RSC neurons starts at E16 and is finished around E20, and is topographically graded so that rostral A29 is slightly older than caudal A30 (Bayer, 1990b). The migration of A29 layer II pyramidal cells is not finished until P7 and the neurons obtain adult-like dendritic morphology before P10 (Zgraggen et al., 2012).

Intrinsic connectivity within HF-PHR develops in parallel with neurogenesis and neuronal migration (for a summary see Table 1). There are two important features which should be stressed. First, in all projections investigated, the first axons to arrive in their place of termination already are distributed topographically according to the adult patterns. For instance the projection from EC to HF is organized similar to adults both with respect to the distribution along the laminar-, transverse- and dorsoventral axes (Fricke and Cowan, 1977; Borrell et al., 1999; O'Reilly et al., 2014). Second, several of the intrinsic HF-PHR projections develop before the cells issuing the projection- and the future posts-synaptic cells have migrated to their final location. For instance, axons originating in EC arrive in DG before the dendrites of the future post-synaptic granule cells are developed, which suggest that cues on the postsynaptic neurons are not important to direct axons into their field of termination (Jones et al., 2003). Instead it has been suggested that certain early born neurons provide ‘scaffolds’ for the growing axons, similar to what has been reported for thalamocortical projections (Allendoerfer and Shatz, 1994). For instance, the EC-HF projection is dependent on calretinin- and reelin expressing Cajal-Retzius cells located in the outer marginal zone of HF (Borrell et al., 1999). In both rats, mice, and humans, the Cajal-Retzius cells are born before the principal neurons of HF, and make up a transient population which disappears early in the postnatal period, possibly because of increased activity in the network (Del Rio et al., 1996; Meyer and Goffinet, 1998; Deng et al., 2007). The Cajal-Retzius cells project ‘pioneer’ axons to EC and these axons are used as scaffolds for the HF-projecting neurons in EC which grow along the Cajal-Retzius axons. Arriving in HF, the EC axons transiently synapse on the Cajal-Retzius cells before they form synapses on their final postsynaptic targets. Similarly, to the EC-HF projection,

commissural HF fibers and the septal-HF projection use distinct pioneer populations of neurons as a scaffold to reach HF, suggesting that this phenomenon might be general for several HF afferents (Super and Soriano, 1994; Super et al., 1998).

Even though axons are located in their final field of termination, several studies suggest that the majority of synaptogenesis happens postnatally, several days after the first axons arrive (Crain et al., 1973; Deguchi et al., 2011). In another set of experiments in our lab we investigated when these synapses become functional. The first connections turning functional are the Schaffer collaterals and mossy fiber projections which can be recorded from P6, followed by EC-HF and SUB-EC which can be recorded from P9 (Koganezawa and Witter, 2010). In PHR, connections from PaS and PrS to EC are functional from P8 and P9 respectively (Canto et al., 2011). Within EC, development of excitatory and inhibitory circuits seems to be distinct. Excitatory connections from deep to superficial layers are functional already from P7 (van Haeften et al., 2003; O'Reilly et al., 2010b). However stellate cells within layer II of MEC do not display synchronized subthreshold membrane potentials until P22, a finding which likely relates to the development of adult-like connectivity between stellate cells and fast-spiking interneurons in the same period (Langston et al., 2010; Couey et al., 2013). These findings suggest that MEC circuits involving inhibitory interneurons develop later than long- and short range excitatory connections. This assumption is supported by the finding that excitatory depolarizations in MEC after stimulations of PrS and PaS declines at the end of the second postnatal week, suggestive of overall increased inhibition late in postnatal development (Koganezawa et al., 2010).

Mouse	Rat	Origin	Termination	Note	Reference
<E14	<E17	HF OMZ	Ipsilateral EC	Calretinin+ Cajal-Retzius cells issue the projection. Disappears by P15	(Super et al., 1998; Ceranik et al., 1999; Deng et al., 2007)
<E15		HF IMZ+SR	(Assumed: contralateral HF)	Calbindin+, and GABA+ neurons issue the projection. Disappears by P15	(Super et al., 1998)
E15		EC	Ipsilateral HF WM		(Super and Soriano, 1994; Super et al., 1998)
E15		HF	Ipsilateral medial septum	Disappears by E17	(Super and Soriano, 1994)
E16	E17	EC	Ipsilateral CA SLM	Adult-like topography	(Super and Soriano, 1994; Super et al., 1998; Borrell et al., 1999; Deng et al., 2007)
E17		HF	Ipsilateral lateral septum		(Super and Soriano, 1994)
E17		Septum	Ipsilateral HF		(Super and Soriano, 1994)
E18		CA3	Ipsilateral CA1 SR		(Super et al., 1998)
E18		EC	Contralateral HF		(Super and Soriano, 1994)
	E17	CA1	Ipsilateral EC		(Deng et al., 2007)
E19	P2	EC	Ipsilateral DG OLM		(Super and Soriano, 1994; Borrell et al., 1999; Deng et al., 2007)
P0	<P6	HF	Contralateral CA1 SR+SO		(Fricke and Cowan, 1977; Super et al., 1998)
P2		EC	Contralateral DG		(Super and Soriano, 1994)
	<P0	HF	EC	Adult-like topography	(O'Reilly et al., 2010a)

	<P2	EC	Ipsilateral DG SM + CA	Adult-like topography	(Fricke and Cowan, 1977; O'Reilly et al., 2014)
	<P3	DG	Ipsilateral CA3		(Fricke and Cowan, 1977)
	<P7	SUB	PrS, PaS, EC	Adult-like topography	(O'Reilly et al., 2013)

Table 1. Overview of reported connectivity in the developing rodent HF-PHR. The two leftmost columns indicate the ages the connections have been observed in the mouse and rat. The third and fourth column indicate the area of origin and termination. Abbreviations: hippocampal formation (HF), entorhinal cortex (EC), dentate gyreus (DG), subiculum (SUB), outer/inner molecular zone (OMZ/IMZ), stratum radiatum (SR), stratum oriens (SO), stratum radium moleculare (SLM), outer molecular layer (OLM), white matter (WM).

Objective II

The current knowledge about development of intrinsic HF-PHR circuitry suggests that there are several temporally distinct periods of maturation. To study developmental changes in anatomy and functionality within HF-PHR seems therefore to be a powerful approach to understand the relationship between anatomical and functional features.

In paper III and IV I aimed to investigate the development of interconnectivity between RSC and HF-PHR between P0 and the third postnatal week. Anterograde- (paper 3) and retrograde tracers (paper 4) were injected into RSC. I first asked when RSC is interconnected to HF-PHR. The second aim was to investigate when these connections were organized in adult-like topographies and adult-like densities. Since RSC has a functional overlap between HF-PHR and contains head-direction cells, I hypothesized that RSC–HF-PHR interconnectivity is present and adult-like when the first head-direction cells can be recorded by P11.

Synopsis of methods

Paper 1

A search was performed on publications reporting tract-tracing studies on intrinsic RSC and RSC – HF–PHR connections in PubMed and Embase (see www.temporal-lobe.com for queries and subsequent search strategies). The following inclusion criteria were used: (1) tract-tracing studies or studies which report intracellular filling of single neurons; (2) studies which used healthy, genetically un-altered, untreated adult rats were included; (3) publications written or translated into English or in a language using roman print. The database queries retrieved 816 papers of which 46 contained relevant information. The connectional information was retrieved from these papers, including information from tables and figures, using the following criteria: (1) it was clear where anterogradely filled terminals or retrogradely labeled cell bodies were located; (2) the location of the injection site was clearly described; (3) injection sites did not include multiple brain areas or fiber bundles; (4) only non-lesioned animals were included; (5) explicitly reported non-excitatory projections were excluded; (6) contralateral projections were excluded. The information about these connections was stored in a custom-made relational database (Microsoft Access; Microsoft Corporation, WA, USA). Before data were entered into this database, the accuracy was verified by at least two of the authors. Next, results from independent retrograde and anterograde experiments were combined, such that both the layers of origin and termination could be determined. The connections were added to the existing HF–PHR connectome (van Strien et al., 2009) which was drawn in Visio (Microsoft Corporation, WA, USA) and exported to PDF (Adobe Acrobat Pro; Adobe Systems Inc., CA, USA).

Paper 2

Sprague Dawley rats (n=30) were anesthetized with isoflurane and mounted in a stereotaxic frame. Three different experimental methods were used. First, the anterograde tracer BDA was injected into RSC, in 19 rats. Second, eight of the rats receiving BDA injections also received injections with the retrograde tracer FB in superficial layers of MEC. Third, rAAV-CaMKIIα-ChIEF-mCherry was injected into RSC of 11 rats.

After 9 –21 days of survival, rats injected with BDA and FB were anesthetized and subsequently transcardially perfused with Ringer's solution followed by PFA. Brains only containing BDA injections were horizontally cut with a vibratome at 50 μm. BDA positive axons in layer V of MEC were visualized by tagging BDA with fluorescent markers for visualization in the light microscope or by tagging BDA with an electron dense reaction product for visualization in the EM. Sections processed for light microscopy were used to document the location of the injection, the location of the axonal plexus and guide the dissection of MEC in the tissue processed for EM. In sections processed for EM, MEC was dissected from the section and mounted in epoxy resin. Series of 60-70 nm thick sections were cut and inspected with the use of a transmission electron microscope. Synapse properties in terms of presynaptic

varicosities and postsynaptic targets were determined on the basis of their overall morphology in a series of sections.

Brains containing both BDA and FB tracer injections, were horizontally cut in alternating 100 µm and 400 µm thick sections with a vibratome. The 100 µm thick sections were stained for the presence of BDA and assessed with fluorescence microscopy to verify the location of the injection site and the overlap of BDA positive axons and FB labeled neurons. In adjacent 400 µm sections, randomly selected FB-positive neurons in layer V of MEC were intracellularly injected with a fluorescent dye to visualize the soma and its dendrites. Subsequently, the 400 µm slices were incubated with Alexa-conjugated streptavidin to visualize BDA positive axons originating in RSC. In case of four intracellularly filled MEC layer V neurons, we stained for the presence of postsynaptic and presynaptic markers. The sections were resliced to 50 µm sections, incubated with anti-PSD-95 antibody and anti-synaptophysin antibody, and these antibodies were subsequently tagged with fluorescent markers. All sections were imaged with the use of a confocal microscope to identify putative synaptic contacts between RSC axon terminals and superficially projecting neurons in layer V.

After a survival time of up to six weeks after injections of rAAV, animals were anesthetized and transcardially perfused with ACSF. The brains were quickly dissected, and horizontal slices of RSC and MEC were cut with vibratome. Multiple whole-cell recordings were made with glass micropipettes. Biocytin was included in the pipette for later anatomical verification of cell location and morphology. Up to four neighboring neurons were targeted for whole-cell patch. Recordings were made in current-clamp mode with the membrane potential maintained between 60 and 65 mV. Recorded responses to steps of current injection allowed to electrophysiologically classify each cell. For photostimulation of RSC afferents in layer V of MEC, a beam diameter of ~5 µm was used. Stimuli were arranged in a rectangular 8×6 grid with 20 µm spacing, positioned over the recorded cluster. Voltage deflections were identified as a response at a threshold of 10 SDs beyond the average variation of the membrane potential. The voltage responses obtained from stimulation of each unique location in the grid were averaged and onset times and amplitudes were determined for each location. In several slices, action potentials were blocked by adding tetrodotoxin. After each recording session, the slices were fixated in paraformaldehyde and biocytin filled neurons, mCherry positive axons and neuronal cell bodies were tagged with fluorescent markers. Stained sections were imaged with the use of a confocal microscope.

Paper 3 and 4

82 (paper 3) and 51 (paper 4) Long Evans rats aged between P0 and P28 received multiple injections of anterograde tracers (paper 3) or retrograde tracers (paper 4) in RSC. After a survival time of 18-30 hours, the animals were anesthetized and transcardially perfused and the brains were left in fixative for 24 hours before they were cryoprotected. Brains were cut with a freezing microtome in horizontal sections and the sections were processed to allow for visualization of retrogradely labeled neurons or

anterogradely labeled axons in the fluorescent microscope. All subdivisions within PHR were delineated using cytoarchitectonic characteristics of the different subdivisions. Borders were established in fluorescent sections overlaid with the adjacent nissl-stained section. I carefully described the anterogradely labeled fibers in HF-PHR (paper 3) or the retrogradely labeled neurons in HF-PHR (paper 4) after injections in different parts of RSC and in animals of different ages.

After injections of anterograde tracers (paper 3) I produced flatmaps of PHR and plotted the position of the labeled fibers in a canonical average flatmap. Injections were grouped according to the localization of the injections and/or the age of the animal. Projection patterns within different groups of interest were pooled and the combined flatmaps of the different groups of interest were compared. Additionally I calculated the center of mass of the projection pattern within layer I and III of PrS combined, layer V-VI of PrS and PaS combined and layer V-VI of MEC and LEC combined. These values were used for statistical testing with multiple regression. The average center of mass of different groups of interest were compared.

Synopsis of results

Paper 1

There are strong intrinsic connections in RSC subdivisions. All rostrocaudal levels within both A29c and A30 issue projections to their respective rostrocaudal extents. A29b projections have a strict topography from rostral-to-rostral and from caudal-to-caudal; A29a only has a caudal-to-caudal projection. There are also strong reciprocal connections between RSC subdivisions. All rostrocaudal levels of one subdivision project to all rostrocaudal levels of all other subdivisions, but there are some exceptions: (1) caudal A29a projects only to caudal A29b, A29c, and A30; (2) caudal A29b does not project to rostral A29c; (3) rostral A29c does not project to caudal A30; (4) rostral and midrostrocaudal A30 only projects to caudal A29b and the return projection from A29b only terminates in caudal A30.

The RSC projects to all PHR subdivisions and SUB. Only the projections of RSC to PrS and SUB show a topographical organization such that the rostrocaudal axis of origin in RSC correlates to a dorsoventral terminal distribution in PrS and SUB. The projections to PrS are among the densest of RSC–PHR connections (Jones and Witter, 2007) and this is particularly true for projections from caudal RSC (Shibata, 1994). Areas 30 and 29c receive input from the whole PHR and SUB, while PrS and SUB are the only areas which project to A29b and A29ab. Dorsal CA1 projects only to A29ab and A29c.

Paper 2

All injections in caudal RSC resulted in a densely labeled terminal plexus in layer V of the dorsal and intermediate dorsoventral MEC and layer III and V of dorsal presubiculum. Sparse labeling was observed in layer III of MEC. In series of ultrathin sections of MEC layer V, we observed both presynaptic elements forming synapses with one postsynaptic element, so-called single synaptic boutons

(SSBs) and presynaptic boutons forming multiple synapses, so-called multiple synaptic boutons (MSBs). Boutons (n=262) making asymmetrical or symmetrical synapses (n=301) with dendritic shafts and dendritic spines as post-synaptic targets were observed. The distribution of synapse types and post-synaptic targets is presented in table 1.

No. of boutons	*No. of synapses*	*Asymm. - spine*	*Asymm. - shaft*	*Symm. - spine*	*Symm. - shaft*	*Undet.*
262	*301*	*90%*	*8%*	*1%*	*1%*	*0%*

Table 2. *Distribution of asymmetrical and symmetrical synapses and their postsynaptic targets.*

Of the asymmetrical synapses, 13% (n=34) were of the MSB type. These boutons made synapses with two to four postsynaptic elements. The MSBs contacted either only dendritic spines (n=29) or both dendritic spines and dendritic shafts (n=5). Furthermore, 22% (n=59) of the asymmetrical synapses were of the perforated type, and they contacted dendritic spines (n=56) or dendritic shafts (n=3). In 36% (n=10) of the synapses onto dendritic shafts, these shafts showed additional multiple unlabeled synaptic contacts showing a circular arrangement around the shaft.

The morphological quantification of the majority of RSC synapses in MEC as asymmetrical onto spines indicated the presence of a direct, primarily excitatory input from RSC into spiny neurons in layer V of MEC (Gray, 1959; Eccles, 1964; Uchizono, 1965; Colonnier, 1968). To functionally validate this morphologically based inference, an optogenetic in vitro approach by expressing ChIEF in RSC neurons projecting to layer V of MEC was applied. In MEC, layer V neurons within the plexus were identified, pseudo-randomly selected cells were patched, and main electrophysiological properties were determined. The vast majority of the cells (n=66, 94% of total) was classified as layer V principal excitatory cells. The postsynaptic cells responded with EPSPs after stimulation in a subset of grid locations located over the basal dendrites. We reconstructed and analyzed the axonal trajectories of 22 principal cells after the optogenetic experiments to determine whether neurons post-synaptic to RSC inputs have axons directed for the angular bundle or have axons directed towards the superficial layers. All reconstructed cells had axons projecting toward angular bundle. In a substantial fraction of neurons (n=11), axonal collaterals were present in superficial layers.

Next, we aimed to identify cells in layer V that project to superficial layers II and III in MEC and to assess the overall distribution of RSC inputs onto the dendrites of these cells. In fixed slices containing anterogradely labeled RSC axons, we identified retrogradely labeled superficially projecting layer V neurons and filled pseudo-randomly selected cells intracellularly with fluorescent dye (n=27). Consistent with the earlier studies, the majority of the cells were multidirectional pyramidal cells (n=22), although several horizontal cells were included (n=5). After neuron reconstruction, the proximity of the BDA-positive fibers was mapped onto the rendered dendritic surface. Each individual putative contact

between presynaptic and postsynaptic label was then verified for the presence of a presynaptic bouton. Of these putative presynaptic terminals, 84% (580 of 692) contacted spines, whereas the remaining 16% (112 of 692) terminated on shafts. We performed additional immunostaining of marker proteins for presynaptic terminals (synaptophysin) and for PSDs (PSD-95) and reconstructed 88 previously imaged putative contacts from four neurons. Of these, 68 contacted spines and 20 contacted shafts. In 78% of the putative spine contacts (n=53 of 68) and in 55% of the putative shaft contacts (n=11 of 20), both presynaptic and postsynaptic markers were found, and these contacts could therefore be confirmed as synaptic. Extrapolating these percentages to the entire pool of putative synaptic contacts implies that 88% (452 of 514) of the axon terminals originating in RSC contacted spines, whereas 12% (62 of 514) contacted shafts. From these results, I conclude that RSC provides a major excitatory drive to neurons in layer V. Further, superficially projecting principal neurons in layer V were identified as a main postsynaptic target of RSC inputs. These neurons may relay information from RSC to HF since these layers harbor neurons projecting to HF.

Paper 3

The postnatal RSC projects densely to all layers of PrS and posterior POR and deep layers of PaS and MEC and weakly to deep layers of LEC and to SUB. Our retrograde experiments showed that the origin of these projections were neurons located in superficial parts of layer V of RSC. These projection patterns are in line with those reported for the adult (Wyss and Van Groen, 1992; Insausti et al., 1997; Jones and Witter, 2007; Honda et al., 2011). Additionally, I report that the RSC projections to PrS, PaS and EC in the youngest postnatal rats are organized similarly to adults. First, the rostral RSC projects to dorsal PHR, while caudal RSC projects to additional more ventral parts of PHR. Second, dorsal RSC (A30) projects preferentially to distal PrS, PaS and medial MEC, while more ventral parts of RSC (A29) project significantly more to proximal PrS and more lateral parts of MEC, but not PAS.

During the postnatal period an overall increase in the density of labeled axonal branches in all PHR subregions was observed. Even though I did not perform a formal quantification of the number of labeled fibers in PHR, only single unbranching fibers were observed in animals aged P1-2. During the first postnatal week, the number of axons generally increased, and the fibers displayed several branching points.

Our temporal analysis revealed that RSC axons destined for PHR migrate directly into their area of termination and thereafter keeps their position constant while the number of axonal branches and the total axonal spread increases gradually until they reach adult-like plexus features. This observation is supported by our center of mass analyses of the early perinatal RSC to PHR projections, showing that projections originating in different parts of RSC show a striking terminal topography already during the first postnatal week.

Paper 4

The postnatal SUB, PrS, PaS and MEC project densely to RSC. Additional weak projections arise from LEC, PER and CA1. The distal half of SUB is the main origin of HF-PHR outputs terminating in RSC. HF-PHR projections to RSC in the rat pup are topographically organized along the dorsoventral axis of HF-PHR. Projections from SUB and PrS are organized so that caudal A30 receives projections from the entire dorsoventral SUB and PrS, while rostral A30 and the whole rostrocaudal extend of A29 receive afferents from neurons in dorsal SUB and dorsal PrS, partly similar to what has been reported in adults (van Groen and Wyss, 1990c, 1992, 2003; Aggleton et al., 2012).

We further report that the projections originating in SUB, PrS and PaS are topographically organized along the transverse plane of HF-PHR. Distal SUB projects to dorsal RSC (A30), while more proximal parts of SUB project to ventral RSC (A29). Distal PrS and whole PaS preferentially project to A30 while more proximal PrS (but not PaS) preferentially projects to A29. The sparse projection from EC to RSC are organized so rostral parts and the whole rostrocaudal extend of A29 receive projections from dorsolateral EC, while caudal A30 receives projections from the intermediate dorsolateral-ventromedial EC. To our knowledge these topographical organizations have not been reported in earlier work.

The retrogradely labeled neurons in PrS, PaS and EC were located in superficial layer V. Our anterograde injections in SUB and PrS suggest that these neurons issue axons mainly to layer I and IV of RSC while a few fibers are present in layer V-VI.

Our temporal analysis shows that all of the individual HF-PHR projections to caudal RSC are present at P1. Even though we did not perform a formal quantification of the number of retrogradely labeled neurons in HF-PHR, it was obvious that in the youngest animals only a few retrogradely labeled neurons were present in HF-PHR. During the first postnatal week, the number of retrogradely labeled neurons increased reaching adult-like densities between P5 and P10. Since we were not able to show retrogradely labeled neurons in HF-PHR in animals younger than P3 with injections in rostral RSC, we suggest that the projections to rostral RSC seems to develop a few days later than the projections to caudal RSC. We therefore conclude that HF-PHR projections to RSC are present very early during postnatal development and that these early projections are topographically organized already when the first axons arrive in RSC.

General discussion

RSC plays a role in spatial cognition and episodic memory formation. Functionally, it shows a striking overlap with the attributes of HF–PHR, suggesting a relationship between the areas. In this thesis, I explored the connections between RSC and HF-PHR and how the information carried by these connections may interact with the various components of the local HF-PHR network. I first reviewed the anatomical framework of how functional interactions between RSC and HF-PHR can occur (paper 1). One of the most dominant pathways, are the dense RSC projections to layer V of the medial entorhinal cortex (MEC). In the first experimental paper, I explored the synaptic organization and the postsynaptic targets of RSC to MEC connections and revealed that RSC afferents in MEC mainly target principal neurons in layer V with excitatory synapses (paper 2). Among the postsynaptic layer V neurons we identified a population of superficially projecting neurons, thereby providing a route for information provided by RSC to reach the superficial layers of MEC, thus likely influencing the neurons providing the main input to HF (Segal and Landis, 1974). Next, I used a developmental approach and revealed that projections from RSC to HF-PHR, throughout development are organized similar to what has been reported in adults (Jones et al., 2005). Already from the earliest postnatal ages specific parts of RSC subdivisions are connected with specific parts of HF-PHR subregions (paper 3 and 4). A29 is preferentially connected to more proximal parts of the distal half of SUB, proximal PrS, and lateral parts of MEC, while A30 is preferentially connected to the most distal part of SUB, distal PrS and medial parts of MEC.

Taken together, the experimental data reported in this thesis show that different parts of RSC are connected to different parts of the HF-PHR circuitry. These results suggest that RSC and HF-PHR interact through several parallel processing pathways. Since different parts of HF-PHR process qualitatively different information, likely mediating different functions (Kerr et al., 2007; Knierim et al., 2014), these findings suggest that also RSC is heterogeneous with respect to information processing, which is in line with previously reported functional heterogeneity in RSC (Vann et al., 2009). Our developmental experiments revealed that RSC axons migrate directly into their area of termination and thereafter keep their position constant while the number of axonal branches increases gradually until they reach adult-like plexus features. In the adult, the projection to MEC terminates partly on a population of principal neurons which project to superficial layers of MEC. These neurons may relay information from RSC to HF since the superficial layers of MEC harbor neurons projecting to HF. The experience independent topographic organization of RSC – HF-PHR interconnections suggests that RSC and HF-PHR are parts of one tightly coupled system and that RSC – HF-PHR interaction is necessary for proper functioning of the two regions.

Methodological considerations

Tract tracing

The data presented in all papers in this thesis involve the use of various tract tracing techniques. For anterograde tracings I mostly used 10 kDa dextran amine (DA) which was either biotinylated (BDA) or conjugated with an Alexa fluorochrome. These tracers were chosen since DA is reliably taken up by dendrites and neuronal cell bodies within the injection site, eventually homogeneously filling the axonal processes (Veenman et al., 1992). Therefore the biotinylated version of the molecule (together with *Phaseolus vulgaris leucoagglutinin*, PHA-L) has for a long time been regarded as gold standard for anterograde neuroanatomical tracing.

Even though DA is regarded as reliable anterograde tracers, there are some consideration with the use of this class of tracers. First, it is not known whether they have any preference for certain types of neurons, pathways or brain areas; it is assumed that all neurons within the injection site take up and transport the tracer. However, the mechanisms of uptake are not yet exactly known (Lanciego and Wouterlood, 2011). Even though the tracer efficacy is considered to be not depending on its neuronal targets, there is a theoretical possibility that the axonal projections observed by the use of DA represents only a part of the population of projecting neurons. For instance, small differences between two commonly used anterograde tracers, PHA-L and BDA have been reported, which suggest that not all classical anterograde tracers have similar mechanisms of uptake and transport, and might therefore display different features of a neuronal pathway under investigation (Dolleman-Van der Weel et al., 1994). Another example of tracers with heterogeneous transport mechanisms are the recently developed viral tracers, which have revealed several anatomical pathways which has not been reported or underappreciated in experiments using classical tract tracers (Rowland et al., 2013; Rajasethupathy et al., 2015). These results exemplifies that different groups of tracers have different affinities for certain neural pathways.

Second, the distance DA is transported is related to the survival time of the animal after injection. Transportation speed has been estimated to be 15–20 mm per week (Lanciego and Wouterlood, 2011). In paper 2, I used survival times of more than ten days, which were more than enough for transport to MEC at a distance of about ~5 mm. However, in the developmental experiments, I used survival times of 24 hours to obtain the necessary temporal resolution of my experiments. It could be argued that such short survival times do not allow for visualization of the most distant projections, for example to the most ventral part of PHR. However, in earlier publications from our lab, short survival times have successfully been used to trace developing projections (O'Reilly et al., 2013; O'Reilly et al., 2014). In addition, labeled axons were observed in the brainstem, which is further away from RSC compared to PHR. I therefore regard 24 hours survival time in young postnatal animals as sufficient to label axons throughout HF-PHR.

Third, retrograde transport of DA may occur (Veenman et al., 1992; Wang et al., 2014). Some retrogradely labeled neurons in anterior nuclei of the thalamus and in SUB were observed in some of the experiments. This could potentially be an issue since the retrogradely labeled neurons could result in "false" anterograde labeling of axon collaterals belonging to these retrogradely labeled neurons (Chen and Aston-Jones, 1998). Therefore, it cannot be ruled out that DA is transported anterogradely from retrograde labeled neurons in SUB, labeling axon collaterals terminating in the PrS and MEC, thus biasing the results. However, I find this very unlikely as the number of retrogradely filled neurons in SUB was very low, I never observed BDA filled axons leaving SUB towards the PHR and SUB neurons seldom have divergent extrinsic axon collaterals, implying that retrogradely labeled cells, therefore projecting to RSC, do not likely project to PrS or MEC as well (Naber and Witter, 1998).

Using flatmaps to analyze organization of anatomical connections

In paper 3 I decided to use flatmaps of RSC and PHR to obtain comparable measures of injection sites and location of labeled fibers in all experiments. This is an efficient and schematic way of visually representing large amount of anatomical data. In addition, the flatmaps allow for comparisons between groups of experiments, for example between animals of different ages.

However there are several methodological issues with the use of flatmaps. In our procedure I averaged each brain into one "average brain" and represented the projection patterns within this average brain. However, care should be taken since averaging could mask unknown differences across groups of rats. For instance, I noticed that the EC in young animals was positioned relatively more dorsally in the brain compared to PrS and PaS, while in older animals the relative position of EC was more ventral. In fig 3, I plotted the relative location of the border between MEC and LEC in the transverse plane (y-axis) as a function of age (x-axis) and the different dorsoventral levels in the brain (the different panels). The figure illustrates that in younger animals the dorsal pole of MEC, the dorsal pole of LEC and the ventral pole of MEC appears relatively more dorsally in the brain compared to older animals. Therefore, EC seems to "move" to a more ventral position relative to PrS and PaS, resulting in young animals having a dorsal border of EC positioned more dorsally compared to PrS, while in older animals the dorsal border of EC was positioned more ventrally (Fig 3). These differences likely reflect developmental growth patterns since similar growth patterns have been observed also for the ventral HF which shifts its position ventrally in the brain during postnatal development (O'Reilly et al., 2014). If the dorsoventral positions of each subregion had been normalized to the total dorsoventral extend of PHR, I would most probably see a relationship for older animals to have labeled fibers located more ventrally than in younger animals. Such a result would be biased since the labeled fibers in reality are located at the same absolute position within EC. To avoid such biases I decided to normalize each subregion separately, assuming that the shape and composition of *each subregion* is constant throughout development. To produce flatmaps I assumed that the PHR subregions (and RSC) were similarly organized in animals of different ages and therefore averaged each of these areas.

Second, in the algorithm to produce flatmaps, I used straight lines between defined cytoarchitectonic borders to measure the sizes of the different brain regions. This is obviously an approximation since most brain regions are to some extent curved. With our approach, the extent of curved structures will be underestimated. However, in horizontal sections this effect is minimal for PrS, PaS and MEC since these areas are relatively straight in the transverse plane. However, in horizontal sections, LEC is generally more curved. A possible risk might be that structures located laterally in EC might be positioned more lateral than calculated by our approach. However, I did not observe a substantial amount of labeled fibers in LEC and such a bias is thus minimally relevant in our dataset.

Third, to measure the location of labeled fibers in PHR two different approaches were used. In animals with a few labeled fibers, the position of each labeled fiber was measured, while in animals with a dense plexus, I chose to measure the outlines by marking the borders of each plexus. In addition, I set the density of each fiber plexus on a scale ranging from 1 to 3. Such an approach is based on several subjective evaluations. First, plexus densities are continuous gradients and binning the densities of these plexuses can be challenging. Second, the borders of plexuses are never absolute, often displaying gradients from the densest core of a plexus to areas containing fewer fibers at the periphery of the plexus. One might argue that the two approaches used to register data for the flatmaps cannot be directly compared. With respect to the production of flatmaps, such an argument is to some extend true such that experiments with more labeled bins will be overrepresented in the flatmaps. A better approach would be to implement quantitative estimations of the number of fibers in each area of the plexus. Or even better, to implement a synaptic stain and quantify the number of pixels containing both synaptic stains and fluorescent tracer and use these numbers to calculate a 2D flatmap of the projections (Wouterlood et al., 2008). Due to time constrains, a far simpler and less sophisticated method to quantify the location of the labeled fibers was used; to calculate the centers of mass of each plexus. The centers of mass represent point measures of the location of the labeled fibers in each structure and were independent of the method used to register each plexus.

To convert histological data into flatmaps is a simplification, which can never represent the full information present in histological sections. However the use of flatmaps has several advantages that make up for the simplification (Van Essen and Maunsell, 1980; Van Essen, 2013). By calculating an average flatmap across all ages, each experiment was morphed into one canonical representation of PHR. This procedure allowed for quantification of the projection patterns by calculating the centers of mass. The flatmaps were an important tool to statistically evaluate potential differences between the distributions of connectivity. Even though the use of flatmaps of both the injection sites and PHR involves many steps of transformations and calculations which potentially can mask details present in the data, I feel confident that the analytical possibilities by using flatmaps outweigh possible biases introduced. I therefore find the flatmaps an important tool to efficiently compare and pool large amounts of data.

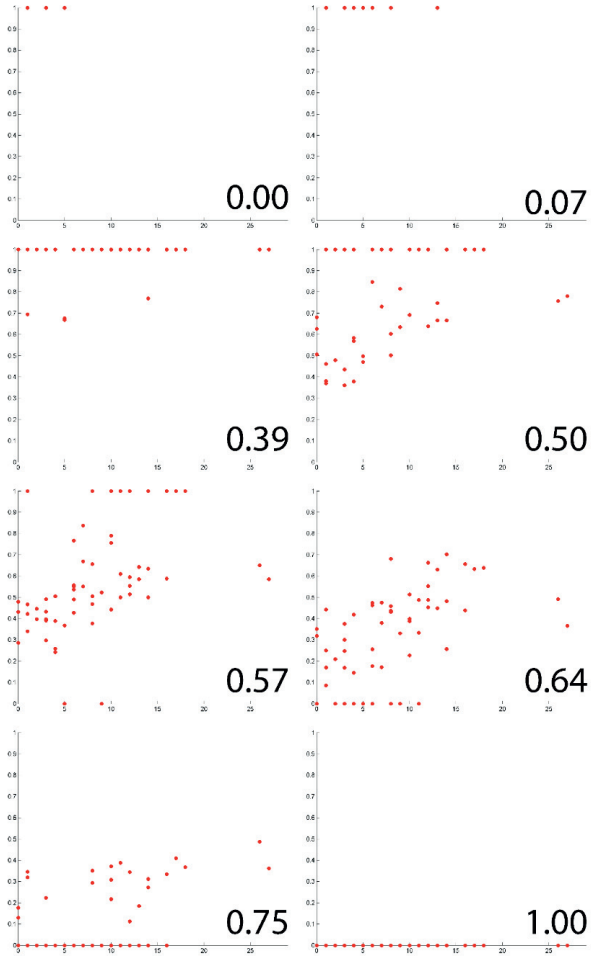

Fig 3. Temporal development of EC

Each of the eight plots represents a dorsoventral level of the brain. The dorsoventral position is normalized to the total dorsoventral extend of the entire PHR and is denoted in the bottom right of each plot. Each dot represents a section from one brain (at the dorsoventral position denoted in the bottom right), and is plotted as a function of age (x-axis) and the ratio between the mediolateral extend of MEC divided by the mediolateral extend of the entire EC ($\frac{MEC}{MEC+LEC}$). The y-axis therefore represents sections containing only MEC (1), sections containing MEC and LEC (between 0 and 1) and sections only containing LEC (0). In dorsal sections only young animals have a MEC in their sections (0.00 and 0.07). At intermediate dorsoventral levels all animals have sections containing a MEC while young animals also have a LEC (0.39, 0.50 and 0.57). In more ventral sections young animals display only LEC while older animals have sections comprising both MEC and LEC (0.57, 0.64 and 0.75). At the most ventral sections all animals have sections containing only LEC (1.00).

Database of published interconnections within and between HF, PHR and RSC

In paper 1, we present all published tract tracing experiments where connections within or between HF, PHR and/or RSC are reported. In our connectional database, we aimed to describe origin and termination patterns of projections with a relatively high spatial resolution. There are several methodological consideration with respect to sampling of the data and the data model of the database which is discussed in paper 1. Of these, two are worth being highlighted. First, the data model of the database limits the data which can be entered into the database. On the one hand, precise descriptions of connections which are beyond the resolution of the data model may be lost when entered into the database. On the other hand, data which are described in general terms cannot be entered to the database since again the data model does not fit the data. Second, tract tracing experiments usually do not differentiate between excitatory, inhibitory or modulatory connections, nor do they objectively characterize the strength of the connection or the postsynaptic target of the connections. Such information is pivotal for understanding the mechanisms of network functions and care should be taken if hypotheses on neural circuitry are based on data from the database. For instance projections from CA1 to RSC have been reported (Meibach and Siegel, 1977; van Groen and Wyss, 1990d, c; Naber and Witter, 1998; van Groen and Wyss, 2003; paper 4), however this projection differs from the SUB projection to RSC in several ways. First, the CA1 projection is very sparse while the SUB projection is dense. Second, the CA1 projection originates mainly from non-pyramidal cells while the SUB projection originates from pyramidal cells (Miyashita and Rockland, 2007). In George *et al* (2014) information from the database is used to argue that pyramidal cells in CA1 project to RSC. Such a statement is obviously questionable if data from the original references had been presented and the example clearly exemplifies that the database should be used as a library of reported connectivity and not be used uncritically as a ground truth of existing connections. In a recent publication, data on connectivity within the PHR are presented (Agster and Burwell, 2013). In this manuscript the authors use the database to detect knowledge gaps and thereby design their experiments. In addition, they use the database to identify reports of connectivity within the region but clearly state discrepancies in the different reports and possible confounders in the original manuscripts.

In papers 3 and 4, the connections between HF-PHR and RSC as observed in the developing rat brain were described. I did not observe several of the adult connections which are represented in the database. For example, connections between RSC to PER have been reported in the literature, but were not observed by us. There are several possible reasons for this. First, an obvious possibility could be that there are differences between postnatal, adolescent, and adult rats. However, I find this possibility unlikely since I observed adult-like projections and topographies for several other connections. Second, our database does not differentiate between strong and dense connections and our anterograde injections may not have the sensitivity to pick up very sparse projections from a confined part of RSC. For example, the RSC to PER projections are in the original paper reported as *"Area 36 receives relatively*

little input from the cingulate cortex […]. These meager cingulate projections arise from the dorsal […] retrosplenial cortex" (Burwell and Amaral, 1998). This exemplifies that even though a connection is present in the database, it does not imply equal importance or equal density compared with other connections. In this example, a very sparse projection from RSC might not have been picked up by our injections in the postnatal brain. Finally, there could possibly be technical/experimental reasons for why some projections are observed in one set of experiments, but not in others. For instance a prominent projection from RSC to SUB has been reported in some studies (Shibata, 1994) but was neither seen in our experiments nor in other studies in both the adult rat and monkey (Jones and Witter, 2007; Kobayashi and Amaral, 2007). In all reports where dense RSC to SUB projections have been mentioned coronal sections were used. In coronal sections, the exact border between PrS and distal SUB is in most sections extremely difficult to identify. Therefore the putative SUB fibers observed could possibly be proximal PrS fibers mistaken to be distal SUB fibers.

Our database is obviously not exhaustive and hence one could argue that the database is not a real connectome. Full connectomes exist for instance for *C. Elegans* and for the local connectivity of 950 neurons in the inner plexiform layer of the mouse retina (White et al., 1986; Helmstaedter et al., 2013). Even though efforts are made to sample the full connectome of the mouse brain, a complete connectome of a higher developed brain is still beyond the horizon (Mikula and Denk, 2015). Although the database presented in paper 1 is obviously not a complete connectome, it still provides an approximation of a complete and unbiased connectional database of HF-PHR at a subregional level. Additionally the spatial resolution of our database provides a potential for further meta-analysis, such as a graph analysis of the organization of HF-PHR inter-connections (Binicewicz et al., 2015). These analysis revealed that compared to other brain areas, HF-PHR connectivity has several clusters of interconnected subregions. These clusters were organized along the dorsoventral extend of HF-PHR, which fits the observed functional differences along the dorsoventral axis of HF-PHR (Moser et al., 1995). Across the transverse axis of HF-PHR three main modules exist, one comprising HF and two comprising PHR. The PHR modules consist of one module comprising PrS, PaS and MEC and parts of LEC and another module comprising PER, POR, LEC and parts of MEC. These findings are interesting for several reasons. First they confirm that HF is a separate network from PHR and that PrS, PaS and MEC form a functional module concurrent with *in vivo* recordings (Boccara et al., 2010). Second, the authors question whether PER and POR are strictly segregated into two information processing streams and suggest that integration of the two pathways also occur at the level of PER and POR. Finally, the graph analysis suggests that MEC and LEC are involved in both of PHR modules and point to EC as a central hub within HF-PHR integrating information from all of the three modules. This example proves that the database is not only a useful library, but can also be used to reveal patterns of connectivity within already published data. It would thus be interesting to add the RSC-HF-PHR connections which are already incorporated in the database (Sugar et al., 2011) to carry out comparable connectional analyses.

Two routes for RSC to reach HF

The overlapping functional attributes of HF and RSC have been noted in a number of publications. First the human RSC and HF are both simultaneously activated during several behavioral tasks (Iaria et al., 2007). Further, episodic memory, classically attributed to HF, can also be mediated by RSC (Cowansage et al., 2014). Additionally, *in vivo* recordings in rats have revealed that spatially modulated neurons are present in both RSC and HF-PHR (O'Keefe and Dostrovsky, 1971; Taube et al., 1990; Cho and Sharp, 2001; Smith et al., 2012) and that inactivation of RSC leads to place-cell remapping in HF (Cooper and Mizumori, 2001). These HF-RSC interactions are likely mediated partly by the dense projections from SUB to RSC. However, reciprocal projections from RSC to HF do not exist, suggesting that alternative pathways must exist for RSC to communicate with HF. In paper 2, this issue was addressed by examining the possibility that RSC inputs to HF are mediated through the neurons in deep layers of MEC to HF-projecting neurons in layer II/III of MEC. Anterograde transport of BDA and ChR-expressing rAAV was used to identify axons and terminals in layer V of MEC originating in RSC. Our assessments revealed that a majority of the presynaptic elements was excitatory and that the postsynaptic targets were spiny principal neurons. The latter comprise neurons with at least two different projection patterns, one that projects both superficially and extrinsically to a number of cortical and subcortical areas, and one that projects extrinsically with only local collaterals in layer V (Insausti et al., 1997; Quilichini et al., 2010; Canto and Witter, 2012a). The data presented in paper 2 lead us to conclude that both types of layer V pyramidal neurons receive excitatory RSC input. EC layer II and III harbor neurons projecting directly to HF, which possibly could be among the postsynaptic targets of the RSC-targeted layer V neurons. We thus propose that the superficially projecting layer V neurons in MEC mediate one of two pathways by which RSC information can reach superficial layers of MEC and thereby indirectly reach the HF.

The other indirect route for RSC to reach MEC and HF is through PrS, the latter receiving a projection from RSC as dense as that to MEC (Jones and Witter, 2007). A recent study examining RSC to PrS to MEC projections concluded that more than half of the synapses target proximal shafts of dendrites of sparsely spiny neurons in PrS layer III, which project to MEC (Kononenko and Witter, 2012). A small fraction of RSC fibers contact non-spiny MEC-projection neurons, and these likely represent the GABAergic neurons projecting to MEC (van Haeften et al., 1997). Both anatomical and electrophysiological studies have shown that the PrS to MEC projection terminates on principal neurons in layers II, III and V, exerting excitatory effects (van Haeften et al., 1997; Wouterlood et al., 2004; Canto et al., 2012). Thus, the parallel projections 'RSC to MEC layer V to MEC layer II/III' and 'RSC to PrS layer III to MEC layer II, III, V "converge" in LII/III and in LV of MEC, possibly targeting HF projecting neurons in these layers (Deller et al., 1996). These pathways are of interest for two reasons. First, they are potential pathways for RSC to reach HF and thereby mediate the overlapping functionality between HF and RSC. Second, these pathways may also modulate the firing properties of neurons within

MEC. Neurons in PrS and in layer III-VI of MEC show remarkably similar spatial properties in vivo (Sargolini et al., 2006; Boccara et al., 2010). This has initiated a debate on whether such properties might be inherited from one structure to the next within PHR, or whether this may indicate a common input that provides both PrS and MEC with the required information to generate these firing properties independently from each other (Boccara et al., 2010; Giocomo and Moser, 2011; Tocker et al., 2015). One such common input might be SUB, which projects to both layer V of MEC and PrS (Cappaert et al., 2015) and contain spatially modulated neurons (Sharp and Green, 1994). Another plausible candidate, as emerging from my studies, is RSC which has prominent projections to both PrS and layer V of MEC. To reveal whether RSC is important for the spatially modulated cells in MEC, inactivation of RSC in behaving animals, while recording neuronal responses of PHR neurons should be performed.

Principal neurons in layer V of EC are the integrating unit of entorhinal cortex

In the 'traditional representation' of the functional organization of MEC, layer V neurons are considered as the output neurons, while neurons in layers II and III are the recipients of information, which is forwarded to the HF (Fig 2A). In that perspective, the projections from RSC to layer V are particularly intriguing. Above, it was argued that these layer V neurons could forward RSC information to superficial layers, acting as an input pathway to HF. However, the principal neurons in layer V of MEC possess key anatomical and physiological features to act as a local integrator of inputs to EC. Neurons in layer V possess dendrites spanning all layers of EC. In contrast, principal neurons in layers II, III and VI possess dendrites which are restricted to respectively superficial layers and layer VI. Principal neurons in layer V are therefore the only principal neurons in EC with the potential to receive inputs terminating in all EC layers. With respect to dendritic morphology, three main types of principal neurons exist in layer V of MEC. First, the pyramidal cells, which come in two subtypes. Large pyramidal neurons occupy the most superficial part of layer V directly underneath lamina dissecans (Hamam et al., 2000; Canto and Witter, 2012a). They possess an apical dendrite reaching the pia and have a dendritic tuft in layers I and II. They also have a set of basal dendrites which extends in all directions in layer V. Most of these neurons have an axon directed for the angular bundle and/or superficial layers of EC (Lingenhohl and Finch, 1991; Canto and Witter, 2012a). Small pyramidal cells are located deeper in layer V and are morphologically similar to the large pyramids except that their basal dendrites extend into deeper parts of layer V and into layer VI. These neurons have been reported to only have local axonal harbors which do not leave MEC (Lingenhohl and Finch, 1991). In the mouse, pyramidal cells in layer V have been subdivided in two groups based on molecular markers. Etv1 is expressed in large, superficially located pyramidals, close to the lamina dissecans, while Ctip2 is expressed in smaller pyramidals deeper in layer V (Surmeli et al., 2015). Interestingly, Ctip2 and Etv1 positive neurons have different connectional schemes. The former receive input from layer II stellate cells and do not project to other brain regions. Conversely, the latter do not receive input from layer II stellate cells and project to extra hippocampal brain regions. Based on the anatomical distribution of these markers, the

morphology of the somata of the positive cells and the axonal arborization of neurons within each of these populations, these markers probably label similar population of neurons in the mouse as the large and small neurons observed in respectively superficial and deep layer V in the rat.

A second group of principal cells is formed by neurons having an apical dendrite similar to the pyramidal cells and basal dendrites which extend in the laminar plane. Third, polymorphic multipolar neurons and horizontal neurons do not have an apical dendrite. However, their dendrites cover long distances in the laminar plane of layers V and VI and even reach areas outside of MEC, such as SUB. The pyramidal neurons thus have the morphology to receive inputs terminating in all layers, while the polymorph and horizontal cells seem to be uniquely positioned to integrate information that targets different parts of layer V.

Layer V neurons receive inputs from axons within layers I–III (Medinilla et al., 2013), including those from the parasubiculum and presubiculum (Canto and Witter, 2012a). Moreover, layer V principal neurons receive hippocampal output, arising from CA1 and the subiculum (van Haeften et al., 1995). The latter input has been shown to converge onto single EC layer V neurons with inputs from RSC (Simonsen et al., 2012). The notion that both HF and RSC projections converge on layer V neurons is of interest in view of the overlapping functional attributes of both HF and RSC as argued above. Therefore, a possibility that has not yet been explored is whether the common phenotype seen after lesions of HF and RSC respectively are not caused by the removal of the HF and RSC *per se* but are caused by the loss of inputs to layer V of MEC. A possible way to test this alternative hypothesis is to have optogenetic or pharmacogenetic access to populations of neurons in layer V. If achieved, the phenotype seen after inactivation of layer V could be compared to the phenotype seen after inactivating or lesioning HF or RSC. Pharmacogenetic or optogenetic access to layer V neurons can be achieved in several ways. For instance by injection of viral vectors such as AAV directly into layer V, injection of a retrogradely transported rabies virus into any of the areas receiving projections from layer V of EC or by using a transgenic animal specific for populations of layer V neurons, similar to approaches used in case of layer II or layer III or MEC (Suh et al., 2011; Rowland et al., 2013). Alternatively, a more specific experiment would be to only target the projections to layer V originating in RSC and/or HF. This could be done by transfecting SUB and RSC neurons with an optogenetic silencer such as halorhodopsin, and simultaneously implanting a laser in deep layers of MEC. If both these layer V inputs are equally important for memory encoding, irrespective of their origin, the same phenotype should be seen if axon terminals in layer V originating in RSC and HF are inhibited. If the resulting similar phenotype is also similar to that reported as the result of lesions in RSC and HF, neurons in layer V of MEC are clearly implicated as the common/shared mediator of these shared functionalities.

Topographies in HF-PHR – RSC interconnections

In paper 1, I review data indicating that RSC connects to all subdivisions of PHR and SUB, and in papers 3 and 4, I further describe the topographies of these projections in pups and adults, concluding that two main organizational patterns, seen in the adult brain, are present already in the early postnatal period of brain development. First, different rostrocaudal levels of RSC are connected with different dorsoventral levels of HF-PHR. Rostral RSC projects to more dorsal parts of PHR, while caudal RSC projects to more ventral parts of PHR. This finding is in line with earlier published work in the adult (Wyss and Van Groen, 1992; Shibata, 1994; Jones and Witter, 2007). The projections originating in HF-PHR and terminating in RSC are comparably organized such that caudodorsal RSC receives projections from the entire dorsoventral SUB, PrS, and intermediate dorsolateral-ventromedial EC, while rostral and ventral RSC receive afferents only from neurons in dorsal SUB, PrS, PaS, and dorsolateral EC. Such an organization is partly similar to what has been reported for adult SUB/PrS to RSC projections (van Groen and Wyss, 1990b; Wyss and Van Groen, 1992; van Groen and Wyss, 2003).

Second, I found that different dorsoventral levels of RSC are connected with different transverse levels of HF-PHR. Dorsal RSC projects to distal PrS, PaS and medial MEC, while ventral RSC projects to proximal PrS and lateral MEC. The SUB, PrS and PaS projections to RSC are similarly organized. Distal SUB and distal PrS and PaS project to dorsal RSC, while more proximal parts of SUB and proximal PrS project to ventral RSC. The EC projection to RSC seems to not share a directly comparable organization since dorsolateral MEC projects to rostral A30 and the full rostrocaudal extend of A29 while more ventromedial parts project to caudal A30.

These topographies have not been reported in earlier work in rodents, however Jones and Witter (2007) summarize in fig. 13 the projections from RSC to PHR and report that A29 projects weakly to LEC while A30 only projects to MEC. This finding is probably an effect of the same wiring-patterns reported in paper 3. Hints of the existence of a similar topography have also been presented, although not explicitly mentioned in the monkey. In fig. 6 in a paper by Kobayashi and Amaral (2007), two cases of anterograde injections into RSC are reported. One injection located in rostral A29 displays anterograde labeling in layers I and III of proximal PrS and layers V-VI of lateral parts of EC. The other injection, located in caudal A30 displays anterograde labeling in layers I, III and V-VI of distal PrS and layers V-VI of medial parts EC. Based on two injections it is not possible to differentiate whether the observed projections are a result of the different rostrocaudal or dorsoventral positions of the injections. However, the sparse description of these cases suggest that the topography observed in the rat is also present in the monkey.

One could speculate why several of the topographies I have reported have not been reported in earlier publications. Methodological issues are one possible reason. First of all most authors have subdivided RSC into A29ab, A29c and A30 based on cytoarchitectonic features and analyzed the connection

patterns of these areas individually without a focus on inter-areal differences. In most of the papers the topography within each of these areas, i.e. along the rostrocaudal axis of RSC has been emphasized. Potential differences across the dorsoventral axis might have been depreciated because each area has been analyzed separately and since the dorsoventral extend of each subarea is too small for an evaluation of topographies across this axis. Second, caudal RSC is curved both in the dorsoventral and mediolateral plane. In many of the publications it is not clear whether the dorsoventral axis of RSC relates to the dorsoventral axis of the brain or is defined as perpendicular to the rostrocaudal axis of RSC as in our analyses. Third, an objective evaluation of the dorsoventral level of an injection is challenging, which is alleviated by the use of a 3D-atlas or 3D-reconstruction to define the location of each injection site (Boccara et al., 2015). The use of flatmaps of RSC is also a powerful tool to calculate the relative positions of injections and probably increased the sensitivity of the analysis. A fourth reason for why the topographies have not been reported could be that coronal sections have been used in most of the previous studies. To evaluate the transverse termination pattern in PrS, PaS and EC in coronal sections is, again, a challenging task. First of all, the plexus in deep layers of EC will only appear in one or two coronal sections depending on section thickness and the number of series examined for tracer transport. Additionally, the plexus appearance in the most caudal coronal sections is to a large extend dependent on the cutting angle. If the cutting plane varies with only a few degrees between animals, the position of the plexus relative to the section borders will be variable across animals. Therefore, the evaluation of mediolateral termination pattern in EC has to depend purely on evaluation of cytoarchitectonic features. In such cases the comparisons of the specific mediolateral distribution of projections across animals is an extremely difficult exercise. In our experiments, horizontal sections were used. Since the labeled structures and HF-PHR are mostly cut perpendicular to their long axis, our structure of interest is visible in multiple sections and the transverse position of the plexus is therefore easier to evaluate.

All together, our investigations of topographical patterns of HF-PHR – RSC interconnections reveal a clear pattern. A30 is preferentially connected to distal SUB, distal PrS, PaS and medial MEC, while A29 is connected preferentially more proximal SUB, proximal PrS and more lateral parts of MEC, but not to PaS. These connectional schemes are interesting in view of reported functional differentiation of non-spatial and spatial information streams within HF-PHR and the different wiring patterns, which exist within HF-PHR. The PrS to MEC projection is topographically organized such that distal PrS projects to medial MEC, while proximal PrS projects to more lateral parts of MEC (Fig 4; Shipley, 1975; Caballero-Bleda and Witter, 1994; Honda and Ishizuka, 2004). Furthermore, these partner domains in PrS and MEC are selectively innervated by different areas of SUB along its transverse axis such that distal SUB projects to distal PrS and medial MEC, while more proximal parts of SUB, with the exclusion of the very proximal part, project to proximal PrS and more lateral MEC (Fig 4; Witter, 2006; O'Reilly et al., 2013). Regarding the EC to RSC projection, we related our observations to the known organization of HF-EC interconnections which show a marked dorsolateral to ventromedial organization. In general,

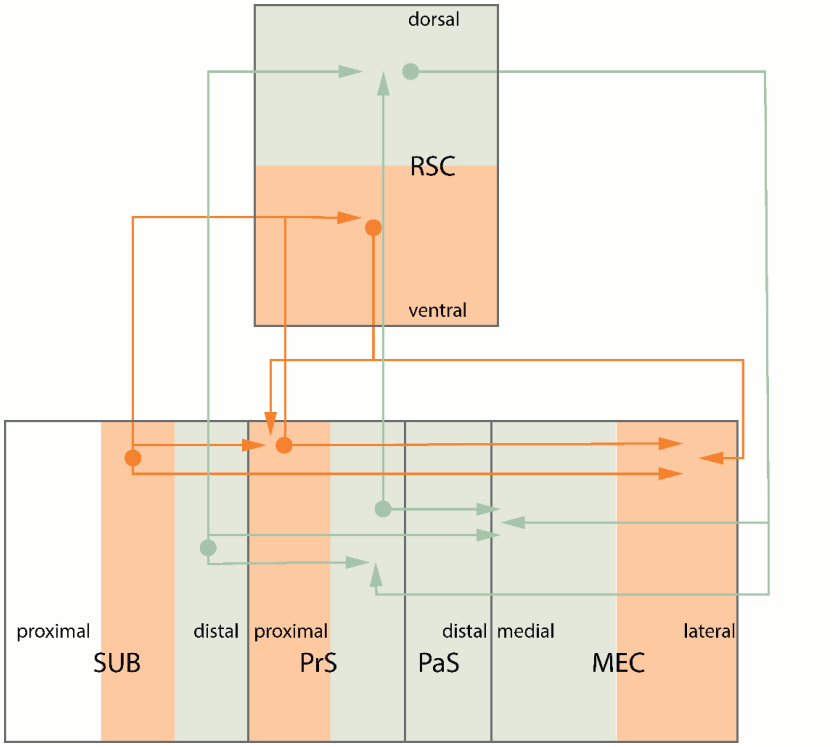

Figure 4. Schematic representation of connections between RSC and HF-PHR and within HF-PHR.

Dorsal RSC, distal SUB, distal PrS, PAS and medial MEC are preferentially connected, while ventral RSC, more proximal parts of SUB, proximal PrS and more lateral parts of MEC are preferentially connected. For illustrative purposes each subarea has been colorcoded in discrete colors even though the topographies are continuous gradients.

neurons with a dorsolateral position in EC project to rostral and ventral parts of RSC, while neurons located more ventromedially in EC project to more caudal and dorsal RSC. These observations thus indicate the existence of a connectional route linking A30, medial MEC, distal SUB and distal PrS to each other and a parallel route linking A29 with more lateral MEC, more proximal SUB and proximal PrS. Although no clear transverse gradients in spatial modulation have been reported in MEC, electrophysiological properties of neurons show a transverse gradient, which has been suggested to relate to the levels of spatial tuning (Burgess et al., 2007; Canto and Witter, 2012a, b). Furthermore, neurons in distal SUB are more spatially modulated compared to those in proximal SUB (Sharp and Green, 1994). All observations thus point to a differentiation of A29 and A30 where A30 is connected preferentially to more spatially modulated neurons in medial MEC and distal SUB.

Development of topographies

In papers 3 and 4 I explored the development of projections between HF-PHR and RSC and showed that these projections are topographically organized already when the first axons arrive in their target

regions. These findings imply that the final position of the RSC – HF-PHR axons are determined before the axons arrive at their final destination. In early developmental experiments, Sperry and colleagues investigated behavioral- and anatomical features in the newt, fish and tadpoles after a series of manipulations of the retinotectal projections. By rotating and/or mirroring retinas, Sperry revealed that regenerating axons grew into the originally correct area of the tectum even though retinal neurons were located in new positions (Sperry, 1943, 1945; Attardi and Sperry, 1963). Thereby the visual scene representation in the tectum was reflected and/or rotated. These experiments led to the conclusion that the spatial organization of regenerating axons in the tectum was highly predetermined and experience independent. Similar conclusions have been reported for developing axons in mammals. For instance, thalamocortical projections in the visual system of both monkeys, cats and ferrets are topographically organized very early during development. Already when the first axons arrive in visual cortex, the projections seems to be topographically organized in ocular dominance columns (Horton and Hocking, 1996; Crowley and Katz, 2000; Crair et al., 2001). Comparable results also exist in the rodent for thalamic projections to somatosensory cortex (Catalano et al., 1996) and for inputs from the nasal epithelium to the olfactory bulb (Lin et al., 2000). These topographically organized projections, present long before neurons encode a receptive field are also independent of activity in sensory receptors, suggesting that the development of topographies in mammals are experience independent.

Whether the strict topographical organization of the first axons is a general phenomenon in the CNS, is a matter of some controversy since in several brain systems projections have been reported to initially be diffuse and later prune into an adult-like topography. This has for instance been observed in the retinogeniculate connections in several species (Rakic, 1976; Linden et al., 1981; Shatz, 1983; Godement et al., 1984), retinotectal projection in mice (McLaughlin et al., 2003) and in *C. Elegans* (Kage et al., 2005). A possible explanation for why pruning of diffuse projections has been observed in some systems, while early topographic organization without pruning has been observed in others could be that there are different mechanisms governing circuit formation in different brain regions. However this suggestion has, to my knowledge, not been yet been systematically tested. In my experiments, the first RSC axons arriving in PHR are topographically organized similarly as adults. However, it still remains to be determined whether the earliest axons are as precisely organized as the adult projections. Unfortunately, our experiments do not have the resolution to answer such questions. Probably single cell tracing is necessary to reveal whether young axons cover larger areas compared to adult axons (Mire et al., 2012). The ideal experiment for addressing this issue would be to perform *in vivo* imaging of the first RSC axons arriving in PHR, and investigate whether axons originating in different parts of RSC will have spatially overlapping axonal branches during the perinatal period and whether these axons prune into discrete plexi during the first postnatal week.

Independent of whether circuits are pruned or not into their adult state, it seems as if the topographic organization of projections are formed by experience independent mechanisms. This suggests that

genetic information sculpts the overall initial architecture of the brain. Thereafter, exposure of the individual to the environment and the physical characteristics of the individual can further shape the individual brain circuitry. For instance, visual deprivation leads to a change of initially organized ocular dominance columns (LeVay et al., 1980) or more generally during so-called critical periods during infancy in several brain regions (Hensch, 2004).

Mechanisms governing topographical organization of circuits

Several mechanisms governing axonal patterning have been suggested. Cajal who was inspired by advances in microbiology suggested that some kind of attractants- and repellents played a role, or as he stated it in one of his books published in 1890; *"[The axons] adopt pre-determined directions and establish connections with defined neural or extra neural elements [...] without deviations or errors, as if guided by an intelligent force"* (Sotelo, 2012). Sperry suggested that the neuronal specificity of the retinotectal projections could be achieved through molecular labeling of pre- and postsynaptic elements so that each neuron could recognize its synaptic partners. Later, Sperry's hypothesis was expanded to also involve gradients- and/or affinities for combinations of molecular markers, which are a more efficient way of genetically encode such patterns. Today we know that several diffusible molecular signals for attraction and repulsion of growing axons exist, probably involved in patterning of axonal projections (Tessier-Lavigne et al., 1988; Alcantara et al., 2000), and for instance the Eph family of receptor protein tyrosine kinases is one of several proteins which has been implicated in topographical mapping of neuronal projections (Vanderhaeghen et al., 2000). In view of the here presented topographies, it would be interesting to know whether molecules known to be important for patterning of axonal projections are topographically organized along the dorsoventral and/or along the transverse axis of PHR and SUB during the perinatal period. Such topographies have been reported in HF (Zhou, 1997; Galimberti et al., 2010). To our knowledge no such topographies have been reported for SUB, PHR or RSC.

Alternatively, activity-patterns in interconnected brain regions have been postulated as crucial for correct patterning of axonal projections. For instance segregation of ipsi- and contralateral retinogeniculate projections in several species is disrupted if retinal activity is hampered/tempered with (Chapman et al., 1986; Stellwagen and Shatz, 2002; Cang et al., 2005). The presence of intermixed axons in early stages of development, followed by an activity dependent segregation, suggests a process, which may include competitive interactions of axons for postsynaptic partners. Spontaneous waves of activity in retinal ganglion cells are believed to induce activity dependent competition in the lateral geniculate nucleus, possibly through classical spike time-dependent plasticity. Similar mechanisms are also thought to be important in the developing neuromuscular junction where motor neurons display activity dependent competition for postsynaptic acetylcholine receptors (Pittman and Oppenheim, 1978), and in induced column formations in the retinotectal projections in fish and xenopus (Boss and Schmidt, 1984; Ruthazer et al., 2003; however see contradicting results for organization of retinotectal

projections in the zebrafish; Gosse et al., 2008). It should be noted that internally generated spontaneous activity is present in CNS long before primary sensory neurons become functional and can therefore not be evoked by sensory stimuli. A possible activity-based competitive mechanism is therefore experience independent.

It would be interesting to carry out electrophysiological recordings in RSC and HF-PHR at different developmental stages to explore whether there are spontaneous waves of network-activity similar to what has been reported in retina, thalamus and primary visual cortex (Hanganu et al., 2006). If such activity is important for selective connectivity patterning in the RSC – HF-PHR system, the activity should be present already before birth, since topographically organized projections are seen already when the first axons arrive in PHR. I would further postulate that A29 displays desynchronized activity patterns with A30 and synchronized activity patterns with proximal PrS and more lateral parts of EC. In contrast, A30 should be synchronized with distal PrS and medial EC. It would also be interesting to investigate whether manipulations of such putative activity in RSC during development could lead to an altered topographical organization in PHR.

Such an induced altered topography would be in line with available data in the adult brain. Entorhinal-, septal-, ipsilateral HF- and contralateral HF afferents terminate in distinct sublayers of the molecular layer of DG. Selective lesions of each of these inputs result in a radial extension of the field of termination of the other remaining inputs such that a larger area of the apical dendrite will be occupied by the remaining terminal plexus (Gottlieb and Cowan, 1972; Cotman et al., 1973; Lynch et al., 1973). These observations have led to the suggestion that there are competitive interactions between presynaptic and postsynaptic partners governing the axonal patterning of HF-PHR projections. It would be interesting to investigate whether RSC inputs to PHR show a similar competition with other projections to PHR. For instance, it is known that single superficially projecting neurons in layer V of MEC are postsynaptic targets of both RSC and SUB inputs (Simonsen et al., 2012). If we were to know the distribution of synapses of both inputs on layer V neurons during development, one could assess a potentially altered distribution if one of the inputs, for example that from RSC, was removed during early development. If there are similar competitive interactions within MEC, I would expect that other afferents, such as the one originating in SUB would take over the vacant spines formerly occupied by RSC inputs.

Another important factor for connectional specificity is the temporal order of events during development. Bayer and Altman noted that there was a correlation between time of neurogenesis and termination patterns of the axonal projection (1987). Their *neurogenetic hypothesis* suggested that the time of neurogenesis predicts which migratory routes will be followed, which position in the brain the neuron will end up in, and where their axons will terminate. For instance, HF issues a topographically organized projection to the septal complex where dorsal HF projects to more medial parts of septum

compared with projections arising in ventral HF. Although neurons along the dorsoventral axis of HF are generated during the same period of neurogenesis, the ones in the dorsal HF are located geometrically closer to the septal complex than their ventral counterparts. Thus the dorsally originating axons may arrive in the septum before the ventral ones. Interestingly more medial parts of the septum contain earlier generated cells compared to more lateral parts of the septum. Therefore, the early arriving axons from dorsal HF target the earlier generated septal neurons. Vice versa, neurons in progressively more ventral parts of HF target the later formed neurons (Bayer, 1980a). Similar topographies exist for a manifold of projections within CNS. For instance, thalamic projections to RSC seem to be organized as a function of distance between the connected regions and the time of neurogenesis of both the pre- and postsynaptic partners (Bayer, 1990b). Within HF, temporal order of neurogenesis seems to play a role, since time of neurogenesis is the deciding factor for which neuronal populations within an area will become connected (Deguchi et al., 2011).

The chronological birth date is not only important for the distance an axon can cover. Work in *Drosophila* suggests that neurons born at different time points, express cell adhesion molecules in distinct temporal windows (Petrovic and Hummel, 2008). Thus, different populations of axons are sensitive to the same ligand at different time points, allowing different populations of axons to innervate different postsynaptic targets at different times. All together, these data indicate that the chronological sequence of neurogenesis is related to the patterns of anatomical interconnections in the adult brain. Phrased in a more general way, one could postulate that neurons born at different time points are primed with different genetically encoded programs and thereby, features such as adult connectivity might already be defined when the neurons starts to migrate from the neuroepithelium (Zhu et al., 2006). In paper 3, I show that A29 projects to more lateral parts of EC compared to A30. Interestingly, A29 neurons are formed earlier compared to A30 neurons (Bayer, 1990b). Neurons in more lateral parts of EC, which preferentially connect with A29 axons, are formed earlier than neurons in more medial parts of EC (Bayer, 1980a). The ontogenetic origin of RSC and EC neurons and the connectional organization between these areas is therefore in line with the neurogenetic hypothesis of Bayer and Altman. It would be of interest to see if the same gradient also holds for the projections to the superficial layers of PrS and deep layers of PrS and PaS. Unfortunately, the data of Bayer does not have the spatial resolution to identify ontogenic gradients within these areas. If the neurogenetic gradient hypothesis is correct, I postulate that proximal PrS neurons are formed earlier than neurons in distal PrS and deep PaS. To reveal possible mechanisms governing axonal patterning, an interesting experiment would be to manipulate the birth date of selective groups of RSC neurons. During neurogenesis in several brain areas, both in *Drosophila* and in rodents, neurons born at different time points express different sets of zinc finger transcription factors (Zhu et al., 2006; Elliott et al., 2008). Likewise, future experiments could manipulate the date of neurogenesis or the "temporal fingerprint" of certain populations of neurons by manipulating the expression of zinc finger transcription factors. If such manipulation could

specifically delay the time of neurogenesis for instance for neurons in A29 compared to A30 I would expect that A29 neurons would display a topographical organization more similar to the later born A30 neurons.

Lastly, work done on development of connections between other brain regions has indicated that axons may reside in the so-called subplate for days or even weeks depending on the species (Lund and Mustari, 1977; Rakic, 1977; Johnson and Casagrande, 1993). The subplate is a transient cortical structure, which is a remnant of the preplate, the first cortical structure which can be observed in the developing brain. Even though the exact function of the waiting period within the subplate is unknown, selective lesions of the subplate disturb the formation of ocular dominance columns (Ghosh et al., 1990). It is therefore suggested that interactions between ingrowing axons and the subplate are required for sorting axons into their correct ocular dominance columns. In our material I did not see any signs of waiting periods where developing RSC axons halts in the subplate and are thereby "sorted" into their correct topographical position within the PHR, suggesting that interactions between RSC axons and the subplate are not necessary for correct topographical organization of the axons.

Temporal development of RSC – HF-PHR connections

In paper 3, I showed that RSC axons are present already at birth. This is comparable to what other studies from our- and other groups have found for projections to, from and within HF-PHR. Since I only investigated postnatal animals it is possible that the first RSC axons arrive in PHR before birth. To reveal earlier ingrowth of axons, it is necessary to perform prenatal injections or injections in prematurely born rats.

In developing projections from EC to HF so-called Cajal-Retzius is present, a transient population of calretinin positive neurons guiding later in-growing axons to HF (Super et al., 1998; Ceranik et al., 1999; Deng et al., 2007). Similar transient populations of neurons also exist for other projection within HF-PHR (Super et al., 1998). It would be interesting to reveal whether the pioneer RSC-axons arriving in HF-PHR are also present in adolescent animals. It could be possible that the first axons arriving are transient "guiding" axons which ultimately degenerates before the network are fully functional. It would also be of interest to reveal whether these first axons make synapses. Our high-resolution images display axons with bouton-like swellings which could possibly be presynaptic terminals. Alternatively the swellings could be growth cones. Electron microscopy of these terminals or to perform a synaptic stain against for instance the synaptic marker bassoon and/or the growth cone marker GAP-43 could reveal whether swellings are actual synapses or growth cones.

In the present studies, I tried to reveal temporal differences between the growth of axons from different subareas of RSC. However, such a measure might not be the most crucial with respect to maturation of neural networks. A more interesting measure would be to reveal when the ingrowing fibers make synapses with their postsynaptic targets. One way to measure such an effect could be to do a synaptic

stain, as described above and measure the number of synapses per axon. Such a measure could reveal temporal differences between synaptogenesis of afferents from different parts of RSC, and ultimately also be compared with synaptogenesis of afferents from other (sub)cortical regions and synaptogenesis in the local circuits of PHR. An indirect measure of synaptogenesis is to quantify the number of axons in the terminal plexus. In our experiments, the axonal densities varied with a number of factors such as size of injection, how much of the injection involved layer V of RSC, the tracer used and also the age of the animal. One additional analysis to overcome this issue is to count the number of axons present in the structure of interest normalized to the number of layer V cells involved in the injection. The latter could be quantified by staining for a neuronal marker such as NeuN together with a stain for the tracer. This number, for each tracer, could be compared across ages to quantify the development of the axonal plexus.

Conclusions

I conclude that there are strong intrinsic connections within and between the RSC subdivisions and there are prominent reciprocal connections between PHR, SUB and RSC.

Further, I conclude that information from RSC could reach the HF through pyramidal neurons in layer V of MEC, which issue projections to the superficial layers of MEC. Neurons in the latter layers may relay information from RSC to HF since these layers harbor neurons projecting to HF. Alternative multisynaptic pathways connecting RSC via PHR to HF likely include RSC projections to postrhinal cortex, pre- and parasubiculum respectively. All three structures receive RSC inputs among others in superficial layers, which harbor neurons projecting to superficial layers of MEC.

The RSC – HF-PHR interconnections are present at birth and the early arriving fibers in PHR display an adult-like topographic organization. Around birth, these connections are very sparse, gradually developing until they reach adult like organization around P12. At all ages, the projections are topographically organized so that rostral RSC is connected with dorsal HF-PHR while caudal RSC is connected with more ventral parts of HF-PHR. In addition, A30 is preferentially connected with distal PrS, PaS and medial MEC, while A29 is preferentially connected with proximal PrS and more lateral parts of MEC, and not PAS. These early postnatal patterns are similar to those observed in adult rats.

The early development of the reciprocal connections between RSC and HF-PHR, already at an early postnatal stage, before neurons are functionally differentiated, suggests that RSC-PHR interconnections are organized by experience-independent mechanisms. This experience independent topographic organization suggests that RSC and HF-PHR are parts of one tightly coupled system and that RSC – HF-PHR interaction is necessary for proper functioning of the two regions.

References

Abellan A, Desfilis E, Medina L (2014) Combinatorial expression of Lef1, Lhx2, Lhx5, Lhx9, Lmo3, Lmo4, and Prox1 helps to identify comparable subdivisions in the developing hippocampal formation of mouse and chicken. Front Neuroanat 8:59. doi: 10.3389/fnana.2014.00059

Aggleton JP, Wright NF, Vann SD, Saunders RC (2012) Medial temporal lobe projections to the retrosplenial cortex of the macaque monkey. Hippocampus 22:1883-1900. doi: 10.1002/hipo.22024

Agster KL, Burwell RD (2009) Cortical efferents of the perirhinal, postrhinal, and entorhinal cortices of the rat. Hippocampus 19:1159-1186. doi: 10.1002/hipo.20578

Agster KL, Burwell RD (2013) Hippocampal and subicular efferents and afferents of the perirhinal, postrhinal, and entorhinal cortices of the rat. Behav Brain Res 254:50-64. doi: 10.1016/j.bbr.2013.07.005

Alcantara S, Ruiz M, De Castro F, Soriano E, Sotelo C (2000) Netrin 1 acts as an attractive or as a repulsive cue for distinct migrating neurons during the development of the cerebellar system. Development 127:1359-1372.

Alexander AS, Nitz DA (2015) Retrosplenial cortex maps the conjunction of internal and external spaces. Nat Neurosci 18:1143-1151. doi: 10.1038/nn.4058

Allendoerfer KL, Shatz CJ (1994) The subplate, a transient neocortical structure: its role in the development of connections between thalamus and cortex. Annual review of neuroscience 17:185-218. doi: 10.1146/annurev.ne.17.030194.001153

Attardi DG, Sperry RW (1963) Preferential selection of central pathways by regenerating optic fibers. Experimental Neurology 7:46-64. doi: http://dx.doi.org/10.1016/0014-4886(63)90093-1

Auger SD, Maguire EA (2013) Assessing the mechanism of response in the retrosplenial cortex of good and poor navigators. Cortex 49:2904-2913. doi: 10.1016/j.cortex.2013.08.002

Auger SD, Mullally SL, Maguire EA (2012) Retrosplenial cortex codes for permanent landmarks. PLoS One 7:e43620. doi: 10.1371/journal.pone.0043620

Awad M, Warren JE, Scott SK, Turkheimer FE, Wise RJ (2007) A common system for the comprehension and production of narrative speech. J Neurosci 27:11455-11464. doi: 10.1523/JNEUROSCI.5257-06.2007

Bar M, Aminoff E (2003) Cortical analysis of visual context. Neuron 38:347-358.

Bayer SA (1980a) Development of the hippocampal region in the rat. I. Neurogenesis examined with 3H-thymidine autoradiography. J Comp Neurol 190:87-114. doi: 10.1002/cne.901900107

Bayer SA (1980b) Development of the hippocampal region in the rat. II. Morphogenesis during embryonic and early postnatal life. J Comp Neurol 190:115-134. doi: 10.1002/cne.901900108

Bayer SA (1990a) Development of the lateral and medial limbic cortices in the rat in relation to cortical phylogeny. Exp Neurol 107:118-131.

Bayer SA (1990b) Neurogenetic patterns in the medial limbic cortex of the rat related to anatomical connections with the thalamus and striatum. Exp Neurol 107:132-142.

Bayer SA, Altman J (1987) Directions in neurogenetic gradients and patterns of anatomical connections in the telencephalon. Progress in neurobiology 29:57-106.

Binicewicz FZ, van Strien NM, Wadman WJ, van den Heuvel MP, Cappaert NL (2015) Graph analysis of the anatomical network organization of the hippocampal formation and parahippocampal region in the rat. Brain Struct Funct. doi: 10.1007/s00429-015-0992-0

Boccara CN, Kjonigsen LJ, Hammer IM, Bjaalie JG, Leergaard TB, Witter MP (2015) A three-plane architectonic atlas of the rat hippocampal region. Hippocampus 25:838-857. doi: 10.1002/hipo.22407

Boccara CN, Sargolini F, Thoresen VH, Solstad T, Witter MP, Moser EI, Moser MB (2010) Grid cells in pre- and parasubiculum. Nat Neurosci 13:987-994. doi: 10.1038/nn.2602

Bontempi B, Laurent-Demir C, Destrade C, Jaffard R (1999) Time-dependent reorganization of brain circuitry underlying long-term memory storage. Nature 400:671-675. doi: 10.1038/23270

Borrell V, Del Rio JA, Alcantara S, Derer M, Martinez A, D'Arcangelo G, Nakajima K, Mikoshiba K, Derer P, Curran T, Soriano E (1999) Reelin regulates the development and synaptogenesis of the layer-specific entorhino-hippocampal connections. J Neurosci 19:1345-1358.

Boss VC, Schmidt JT (1984) Activity and the formation of ocular dominance patches in dually innervated tectum of goldfish. J Neurosci 4:2891-2905.
Brandon MP, Bogaard AR, Libby CP, Connerney MA, Gupta K, Hasselmo ME (2011) Reduction of theta rhythm dissociates grid cell spatial periodicity from directional tuning. Science 332:595-599. doi: 10.1126/science.1201652
Brodmann K (1909) Vergleichende Lokalisationslehre der Grosshirnrinde in ihren Prinzipien dargestellt auf Grund des Zellenbauers. Leipzig.
Brun VH, Leutgeb S, Wu HQ, Schwarcz R, Witter MP, Moser EI, Moser MB (2008) Impaired spatial representation in CA1 after lesion of direct input from entorhinal cortex. Neuron 57:290-302. doi: S0896-6273(07)01029-X [pii]

10.1016/j.neuron.2007.11.034
Buckner RL, Andrews-Hanna JR, Schacter DL (2008) The brain's default network: anatomy, function, and relevance to disease. Ann N Y Acad Sci 1124:1-38. doi: 10.1196/annals.1440.011
Burgalossi A, Herfst L, von Heimendahl M, Forste H, Haskic K, Schmidt M, Brecht M (2011) Microcircuits of functionally identified neurons in the rat medial entorhinal cortex. Neuron 70:773-786. doi: 10.1016/j.neuron.2011.04.003
Burgess N, Barry C, O'Keefe J (2007) An oscillatory interference model of grid cell firing. Hippocampus 17:801-812. doi: 10.1002/hipo.20327
Burgess N, Maguire EA, Spiers HJ, O'Keefe J (2001) A temporoparietal and prefrontal network for retrieving the spatial context of lifelike events. Neuroimage 14:439-453. doi: 10.1006/nimg.2001.0806

S1053-8119(01)90806-7 [pii]
Burwell RD, Amaral DG (1998) Cortical afferents of the perirhinal, postrhinal, and entorhinal cortices of the rat. J Comp Neurol 398:179-205. doi: 10.1002/(SICI)1096-9861(19980824)398:2<179::AID-CNE3>3.0.CO;2-Y [pii]
Burwell RD, Witter MP, Wouterlood FG (2002) Basic anatomy of the parahippocampal region in rats and monkeys. In: The Parahippocampal Region, Organization and Role in Cognitive Functions, pp 35-60. Oxford, UK: Oxford University Press.
Buzsaki G (1996) The hippocampo-neocortical dialogue. Cereb Cortex 6:81-92.
Caballero-Bleda M, Witter MP (1994) Projections from the presubiculum and the parasubiculum to morphologically characterized entorhinal-hippocampal projection neurons in the rat. Exp Brain Res 101:93-108.
Cang J, Renteria RC, Kaneko M, Liu X, Copenhagen DR, Stryker MP (2005) Development of precise maps in visual cortex requires patterned spontaneous activity in the retina. Neuron 48:797-809. doi: 10.1016/j.neuron.2005.09.015
Canto CB, Witter MP (2012a) Cellular properties of principal neurons in the rat entorhinal cortex. II. The medial entorhinal cortex. Hippocampus 22:1277-1299. doi: 10.1002/hipo.20993
Canto CB, Witter MP (2012b) Cellular properties of principal neurons in the rat entorhinal cortex. I. The lateral entorhinal cortex. Hippocampus 22:1256-1276. doi: 10.1002/hipo.20997
Canto CB, Koganezawa N, Witter MP (2011) Development of Functional Projections from Pre- and Parasubiculum to Medial Entorhinal Cortex in the Rat. In: Kavli Institute for Systems Neuroscience and Centre for the Biology of Memory. Trondheim: Norwegian University of Science and Technology.
Canto CB, Koganezawa N, Beed P, Moser EI, Witter MP (2012) All layers of medial entorhinal cortex receive presubicular and parasubicular inputs. J Neurosci 32:17620-17631. doi: 10.1523/JNEUROSCI.3526-12.2012
Cappaert NLM, Van Strien NM, Witter MP (2015) Chapter 20 - Hippocampal Formation. In: The Rat Nervous System (Fourth Edition) (Paxinos G, ed), pp 511-573. San Diego: Academic Press. doi: http://dx.doi.org/10.1016/B978-0-12-374245-2.00020-6
Carpenter F, Manson D, Jeffery K, Burgess N, Barry C (2015) Grid cells form a global representation of connected environments. Curr Biol 25:1176-1182. doi: 10.1016/j.cub.2015.02.037
Catalano SM, Robertson RT, Killackey HP (1996) Individual axon morphology and thalamocortical topography in developing rat somatosensory cortex. J Comp Neurol 367:36-53. doi: 10.1002/(SICI)1096-9861(19960325)367:1<36::AID-CNE4>3.0.CO;2-K

Ceranik K, Deng J, Heimrich B, Lubke J, Zhao S, Forster E, Frotscher M (1999) Hippocampal Cajal-Retzius cells project to the entorhinal cortex: retrograde tracing and intracellular labelling studies. Eur J Neurosci 11:4278-4290.

Chapman B, Jacobson MD, Reiter HO, Stryker MP (1986) Ocular dominance shift in kitten visual cortex caused by imbalance in retinal electrical activity. Nature 324:154-156. doi: 10.1038/324154a0

Chen LL, Lin LH, Green EJ, Barnes CA, McNaughton BL (1994) Head-direction cells in the rat posterior cortex. I. Anatomical distribution and behavioral modulation. Exp Brain Res 101:8-23.

Chen S, Aston-Jones G (1998) Axonal collateral-collateral transport of tract tracers in brain neurons: false anterograde labelling and useful tool. Neuroscience 82:1151-1163.

Cho J, Sharp PE (2001) Head direction, place, and movement correlates for cells in the rat retrosplenial cortex. Behav Neurosci 115:3-25.

Colonnier M (1968) Synaptic patterns on different cell types in the different laminae of the cat visual cortex. An electron microscope study. Brain Research 9:268-287.

Cooper BG, Mizumori SJ (1999) Retrosplenial cortex inactivation selectively impairs navigation in darkness. Neuroreport 10:625-630.

Cooper BG, Mizumori SJ (2001) Temporary inactivation of the retrosplenial cortex causes a transient reorganization of spatial coding in the hippocampus. J Neurosci 21:3986-4001. doi: 21/11/3986 [pii]

Cooper BG, Manka TF, Mizumori SJ (2001) Finding your way in the dark: the retrosplenial cortex contributes to spatial memory and navigation without visual cues. Behav Neurosci 115:1012-1028.

Corcoran KA, Donnan MD, Tronson NC, Guzman YF, Gao C, Jovasevic V, Guedea AL, Radulovic J (2011) NMDA receptors in retrosplenial cortex are necessary for retrieval of recent and remote context fear memory. J Neurosci 31:11655-11659. doi: 10.1523/JNEUROSCI.2107-11.2011

Cotman CW, Matthews DA, Taylor D, Lynch G (1973) Synaptic rearrangement in the dentate gyrus: histochemical evidence of adjustments after lesions in immature and adult rats. Proc Natl Acad Sci U S A 70:3473-3477.

Couey JJ, Witoelar A, Zhang SJ, Zheng K, Ye J, Dunn B, Czajkowski R, Moser MB, Moser EI, Roudi Y, Witter MP (2013) Recurrent inhibitory circuitry as a mechanism for grid formation. Nat Neurosci 16:318-324. doi: 10.1038/nn.3310

Cowansage KK, Shuman T, Dillingham BC, Chang A, Golshani P, Mayford M (2014) Direct reactivation of a coherent neocortical memory of context. Neuron 84:432-441. doi: 10.1016/j.neuron.2014.09.022

Crain B, Cotman C, Taylor D, Lynch G (1973) A quantitative electron microscopic study of synaptogenesis in the dentate gyrus of the rat. Brain Res 63:195-204.

Crair MC, Horton JC, Antonini A, Stryker MP (2001) Emergence of ocular dominance columns in cat visual cortex by 2 weeks of age. J Comp Neurol 430:235-249.

Crowley JC, Katz LC (2000) Early development of ocular dominance columns. Science 290:1321-1324.

Czajkowski R, Sugar J, Zhang SJ, Couey JJ, Ye J, Witter MP (2013) Superficially projecting principal neurons in layer V of medial entorhinal cortex in the rat receive excitatory retrosplenial input. J Neurosci 33:15779-15792. doi: 10.1523/JNEUROSCI.2646-13.2013

Czajkowski R, Jayaprakash B, Wiltgen B, Rogerson T, Guzman-Karlsson MC, Barth AL, Trachtenberg JT, Silva AJ (2014) Encoding and storage of spatial information in the retrosplenial cortex. Proc Natl Acad Sci U S A 111:8661-8666. doi: 10.1073/pnas.1313222111

Deguchi Y, Donato F, Galimberti I, Cabuy E, Caroni P (2011) Temporally matched subpopulations of selectively interconnected principal neurons in the hippocampus. Nat Neurosci 14:495-504. doi: 10.1038/nn.2768

Del Rio JA, Heimrich B, Super H, Borrell V, Frotscher M, Soriano E (1996) Differential survival of Cajal-Retzius cells in organotypic cultures of hippocampus and neocortex. J Neurosci 16:6896-6907.

Deller T, Martinez A, Nitsch R, Frotscher M (1996) A novel entorhinal projection to the rat dentate gyrus: direct innervation of proximal dendrites and cell bodies of granule cells and GABAergic neurons. J Neurosci 16:3322-3333.

Demonet JF, Thierry G, Cardebat D (2005) Renewal of the neurophysiology of language: functional neuroimaging. Physiological reviews 85:49-95. doi: 10.1152/physrev.00049.2003
Deng JB, Yu DM, Wu P, Li MS (2007) The tracing study of developing entorhino-hippocampal pathway. Int J Dev Neurosci 25:251-258. doi: 10.1016/j.ijdevneu.2007.03.002
Deshmukh SS, Knierim JJ (2011) Representation of non-spatial and spatial information in the lateral entorhinal cortex. Front Behav Neurosci 5:69. doi: 10.3389/fnbeh.2011.00069
Dolleman-Van der Weel MJ, Wouterlood FG, Witter MP (1994) Multiple anterograde tracing, combining Phaseolus vulgaris leucoagglutinin with rhodamine- and biotin-conjugated dextran amine. J Neurosci Methods 51:9-21.
Eccles JC (1964) The physiology of synapses. Berlin: Springer Verlag.
Eichenbaum H, Yonelinas AP, Ranganath C (2007) The medial temporal lobe and recognition memory. Annual review of neuroscience 30:123-152. doi: 10.1146/annurev.neuro.30.051606.094328
Elduayen C, Save E (2014) The retrosplenial cortex is necessary for path integration in the dark. Behav Brain Res 272:303-307. doi: 10.1016/j.bbr.2014.07.009
Elliott J, Jolicoeur C, Ramamurthy V, Cayouette M (2008) Ikaros confers early temporal competence to mouse retinal progenitor cells. Neuron 60:26-39. doi: 10.1016/j.neuron.2008.08.008
Epstein RA, Higgins JS (2007) Differential parahippocampal and retrosplenial involvement in three types of visual scene recognition. Cereb Cortex 17:1680-1693. doi: bhl079 [pii]

10.1093/cercor/bhl079
Fahy FL, Riches IP, Brown MW (1993) Neuronal activity related to visual recognition memory: long-term memory and the encoding of recency and familiarity information in the primate anterior and medial inferior temporal and rhinal cortex. Exp Brain Res 96:457-472.
Fricke R, Cowan WM (1977) An autoradiographic study of the development of the entorhinal and commissural afferents to the dentate gyrus of the rat. J Comp Neurol 173:231-250. doi: 10.1002/cne.901730203
Furtak SC, Wei SM, Agster KL, Burwell RD (2007) Functional neuroanatomy of the parahippocampal region in the rat: the perirhinal and postrhinal cortices. Hippocampus 17:709-722. doi: 10.1002/hipo.20314
Fyhn M, Molden S, Witter MP, Moser EI, Moser MB (2004) Spatial representation in the entorhinal cortex. Science 305:1258-1264. doi: 10.1126/science.1099901

305/5688/1258 [pii]
Gabriel M, Sparenborg SP, Stolar N (1987) Hippocampal control of cingulate cortical and anterior thalamic information processing during learning in rabbits. Exp Brain Res 67:131-152.
Gabriel M, Vogt BA, Kubota Y, Poremba A, Kang E (1991) Training-stage related neuronal plasticity in limbic thalamus and cingulate cortex during learning: a possible key to mnemonic retrieval. Behav Brain Res 46:175-185.
Galimberti I, Bednarek E, Donato F, Caroni P (2010) EphA4 signaling in juveniles establishes topographic specificity of structural plasticity in the hippocampus. Neuron 65:627-642. doi: 10.1016/j.neuron.2010.02.016
Garden DL, Dodson PD, O'Donnell C, White MD, Nolan MF (2008) Tuning of synaptic integration in the medial entorhinal cortex to the organization of grid cell firing fields. Neuron 60:875-889. doi: 10.1016/j.neuron.2008.10.044
George S, Ronnback A, Gouras GK, Petit GH, Grueninger F, Winblad B, Graff C, Brundin P (2014) Lesion of the subiculum reduces the spread of amyloid beta pathology to interconnected brain regions in a mouse model of Alzheimer's disease. Acta Neuropathol Commun 2:17. doi: 10.1186/2051-5960-2-17
Ghosh A, Antonini A, McConnell SK, Shatz CJ (1990) Requirement for subplate neurons in the formation of thalamocortical connections. Nature 347:179-181. doi: 10.1038/347179a0
Giocomo LM, Moser EI (2011) Spatial representation: maps in a temporal void. Curr Biol 21:R962-964. doi: 10.1016/j.cub.2011.10.024
Gloveli T, Dugladze T, Schmitz D, Heinemann U (2001) Properties of entorhinal cortex deep layer neurons projecting to the rat dentate gyrus. Eur J Neurosci 13:413-420. doi: ejn1405 [pii]

Godement P, Salaun J, Imbert M (1984) Prenatal and postnatal development of retinogeniculate and retinocollicular projections in the mouse. J Comp Neurol 230:552-575. doi: 10.1002/cne.902300406

Gosse NJ, Nevin LM, Baier H (2008) Retinotopic order in the absence of axon competition. Nature 452:892-895. doi: 10.1038/nature06816

Gottlieb DI, Cowan WM (1972) Evidence for a temporal factor in the occupation of available synaptic sites during the development of the dentate gyrus. Brain Res 41:452-456.

Gray EG (1959) Electron microscopy of synaptic contacts on dendrite spines of the cerebral cortex. Nature 183:1592-1593.

Greicius MD, Supekar K, Menon V, Dougherty RF (2009) Resting-state functional connectivity reflects structural connectivity in the default mode network. Cereb Cortex 19:72-78. doi: 10.1093/cercor/bhn059

Guterstam A, Bjornsdotter M, Gentile G, Ehrsson HH (2015) Posterior cingulate cortex integrates the senses of self-location and body ownership. Curr Biol 25:1416-1425. doi: 10.1016/j.cub.2015.03.059

Hafting T, Fyhn M, Molden S, Moser MB, Moser EI (2005) Microstructure of a spatial map in the entorhinal cortex. Nature 436:801-806. doi: nature03721 [pii]

10.1038/nature03721

Haglund L, Swanson LW, Kohler C (1984) The projection of the supramammillary nucleus to the hippocampal formation: an immunohistochemical and anterograde transport study with the lectin PHA-L in the rat. J Comp Neurol 229:171-185. doi: 10.1002/cne.902290204

Hales JB, Schlesiger MI, Leutgeb JK, Squire LR, Leutgeb S, Clark RE (2014) Medial entorhinal cortex lesions only partially disrupt hippocampal place cells and hippocampus-dependent place memory. Cell Rep 9:893-901. doi: 10.1016/j.celrep.2014.10.009

Hamam BN, Kennedy TE, Alonso A, Amaral DG (2000) Morphological and electrophysiological characteristics of layer V neurons of the rat medial entorhinal cortex. J Comp Neurol 418:457-472. doi: 10.1002/(SICI)1096-9861(20000320)418:4<457::AID-CNE7>3.0.CO;2-L [pii]

Hanganu IL, Ben-Ari Y, Khazipov R (2006) Retinal waves trigger spindle bursts in the neonatal rat visual cortex. J Neurosci 26:6728-6736. doi: 10.1523/JNEUROSCI.0752-06.2006

Hardcastle K, Ganguli S, Giocomo LM (2015) Environmental boundaries as an error correction mechanism for grid cells. Neuron 86:827-839. doi: 10.1016/j.neuron.2015.03.039

Hargreaves EL, Rao G, Lee I, Knierim JJ (2005) Major dissociation between medial and lateral entorhinal input to dorsal hippocampus. Science 308:1792-1794. doi: 10.1126/science.1110449

Hashimoto R, Tanaka Y, Nakano I (2010) Heading disorientation: a new test and a possible underlying mechanism. Eur Neurol 63:87-93. doi: 10.1159/000276398

Hassabis D, Maguire EA (2007) Deconstructing episodic memory with construction. Trends Cogn Sci 11:299-306. doi: S1364-6613(07)00125-8 [pii]

10.1016/j.tics.2007.05.001

Hasselmo ME, Giocomo LM, Zilli EA (2007) Grid cell firing may arise from interference of theta frequency membrane potential oscillations in single neurons. Hippocampus 17:1252-1271. doi: 10.1002/hipo.20374

Helmstaedter M, Briggman KL, Turaga SC, Jain V, Seung HS, Denk W (2013) Connectomic reconstruction of the inner plexiform layer in the mouse retina. Nature 500:168-174. doi: 10.1038/nature12346

Henriksen EJ, Colgin LL, Barnes CA, Witter MP, Moser MB, Moser EI (2010) Spatial representation along the proximodistal axis of CA1. Neuron 68:127-137. doi: 10.1016/j.neuron.2010.08.042

Hensch TK (2004) Critical period regulation. Annual review of neuroscience 27:549-579. doi: 10.1146/annurev.neuro.27.070203.144327

Hindley EL, Nelson AJ, Aggleton JP, Vann SD (2014a) The rat retrosplenial cortex is required when visual cues are used flexibly to determine location. Behav Brain Res 263:98-107. doi: 10.1016/j.bbr.2014.01.028

Hindley EL, Nelson AJ, Aggleton JP, Vann SD (2014b) Dysgranular retrosplenial cortex lesions in rats disrupt cross-modal object recognition. Learn Mem 21:171-179. doi: 10.1101/lm.032516.113

Honda Y, Ishizuka N (2004) Organization of connectivity of the rat presubiculum: I. Efferent projections to the medial entorhinal cortex. J Comp Neurol 473:463-484. doi: 10.1002/cne.20093
Honda Y, Ishizuka N (2015) Topographic distribution of cortical projection cells in the rat subiculum. Neurosci Res 92:1-20. doi: 10.1016/j.neures.2014.11.011
Honda Y, Furuta T, Kaneko T, Shibata H, Sasaki H (2011) Patterns of axonal collateralization of single layer V cortical projection neurons in the rat presubiculum. J Comp Neurol 519:1395-1412. doi: 10.1002/cne.22578
Horton JC, Hocking DR (1996) An adult-like pattern of ocular dominance columns in striate cortex of newborn monkeys prior to visual experience. J Neurosci 16:1791-1807.
Hunsaker MR, Chen V, Tran GT, Kesner RP (2013) The medial and lateral entorhinal cortex both contribute to contextual and item recognition memory: a test of the binding of items and context model. Hippocampus 23:380-391. doi: 10.1002/hipo.22097
Iaria G, Chen JK, Guariglia C, Ptito A, Petrides M (2007) Retrosplenial and hippocampal brain regions in human navigation: complementary functional contributions to the formation and use of cognitive maps. Eur J Neurosci 25:890-899. doi: 10.1111/j.1460-9568.2007.05371.x
Insausti R, Herrero MT, Witter MP (1997) Entorhinal cortex of the rat: cytoarchitectonic subdivisions and the origin and distribution of cortical efferents. Hippocampus 7:146-183. doi: 10.1002/(SICI)1098-1063(1997)7:2<146::AID-HIPO4>3.0.CO;2-L
Jarrard LE (1978) Selective hippocampal lesions: differential effects on performance by rats of a spatial task with preoperative versus postoperative training. Journal of Comparative and Physiological Psychology 92:1119-1127.
Johnson JK, Casagrande VA (1993) Prenatal development of axon outgrowth and connectivity in the ferret visual system. Vis Neurosci 10:117-130.
Jones BF, Witter MP (2007) Cingulate cortex projections to the parahippocampal region and hippocampal formation in the rat. Hippocampus 17:957-976. doi: 10.1002/hipo.20330
Jones BF, Groenewegen HJ, Witter MP (2005) Intrinsic connections of the cingulate cortex in the rat suggest the existence of multiple functionally segregated networks. Neuroscience 133:193-207. doi: S0306-4522(05)00224-1 [pii]

10.1016/j.neuroscience.2005.01.063
Jones SP, Rahimi O, O'Boyle MP, Diaz DL, Claiborne BJ (2003) Maturation of granule cell dendrites after mossy fiber arrival in hippocampal field CA3. Hippocampus 13:413-427. doi: 10.1002/hipo.10121
Kage E, Hayashi Y, Takeuchi H, Hirotsu T, Kunitomo H, Inoue T, Arai H, Iino Y, Kubo T (2005) MBR-1, a novel helix-turn-helix transcription factor, is required for pruning excessive neurites in Caenorhabditis elegans. Curr Biol 15:1554-1559. doi: 10.1016/j.cub.2005.07.057
Katche C, Dorman G, Slipczuk L, Cammarota M, Medina JH (2013a) Functional integrity of the retrosplenial cortex is essential for rapid consolidation and recall of fear memory. Learn Mem 20:170-173. doi: 10.1101/lm.030080.112
Katche C, Dorman G, Gonzalez C, Kramar CP, Slipczuk L, Rossato JI, Cammarota M, Medina JH (2013b) On the role of retrosplenial cortex in long-lasting memory storage. Hippocampus 23:295-302. doi: 10.1002/hipo.22092
Keene CS, Bucci DJ (2008a) Contributions of the retrosplenial and posterior parietal cortices to cue-specific and contextual fear conditioning. Behav Neurosci 122:89-97. doi: 2008-01943-010 [pii]

10.1037/0735-7044.122.1.89
Keene CS, Bucci DJ (2008b) Involvement of the retrosplenial cortex in processing multiple conditioned stimuli. Behav Neurosci 122:651-658. doi: 2008-06403-017 [pii]

10.1037/0735-7044.122.3.651
Kerr KM, Agster KL, Furtak SC, Burwell RD (2007) Functional neuroanatomy of the parahippocampal region: the lateral and medial entorhinal areas. Hippocampus 17:697-708. doi: 10.1002/hipo.20315
Killian NJ, Jutras MJ, Buffalo EA (2012) A map of visual space in the primate entorhinal cortex. Nature 491:761-764. doi: 10.1038/nature11587

Knierim JJ, Neunuebel JP, Deshmukh SS (2014) Functional correlates of the lateral and medial entorhinal cortex: objects, path integration and local-global reference frames. Philos Trans R Soc Lond B Biol Sci 369:20130369. doi: 10.1098/rstb.2013.0369

Kobayashi Y, Amaral DG (2000) Macaque monkey retrosplenial cortex: I. three-dimensional and cytoarchitectonic organization. J Comp Neurol 426:339-365.

Kobayashi Y, Amaral DG (2003) Macaque monkey retrosplenial cortex: II. Cortical afferents. J Comp Neurol 466:48-79. doi: 10.1002/cne.10883

Kobayashi Y, Amaral DG (2007) Macaque monkey retrosplenial cortex: III. Cortical efferents. J Comp Neurol 502:810-833. doi: 10.1002/cne.21346

Koganezawa N, Witter MP (2010) Entorhinal-hippocampal circuits in rat are functional around the moment of eye opening. In: Poster 101.7. Society for Neuroscience. San Diego.

Koganezawa N, Canto CB, Witter MP (2010) Postnatal development of functional connectivity from pre- and parasubiculum to medial entorhinal cortex. In: Poster 087.30. Federation of European Neuroscience Societies. Amsterdam.

Koganezawa N, Gisetstad R, Husby EM, Witter MP (2009) Functional organization of postrhinal to medial entorhinal cortex connectivity in the rat. In: Poster 101.14. Society of Neuroscience. Chicago.

Kononenko NL, Witter MP (2012) Presubiculum layer III conveys retrosplenial input to the medial entorhinal cortex. Hippocampus 22:881-895. doi: 10.1002/hipo.20949

Krieg WJ (1946) Connections of the cerebral cortex; the albino rat; structure of the cortical areas. Journal of Comparative Neurology 84:277-323.

Kropff E, Carmichael JE, Moser MB, Moser EI (2015) Speed cells in the medial entorhinal cortex. Nature 523:419-424. doi: 10.1038/nature14622

Krupic J, Bauza M, Burton S, Lever C, O'Keefe J (2014) How environment geometry affects grid cell symmetry and what we can learn from it. Philos Trans R Soc Lond B Biol Sci 369:20130188. doi: 10.1098/rstb.2013.0188

Lanciego JL, Wouterlood FG (2011) A half century of experimental neuroanatomical tracing. J Chem Neuroanat 42:157-183. doi: 10.1016/j.jchemneu.2011.07.001

Langston RF, Ainge JA, Couey JJ, Canto CB, Bjerknes TL, Witter MP, Moser EI, Moser MB (2010) Development of the spatial representation system in the rat. Science 328:1576-1580. doi: 10.1126/science.1188210

Leitner FC, Melzer S, Lutcke H, Pinna R, Seeburg PH, Helmchen F, Monyer H (2016) Spatially segregated feedforward and feedback neurons support differential odor processing in the lateral entorhinal cortex. Nat Neurosci. doi: 10.1038/nn.4303

LeVay S, Wiesel TN, Hubel DH (1980) The development of ocular dominance columns in normal and visually deprived monkeys. J Comp Neurol 191:1-51. doi: 10.1002/cne.901910102

Lin DM, Wang F, Lowe G, Gold GH, Axel R, Ngai J, Brunet L (2000) Formation of precise connections in the olfactory bulb occurs in the absence of odorant-evoked neuronal activity. Neuron 26:69-80.

Linden DC, Guillery RW, Cucchiaro J (1981) The dorsal lateral geniculate nucleus of the normal ferret and its postnatal development. J Comp Neurol 203:189-211. doi: 10.1002/cne.902030204

Lingenhohl K, Finch DM (1991) Morphological characterization of rat entorhinal neurons in vivo: soma-dendritic structure and axonal domains. Experimental Brain Research 84:57-74.

Lund RD, Mustari MJ (1977) Development of the geniculocortical pathway in rats. J Comp Neurol 173:289-306. doi: 10.1002/cne.901730206

Lynch GS, Mosko S, Parks T, Cotman CW (1973) Relocation and hyperdevelopment of the dentate gyrus commissural system after entorhinal lesions in immature rats. Brain Res 50:174-178.

Maguire EA (2001) The retrosplenial contribution to human navigation: a review of lesion and neuroimaging findings. Scand J Psychol 42:225-238.

Maguire EA, Nannery R, Spiers HJ (2006) Navigation around London by a taxi driver with bilateral hippocampal lesions. Brain 129:2894-2907.

Marchette SA, Vass LK, Ryan J, Epstein RA (2014) Anchoring the neural compass: coding of local spatial reference frames in human medial parietal lobe. Nat Neurosci 17:1598-1606. doi: 10.1038/nn.3834

Maviel T, Durkin TP, Menzaghi F, Bontempi B (2004) Sites of neocortical reorganization critical for remote spatial memory. Science 305:96-99. doi: 10.1126/science.1098180

305/5680/96 [pii]
McLaughlin T, Torborg CL, Feller MB, O'Leary DD (2003) Retinotopic map refinement requires spontaneous retinal waves during a brief critical period of development. Neuron 40:1147-1160.
McNaughton BL, Barnes CA, Meltzer J, Sutherland RJ (1989) Hippocampal granule cells are necessary for normal spatial learning but not for spatially-selective pyramidal cell discharge. Exp Brain Res 76:485-496.
McNaughton BL, Battaglia FP, Jensen O, Moser EI, Moser MB (2006) Path integration and the neural basis of the 'cognitive map'. Nat Rev Neurosci 7:663-678. doi: nrn1932 [pii]

10.1038/nrn1932
Medinilla V, Johnson O, Gasparini S (2013) Features of proximal and distal excitatory synaptic inputs to layer V neurons of the rat medial entorhinal cortex. J Physiol 591:169-183. doi: 10.1113/jphysiol.2012.237172
Meibach RC, Siegel A (1977) Subicular projections to the posterior cingulate cortex in rats. Exp Neurol 57:264-274. doi: 0014-4886(77)90062-0 [pii]
Meyer G, Goffinet AM (1998) Prenatal development of reelin-immunoreactive neurons in the human neocortex. J Comp Neurol 397:29-40.
Mikula S, Denk W (2015) High-resolution whole-brain staining for electron microscopic circuit reconstruction. Nat Methods 12:541-546. doi: 10.1038/nmeth.3361
Miller VM, Best PJ (1980) Spatial correlates of hippocampal unit activity are altered by lesions of the fornix and endorhinal cortex. Brain Res 194:311-323.
Mire E, Mezzera C, Leyva-Diaz E, Paternain AV, Squarzoni P, Bluy L, Castillo-Paterna M, Lopez MJ, Peregrin S, Tessier-Lavigne M, Garel S, Galceran J, Lerma J, Lopez-Bendito G (2012) Spontaneous activity regulates Robo1 transcription to mediate a switch in thalamocortical axon growth. Nat Neurosci 15:1134-1143. doi: 10.1038/nn.3160
Miyashita T, Rockland KS (2007) GABAergic projections from the hippocampus to the retrosplenial cortex in the rat. Eur J Neurosci 26:1193-1204. doi: EJN5745 [pii]

10.1111/j.1460-9568.2007.05745.x
Morris R, Petrides M, Pandya DN (1999) Architecture and connections of retrosplenial area 30 in the rhesus monkey (Macaca mulatta). Eur J Neurosci 11:2506-2518. doi: ejn672 [pii]
Moscovitch M, Cabeza R, Winocur G, Nadel L (2016) Episodic Memory and Beyond: The Hippocampus and Neocortex in Transformation. Annu Rev Psychol 67:105-134. doi: 10.1146/annurev-psych-113011-143733
Moser MB, Moser EI, Forrest E, Andersen P, Morris RG (1995) Spatial learning with a minislab in the dorsal hippocampus. Proc Natl Acad Sci U S A 92:9697-9701.
Naber PA, Witter MP (1998) Subicular efferents are organized mostly as parallel projections: a double-labeling, retrograde-tracing study in the rat. J Comp Neurol 393:284-297.
Naber PA, Lopes da Silva FH, Witter MP (2001) Reciprocal connections between the entorhinal cortex and hippocampal fields CA1 and the subiculum are in register with the projections from CA1 to the subiculum. Hippocampus 11:99-104. doi: 10.1002/hipo.1028
Naya Y, Suzuki WA (2011) Integrating what and when across the primate medial temporal lobe. Science 333:773-776. doi: 10.1126/science.1206773
Nelson AJ, Hindley EL, Haddon JE, Vann SD, Aggleton JP (2014) A novel role for the rat retrosplenial cortex in cognitive control. Learn Mem 21:90-97. doi: 10.1101/lm.032136.113
O'Keefe J, Dostrovsky J (1971) The hippocampus as a spatial map. Preliminary evidence from unit activity in the freely-moving rat. Brain Res 34:171-175. doi: 0006-8993(71)90358-1 [pii]
O'Keefe J, Nadel L (1978) The Hippocampus as a cognitive map. Oxford: Clarendon Press.
O'Reilly KC, Kruge IU, Witter MP (2010a) Postnatal development of hippocampal-to-entorhinal connections in the rat. In: Poster 087.33 Forum of European Neuroscience. Amsterdam.
O'Reilly KC, Koganezawa N, Kruge IU, Witter MP (2010b) Postnatal development of medial entorhinal intrinsic connectivity in the rat. In: Poster 101.10. Society for Neuroscience. San Diego.

O'Reilly KC, Gulden Dahl A, Ulsaker Kruge I, Witter MP (2013) Subicular-parahippocampal projections revisited: development of a complex topography in the rat. J Comp Neurol 521:4284-4299. doi: 10.1002/cne.23417

O'Reilly KC, Flatberg A, Islam S, Olsen LC, Kruge IU, Witter MP (2014) Identification of dorsal-ventral hippocampal differentiation in neonatal rats. Brain Struct Funct. doi: 10.1007/s00429-014-0831-8

Osawa A, Maeshima S, Kunishio K (2008) Topographic disorientation and amnesia due to cerebral hemorrhage in the left retrosplenial region. Eur Neurol 59:79-82. doi: 10.1159/000109572

Park S, Chun MM (2009) Different roles of the parahippocampal place area (PPA) and retrosplenial cortex (RSC) in panoramic scene perception. Neuroimage 47:1747-1756. doi: 10.1016/j.neuroimage.2009.04.058

Parron C, Poucet B, Save E (2004) Entorhinal cortex lesions impair the use of distal but not proximal landmarks during place navigation in the rat. Behav Brain Res 154:345-352. doi: 10.1016/j.bbr.2004.03.006

Petrovic M, Hummel T (2008) Temporal identity in axonal target layer recognition. Nature 456:800-803. doi: 10.1038/nature07407

Pitkanen A, Pikkarainen M, Nurminen N, Ylinen A (2000) Reciprocal connections between the amygdala and the hippocampal formation, perirhinal cortex, and postrhinal cortex in rat. A review. Ann N Y Acad Sci 911:369-391.

Pittman RH, Oppenheim RW (1978) Neuromuscular blockade increases motoneurone survival during normal cell death in the chick embryo. Nature 271:364-366.

Pothuizen HH, Aggleton JP, Vann SD (2008) Do rats with retrosplenial cortex lesions lack direction? Eur J Neurosci 28:2486-2498. doi: EJN6550 [pii]

10.1111/j.1460-9568.2008.06550.x

Pothuizen HH, Davies M, Albasser MM, Aggleton JP, Vann SD (2009) Granular and dysgranular retrosplenial cortices provide qualitatively different contributions to spatial working memory: evidence from immediate-early gene imaging in rats. Eur J Neurosci 30:877-888. doi: 10.1111/j.1460-9568.2009.06881.x

Quilichini P, Sirota A, Buzsaki G (2010) Intrinsic circuit organization and theta-gamma oscillation dynamics in the entorhinal cortex of the rat. Journal of Neuroscience 30:11128-11142. doi: 10.1523/jneurosci.1327-10.2010

Rajasethupathy P, Sankaran S, Marshel JH, Kim CK, Ferenczi E, Lee SY, Berndt A, Ramakrishnan C, Jaffe A, Lo M, Liston C, Deisseroth K (2015) Projections from neocortex mediate top-down control of memory retrieval. Nature 526:653-659. doi: 10.1038/nature15389

Rakic P (1976) Prenatal genesis of connections subserving ocular dominance in the rhesus monkey. Nature 261:467-471.

Rakic P (1977) Prenatal development of the visual system in rhesus monkey. Philos Trans R Soc Lond B Biol Sci 278:245-260.

Ranganath C, Ritchey M (2012) Two cortical systems for memory-guided behaviour. Nat Rev Neurosci 13:713-726. doi: 10.1038/nrn3338

Reep RL, Chandler HC, King V, Corwin JV (1994) Rat posterior parietal cortex: topography of corticocortical and thalamic connections. Exp Brain Res 100:67-84.

Robinson S, Keene CS, Iaccarino HF, Duan D, Bucci DJ (2011) Involvement of retrosplenial cortex in forming associations between multiple sensory stimuli. Behav Neurosci 125:578-587. doi: 10.1037/a0024262

Robinson S, Todd TP, Pasternak AR, Luikart BW, Skelton PD, Urban DJ, Bucci DJ (2014) Chemogenetic silencing of neurons in retrosplenial cortex disrupts sensory preconditioning. J Neurosci 34:10982-10988. doi: 10.1523/JNEUROSCI.1349-14.2014

Rowland DC, Weible AP, Wickersham IR, Wu H, Mayford M, Witter MP, Kentros CG (2013) Transgenically targeted rabies virus demonstrates a major monosynaptic projection from hippocampal area CA2 to medial entorhinal layer II neurons. J Neurosci 33:14889-14898. doi: 10.1523/JNEUROSCI.1046-13.2013

Ruthazer ES, Akerman CJ, Cline HT (2003) Control of axon branch dynamics by correlated activity in vivo. Science 301:66-70. doi: 10.1126/science.1082545

Saper CB (1985) Organization of cerebral cortical afferent systems in the rat. II. Hypothalamocortical projections. J Comp Neurol 237:21-46. doi: 10.1002/cne.902370103

Sargolini F, Fyhn M, Hafting T, McNaughton BL, Witter MP, Moser MB, Moser EI (2006) Conjunctive representation of position, direction, and velocity in entorhinal cortex. Science 312:758-762. doi: 312/5774/758 [pii]

10.1126/science.1125572

Scoville WB, Milner B (1957) Loss of recent memory after bilateral hippocampal lesions. J Neurol Neurosurg Psychiatry 20:11-21.

Segal M, Landis S (1974) Afferents to the hippocampus of the rat studied with the method of retrograde transport of horseradish peroxidase. Brain Res 78:1-15.

Sharp PE, Green C (1994) Spatial correlates of firing patterns of single cells in the subiculum of the freely moving rat. J Neurosci 14:2339-2356.

Shatz CJ (1983) The prenatal development of the cat's retinogeniculate pathway. J Neurosci 3:482-499.

Sherrill KR, Erdem UM, Ross RS, Brown TI, Hasselmo ME, Stern CE (2013) Hippocampus and retrosplenial cortex combine path integration signals for successful navigation. J Neurosci 33:19304-19313. doi: 10.1523/JNEUROSCI.1825-13.2013

Shibata H (1994) Terminal distribution of projections from the retrosplenial area to the retrohippocampal region in the rat, as studied by anterograde transport of biotinylated dextran amine. Neurosci Res 20:331-336.

Shipley MT (1975) The topographical and laminar organization of the presubiculum's projection to the ipsi- and contralateral entorhinal cortex in the guinea pig. J Comp Neurol 160:127-145. doi: 10.1002/cne.901600108

Simonsen ØW, Czajkowski R, Witter MP (2012) Retrosplenial And Subicular Efferents Converge On Superficially Projecting Principal Neurons Of Deep Medial Entorhinal Cortex. In: FENS, Abstract P115.15. Barcelona, Spain.

Small DM, Zatorre RJ, Dagher A, Evans AC, Jones-Gotman M (2001) Changes in brain activity related to eating chocolate: from pleasure to aversion. Brain 124:1720-1733.

Smith DM, Barredo J, Mizumori SJ (2012) Complimentary roles of the hippocampus and retrosplenial cortex in behavioral context discrimination. Hippocampus 22:1121-1133. doi: 10.1002/hipo.20958

Smith DM, Freeman JH, Jr., Nicholson D, Gabriel M (2002) Limbic thalamic lesions, appetitively motivated discrimination learning, and training-induced neuronal activity in rabbits. J Neurosci 22:8212-8221.

Sotelo C (2012) The Neurotropic Theory of Santiago Ramón y Cajal. http://ibro.info/wp-content/uploads/2012/12/The-Neurotropic-Theory-of-Santiago-Ram%C3%B3n-y-Cajal.pdf Last updated: 15.12.2012

Sperry RW (1943) Effect of 180 degree rotation of the retinal field on visuomotor coordination. Journal of Experimental Zoology 92:263-279. doi: 10.1002/jez.1400920303

Sperry RW (1945) Restoration of vision after crossing of optic nerves and after contralateral transplantation of eye. J Neurophysiol 8:15-28.

Sripanidkulchai K, Wyss JM (1987) The laminar organization of efferent neuronal cell bodies in the retrosplenial granular cortex. Brain Res 406:255-269. doi: 0006-8993(87)90790-6 [pii]

Steffenach HA, Witter M, Moser MB, Moser EI (2005) Spatial memory in the rat requires the dorsolateral band of the entorhinal cortex. Neuron 45:301-313. doi: 10.1016/j.neuron.2004.12.044

Stellwagen D, Shatz CJ (2002) An instructive role for retinal waves in the development of retinogeniculate connectivity. Neuron 33:357-367.

Stensola T, Stensola H, Moser MB, Moser EI (2015) Shearing-induced asymmetry in entorhinal grid cells. Nature 518:207-212. doi: 10.1038/nature14151

Sugar J, Witter MP, van Strien NM, Cappaert NL (2011) The retrosplenial cortex: intrinsic connectivity and connections with the (para)hippocampal region in the rat. An interactive connectome. Front Neuroinform 5:7. doi: 10.3389/fninf.2011.00007

Suh J, Rivest AJ, Nakashiba T, Tominaga T, Tonegawa S (2011) Entorhinal cortex layer III input to the hippocampus is crucial for temporal association memory. Science 334:1415-1420. doi: 10.1126/science.1210125

Sulpizio V, Committeri G, Lambrey S, Berthoz A, Galati G (2013) Selective role of lingual/parahippocampal gyrus and retrosplenial complex in spatial memory across viewpoint changes relative to the environmental reference frame. Behav Brain Res 242:62-75. doi: 10.1016/j.bbr.2012.12.031

Super H, Soriano E (1994) The organization of the embryonic and early postnatal murine hippocampus. II. Development of entorhinal, commissural, and septal connections studied with the lipophilic tracer DiI. J Comp Neurol 344:101-120. doi: 10.1002/cne.903440108

Super H, Martinez A, Del Rio JA, Soriano E (1998) Involvement of distinct pioneer neurons in the formation of layer-specific connections in the hippocampus. J Neurosci 18:4616-4626.

Surmeli G, Marcu DC, McClure C, Garden DL, Pastoll H, Nolan MF (2015) Molecularly Defined Circuitry Reveals Input-Output Segregation in Deep Layers of the Medial Entorhinal Cortex. Neuron 88:1040-1053. doi: 10.1016/j.neuron.2015.10.041

Suzuki WA, Miller EK, Desimone R (1997) Object and place memory in the macaque entorhinal cortex. J Neurophysiol 78:1062-1081.

Takahashi N, Kawamura M, Shiota J, Kasahata N, Hirayama K (1997) Pure topographic disorientation due to right retrosplenial lesion. Neurology 49:464-469.

Tamamaki N, Nojyo Y (1995) Preservation of topography in the connections between the subiculum, field CA1, and the entorhinal cortex in rats. J Comp Neurol 353:379-390. doi: 10.1002/cne.903530306

Tanaka KZ, Pevzner A, Hamidi AB, Nakazawa Y, Graham J, Wiltgen BJ (2014) Cortical representations are reinstated by the hippocampus during memory retrieval. Neuron 84:347-354. doi: 10.1016/j.neuron.2014.09.037

Taube JS, Muller RU, Ranck JB, Jr. (1990) Head-direction cells recorded from the postsubiculum in freely moving rats. I. Description and quantitative analysis. J Neurosci 10:420-435.

Tessier-Lavigne M, Placzek M, Lumsden AG, Dodd J, Jessell TM (1988) Chemotropic guidance of developing axons in the mammalian central nervous system. Nature 336:775-778. doi: 10.1038/336775a0

Tocker G, Barak O, Derdikman D (2015) Grid cells correlation structure suggests organized feedforward projections into superficial layers of the medial entorhinal cortex. Hippocampus 25:1599-1613. doi: 10.1002/hipo.22481

Todd TP, Meyer HC, Bucci DJ (2015) Contribution of the retrosplenial cortex to temporal discrimination learning. Hippocampus 25:137-141. doi: 10.1002/hipo.22385

Tsao A, Moser MB, Moser EI (2013) Traces of experience in the lateral entorhinal cortex. Curr Biol 23:399-405. doi: 10.1016/j.cub.2013.01.036

Uchizono K (1965) Characteristics of excitatory and inhibitory synapses in the central nervous system of the cat. Nature 207:642-643.

Van Cauter T, Poucet B, Save E (2008) Delay-dependent involvement of the rat entorhinal cortex in habituation to a novel environment. Neurobiol Learn Mem 90:192-199. doi: 10.1016/j.nlm.2008.03.001

Van Cauter T, Camon J, Alvernhe A, Elduayen C, Sargolini F, Save E (2013) Distinct roles of medial and lateral entorhinal cortex in spatial cognition. Cereb Cortex 23:451-459. doi: 10.1093/cercor/bhs033

Van Essen DC (2013) Cartography and connectomes. Neuron 80:775-790. doi: 10.1016/j.neuron.2013.10.027

Van Essen DC, Maunsell JH (1980) Two-dimensional maps of the cerebral cortex. J Comp Neurol 191:255-281. doi: 10.1002/cne.901910208

van Groen T, Wyss JM (1990a) The connections of presubiculum and parasubiculum in the rat. Brain Res 518:227-243.

van Groen T, Wyss JM (1990b) The postsubicular cortex in the rat: characterization of the fourth region of the subicular cortex and its connections. Brain Res 529:165-177.

van Groen T, Wyss JM (1990c) Connections of the retrosplenial granular a cortex in the rat. J Comp Neurol 300:593-606. doi: 10.1002/cne.903000412

van Groen T, Wyss JM (1990d) Extrinsic projections from area CA1 of the rat hippocampus: olfactory, cortical, subcortical, and bilateral hippocampal formation projections. J Comp Neurol 302:515-528. doi: 10.1002/cne.903020308
van Groen T, Wyss JM (1992) Connections of the retrosplenial dysgranular cortex in the rat. J Comp Neurol 315:200-216. doi: 10.1002/cne.903150207
van Groen T, Wyss JM (2003) Connections of the retrosplenial granular b cortex in the rat. J Comp Neurol 463:249-263. doi: 10.1002/cne.10757
van Groen T, Kadish I, Wyss JM (2004) Retrosplenial cortex lesions of area Rgb (but not of area Rga) impair spatial learning and memory in the rat. Behav Brain Res 154:483-491. doi: 10.1016/j.bbr.2004.03.016

S0166432804001123 [pii]
van Haeften T, Jorritsma-Byham B, Witter MP (1995) Quantitative morphological analysis of subicular terminals in the rat entorhinal cortex. Hippocampus 5:452-459. doi: 10.1002/hipo.450050507
van Haeften T, Wouterlood FG, Jorritsma-Byham B, Witter MP (1997) GABAergic presubicular projections to the medial entorhinal cortex of the rat. J Neurosci 17:862-874.
van Haeften T, Baks-te-Bulte L, Goede PH, Wouterlood FG, Witter MP (2003) Morphological and numerical analysis of synaptic interactions between neurons in deep and superficial layers of the entorhinal cortex of the rat. Hippocampus 13:943-952. doi: 10.1002/hipo.10144
van Strien NM, Cappaert NL, Witter MP (2009) The anatomy of memory: an interactive overview of the parahippocampal-hippocampal network. Nat Rev Neurosci 10:272-282. doi: nrn2614 [pii]

10.1038/nrn2614
Vanderhaeghen P, Lu Q, Prakash N, Frisen J, Walsh CA, Frostig RD, Flanagan JG (2000) A mapping label required for normal scale of body representation in the cortex. Nat Neurosci 3:358-365. doi: 10.1038/73929
Vann SD, Aggleton JP (2002) Extensive cytotoxic lesions of the rat retrosplenial cortex reveal consistent deficits on tasks that tax allocentric spatial memory. Behav Neurosci 116:85-94.
Vann SD, Aggleton JP (2004) Testing the importance of the retrosplenial guidance system: effects of different sized retrosplenial cortex lesions on heading direction and spatial working memory. Behav Brain Res 155:97-108. doi: 10.1016/j.bbr.2004.04.005

S0166432804001329 [pii]
Vann SD, Aggleton JP (2005) Selective dysgranular retrosplenial cortex lesions in rats disrupt allocentric performance of the radial-arm maze task. Behav Neurosci 119:1682-1686. doi: 10.1037/0735-7044.119.6.1682
Vann SD, Aggleton JP, Maguire EA (2009) What does the retrosplenial cortex do? Nature reviews Neuroscience 10:792-802. doi: nrn2733 [pii]

10.1038/nrn2733
Vann SD, Kristina Wilton LA, Muir JL, Aggleton JP (2003) Testing the importance of the caudal retrosplenial cortex for spatial memory in rats. Behav Brain Res 140:107-118. doi: S0166432802002747 [pii]
Veenman CL, Reiner A, Honig MG (1992) Biotinylated dextran amine as an anterograde tracer for single- and double-labeling studies. J Neurosci Methods 41:239-254.
Vogt B, Vogt L, Farber NB (2004) Cingulate cortex and disease models. In: The Rat Nervous System, 3rd ed Edition (Paxinos G, ed), pp 705-727. San Diego, CA: Elsevier Academic Press.
Vogt BA (2015) Chapter 3 - Architecture, Neurocytology and Comparative Organization of Monkey and Human Cingulate Cortices. In: The Rat Nervous System (Fourth Edition) (Paxinos G, ed), pp 66-91. San Diego: Academic Press. doi: http://dx.doi.org/10.1016/B978-0-12-374245-2.00021-8
Vogt BA, Miller MW (1983) Cortical connections between rat cingulate cortex and visual, motor, and postsubicular cortices. J Comp Neurol 216:192-210. doi: 10.1002/cne.902160207
Vogt BA, Rosene DL, Peters A (1981) Synaptic termination of thalamic and callosal afferents in cingulate cortex of the rat. J Comp Neurol 201:265-283. doi: 10.1002/cne.902010210

Wang Q, Henry AM, Harris JA, Oh SW, Joines KM, Nyhus J, Hirokawa KE, Dee N, Mortrud M, Parry S, Ouellette B, Caldejon S, Bernard A, Jones AR, Zeng H, Hohmann JG (2014) Systematic comparison of adeno-associated virus and biotinylated dextran amine reveals equivalent sensitivity between tracers and novel projection targets in the mouse brain. J Comp Neurol 522:1989-2012. doi: 10.1002/cne.23567

Warburton EC, Brown MW (2015) Neural circuitry for rat recognition memory. Behav Brain Res 285:131-139. doi: 10.1016/j.bbr.2014.09.050

Wernicke C (1874) Der aphasische Symptomencomplex. Breslau: Max Cohn & Weigert.

Whishaw IQ, Maaswinkel H, Gonzalez CL, Kolb B (2001) Deficits in allothetic and idiothetic spatial behavior in rats with posterior cingulate cortex lesions. Behav Brain Res 118:67-76. doi: S0166-4328(00)00312-0 [pii]

White JG, Southgate E, Thomson JN, Brenner S (1986) The structure of the nervous system of the nematode Caenorhabditis elegans. Philos Trans R Soc Lond B Biol Sci 314:1-340.

Whitlock JR, Pfuhl G, Dagslott N, Moser MB, Moser EI (2012) Functional split between parietal and entorhinal cortices in the rat. Neuron 73:789-802. doi: 10.1016/j.neuron.2011.12.028

Wik G, Fischer H, Finer B, Bragee B, Kristianson M, Fredrikson M (2006) Retrospenial cortical deactivation during painful stimulation of fibromyalgic patients. The International journal of neuroscience 116:1-8. doi: 10.1080/00207450690962208

Wilson DI, Langston RF, Schlesiger MI, Wagner M, Watanabe S, Ainge JA (2013) Lateral entorhinal cortex is critical for novel object-context recognition. Hippocampus 23:352-366. doi: 10.1002/hipo.22095

Witter MP (2006) Connections of the subiculum of the rat: topography in relation to columnar and laminar organization. Behav Brain Res 174:251-264. doi: 10.1016/j.bbr.2006.06.022

Witter MP, Amaral DG (2004) Hippocampal Formation. In: The Rat Nervous System (Paxinos G, ed), pp 637-703: Elsevier Academic Press.

Witter MP, Chan-Palay V, Köhler C (1989) Connectivity of the rat hippocampus. In: The Hippocampus-New Vistas, pp 53-69. New York: Allen R. Liss.

Witter MP, Naber PA, van Haeften T, Machielsen WC, Rombouts SA, Barkhof F, Scheltens P, Lopes da Silva FH (2000) Cortico-hippocampal communication by way of parallel parahippocampal-subicular pathways. Hippocampus 10:398-410. doi: 10.1002/1098-1063(2000)10:4<398::AID-HIPO6>3.0.CO;2-K

Wouterlood FG, Boekel AJ, Kajiwara R, Belien JA (2008) Counting contacts between neurons in 3D in confocal laser scanning images. J Neurosci Methods 171:296-308. doi: 10.1016/j.jneumeth.2008.03.014

Wouterlood FG, van Haeften T, Eijkhoudt M, Baks-Te Bulte LT, Goede PH, Witter MP (2004) Input from the presubiculum to dendrites of layer-V neurons of the medial entorhinal cortex of the rat. Brain Research 1013:1-12.

Wright NF, Erichsen JT, Vann SD, O'Mara SM, Aggleton JP (2010) Parallel but separate inputs from limbic cortices to the mammillary bodies and anterior thalamic nuclei in the rat. J Comp Neurol 518:2334-2354. doi: 10.1002/cne.22336

Wyss JM, Van Groen T (1992) Connections between the retrosplenial cortex and the hippocampal formation in the rat: a review. Hippocampus 2:1-11. doi: 10.1002/hipo.450020102

Yartsev MM, Witter MP, Ulanovsky N (2011) Grid cells without theta oscillations in the entorhinal cortex of bats. Nature 479:103-107. doi: 10.1038/nature10583

Young CK, McNaughton N (2009) Coupling of theta oscillations between anterior and posterior midline cortex and with the hippocampus in freely behaving rats. Cereb Cortex 19:24-40. doi: 10.1093/cercor/bhn055

Zgraggen E, Boitard M, Roman I, Kanemitsu M, Potter G, Salmon P, Vutskits L, Dayer AG, Kiss JZ (2012) Early postnatal migration and development of layer II pyramidal neurons in the rodent cingulate/retrosplenial cortex. Cereb Cortex 22:144-157. doi: 10.1093/cercor/bhr097

Zhou R (1997) Regulation of topographic projection by the Eph family receptor Bsk (EphA5) and its ligands. Cell Tissue Res 290:251-259.

Zhu S, Lin S, Kao CF, Awasaki T, Chiang AS, Lee T (2006) Gradients of the Drosophila Chinmo BTB-zinc finger protein govern neuronal temporal identity. Cell 127:409-422. doi: 10.1016/j.cell.2006.08.045

frontiers in
NEUROINFORMATICS

REVIEW ARTICLE
published: 27 July 2011
doi: 10.3389/fninf.2011.00007

The retrosplenial cortex: intrinsic connectivity and connections with the (para)hippocampal region in the rat. An interactive connectome

Jørgen Sugar[1], Menno P. Witter[1], Niels M. van Strien[2†] and Natalie L. M. Cappaert[3*†]

[1] *Kavli Institute for Systems Neuroscience, Centre for the Biology of Memory, Faculty of Medicine, Norwegian University of Science and Technology, Trondheim, Norway*
[2] *FMRI-group, Department of Circulation and Medical Imaging, Faculty of Medicine, Norwegian University of Science and Technology, Trondheim, Norway*
[3] *Center for NeuroScience, Swammerdam Institute for Life Science, University of Amsterdam, Netherlands*

Edited by:
Trygve B. Leergaard, University of Oslo, Norway

Reviewed by:
Rebecca D. Burwell, Brown University, USA
Mihail Bota, University of Southern California, USA
Andreas H. Burkhalter, Washington University School of Medicine, USA

****Correspondence:***
Natalie L. M. Cappaert, SILS – Center for NeuroScience, University of Amsterdam, Science Park 904, 1098 XH Amsterdam, Netherlands.
e-mail: correspondence@temporal-lobe.com

†Niels M. van Strien and Natalie L. M. Cappaert shared last authorship.

A connectome is an indispensable tool for brain researchers, since it quickly provides comprehensive knowledge of the brain's anatomical connections. Such knowledge lies at the basis of understanding network functions. Our first comprehensive and interactive account of brain connections comprised the rat hippocampal–parahippocampal network. We have now added all anatomical connections with the retrosplenial cortex (RSC) as well as the intrinsic connections of this region, because of the interesting functional overlap between these brain regions. The RSC is involved in a variety of cognitive tasks including memory, navigation, and prospective thinking, yet the exact role of the RSC and the functional differences between its subdivisions remain elusive. The connectome presented here may help to define this role by providing an unprecedented interactive and searchable overview of all connections within and between the rat RSC, parahippocampal region and hippocampal formation.

Keywords: connectivity, retrosplenial cortex, hippocampal formation, parahippocampal region, interactive, connectome, tract tracing

INTRODUCTION

A connectome is a comprehensive description of the network elements and connections that form the brain (Sporns et al., 2005). Such clear and comprehensive knowledge of anatomical connections lies at the basis of understanding network functions (Crick and Koch, 2003). For example, the existence of a connection between two brain regions ascertains that information transfer can occur. Likewise, when inputs from different brain regions converge onto another region, this can be interpreted as an anatomical substrate for information integration (Sporns and Tononi, 2007). Here, we review the current state of the art knowledge on connectivity of the rat retrosplenial cortex (RSC) with the hippocampal–parahippocampal region (HF–PHR). Apart from this written account, the results will be presented graphically in a comprehensive, interactive, and searchable connectome.

The RSC is the most caudal subdivision of the strip of cortex around the corpus callosum that is generally referred to as the cingulate cortex. In primates, the cingulate cortex is subdivided into an anterior and a posterior part and the most caudoventral subdivision of the posterior cingulate cortex is called RSC, whereas in rodents the RSC comprises the entire posterior cingulate cortex (Vogt and Peters, 1981). Compared to well-investigated brain regions such as the hippocampus, relatively little research has been carried out on the anatomy and functions of the RSC. Recently, discoveries that suggest an important role for the RSC in cognitive functions have sparked increased interest in its anatomy and functions. In humans, the RSC is activated in (autobiographical) memory tasks, navigation, and prospective thinking (Vann et al., 2009). These cognitive functions are also known to be affected in patients with RSC lesions, in whom topographical disorientation and learning deficits are commonly observed (Maguire, 2001). Additional evidence for the involvement of the RSC in cognitive functions stems from the observation that the RSC is a component of the so-called default mode network. The default mode network is an interconnected system of brain regions, involving the lateral and medial parietal areas, the medial frontal and medial temporal lobe region, and the RSC (Buckner et al., 2008; Greicius et al., 2009). This network of brain regions is not only active during retrieval of autobiographical memories, but also when an individual is not focused on the outside world and instead is performing internal tasks such as daydreaming, envisioning the future, retrieving memories, and probing emotions and actions of others (Buckner et al., 2008). Although the function of the default mode network and the role of the RSC within it remains elusive, it has been argued that the RSC plays an active part in memory retrieval and visualization of memories (Greicius et al., 2009).

The cognitive functions in which the RSC is engaged show a striking similarity with those that engage the medial temporal lobe system; a system that comprises the HF–PHR. The loss of cognitive capabilities as seen in patients with RSC lesions is remarkably similar to those seen in patients with HF–PHR damage (Scoville and Milner, 1957; Henderson et al., 1989; Reed and Squire, 1997; Maguire, 2001). Furthermore, in Alzheimer's disease, both HF–PHR as well as RSC show progressive atrophy (Villain et al., 2008; Raji et al., 2009; Pengas et al., 2010).

As in humans, the RSC of rats is thought to be important for a variety of cognitive tasks. RSC lesions impair performance in spatial memory tasks (Sutherland et al., 1988), allocentric working memory tasks (Vann and Aggleton, 2004), egocentric memory tasks (Cooper and Mizumori, 1999; Whishaw et al., 2001), and tasks in which animals have to detect if a spatial arrangement is novel or familiar (Vann and Aggleton, 2002). Particularly within the field of spatial learning and memory, functional attributes of the RSC show a large overlap with those of HF–PHR. The presence of so called head direction cells in the RSC, which have been implicated in navigation, provides strong support to the notion that the RSC has a role in spatial cognition (Chen et al., 1994; Muller et al., 1996; Cho and Sharp, 2001). Head direction cells fire when the animal's head points in a specific direction, and such neurons are also present in a number of subdivisions of PHR, in particular in the presubiculum, parasubiculum, and entorhinal cortex (Boccara et al., 2010). These three areas of PHR are reciprocally connected with RSC and in addition, they receive input from CA1 (Cornu Ammonis; see Nomenclature of HF and PHR) and subiculum (Insausti et al., 1997; Naber et al., 2001; Jones and Witter, 2007), which are both involved in navigation (O' Keefe and Dostrovsky, 1971; Sharp and Green, 1994). The RSC also receives direct input from CA1 and subiculum (Vogt and Miller, 1983; Van Groen and Wyss, 1990b, 1992, 2003; Insausti et al., 1997).

The functional relevance of the RSC and the striking overlap with the functional connotations attributed to HF–PHR strongly suggests a functional relationship between these areas. Knowledge about the connectome that underlies this relationship is relevant, but presently not available in an accessible format. In this review, all reported anatomical connections within the RSC and between the RSC and the HF–PHR in the rat are presented. The general patterns of connectivity will be presented in a condensed written form and specific connection patterns will be highlighted to evaluate possible functional implications. Additionally, all published connections between the RSC and HF–PHR and the intrinsic connectivity of the RSC were integrated in the already published interactive diagram of all published connections of the rat HF–PHR (Van Strien et al., 2009). The current version of the interactive and now searchable diagram, represents without doubt the fullest and most detailed account ever of the brain connections between the HF, PHR, and RSC. We hope that this contribution will help to further understanding of the functional interactions between those brain structures.

MATERIALS AND METHODS

NOMENCLATURE OF THE RSC

Multiple definitions and nomenclatures for the rat cortical mantle exist. Krieg (1946) was the first to delineate the RSC in the rat, based on the anatomical account of Brodmann, who subdivided the RSC in rabbit and named it area (A)29 (Brodmann, 1909). For this review, the nomenclature as described by Vogt et al. (2004) is followed. According to this definition, the rat RSC is subdivided into four areas referred to as A29a, A29b, A29c, and A30. Most of the connectional papers do not separate A29a from A29b and the combined region will be referred to as A29ab in this paper (**Figure 1**). Where necessary, we converted the original nomenclature used in individual papers into the nomenclature of Vogt. For this purpose, a "Rosetta table" was created, which allows easy conversion between different nomenclatures of the RSC (**Table 1**).

DELINEATION OF RSC

The RSC is a neocortical structure situated in the midline of the cerebrum. It arches around the dorsocaudal half of the corpus callosum in the rat, where it is bordered rostrally by the anterior cingulate cortex, caudoventrally by the PHR and laterally by the parietal and visual cortices. The coordinate system that defines position within the RSC is explained in **Figure 1**. The delineation of the subareas of RSC is based on cytoarchitectonic features (**Figure 2**). A29a is the most ventral subdivision and it differs from the dorsally adjacent A29b since it lacks a fully differentiated layered structure. Cytoarchitectonically, A29a has a homogenous layer II/III, while in A29b this layer is divided into a thin superficial densely packed zone and a less dense deeper zone (Vogt and Peters, 1981). A29a and A29b are distinguished from A29c most strikingly in layer III, which in A29ab has cells arranged in bands parallel to the pial surface, while in A29c layer III is thinner and the pyramidal cell bodies are randomly spaced (Van Groen and Wyss, 1990b). An additional way to compare sub-regions is by looking at chemoarchitectonic features. A29ab shows parvalbumin stained cells in layers II, V, and VI, which are not as apparent in A29c (Jones et al., 2005). In AChE stained sections A29c layer IV shows a widening and increased strength of AChE staining compared to layer IV of A29b (Vogt and Peters, 1981; Sripanidkulchai and Wyss, 1987; Van Groen and Wyss, 1990b; Jones et al., 2005). Cytoarchitectonically, A30 shows an abrupt widening and a less dense packing of layer II/III compared to A29b and A29c (Vogt and Peters, 1981; Sripanidkulchai and Wyss, 1987; Van Groen and Wyss, 1992; Jones et al., 2005). Also, A30 layer IV is wider than in A29b/A29c and A30 layer V neuronal cell bodies tend to be larger (Krieg, 1946; Van Groen and Wyss, 1992). In AChE stained sections, layer I–IV of A30 are evenly and darkly stained (Van Groen and Wyss, 1992), whereas in A29c superficial and deep parts of layer I and layer IV are most densely stained (Sripanidkulchai and Wyss, 1987).

NOMENCLATURE OF HF AND PHR

The HF is a C-shaped structure situated bilaterally in the caudal part of the brain. It is subdivided into the dentate gyrus (DG), the Cornu Ammonis (subdivided into CA3, CA2, and CA1), and the subiculum (Sub). The HF consists of three layers, a deep polymorph layer, a more superficial cell layer and on the outside a molecular layer that is almost devoid of neurons. The deep layer is called hilus in the DG and stratum oriens in CA and is not really differentiated in Sub. In DG the cell layer consists of granule cell bodies. In CA and Sub, the cell layer contains pyramidal cells. The superficially positioned molecular layer in DG and Sub is not further subdivided, whereas in CA3, it is divided into three sub-layers: stratum lucidum, stratum radiatum, and stratum lacunosum-moleculare. The lamination of CA2 and CA1 is the same, with the exception that the stratum lucidum is missing.

The PHR borders HF caudally and medially. It is subdivided into the presubiculum (PrS), the parasubiculum (PaS), the entorhinal cortex (EC), further subdivided into the medial and lateral

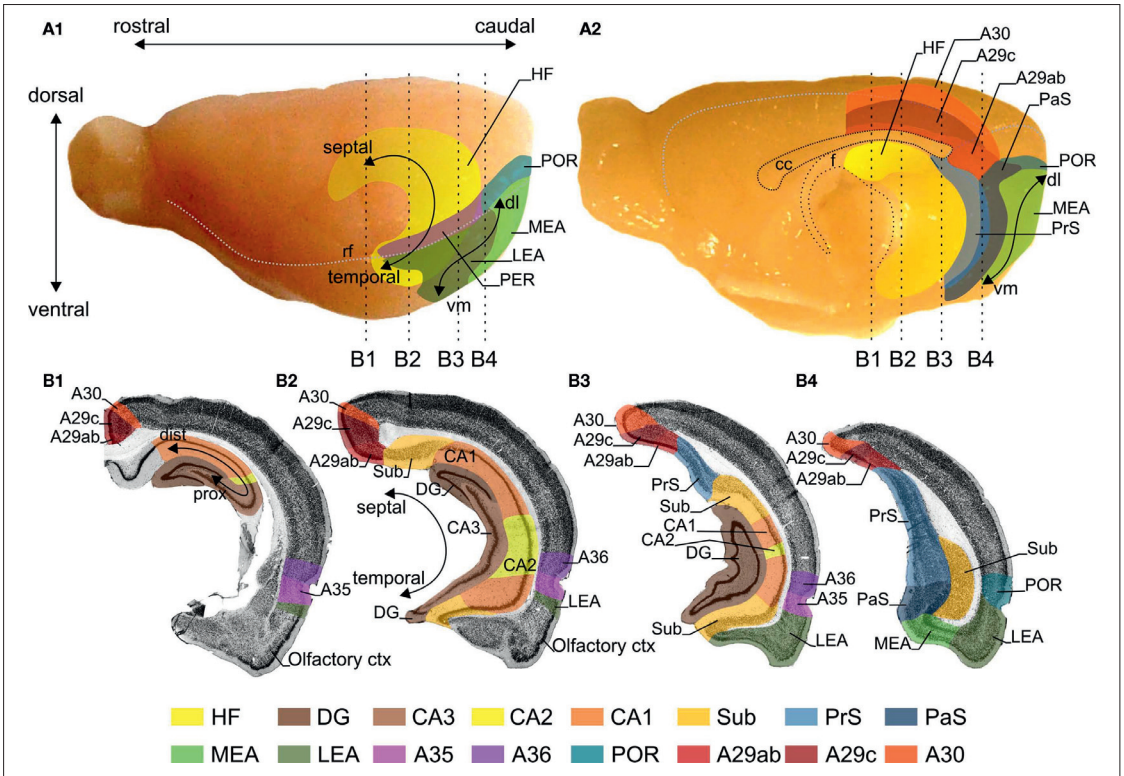

FIGURE 1 | Representations of the retrosplenial cortex (RSC), hippocampal formation (HF) and the parahippocampal region (PHR) in the rat brain. Lateral **(A1)** and midsagittal **(A2)** views of the rat brain. The RSC is subdivided into A29ab, A29c, and A30. For orientation a rostrocaudal and dorsoventral axis is indicated **(A1)**. The HF consists of the dentate gyrus (DG), CA3, CA2, CA1, and the subiculum (Sub). The PHR is subdivided into the presubiculum (PrS), parasubiculum (PaS), the entorhinal cortex, which has a lateral (LEA) and a medial (MEA) subdivision, the perirhinal cortex (PER; consisting of Brodmann areas (A)35 and A36) and the postrhinal cortex (POR). For orientation in HF the long or septotemporal axis is used [also referred to as the dorsoventral axis; **(A1,B2)**]. Another commonly used axis is referred to as the proximodistal axis which indicates a position closer to DG or closer to PHR, respectively **(B1)**. The main axis applied in case of PrS and PaS is also the septotemporal axis, in PER and POR a rostrocaudal axis and in the entorhinal cortex is a dorsolateral-to-ventromedial axis [dl and vm; **(A1,A2)**]. The dashed vertical lines in panels **(A1,A2)** indicate the levels of four coronal sections **(B1–B4)**, which are shown in **(B)**. The gray stippled line in **(A1)** represents the position of the rhinal fissure (rf) and in **(A2)** they represent the global delineation from the dorsal surface of the brain with the midsagittal and occipital surfaces. **(B)** Four coronal sections of the rat brain; the levels of these sections are indicated in **(A)**. The subfields of the HF, PHR and RSC are color-coded, see color panel below **(B)**.

entorhinal area (MEA and LEA respectively), the perirhinal cortex (PER; divided into Brodmann's areas 35 and 36) and the postrhinal cortex (POR). The PHR is generally described as having six layers. The delineation and the HF–PHR connections are extensively described in earlier publications (Witter and Amaral, 2004; Van Strien et al., 2009). The coordinate system that defines position within the HF and the PHR is explained in **Figure 1**.

DATA COLLECTION AND VISUALIZATION

A search was performed on publications reporting tract-tracing studies on intrinsic RSC and RSC – HF–PHR connections in PubMed[1] and Embase[2] (see www.temporal-lobe.com for queries). The following inclusion criteria were used: (1) tract-tracing studies or studies which report intracellular filling of single cells; (2) studies which used healthy, genetically un-altered, untreated adult rats were included; (3) publications written or translated into English or in a language using roman print. The database queries retrieved 816 papers of which 46 contained relevant information. The connectional information was retrieved from these papers, including information from tables and figures, using the following criteria: (1) it was clear where anterogradely filled terminals or retrogradely labeled cell bodies were located; (2) the location of the injection site was clearly described; (3) injection sites did not include multiple brain areas or fiber bundles; (4) lesion studies were discarded; (5) explicitly reported non-excitatory projections were excluded; (6) contralateral projections were excluded. The information about these connections was stored in a custom-made relational database

[1]www.PubMed.gov
[2]www.embase.com

Table 1 | Comparison of nomenclatures of the retrosplenial cortex (RSC).

Vogt et al. (2004)	Brodmann (1909)†	Rose (1927)‡	Krieg (1946)	Rose and Woolsey (1948)†	
A30	A29d	RSag (rostral and intermediate A30)	29c	Area cingularis	
A29c	A29c	RSgβ (caudal A30 and A29c)	29b	Area cingularis	
A29ab		RSgα		Retrosplenial area	
A29b	A29b				
A29a	A29a				
Vogt et al. (2004)	**Meibach and Siegel (1977)**	**Krettek and Price (1977)§**	**Sripanidkulchai and Wyss (1987)**	**Van Groen and Wyss (1992)**	**Shibata (1994)**
A30	RSAG	RsAg	Rag	Rdg	RSA
A29c	RSGd	RsG	Rgb	Rgb	RSG
A29ab	RSGv	RsG	Rga	Rga	RSG
A29b					
A29a					
Vogt et al. (2004)	**Zilles and Wree (1995)**	**Burwell and Amaral (1998)**	**Jones et al. (2005)**	**Shibata et al. (2009)**	
A30	RSA	RSPd	Rostral and intermediate Rsd	29d	
A29c	RSG	RSPv	RSv-b	29c	
A29ab	RSG		RSv-a and caudal RSd		
A29b				29b	
A29a				29a	

In the present paper, RSC is subdivided into A29a, A29b, A29c, and A30 according to Vogt et al. (2004).
†Rabbit.
‡Mouse.
§Nomenclature described in Zilles and Wree (1995).
Rose (1927): RSag, retrosplenialis agranaluris; RSgβ, retrosplenialis granularis dorsalis; RSgα, retrosplenialis granularis ventralis; Meibach and Siegel (1977): RSAG, retrosplenialis agranularis; RSGd, retrosplenialis granularis dorsalis; RSGv, retrosplenialis granularis ventralis; Krettek and Price (1977): RsAg, agranular retrosplenial area; RsG, granular retrosplenial area; Sripanidkulchai and Wyss (1987): Rag, retrosplenial agranular cortex; Rgb, retrosplenial granular cortex b; Rga, retrosplenial granular cortex a; Van Groen and Wyss (1992):Rdg, retrosplenial dysgranular cortex; Rgb, retrosplenial granular b cortex; Rga, retrosplenial granular a cortex; Shibata (1994): RSA, retrosplenial agranular area; RSG, retrosplenial granular area; Zilles and Wree (1995):RSA, agranular retrosplenial cortex; RSG, granular retrosplenial cortex; Burwell and Amaral (1998): RSPd, dorsal retrosplenial area; RSPv, ventral retrosplenial area; Jones et al. (2005): RSd, dorsal retrosplenial cortex; RSv-b, ventral retrosplenial cortex dorsal part; RSv-a, ventral retrosplenial cortex ventral part.

(Microsoft Access; Microsoft Corporation, WA, USA). Before data was entered into this database, the accuracy was verified by at least two of the authors.

Next, results from independent retrograde and anterograde experiments were combined, such that both the layers of origin and termination could be determined. The connections were added to the existing HF–PHR connectome (Van Strien et al., 2009) which was drawn in Visio (Microsoft Corporation, WA, USA) and exported to PDF (Adobe Acrobat Pro; Adobe Systems Inc., CA, USA), see **Figure 3** for an overview of the connectome. In total, the database now includes 223 references in 710 records, describing approximately 2600 connections. Compared to the initial interactive connectome, the usability of the current version is improved by adding a search dialog, help section and a tutorial, developed using AcroDialogs and AcroButtons (Windjack Solutions, Inc., OR, USA). Updated and extended support information (e.g., manual, references, and RSC nomenclature) is available on http://www.temporal-lobe.com.

RESULTS

In the following section, the intrinsic connections between RSC subdivisions and connections between RSC subdivisions and the HF and PHR are summarized in a condensed written form (for a condensed overview see **Table 2**). These connections are also visually presented in the interactive connectome (Supplementary Material).

CONNECTIONS WITHIN RSC

A29a and A29b

Intrinsic projections are those confined to a defined cytoarchitectonic subarea. In case of A29a and A29b, reports either describe those separately or the two areas have been combined into one A29ab. We therefore deal with the two areas in this section together. The intrinsic projections of A29a originate in layer III–VI and terminate in layers I, II, III, and V. Those of A29b follow a rostral-to-rostral and a caudal-to-caudal pattern. Rostral projections originate in layers II, III, V, and VI and terminate rostrally in all layers. Caudal

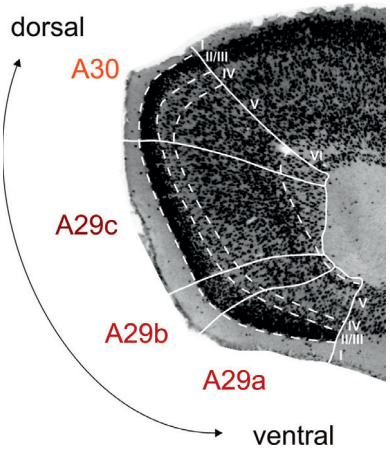

FIGURE 2 | Cytoarchitecture of rat retrosplenial cortex (RSC). Photomicrograph of a coronal section stained for NeuN (high power image taken from the section shown in **Figure 1B2**), illustrating the cytoarchitectonic characteristics of A29a, A29b, A29c, and A30. A29a has a homogenous layer II/III and lacks fully differentiated deep layers. In A29b layer II/III is divided into a thin superficial densely packed zone and a less dense deeper zone. A29c has a more differentiated layer V and a more equally dense layer II/III compared to A29b and a thinner layer IV compared to A30. A30 shows a widening and a less dense packing of layer II/III and layer V neuronal cell bodies tend to be larger. Layer VI is mostly developed in A30 and A29c and almost absent in A29a and b (for more details see Vogt et al., 2004; Jones et al., 2005).

projections terminate caudally in layers I, II, III, and V (Shibata et al., 2009). The A29a projection to rostral and caudal A29b originates in all cell layers and terminates in layers I, II, III, and V (Shibata et al., 2009). Caudal A29b projects to caudal A29a and rostral A29b projects to rostral A29a and the projections originate in all cell layers and terminate in layers I, II, III, and V (Shibata et al., 2009). The terminal patterns, when combined, are essentially in line with the reported terminal distribution in layers I, III, V, and VI for the combined area A29ab (Van Groen and Wyss, 1990b; Jones et al., 2005; Miyashita and Rockland, 2007).

Both A29a and A29b project to the entire rostrocaudal extent of A29c (Vogt and Miller, 1983; Shibata et al., 2009). Projections that arise from layer V of caudal A29a terminate in layers I, II, III, and VI of the intermediate rostrocaudal and caudal parts of A29c. Rostral A29b projects to rostral and intermediate rostrocaudal A29c, and caudal A29b projects to caudal A29c. Projections originate in layers II, III, V, and VI and terminate in all layers of A29c. When described together (Van Groen and Wyss, 1990b, 2003; Jones et al., 2005; Miyashita and Rockland, 2007), the only striking deviation from the combined separate patterns is that the terminal distribution of the projection from A29ab to rostral A29c is restricted to layers II and III (Van Groen and Wyss, 1990b).

Neurons in layers V and VI of the caudal part of A29a project to caudal levels of A30, terminating in layers I, II, III, and V (Shibata et al., 2009). In case of A29b these projections arise from the entire rostrocaudal extent, but also target caudal portions of A30, showing the same laminar distribution as those of A29a (Vogt and Miller, 1983; Shibata et al., 2009). In line with these observations, the projections from A29ab originate caudally in layer VI and more rostrally in layers III–V projecting to the midrostrocaudal portion of A30 (Van Groen and Wyss, 1990b, 1992; Jones et al., 2005).

A29c

The intrinsic connections of A29c arise from the entire rostrocaudal extent and project to the entire rostrocaudal extent (Vogt and Miller, 1983; Van Groen and Wyss, 2003; Jones et al., 2005; Miyashita and Rockland, 2007; Shibata et al., 2009). These projections originate in layers II, III, V, and VI and terminate in layers I–V. Projections from A29c to caudal A29a exist (Shibata et al., 2009) and the caudal and midrostrocaudal origin is in layer V and that of the rostrally originating projections in layers V and VI. The projections from A29c to A29ab or A29b arise from the entire rostrocaudal extent and project to the entire rostrocaudal extent (Van Groen and Wyss, 1990b, 2003; Jones et al., 2005; Miyashita and Rockland, 2007; Shibata et al., 2009). Rostrally, projections arise from layers V and VI, whereas in caudal A29c projections arise from layers II, III, V, and VI. Termination of these projections in A29b occurs in layers I, II, III, and V. The projection from A29c to A30 originates and terminates in all layers (Vogt and Miller, 1983; Sripanidkulchai and Wyss, 1987; Audinat et al., 1988; Van Groen and Wyss, 1992, 2003; Jones et al., 2005; Shibata et al., 2009). A topographical organization is present, such that rostral A29c projects to rostral and mid-rostrocaudal A30 and caudal A29c projects to the entire rostrocaudal extent of A30.

A30

The intrinsic connections of A30 arise from the entire rostrocaudal extent and project to the entire rostrocaudal extent, whereby layers II–VI project to all layers (Vogt and Miller, 1983; Audinat et al., 1988; Van Groen and Wyss, 1992; Jones et al., 2005; Shibata et al., 2009). Projections to A29a arise from the entire rostrocaudal extent of A30 and terminate caudally (Vogt and Miller, 1983; Shibata et al., 2009). At rostral and intermediate rostrocaudal levels, the projections originate in layer V, whereas caudally the projections arise from layer II–VI. A30 also projects to A29b (Vogt and Miller, 1983; Shibata et al., 2009). This projection arises rostrally from layers V and VI and caudally from layers II–VI. Termination in A29b occurs in layers I, II, III, and V. The caudal and midrostrocaudal projections of A30 to A29ab terminate in all layers (Van Groen and Wyss, 1992; Jones et al., 2005). A30 projects to A29c and the projection does not show a topographical rostrocaudal organization. Projections arise from layers II, III, V, and VI and terminate in all layers of A29c (Vogt and Miller, 1983; Van Groen and Wyss, 1992, 2003; Jones et al., 2005; Shibata et al., 2009).

RSC PROJECTIONS TO THE PHR

A29a and A29b

A29ab projects to all subdivisions of PHR. Dense projections exist from A29ab to PrS (Van Groen and Wyss, 1990a,b,d; Shibata, 1994; Jones and Witter, 2007). More specifically, layers II and V of A29ab target PrS layers I, III, V, and VI. The A29ab projection to PrS is topographically organized, such that caudal A29ab targets the entire septotemporal extent of PrS, whereas rostral A29ab targets septal PrS only. The projection to PaS originates in layers II, III,

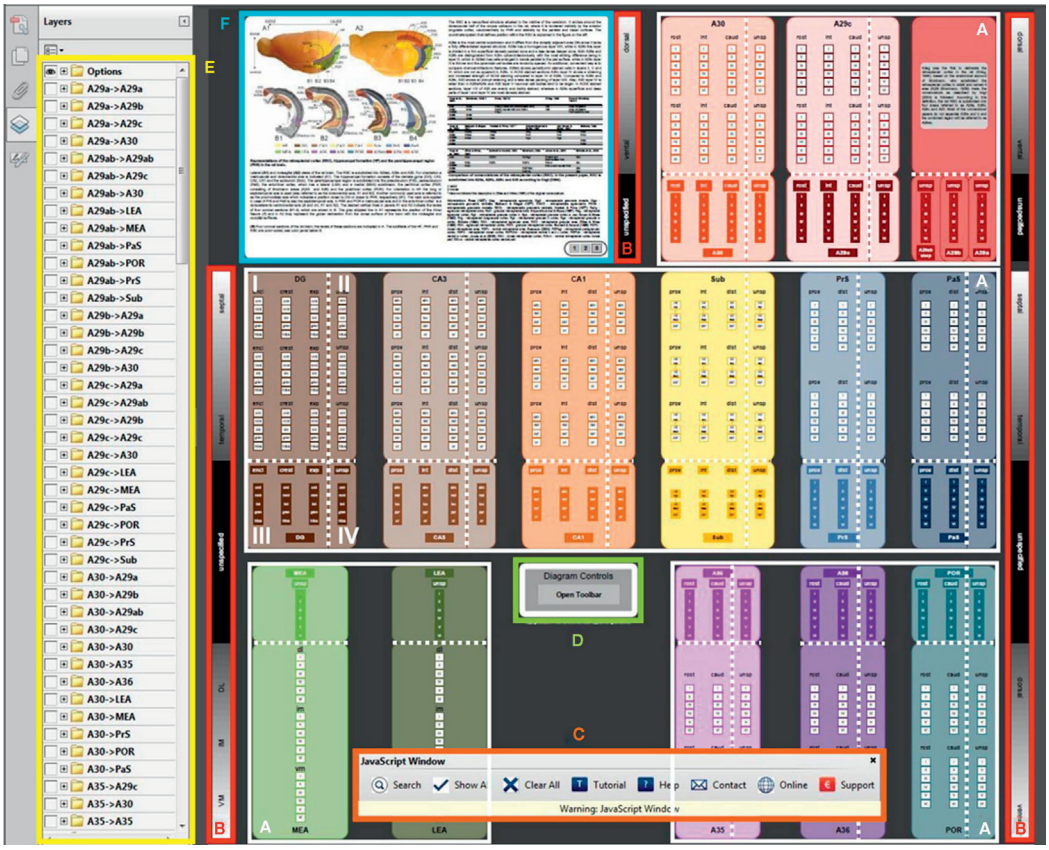

FIGURE 3 | Retrosplenial and hippocampal–parahippocampal connectome. The connectome (see ratbrain_connectome.pdf in Supplementary Material) consists of 14 large, color-coded boxes, which represent the sub-regions of the hippocampal formation, parahippocampal region, and retrosplenial cortex. In this figure, the user interface elements of the connectome are indicated with color-coded outlines and their meaning/purpose is explained. **(A)** In the white outlines, the 14 anatomical sub-regions are displayed. **(B)** The 14 anatomical sub-regions are three-dimensionally organized. However, the origin and termination of connections are not always described in full detail in the literature. Therefore, area boxes are divided into four quadrants. Quadrant I has full topological information, whereas the other quadrants have less topological detail. In *quadrant I*, the vertical axis in the connectome represents the septotemporal axis of dentate gyrus (DG), Cornu Ammonis (CA3 and CA1), subiculum (Sub), presubiculum (PrS) and parasubiculum (PaS), and the dorsoventral axis of medial and lateral entorhinal area (MEA and LEA), retrosplenial cortex (A29 and A30), perirhinal cortex (A35 and A36) and postrhinal cortex (POR). The sidebars **(B)** display the dorsoventral and septotemporal axes of the anatomical sub-regions. The horizontal axis within quadrant I and III represents the proximodistal axis in CA3, CA1, Sub, PrS, and PaS; the rostrocaudal axis in A29c, A30, A35, A36, and POR and the DG is subdivided into the inner/outer blades and crest region. Within the area boxes, the layers for each specific subarea are outlined. In *quadrant II*, the information of the vertical axis and the layers are specified, but no details of the horizontal axis are presented. In *quadrant III* the horizontal axis and the layers are represented, while in *quadrant IV*, only layer information is present. **(C)** The interactive connectome allows visualization of detailed connectivity patterns within and between sub-regions. To search for connections, use the search button on the toolbar **(C)**. The toolbar has eight buttons (from left to right): Search for connections, show all connections, clear all connections, a short tutorial on how to search for connections, a help section, contact information, a link to the project website www.temporal-lobe.com and information about how to support this project. **(D)** If the toolbar is closed, clicking the "open toolbar" button will restore it. **(E)** After a search is carried out, the retrieved connections will be drawn in the diagram between the appropriate areas and quadrants. Additionally, an eye-icon will appear in the layers panel on the left **(E)**. This is an alphabetically sorted list of "from → to" connection groups that can also be switched on or off manually. In front of each group is a "+" icon. Clicking this icon expands the list of individual connections that make up the group, allowing one to select connections originating from a specific cortical layer or according to a specific three-dimensional projection pattern. **(F)** The figure panel provides a detailed anatomical description of the retrosplenial cortex, the hippocampal formation and the parahipppcampal region, together with translation tables for nomenclature. Use the buttons in this panel to switch between the figures.

and V and the caudal A29ab projects to the whole septotemporal axis of the PaS (Van Groen and Wyss, 1990a,b; Shibata, 1994; Jones and Witter, 2007). The projections to PER originate in caudal and intermediate rostrocaudal A29ab and terminate in layers V and VI (Shibata, 1994; Jones and Witter, 2007). The POR projection originates in layer II and V and terminates in all layers (Jones

Table 2 | Anatomical connections between subareas of the hippocampal formation, the parahippocampal region and the retrosplenial cortex.

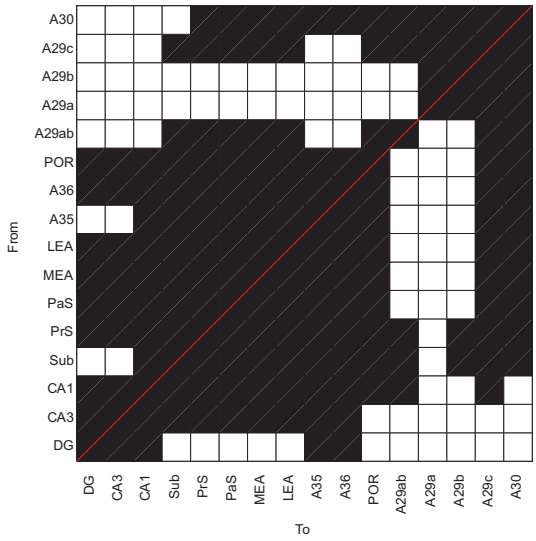

Connections that are present are shown as black squares, absent connections are shown as white squares. DG, dentate gyrus; CA, Cornu Ammonis 1 and 3; Sub, subiculum; PrS, presubiculum; PaS, parasubiculum; MEA, medial entorhinal area; LEA, lateral entorhinal area; A35: perirhinal cortex – Brodmann area 35; A36: perirhinal cortex – Brodmann area 36; POR postrhinal cortex. Brodmann area A29ab, A29a, A29b, A29c, and A30.

and Witter, 2007). The projection to LEA layers I, II, III, V, and VI and MEA layers I, V, and VI originates in caudal A29ab (Jones and Witter, 2007).

A29c

A29c also projects to all subdivisions of PHR. The projection to PrS is topographically organized along the rostrocaudal axis, such that caudal A29c projects to the entire septotemporal extent of PrS, intermediate A29c projects to intermediate and septal PrS, whereas rostral A29c only projects to septal PrS (Meibach and Siegel, 1977; Vogt and Miller, 1983; Van Groen and Wyss, 1990a,d, 2003; Shibata, 1994; Gonzalo-Ruiz and Bayona, 2001; Jones and Witter, 2007). Projections to temporal PrS originate in layers II and V, whereas projections that terminate in septal PrS are reported to originate only in layer V. Termination has been reported in all layers of PrS. The projection to PaS originates in layer V and terminates in all layers (Vogt and Miller, 1983; Finch et al., 1984; Van Groen and Wyss, 1990a; Shibata, 1994; Jones and Witter, 2007). Whether or not this projection shows a topographical organization is unclear. The projection to PER that arises from midrostrocaudal A29c terminates in layer V and VI of PER, whereas the caudal A29c projection terminates in all layers of PER (Guldin and Markowitsch, 1983; Shibata, 1994; Jones and Witter, 2007). The projection to POR originates in layers II and V of A29c and terminates in all layers (Burwell and Amaral, 1998; Jones and Witter, 2007). Both MEA and LEA are targeted by projections that originate in caudal A29c. Termination in EC has been reported to include both superficial layers and deep layers (Shibata, 1994; Jones and Witter, 2007).

A30

Similar to A29ab and A29c, A30 also projects to all subdivisions of the PHR. The projections to PrS originate in layers II and V and terminate in layers I, II, III, V, and VI (Vogt and Miller, 1983; Van Groen and Wyss, 1990a, 1992; Shibata, 1994; Jones and Witter, 2007). The topographical organization of this projection is such that rostral A30 projects to septal PrS, whereas caudal and midrostrocaudal A30 project to the entire septotemporal extent of PrS. The projection to PaS originates along the entire rostrocaudal extent of A30 (Vogt and Miller, 1983; Van Groen and Wyss, 1992; Shibata, 1994; Jones and Witter, 2007). The layers from which these projections originate have not been determined, and the projections terminate in all layers of PaS. The projections to PER originate from the rostrocaudal extent of A30. Rostral A30 projections to PER show terminal labeling in layers V and VI. Caudal projections originate in layers II, III, and V and terminate in all layers of PER (Deacon et al., 1983; Shibata, 1994; Burwell and Amaral, 1998; Jones and Witter, 2007). A30 projections to POR originate in layers II and V and terminate in all layers of POR. No topographical organization has been reported (Burwell and Amaral, 1998; Jones and Witter, 2007). A30 to EC projections show the following pattern: Layer V of A30 projects to all layers of MEA. However, caudal A30 was shown to project to LEA and MEA layers V and VI, whereas intermediate rostrocaudal A30 was shown to project to MEA layers I, II, and III (Van Groen and Wyss, 1992; Shibata, 1994; Burwell and Amaral, 1998; Jones and Witter, 2007).

PHR PROJECTIONS TO THE RSC

A29a and A29b

Some PHR sub-regions send return projections to A29ab. Septal and temporal PrS layer V neurons project to A29ab layers I–V (Finch et al., 1984; Van Groen and Wyss, 1990a,b,d). A projection from EC to A29ab has been reported, but topographical information for this projection is absent (Miyashita and Rockland, 2007). Although PaS, PER, and POR receive connections from A29ab, return projections have not been described.

A29c

Neurons in PrS layer V project to layers I and III of A29c. Septal PrS projections terminate in the whole rostrocaudal extent of A29c (Vogt and Miller, 1983; Finch et al., 1984; Van Groen and Wyss, 1990a,d, 2003). Neurons in PaS layer V project to layer II and III of A29c (Vogt and Miller, 1983; Finch et al., 1984). Similarly, projections from PER (A35, A36) and POR to A29c have been reported, but no additional information about these projections is available (Agster and Burwell, 2009). Finally, layer V of both LEA (Agster and Burwell, 2009) and MEA (Frohlich and Ott, 1980; Insausti et al., 1997; Agster and Burwell, 2009) project to A29c. MEA is known to project to layers I, II, and IV of A29c (Frohlich and Ott, 1980; Insausti et al., 1997).

A30

Neurons in layers V and VI of septal PrS project to layers I, III, IV, and V of A30 (Vogt and Miller, 1983; Finch et al., 1984; Witter et al., 1990; Van Groen and Wyss, 1992). PaS layer V

projects to A30, but the layers of termination are unknown (Vogt and Miller, 1983). A35 and A36 also project to A30 (Agster and Burwell, 2009), where caudal A36 projects to caudal A30. POR projects to A30, but layer specific information is absent (Agster and Burwell, 2009). Finally, both LEA (Agster and Burwell, 2009) and MEA (Insausti et al., 1997; Agster and Burwell, 2009) have been reported to project to A30, but only for MEA a termination in layers I and II of A30 has been described (Insausti et al., 1997).

RSC PROJECTION TO THE HF

A29a and A29b

Neurons in layer V of A29ab project to Sub in the HF (Van Groen and Wyss, 1990b; Shibata, 1994). This projection is topographically organized such that caudal A29ab projects to temporal Sub, where termination occurs in the stratum moleculare and stratum pyramidale, whereas rostral and intermediate A29ab projects to intermediate septotemporal levels of Sub, where termination occurs in the stratum pyramidale.

A29c

Also for A29c, Sub is the only HF target (Meibach and Siegel, 1977; Shibata, 1994; Gonzalo-Ruiz and Bayona, 2001; Van Groen and Wyss, 2003). This projection is topographically organized along the rostrocaudal axis, such that rostral A29c projects to septal and intermediate septotemporal levels of Sub, intermediate A29c projects to intermediate septotemporal levels and caudal A29c projects to temporal and intermediate septotemporal levels of Sub. Caudal projections to temporal Sub have been described to terminate in stratum moleculare and stratum pyramidale, whereas projections from rostral A29c to intermediate septotemporal Sub terminate in stratum pyramidale.

HF PROJECTIONS TO THE RSC

A29a and A29b

The HF projections to A29ab originate in Sub and CA1. Sub projections to A29ab terminate in layers I, II, and III and mimic the topographical organization of the retrosplenial projections to Sub. The projection from CA1 to A29ab originates from the septal portion (Van Groen and Wyss, 1990b; Naber and Witter, 1998; Miyashita and Rockland, 2007).

A29c

The HF projections to A29c also originate in Sub and CA1. The proximal part of the septal Sub projects to rostral A29c. Intermediate septotemporal and distal Sub project to caudal A29c (Vogt and Miller, 1983; Finch et al., 1984; Naber and Witter, 1998; Van Groen and Wyss, 2003; Miyashita and Rockland, 2007). These projections typically terminate in layers II and III. No information about temporal Sub to A29c projections has been published. The distal portion of septal CA1 also projects to A29c. The projection originates in neurons in stratum pyramidale and at the border between stratum moleculare and stratum radiatum and terminates in layers II, III, and IV (Meibach and Siegel, 1977; Van Groen and Wyss, 1990c, 2003; Naber and Witter, 1998; Miyashita and Rockland, 2007).

A30

The HF projections to A30 only originate in Sub. The distal portion of the septal Sub, as well as the intermediate proximodistal portion of intermediate septotemporal Sub project to layers I and II of A30 (Vogt and Miller, 1983; Finch et al., 1984; Kohler, 1985; Witter et al., 1990).

SUMMARY OF INTRINSIC RSC CONNECTIONS

There are strong intrinsic connections within the RSC subdivisions. All rostrocaudal levels within both A29c and A30 issue projections to their respective rostrocaudal extents. A29b projections have a strict topography from rostral-to-rostral and from caudal-to-caudal; A29a only has a caudal-to-caudal projection. There are also strong reciprocal connections between the RSC subdivisions. All rostrocaudal levels of one subdivision project to all rostrocaudal levels of all other subdivisions, but there are some exceptions: (1) caudal A29a projects only to caudal A29b, A29c, and A30; (2) caudal A29b does not project to rostral A29c; (3) rostral A29c does not project to caudal A30; (4) rostral and midrostrocaudal A30 only projects to caudal A29b and the return projection from A29b only terminates in caudal A30.

SUMMARY OF RSC – HF/PHR CONNECTIONS

The RSC projects to all PHR subdivisions and Sub. Only the projections of RSC to PrS and Sub show a topographical organization such that the rostrocaudal axis of origin in RSC correlates to a septotemporal terminal distribution in PrS and Sub. The projections to PrS are among the densest of RSC–PHR connections (Jones and Witter, 2007) and this is particularly true for projections from caudal RSC (Shibata, 1994). A topographical pattern for reciprocal connections has not been identified. Areas 30 and 29c receive input from the whole PHR and Sub, while PrS and Sub are the only areas which project to A29b and A29ab. Dorsal CA1 projects only to A29ab and A29c.

DISCUSSION

The connectome of the rat brain should describe all network elements and connections in a clear and comprehensible way. Compared to the comprehensiveness that a connectome implies, current knowledge is in its infancy. When considering the vast number of neurons in the rat nervous system and their connections, together with the currently available technologies to collect and handle information about them, creating a connectome is an expensive, time consuming, and complicated task. Scientists will eventually have a comprehensive map of the rat brain available, and just like the usefulness of an easily accessible map of all the roads in the world, such a connectome will be an indispensible foundation for basic and applied neurobiological research (Sporns et al., 2005). Therefore, regardless of the complexity and duration of the undertaking to create a connectome, the challenge to create a connectome of the mouse, rat, monkey, and human brain has been readily accepted by scientists [e.g., Brain Architecture Management System (BAMS), CoCoMac, The Rodent Brain Workbench, BrainNavigator, Blue Brain Project, The Allen brain atlas, Neuroscience Information Network (NIF). For a complete overview of projects see the International Coordinating Facility (INCF)].

With this publication, we present the current version of our partial rat brain connectome, which to the best of our knowledge represents all current information on the ipsilateral pathways within and between the HF, PHR, and RSC. A different approach from that of a traditional meta-analysis was taken, to create this connectome. In a traditional meta-analysis, typically only a subset of data is selected, summarized, and organized according to the author's views. The resulting reduction in detail of anatomical networks is useful for creating scientific hypotheses, but contradicts with a fundamental characteristic of a connectome: to be an exhaustive knowledge resource. Therefore, we chose the approach to present the anatomical data of the selected regions in the fullest available detail, which allows scientists to prune this information themselves to match their hypotheses, or design competing anatomical hypotheses.

We realize that the current state of knowledge is not exhaustive and hence one could argue that the connectome presented here is not a real connectome. Nevertheless, the connectome presented here provides the best approximation of a full connectome at the current point in time. With future publications we aim to continually update and expand the database. Still, users of connectomes should always keep a perspective on where the current state of knowledge stands compared to having absolute knowledge. For this reason, this discussion will first touch upon some of the challenges of anatomical connectomes that remain to be resolved, after which the potentials of connectomes will be exemplified using the information presented in this review.

CHALLENGE 1: BORDERS IN THE BRAIN

Combining data produced by many researchers, over 100 years, using many different techniques in a great number of tract-tracing experiments, leads to a number of challenges on demarcation of brain areas and designation of names in research reports. Such nomenclature issues exist not only for the RSC, but for almost all brain regions. These issues have arisen because different histological techniques produce different definitions of borders in the brain, or simply because researchers disagree on the demarcation.

Krieg (1946) was the first to delineate the RSC in the rat. Based on the nomenclature of Brodmann (1909) who subdivided the RSC in rabbit and dubbed it A29, Krieg divided it into a ventral subdivision (A29b) and a dorsal subdivision (A29c) in the rat (**Table 1**). In the 1970s of the last century, Krettek and Price (1977) divided the RSC in a granular and an agranular subdivision, the RsG and the RsAg. The granular part was further differentiated into a dorsal and a ventral part by Meibach and Siegel (1977). Vogt and Peters (1981) divided the granular subdivision into three areas, A29a, b, and c based on termination patterns of callosal fibers. In this century, Jones et al. (2005), Jones and Witter (2007) delineated the RSC borders based on parvalbumin stainings and classified the most caudal part of A29ab with A30 into the dorsal retrosplenial cortex (RSd). Although no standardization of nomenclatures has become apparent, dealing flexibly with the diverse nomenclatures may allow to efficiently generate inspiring insights into the organization of the RSC. Therefore, in the current HF–PHR–RSC connectome, we selected one nomenclature to express ourselves. For RSC we used the nomenclature of Vogt et al. (2004) and for HF–PHR the nomenclature of Witter and Amaral (2004). We provided what we call a "Rosetta table" of nomenclatures. The "Rosetta table" of nomenclatures is a necessary translation tool that lists all available nomenclatures (for a given structure in a given species) and facilitates translating between different nomenclatures. For such translations, different methods have been developed, and we applied careful comparison of all cyto- and chemoarchitectural features described in the original publications (Bota and Swanson, 2010).

CHALLENGE 2: LEVEL OF DETAIL

Aspecific reporting

Even when using technically advanced methods to clarify projection patterns, the usefulness of a scientific report on anatomical connections depends to a great extent on how detailed the authors report their results and the way they present the data in figures to support their observations. When reviewing the projections from RSC to HF and PHR, only in a few studies information was provided on the layers of origin or termination, or specific projection patterns. For example, projections from A29ab, A29c, and A30 to LEA and MEA exist (Van Groen and Wyss, 1992; Burwell and Amaral, 1998; Jones and Witter, 2007) and although LEA and MEA show an overall dorsolateral-to-ventromedial connectional and functional gradient, none of these reports provide comparable termination information. Even less specific accounts inform us that RSC projects to the EC, without indicating if the projections terminated in the lateral or medial subdivision (Audinat et al., 1988; Van Groen and Wyss, 1990b; Shibata, 1994). This is regrettable, since more detailed information about the origin and termination could be related to the function of a connection. It is known that functional differences between the LEA and MEA exist. Neurons in the MEA exhibit spatial selectivity, while LEA cells display only weak spatial modulation (Fyhn et al., 2004; Hargreaves et al., 2005). Since projections from RSC to EC mainly target MEA, it could be hypothesized that this input is relevant to spatial firing properties of MEA neurons. Unfortunately, the current level of detail is such that almost nothing is known about the topography and lamination of the HF and PHR projections to the RSC and vice versa. In our connectome, this information is displayed as connecting areas with an unspecified origin or termination. This lack of detailed information makes it difficult to predict the function of projections or small networks. Fortunately, more advanced methods to explore brain networks are continuously being developed, making it likely that future expansions of the connectome can include for example, information about the nature of postsynaptic targets or the distribution of synapses on the dendritic tree.

Displaying layer specificity

To obtain information about layer specificity of projections, ideally anterograde and retrograde tract-tracing experiments are combined. For example, an anterograde tracer injection is placed in midrostrocaudal A30, thereby discovering regions of termination including layers I, II, III, and V of rostral A29c. This experiment should be completed by placing a retrograde tracer in rostral A29c, to reveal the layers of origin of this projection in midrostrocaudal A30, i.e., layer II, III, V, and VI (Shibata et al., 2009). A strength

of our current approach is that a database of connections allows easy combination of anterograde and retrograde experiments, even across publications. But when representing this information in a connectome, should one draw projections from all origin layers to all target layers, or could it be that a more specific pattern exists, e.g., that layer II cells only project to layer V of the target region? Therefore, only when single cells are fully traced (e.g., Honda et al., 2011), one can accurately describe layer specificity of projections.

Displaying projection topographies

Apart from layer specificity, projections may be topographically organized. For example, the rostral RSC projects weaker to EC than caudal RSC. Often, such topographies show a gradient in projection strength, but one cannot rigorously claim that only caudal RSC projects to EC. In the current version of our connectome, such topographies are not visible since no information on relative density is included. We chose this approach, in view of the risk that by emphasizing some brain connections over others, the less emphasized ones may be erased from the scientific working memory. However, users should not forget that brain connections typically have different strengths and may show topographical gradients that are not apparent in the interactive connectome.

CHALLENGE 3: FUNCTIONAL CONNECTIVITY

When using our connectome, it is important to keep in mind that two connections symbolized by two similar looking lines may be different from one another for a number of reasons.

Excitatory – inhibitory, modulation

Our connectome is based on tract-tracing data and thus comes with certain limitations related to this technique. One important limitation is that tract-tracing does not reveal if a connection is excitatory or inhibitory, whereas this information is of functional relevance. By combining immunohistochemistry with either confocal or electron microscopy, it can be established if a projection is excitatory or inhibitory (Van Haeften et al., 1997). Alternatively, electrophysiological data can help determine this functional property and such information will eventually be incorporated into the connectome.

In our current connectome, known GABA-ergic connections are not specifically included, although some projections are likely GABA-ergic. There is a dense GABA-ergic projection from CA1 to the RSC, starting from all layers except the stratum lacunosum-moleculare (Miyashita and Rockland, 2007). Non-pyramidal cells, which could be GABA-ergic, of the septal Sub are projecting to layer I of the RSC as well (Van Groen and Wyss, 1992, 2003; Miyashita and Rockland, 2007). Hippocampal GABA-ergic neurons also project intra-hippocampally (Jinno, 2009). Inhibitory GABA-ergic projections are involved in regulation of neural oscillations (Somogyi and Klausberger, 2005). Theta oscillations (4–12 Hz) for instance, have been postulated to support memory formation in the HF and the cortex (Klausberger et al., 2003). Theta oscillations have also been recorded in the RSC (Borst et al., 1987; Talk et al., 2004) and are in coherence with oscillations in CA1 (Young and Mcnaughton, 2009). Although this coherence may be a product of volume conduction from the hippocampus, the GABA-ergic projections from CA1 and Sub to RSC could play a role as well.

Weak – strong connections

Most anatomical reports contain subjective descriptions of the strengths of projections. Such subjective reports are impossible to quantify and therefore such information cannot be incorporated in the connectome. Yet, in reality differences in strengths exist. For instance, the projection from A29ab to MEA is reported to terminate in both superficial and deep layers. When assessing this connection in detail, clear differences between superficial and deep layers exist. There is dense terminal labeling in layer V of MEA, whereas terminal labeling in layer III is very light (Jones and Witter, 2007). Therefore, it would be reasonable to suggest that the major effect of A29ab on MEA is mediated through layer V, not through layer III. Moreover a strong projection could arise from a small number of neurons that supply a highly collateralized terminal plexus, but a similarly strong projection may also result from many cells sending less collateralized axons to the target area. This type of information is almost never available in the literature. Yet a connectome ideally would describe this information.

CHALLENGE 4: NOT REPORTED OR NO CONNECTION?

Another challenge is how to interpret "negative information." There are two types of negative information: (1) there is data that indicate that a connection between area A and area B is very unlikely, or (2) a connection between area A and area B was not reported, but may exist. For example, the current literature assessment shows that A29c and A29ab both project to Sub, whereas data on a projection from A30 to Sub are lacking. Should one now conclude that a projection from A30 to Sub is not present in the rat brain, or could it be that this projection is present, but perhaps remained undetected or was detected but not reported? This issue has been dealt with in other databases, where connections that are explicitly reported to not exist have been collated (Stephan et al., 2000; Bota and Arbib, 2004). In a future version of our database we plan to implement a similar solution. Currently, some caution is required when drawing conclusions on the basis of the connectome alone.

CHALLENGE 5: INCLUSION OF INCORRECT DATA

Although it is assumed that researchers aim to report as accurately as possible the results of their tract-tracing experiments, it does not exclude the possibility that brain connections are reported that do not exist. Tract-tracing techniques were much refined over time, such that injections of modern tracers such as Phaseolus Vulgaris-leucoagglutinin or biotinylated dextran-amine can now be injected region or cell layer selective (Gerfen and Sawchenko, 1984; Wouterlood and Jorritsma-Byham, 1993). Compared to modern tract-tracing studies, many of the old reports are coarse and provide little information for the current connectome. Such reports are only of interest when they seem valid and provide the only available source of knowledge about a particular connection.

A bigger problem occurs when a report provides many connection details, but too little evidence is presented to confirm the claims of authors. In such cases, one can only trust the author's interpretation of the data, in the absence of proof against it. However, when sufficient proof against the existence of a connection is available, such information is registered in our connection database, but

excluded or removed from the connectome. An example of a connection that was reported but is not in the current connectome is based on an injection in A30 and A29c with terminal labeling in Sub, septal PrS and PaS (Vogt and Miller, 1983) or an injection in Sub, PrS, and CA1 (Long et al., 1995). These data were excluded from the connectome because the tracer injections covered more than one defined region or targeted fiber bundles. Another possible confounder occurs if described results do not match those in the referred figures or tables. In such cases they were either corrected to match the figure or table or if that was impossible, they were excluded entirely. Nevertheless, such "false positive" reports are taken up in the reference tables on our website, which displays in which papers connections were reported, such that scientists can evaluate such reports for themselves.

ADVANTAGE 1: EDUCATION

Apart from scientific value, a connectome is useful as an educational tool to get an overview of an ever increasing amount of literature. Instead of having to search through many papers, basic anatomical facts such as the three dimensional organization of a structure, but also complex issues such as differences in nomenclature and perhaps most complex, the numerous connections between brain regions, are neatly organized, such that users can easily get an exhaustive overview of information at the level of detail that they choose. This is useful for novice researchers who just started to learn about the organization of the brain, as well as researchers who wish to expand their research into new brain regions that are charted in the connectome.

ADVANTAGE 2: SCIENTIFIC VALUE

There are several scientific uses of connectomes. A connectome can help detect knowledge gaps, it will improve the interpretation of experimental results and may facilitate the design of new experiments. Depending on the level of detail of the available information, the scientific value varies between these uses. If little information is available, a connectome will mainly help detect knowledge gaps. When a reasonable amount of details are known, it will help better understand completed experiments. The true potential of a connectome becomes apparent only when the level of detail of information goes beyond the point where one can easily keep track of all the known facts.

Detection of knowledge gaps

Even though the current connectome may look overwhelming already, a close look immediately points to gaps in our knowledge. For example, there are no experiments evaluating the topographical organization of the connections between A29a or A29b and HF–PHR. Anterograde or retrograde injections in A29a or A29b and the topography of terminating patterns or labeling of neurons in PHR have not yet been described. Similarly, injections in HF–PHR and descriptions of the terminating patterns in A29a or A29b are missing. Another example concerns the topography of the projection from PrS to RSC. It is known that temporal PrS projects specifically to A29ab, whereas septal PrS projects to all RSC subdivisions. It is likely that a more specified topography exists, for example along the rostrocaudal axis of RSC, but such information is presently unknown.

Understanding experiments

Another useful scientific application is the graphical representation of hypotheses. Sometimes it is easier to understand a hypothesis by looking at a graphical representation of the connections. For example, it was hypothesized that information transfer between the RSC and PHR–HF is crucial for adequate navigation and spatial memory. This is supported by the observation that extensive lesions, including A29ab and A29c disrupt spatial memory tasks (Pothuizen et al., 2010). However, it is also likely that different subdivisions of the RSC have different roles in navigation and spatial memory, since lesioning A29c and A30 results in impaired performance on spatial learning tests, whereas selective lesions of A29ab do not interfere with the performance in spatial tasks (Van Groen et al., 2004; Vann and Aggleton, 2005). When looking at the connectome, it can be seen that A29ab receives information from septal and temporal PrS, septal and temporal Sub and septal CA1, whereas A30 and A29c receive inputs from LEA, MEA, A35, A36, POR, PaS, next to input from PrS, Sub, and CA1. These connectional differences may partially explain the lesion data, but likely will also lead to new concepts or new experiments.

Another example of an inferred experiment, based on the connectome follows from the topography observed in the RSC – HF–PHR projections. The traditional emphasis on the topography of RSC – HF–PHR projections relies on the observation that there is a gradient in the RSC to HF–PHR projections, such that rostral RSC (A29c) projects primarily to septal parts of HF–PHR (PrS) and caudal RSC (A29c/A30) projects both to septal and temporal HF–PHR (PrS). Upon close inspection, a more striking topography is apparent in the projections of Sub to A29c. The transverse axis of Sub relates to the rostrocaudal axis in A29c such that proximal Sub projects to the rostral part of A29c and distal Sub projects to the caudal of A29c. This topography could be of functional relevance, since LEA projects to proximal parts of Sub, whereas MEA projects distally (Tamamaki and Nojyo, 1995; Naber et al., 2001; Baks-Te Bulte et al., 2005). This suggests that MEA related input is selectively transferred to caudal portions of A29c and LEA related input to more rostral levels. Since the projections from CA1 to Sub follow a matching proximodistal organization and CA1 also projects to A29c, it would be of interest to know whether the CA1 to A29c projection is in register, such that distal CA1 projects to rostral A29c and proximal CA1 projects to caudal A29c.

The current connectome, as presented here, is far from complete and differences exist in the amount of information that is available about anatomical demarcation and connectivity of different brain areas. The HF connectivity is relatively well covered, followed by the PHR – HF connections and least is known about HF – RSC connectivity. As indicated, the amount of available information is largely decisive for the type of questions a connectome can assist with. We do not see these issues as shortcomings undermining the value of this approach. Connectomes can continuously be updated and extended and therefore will always provide an exhaustive and up to date account of the current knowledge. These two factors precisely define the value of connectomes. Moreover, anatomical connectivity characterizes the brain at an intermediate information level, allowing to easily link this to, e.g., functional properties of individual cells or effective connectivity (Friston, 2011). Such linking is a key prerequisite to fully understand brain function. A

connectome therefore does not only describe the architecture of the brain, it also is a key linking system to understand brain function at multiple scales.

ACKNOWLEDGMENTS

We like to thank Ingrid Riphagen for designing and performing the initial literature searches. Niels M. van Strien was supported by the Norwegian Research Council, Independent projects – Biology and Biomedicine grant number 197245. Menno P. Witter and Jørgen Sugar received support from the Kavli Foundation and the Norwegian Research Council, centre of excellence grant number 145993.

SUPPLEMENTARY MATERIAL

The Supplementary Material for this article can be found online at http://www.frontiersin.org/Neuroinformatics/10.3389/fninf.2011.00007/abstract

REFERENCES

Agster, K. L., and Burwell, R. D. (2009). Cortical efferents of the perirhinal, postrhinal, and entorhinal cortices of the rat. *Hippocampus* 19, 1159–1186.

Audinat, E., Conde, F., and Crepel, F. (1988). Cortico-cortical connections of the limbic cortex of the rat. *Exp. Brain Res.* 69, 439–443.

Baks-Te Bulte, L., Wouterlood, F. G., Vinkenoog, M., and Witter, M. P. (2005). Entorhinal projections terminate onto principal neurons and interneurons in the subiculum: a quantitative electron microscopical analysis in the rat. *Neuroscience* 136, 729–739.

Boccara, C. N., Sargolini, F., Thoresen, V. H., Solstad, T., Witter, M. P., Moser, E. I., and Moser, M. B. (2010). Grid cells in pre- and parasubiculum. *Nat. Neurosci.* 13, 987–994.

Borst, J. G., Leung, L. W., and Macfabe, D. F. (1987). Electrical activity of the cingulate cortex. II. Cholinergic modulation. *Brain Res.* 407, 81–93.

Bota, M., and Arbib, M. A. (2004). Integrating databases and expert systems for the analysis of brain structures: connections, similarities, and homologies. *Neuroinformatics* 2, 19–58.

Bota, M., and Swanson, L. W. (2010). Collating and curating neuroanatomical nomenclatures: principles and use of the brain architecture knowledge management system (BAMS). *Front. Neuroinform.* 4:3. doi: 10.3389/fninf.2010.00003.

Brodmann, K. (1909). *Vergleichende Lokalisationslehre der Grosshirnrinde in ihren Prinzipien dargestellt auf Grund des Zellenbauers.* Leipzig: Verlag von Johann Ambrosius Barth.

Buckner, R. L., Andrews-Hanna, J. R., and Schacter, D. L. (2008). The brain's default network: anatomy, function, and relevance to disease. *Ann. N. Y. Acad. Sci.* 1124, 1–38.

Burwell, R. D., and Amaral, D. G. (1998). Cortical afferents of the perirhinal, postrhinal, and entorhinal cortices of the rat. *J. Comp. Neurol.* 398, 179–205.

Chen, L. L., Lin, L. H., Green, E. J., Barnes, C. A., and Mcnaughton, B. L. (1994). Head-direction cells in the rat posterior cortex. I. Anatomical distribution and behavioral modulation. *Exp. Brain Res.* 101, 8–23.

Cho, J., and Sharp, P. E. (2001). Head direction, place, and movement correlates for cells in the rat retrosplenial cortex. *Behav. Neurosci.* 115, 3–25.

Cooper, B. G., and Mizumori, S. J. (1999). Retrosplenial cortex inactivation selectively impairs navigation in darkness. *Neuroreport* 10, 625–630.

Crick, F., and Koch, C. (2003). A framework for consciousness. *Nat. Neurosci.* 6, 119–126.

Deacon, T. W., Eichenbaum, H., Rosenberg, P., and Eckmann, K. W. (1983). Afferent connections of the perirhinal cortex in the rat. *J. Comp. Neurol.* 220, 168–190.

Finch, D. M., Derian, E. L., and Babb, T. L. (1984). Afferent fibers to rat cingulate cortex. *Exp. Neurol.* 83, 468–485.

Friston, K. J. (2011). Functional and effective connectivity: a review. *Brain Connect.* 1, 13–36.

Frohlich, J., and Ott, T. (1980). Autoradiographic analysis of projections from the medial entorhinal cortex to limbic areas. *Folia Morphol. (Praha)* 28, 240–245.

Fyhn, M., Molden, S., Witter, M. P., Moser, E. I., and Moser, M. B. (2004). Spatial representation in the entorhinal cortex. *Science* 305, 1258–1264.

Gerfen, C. R., and Sawchenko, P. E. (1984). An anterograde neuroanatomical tracing method that shows the detailed morphology of neurons, their axons and terminals: immunohistochemical localization of an axonally transported plant lectin, Phaseolus vulgaris leucoagglutinin (PHA-L). *Brain Res.* 290, 219–238.

Gonzalo-Ruiz, A., and Bayona, I. (2001). Localization of excitatory amino acid and neuropeptide markers in neurons of the subicular complex projecting to the retrosplenial granular cortex of the rat. *Eur. J. Anat.* 5, 119–132.

Greicius, M. D., Supekar, K., Menon, V., and Dougherty, R. F. (2009). Resting-state functional connectivity reflects structural connectivity in the default mode network. *Cereb. Cortex* 19, 72–78.

Guldin, W. O., and Markowitsch, H. J. (1983). Cortical and thalamic afferent connections of the insular and adjacent cortex of the rat. *J. Comp. Neurol.* 215, 135–153.

Hargreaves, E. L., Rao, G., Lee, I., and Knierim, J. J. (2005). Major dissociation between medial and lateral entorhinal input to dorsal hippocampus. *Science* 308, 1792–1794.

Henderson, V. W., Mack, W., and Williams, B. W. (1989). Spatial disorientation in Alzheimer's disease. *Arch. Neurol.* 46, 391–394.

Honda, Y., Furuta, T., Kaneko, T., Shibata, H., and Sasaki, H. (2011). Patterns of axonal collateralization of single layer V cortical projection neurons in the rat presubiculum. *J. Comp. Neurol.* 519, 1395–1412.

Insausti, R., Herrero, M. T., and Witter, M. P. (1997). Entorhinal cortex of the rat: cytoarchitectonic subdivisions and the origin and distribution of cortical efferents. *Hippocampus* 7, 146–183.

Jinno, S. (2009). Structural organization of long-range GABAergic projection system of the hippocampus. *Front. Neuroanat.* 3:13. doi: 10.3389/neuro.05.013.2009

Jones, B. F., Groenewegen, H. J., and Witter, M. P. (2005). Intrinsic connections of the cingulate cortex in the rat suggest the existence of multiple functionally segregated networks. *Neuroscience* 133, 193–207.

Jones, B. F., and Witter, M. P. (2007). Cingulate cortex projections to the parahippocampal region and hippocampal formation in the rat. *Hippocampus* 17, 957–976.

Klausberger, T., Magill, P. J., Marton, L. F., Roberts, J. D., Cobden, P. M., Buzsaki, G., and Somogyi, P. (2003). Brain-state- and cell-type-specific firing of hippocampal interneurons in vivo. *Nature* 421, 844–848.

Kohler, C. (1985). Intrinsic projections of the retrohippocampal region in the rat brain. I. The subicular complex. *J. Comp. Neurol.* 236, 504–522.

Krettek, J. E., and Price, J. L. (1977). The cortical projections of the mediodorsal nucleus and adjacent thalamic nuclei in the rat. *J. Comp. Neurol.* 171, 157–191.

Krieg, W. J. (1946). Connections of the cerebral cortex; the albino rat; structure of the cortical areas. *J. Comp. Neurol.* 84, 277–323.

Long, Y., Hardwick, A. L., and Frederickson, C. J. (1995). Zinc-containing innervation of the subicular region in the rat. *Neurochem. Int.* 27, 95–103.

Maguire, E. A. (2001). The retrosplenial contribution to human navigation: a review of lesion and neuroimaging findings. *Scand. J. Psychol.* 42, 225–238.

Meibach, R. C., and Siegel, A. (1977). Subicular projections to the posterior cingulate cortex in rats. *Exp. Neurol.* 57, 264–274.

Miyashita, T., and Rockland, K. S. (2007). GABAergic projections from the hippocampus to the retrosplenial cortex in the rat. *Eur. J. Neurosci.* 26, 1193–1204.

Muller, R. U., Ranck, J. B. Jr., and Taube, J. S. (1996). Head direction cells: properties and functional significance. *Curr. Opin. Neurobiol.* 6, 196–206.

Naber, P. A., Lopes Da Silva, F. H., and Witter, M. P. (2001). Reciprocal connections between the entorhinal cortex and hippocampal fields CA1 and the subiculum are in register with the projections from CA1 to the subiculum. *Hippocampus* 11, 99–104.

Naber, P. A., and Witter, M. P. (1998). Subicular efferents are organized mostly as parallel projections: a double-labeling, retrograde-tracing study in the rat. *J. Comp. Neurol.* 393, 284–297.

O' Keefe, J., and Dostrovsky, J. (1971). The hippocampus as a spatial map. Preliminary evidence from unit activity in the freely-moving rat. *Brain Res.* 34, 171–175.

Pengas, G., Hodges, J. R., Watson, P., and Nestor, P. J. (2010). Focal posterior cingulate atrophy in incipient Alzheimer's disease. *Neurobiol. Aging* 31, 25–33.

Pothuizen, H. H., Davies, M., Aggleton, J. P., and Vann, S. D. (2010). Effects of selective granular retrosplenial cortex lesions on spatial working memory in rats. *Behav. Brain Res.* 208, 566–575.

Raji, C. A., Lopez, O. L., Kuller, L. H., Carmichael, O. T., and Becker, J. T. (2009). Age, Alzheimer disease, and brain structure. *Neurology* 73, 1899–1905.

Reed, J. M., and Squire, L. R. (1997). Impaired recognition memory in patients with lesions limited to the

hippocampal formation. *Behav. Neurosci.* 111, 667–675.
Rose, J. E., and Woolsey, C. N. (1948). Structure and relations of limbic cortex and anterior thalamic nuclei in rabbit and cat. *J. Comp. Neurol.* 89, 279–347.
Rose, M. (1927). Gyrus limbicus anterior und Regio retrosplenialis (Cortex holoprotoptychos quinquestratificatus). Vergleichende Architektonik bei Tier und Mensch. *J. Psychol. Neurol.* 35, 65–173.
Scoville, W. B., and Milner, B. (1957). Loss of recent memory after bilateral hippocampal lesions. *J. Neurol. Neurosurg. Psychiatry* 20, 11–21.
Sharp, P. E., and Green, C. (1994). Spatial correlates of firing patterns of single cells in the subiculum of the freely moving rat. *J. Neurosci.* 14, 2339–2356.
Shibata, H. (1994). Terminal distribution of projections from the retrosplenial area to the retrohippocampal region in the rat, as studied by anterograde transport of biotinylated dextran amine. *Neurosci. Res.* 20, 331–336.
Shibata, H., Honda, Y., Sasaki, H., and Naito, J. (2009). Organization of intrinsic connections of the retrosplenial cortex in the rat. *Anat. Sci. Int.*
Somogyi, P., and Klausberger, T. (2005). Defined types of cortical interneurone structure space and spike timing in the hippocampus. *J. Physiol.* 562, 9–26.
Sporns, O., and Tononi, G. (2007). "Structural determinants of functional brain dynamics," in *Handbook of Brain Connectivity*, eds V. K. Jirsa and A. R. Mcintosh (Berlin: Springer-Verlag), 117–148.
Sporns, O., Tononi, G., and Kotter, R. (2005). The human connectome: a structural description of the human brain. *PLoS Comput. Biol.* 1, e42. doi: 10.1371/journal.pcbi.0010042
Sripanidkulchai, K., and Wyss, J. M. (1987). The laminar organization of efferent neuronal cell bodies in the retrosplenial granular cortex. *Brain Res.* 406, 255–269.
Stephan, K. E., Zilles, K., and Kotter, R. (2000). Coordinate-independent mapping of structural and functional data by objective relational transformation (ORT). *Philos. Trans. R. Soc. Lond. B Biol. Sci.* 355, 37–54.
Sutherland, R. J., Whishaw, I. Q., and Kolb, B. (1988). Contributions of cingulate cortex to two forms of spatial learning and memory. *J. Neurosci.* 8, 1863–1872.
Talk, A., Kang, E., and Gabriel, M. (2004). Independent generation of theta rhythm in the hippocampus and posterior cingulate cortex. *Brain Res.* 1015, 15–24.
Tamamaki, N., and Nojyo, Y. (1995). Preservation of topography in the connections between the subiculum, field CA1, and the entorhinal cortex in rats. *J. Comp. Neurol.* 353, 379–390.
Van Groen, T., Kadish, I., and Wyss, J. M. (2004). Retrosplenial cortex lesions of area Rgb (but not of area Rga) impair spatial learning and memory in the rat. *Behav. Brain Res.* 154, 483–491.
Van Groen, T., and Wyss, J. M. (1990a). The connections of presubiculum and parasubiculum in the rat. *Brain Res.* 518, 227–243.
Van Groen, T., and Wyss, J. M. (1990b). Connections of the retrosplenial granular a cortex in the rat. *J. Comp. Neurol.* 300, 593–606.
Van Groen, T., and Wyss, J. M. (1990c). Extrinsic projections from area CA1 of the rat hippocampus: olfactory, cortical, subcortical, and bilateral hippocampal formation projections. *J. Comp. Neurol.* 302, 515–528.
Van Groen, T., and Wyss, J. M. (1990d). The postsubicular cortex in the rat: characterization of the fourth region of the subicular cortex and its connections. *Brain Res.* 529, 165–177.
Van Groen, T., and Wyss, J. M. (1992). Connections of the retrosplenial dysgranular cortex in the rat. *J. Comp. Neurol.* 315, 200–216.
Van Groen, T., and Wyss, J. M. (2003). Connections of the retrosplenial granular b cortex in the rat. *J. Comp. Neurol.* 463, 249–263.
Van Haeften, T., Wouterlood, F. G., Jorritsma-Byham, B., and Witter, M. P. (1997). GABAergic presubicular projections to the medial entorhinal cortex of the rat. *J. Neurosci.* 17, 862–874.
Van Strien, N. M., Cappaert, N. L., and Witter, M. P. (2009). The anatomy of memory: an interactive overview of the parahippocampal-hippocampal network. *Nat. Rev. Neurosci.* 10, 272–282.
Vann, S. D., and Aggleton, J. P. (2002). Extensive cytotoxic lesions of the rat retrosplenial cortex reveal consistent deficits on tasks that tax allocentric spatial memory. *Behav. Neurosci.* 116, 85–94.
Vann, S. D., and Aggleton, J. P. (2004). Testing the importance of the retrosplenial guidance system: effects of different sized retrosplenial cortex lesions on heading direction and spatial working memory. *Behav. Brain Res.* 155, 97–108.
Vann, S. D., and Aggleton, J. P. (2005). Selective dysgranular retrosplenial cortex lesions in rats disrupt allocentric performance of the radial-arm maze task. *Behav. Neurosci.* 119, 1682–1686.
Vann, S. D., Aggleton, J. P., and Maguire, E. A. (2009). What does the retrosplenial cortex do? *Nat. Rev. Neurosci.* 10, 792–802.
Villain, N., Desgranges, B., Viader, F., De La Sayette, V., Mezenge, F., Landeau, B., Baron, J. C., Eustache, F., and Chetelat, G. (2008). Relationships between hippocampal atrophy, white matter disruption, and gray matter hypometabolism in Alzheimer's disease. *J. Neurosci.* 28, 6174–6181.
Vogt, B. A., and Miller, M. W. (1983). Cortical connections between rat cingulate cortex and visual, motor, and postsubicular cortices. *J. Comp. Neurol.* 216, 192–210.
Vogt, B. A., and Peters, A. (1981). Form and distribution of neurons in rat cingulate cortex: areas 32, 24, and 29. *J. Comp. Neurol.* 195, 603–625.
Vogt, B. A., Vogt, L., and Farber, N. B. (2004). "Cingulate cortex and disease models," in *The Rat Nervous System*, 3rd Edn, ed. G. Paxinos (San Diego, CA: Elsevier Academic Press), 705–727.
Whishaw, I. Q., Maaswinkel, H., Gonzalez, C. L., and Kolb, B. (2001). Deficits in allothetic and idiothetic spatial behavior in rats with posterior cingulate cortex lesions. *Behav. Brain Res.* 118, 67–76.
Witter, M. P., and Amaral, D. G. (2004). "Hippocampal formation," in *The Rat Nervous System*, 3rd Edn. ed. G. Paxinos (Oxford: Elsevier Academic Press), 635–704.
Witter, M. P., Ostendorf, R. H., and Groenewegen, H. J. (1990). Heterogeneity in the dorsal subiculum of the rat. Distinct neuronal zones project to different cortical and subcortical targets. *Eur. J. Neurosci.* 2, 718–725.
Wouterlood, F. G., and Jorritsma-Byham, B. (1993). The anterograde neuroanatomical tracer biotinylated dextran-amine: comparison with the tracer Phaseolus vulgaris-leucoagglutinin in preparations for electron microscopy. *J. Neurosci. Methods* 48, 75–87.
Young, C. K., and Mcnaughton, N. (2009). Coupling of theta oscillations between anterior and posterior midline cortex and with the hippocampus in freely behaving rats. *Cereb. Cortex* 19, 24–40.
Zilles, K., and Wree, A. (1995). "Cortex: areal and laminar structure," *in The Rat Nervous System*, 2nd Edn, ed. G. Paxinos (San Diego, CA: Elsevier Academic Press), 649–685.

Conflict of Interest Statement: The authors declare that the research was conducted in the absence of any commercial or financial relationships that could be construed as a potential conflict of interest.

Received: 18 March 2011; paper pending published: 02 May 2011; accepted: 27 June 2011; published online: 27 July 2011.
Citation: Sugar J, Witter MP, van Strien NM and Cappaert NLM (2011) The retrosplenial cortex: intrinsic connectivity and connections with the (para)hippocampal region in the rat. An interactive connectome. Front. Neuroinform. ***5****:7. doi: 10.3389/fninf.2011.00007*

Systems/Circuits

Superficially Projecting Principal Neurons in Layer V of Medial Entorhinal Cortex in the Rat Receive Excitatory Retrosplenial Input

Rafał Czajkowski,[1,2]* Jørgen Sugar,[1]* Sheng-Jia Zhang,[1] Jonathan J. Couey,[1] Jing Ye,[1] and Menno P. Witter[1]

[1]Kavli Institute for Systems Neuroscience, Centre for Neural Computation, Faculty of Medicine, Norwegian University of Science and Technology, 7491 Trondheim, Norway, and [2]Neurobiology Center, Nencki Institute of Experimental Biology, 02-093 Warsaw, Poland

Principal cells in layer V of the medial entorhinal cortex (MEC) have a nodal position in the cortical–hippocampal network. They are the main recipients of hippocampal output and receive inputs from several cortical areas, including a prominent one from the retrosplenial cortex (RSC), likely targeting basal dendrites of layer V neurons. The latter project to extrahippocampal structures but also relay information to the superficial layers of MEC, closing the hippocampal–entorhinal loop. In the rat, we electrophysiologically and morphologically characterized RSC input into MEC and conclude that RSC provides an excitatory input to layer V pyramidal cells. Ultrastructural analyses of anterogradely labeled RSC projections showed that RSC axons in layer V of MEC form predominantly asymmetrical, likely excitatory, synapses on dendritic spines (90%) or shafts (8%), with 2% symmetrical, likely inhibitory, synapses on shafts and spines. The overall excitatory nature of the RSC input was confirmed by an optogenetic approach. Patterned laser stimulation of channelrhodopsin-expressing presynaptic RSC axons evoked exclusively EPSPs in recorded postsynaptic layer V cells. All responding layer V pyramidal cells had an axon extending toward the white matter. Half of these neurons also sent an axon to superficial layers. Confocal imaging of RSC synapses onto MEC layer V neurons shown to project superficially by way of retrogradely labeling from superficial layers confirmed that proximal dendrites of superficially projecting cells are among the targets of inputs from RSC. The excitatory RSC input thus interacts with both entorhinal–cortical and entorhinal–hippocampal circuits.

Introduction

The entorhinal cortex (EC) is anatomically positioned as a gateway to the hippocampal formation (HF), gathering and preprocessing information from other brain areas and providing the main cortical input to HF (Eichenbaum and Lipton, 2008). HF plays a central role in spatial information processing (O'Keefe and Nadel, 1978), and it contains place cells that fire when an animal is in a certain location (O'Keefe and Dostrovsky, 1971). Layers II and III of the medial entorhinal cortex (MEC) harbor a number of spatially modulated cell types (Hafting et al., 2005; Sargolini et al., 2006; Solstad et al., 2008), contributing a necessary spatial input to hippocampal place cells (Remondes and Schuman, 2004; Brun et al., 2008; Moser and Moser, 2008; Van Cauter et al., 2008; van Strien et al., 2009; Ito and Schuman, 2012; Zhang et al., 2013).

Hippocampally processed information targets dendrites of neurons in EC layer V (van Haeften et al., 1995), and many MEC layer V pyramidal cells send axon collaterals to cortical targets (Insausti et al., 1997). In view of this connectivity, MEC layer V neurons are thought to play an important role in the interaction between the HF and cortex (Chrobak and Buzsáki, 1994; Buzsáki, 1996; Kloosterman et al., 2000, 2003a). MEC layer V neurons also project locally to superficial layers of EC (Kloosterman et al., 2003b; van Haeften et al., 2003), strengthening their nodal position in the network.

The basal dendrites of layer V neurons are not only innervated by inputs from HF but are also embedded in a prominent input from the retrosplenial cortex (RSC; Jones and Witter, 2007). RSC is involved in a variety of behaviors related to spatial navigation. In humans, lesions of RSC cause a deficit in which patients cannot use familiar landmarks or maps to produce a sense of direction (Maguire, 2001). The RSC shows increased activity during route planning (Spiers and Maguire, 2006; Epstein et al., 2007). In rodents, RSC contains head direction cells (Cho and Sharp, 2001), and lesion studies demonstrated an involvement in tasks that depend on spatial memory (Vann and Aggleton, 2002; Pothuizen et al., 2008; Wesierska et al., 2009).

Received June 21, 2013; revised Aug. 6, 2013; accepted Aug. 23, 2013.

Author contributions: R.C., J.S., and M.P.W. designed research; R.C., J.S., and J.J.C. performed research; S.-J.Z. and J.Y. contributed unpublished reagents/analytic tools; R.C., J.S., and J.J.C. analyzed data; R.C., J.S., and M.P.W. wrote the paper.

This work was supported by the Kavli Foundation, Norwegian Research Council Centre of Excellence Grant 145993, Equipment Grant 181676, and Research Grant 191929, and European Commission ("Spacebrain") Grant 200873. We thank Ragnhild Gisetstad for technical assistance with the design of the electron microscopy experiments and Paulo Girão for help with data analysis. The use of the electron microscopy facility at Norwegian University of Science and Technology and the help and advice of Nan Skogaker, Linh Hoang, and Gro Møkkelgjerd is greatly acknowledged.

*R.C. and J.S. contributed equally to this study.

The authors declare no competing financial interests.

Correspondence should be addressed to Menno Witter, Kavli Institute for Systems Neuroscience and Centre for Neural Computation, Norwegian University of Science and Technology, Medical Technical Research Centre, Postboks 8905, NO-7491 Trondheim, Norway. E-mail: menno.witter@ntnu.no.

J. J. Couey's present address: Department of Psychiatry, Erasmus Medical Center, 3015 CE Rotterdam, The Netherlands.

DOI:10.1523/JNEUROSCI.2646-13.2013

 0270-6474/13/3315779-14$15.00/0

Interactions between RSC and the HF–EC circuit have been postulated as crucial for spatial memory formation (Vann et al., 2009). The absence of direct projections from RSC to HF point to layer V neurons in MEC as the likely substrate to mediate the interactions between RSC and HF. However, details about the synaptic organization of the RSC projections to MEC are unknown, and most importantly it is currently not known whether RSC-targeted cells in layer V actually project to superficial layers II and III of MEC. Our aim was to characterize the RSC to layer V projection at the synaptic level, asking first whether it is excitatory or inhibitory and second whether its postsynaptic target cells include superficially projecting pyramidal neurons in layer V. To this end, we combined neuroanatomical and optogenetic *in vitro* electrophysiological experiments.

Materials and Methods

Surgery

Thirty adult female Sprague Dawley rats (Charles River) of 197–257 g weight were used in this study. The rats were housed in individual cages under a controlled environment (21 ± 1°C; humidity, 60%; lights on from 8:00 P.M. to 8:00 A.M.). Food and water were available *ad libitum*. The experimental protocols followed the European Communities Council Directive and the Norwegian Experiments on Animals Act and were approved by the Animal Welfare Committee of the Norwegian University of Science and Technology. Surgeries for tracer and recombinant adeno-associated virus (rAAV) injections were performed as described previously, with minor modifications (Kononenko and Witter, 2012). Animals were anesthetized with isoflurane and mounted in a stereotaxic frame (David Kopf Instruments). For each injection, openings were made in the skull exposing the brain surface over RSC or MEC. The stereotactic coordinates were based on the topographical description of RSC-to-MEC projections (Jones and Witter, 2007) and a stereotaxic rat brain atlas (Paxinos and Watson, 2007). Nomenclature is according to Sugar et al. (2011). The anteroposterior coordinates were measured from the posterior transverse sinus, 2.5 mm laterally to the midsagittal sinus, and the dorsoventral coordinates were measured from the brain surface after removal of the dura.

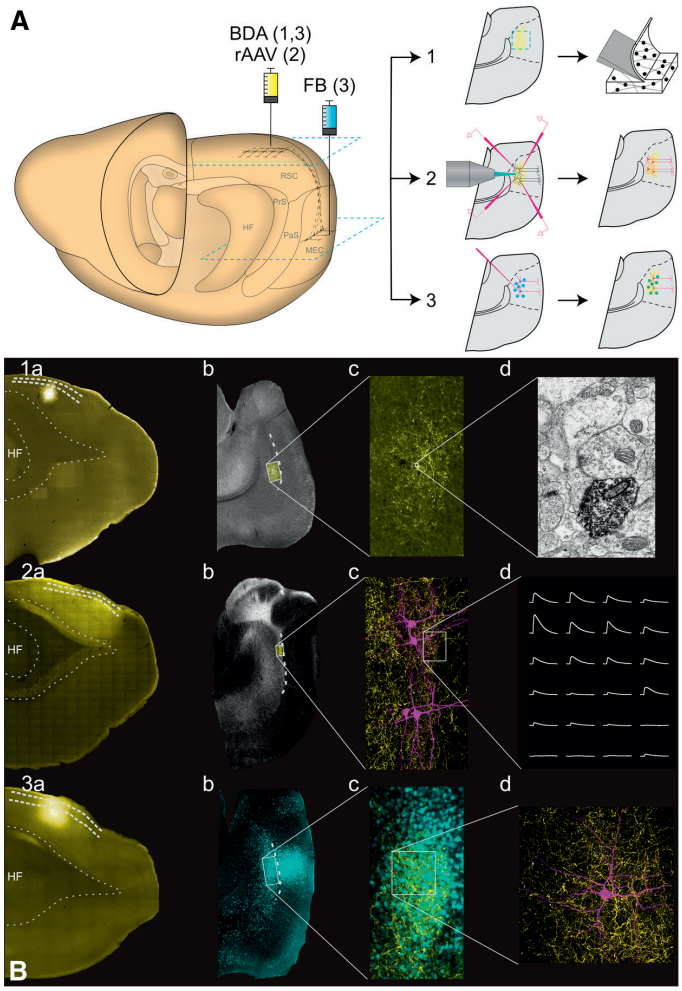

Figure 1. Experimental approaches used in the experiments. ***A***, Schematic drawing of the rat brain and the injection sites (left). ***1***, The anterograde tracer BDA was injected into RSC for EM experiments. ***2***, rAAV was injected in RSC for optogenetic experiments. ***3***, The retrograde tracer FB was injected into superficial layers of MEC and BDA was injected into RSC for confocal experiments. The blue squares depict the level of the horizontal sections of the MEC and RSC shown in ***B***. Each of the three experimental setups resulted in an anterogradely labeled plexus in MEC (yellow), intracellularly filled cells in Experiments 2 and 3 (magenta), and in Experiment 3 also retrogradely labeled neurons in MEC (blue dots). ***B***, Examples of individual experimental protocols. ***1***, For EM experiments, BDA was labeled with AF546-conjugated streptavidin so that injections (***1a***) and an anterograde plexus (***1b***, ***1c***) could be identified (yellow). Sections were processed for EM, and synaptic complexes labeled with DAB were sampled in EM (***1d***). ***2***, For *in vitro* optogenetic experiments, mCherry fluorescence (yellow) was used for identifying the injection in RSC (***2a***), anterograde plexus in MEC (***2b***, ***2c***), where intracellular recordings and axonal reconstructions were performed (***2c***, ***2d***). ***3***, For confocal analysis, BDA was labeled with AF488 (yellow; ***3a***, ***3c***), and FB-positive cells (blue; ***3b***, ***3c***) were filled with AF568 (magenta; ***3d***). PaS, Parasubiculum; PrS, presubiculum.

Three different experimental methods were used (Fig. 1). First we injected rAAV (titer 10^{-12}) into caudal RSC area 29b (A29b) and A29c in 11 rats. Each animal received a total volume of 3 μl, with 1 μl being injected in each of three different dorsoventral positions using a 10 μl NanoFil syringe assembled on a UMP3 pump (WPI). Each injection took 10 min, and we waited for 15 additional minutes before retracting the syringe. Second, the anterograde tracer biotinylated dextran amine [5% BDA, 10,000 molecular weight (Invitrogen) in 0.1 M PBS] was iontophoretically injected (positive-pulsed current of 6 μA, 6 s on, 6 s off for 10 min) into caudal RSC, in 19 rats using a glass micropipette with an inner tip diameter of 9–15 μm. Multiple injections involving different anteroposterior or dorsoventral levels were made aiming to involve at least parts of A29b, A29c, or A30. Third, eight of the rats also received injections with the retrograde tracer fast blue (FB; EMS-Chemie, 1% solution in PBS) in superficial layers of MEC. A volume of 150 nl was delivered with a 1 μl Hamilton syringe over 5 min, and the dye was allowed to diffuse for 15 min before removal of the syringe. Before the end of surgeries, the animals were given a dose of buprenorphine (Temgesic, 0.05 mg/kg; RB Pharmaceuticals) or carprofen (Rimadyl, 5 mg/kg; Pfizer)

subcutaneously. Suturing the skin over the wound completed surgery, and the animal was allowed to recover.

Optogenetic experiments

Viral vector construct and packaging. AAV2/2 was prepared and packaged with the Stratagene AAV Helper-Free System according to the user manual of the manufacturer. The purification, titration, and verification were described previously (Couey et al., 2013; Zhang et al., 2013). It was used to express the optogenetic effector in retrosplenial neurons projecting to MEC layer V. We used a light-gated cation channel ChIEF, a chimera of channelrhodopsin 1 (ChR1) and ChR2 from the unicellular green alga *Chlamydomonas reinhardtii* (ChIEF was provided as a generous gift by Dr. John Y. Lin from the laboratory of Dr. Roger Y. Tsien at the University of California, San Diego, San Diego, CA). It preserves the high ion permeability of ChR2 while gaining the reduced inactivation of ChR1. An additional point mutation, I170V, improves the channel closure rate after stimulation (Lin et al., 2009). The proviral vector containing ChIEF fused with mCherry under control of the calcium/calmodulin-dependent protein kinase II α (αCaMKII) promoter was prepared as described previously (Couey et al., 2013). Before use, all virus batches were titer matched by diluting to 1×10^{12} viral genomic particles/ml in PBS.

In vitro *recordings.* After a survival time of up to 6 weeks after injections of rAAV, animals were anesthetized with isoflurane and perfused through the heart with a small volume of ice-cold artificial CSF (ACSF) cutting solution containing the following (in mM):110 choline chloride, 25 $NaHCO_3$, 25 D-glucose, 11.6 sodium ascorbate, 7 $MgSO_4$, 3.1 sodium pyruvate, 2.5 KCl, 1.25 NaH_2PO_4, and 0.5 $CaCl_2$ (aerated with 95% O_2/5% CO_2 before decapitation). The brain was quickly dissected, and 400-μm-thick horizontal slices of the RSC or MEC were cut with a vibratome (model 3000; Harvard Apparatus) and incubated in oxygenated ACSF containing the following (in mM): 127 NaCl, 25 $NaHCO_3$, 25 D-glucose, 2.5 KCl, 2 $MgSO_4$, 1 $CaCl_2$, and 1.25 NaH_2PO_4 (for 45 min at 37°C). Thereafter, the slices were oxygenated at room temperature until used.

Multiple whole-cell recordings were made with glass micropipettes filled with a standard intracellular solution containing the following (in mM): 120 K-gluconate, 10 KCl, 10 HEPES, 10 K-phosphocreatine, 4 ATP-Mg, and 0.4 GTP, pH adjusted to 7.3 with KOH (270–285 mOsm). Biocytin (3–5 mg/ml; Sigma) was included in the pipette for later anatomical verification of cell location and morphology. All recordings were done at 34°C in ACSF with 1.5 mM $MgSO_4$ and 2 mM $CaCl_2$. Layer V cells in MEC or RSC were first visualized using infrared differential interference contrast (IR-DIC) microscopy. Individual cells or groups of cells ~100 μm deep from the cutting surface were visually identified, and up to four neighboring cells were targeted for whole-cell patch. All cells were first maintained in the "on cell" configuration until all contacts had achieved a +1 GΩ resistance. The entire cluster was then opened to whole-cell configuration. Recordings were made in current-clamp mode with the membrane potential maintained between −60 and −65 mV. After the whole-cell configuration was established, recorded responses to steps of current injection allowed to electrophysiologically classify each cell (Canto and Witter, 2012). Recordings were made using Axon Multiclamp amplifiers (Molecular Devices) sampling at intervals of 100 μs (10 kHz), digitized using an ITC-1600 analog-to-digital interface in combination with custom acquisition software based on Igor Pro version 6.0 (WaveMetrics). The same software was also used to control whole-cell current injection (both timing and levels). Series resistance was compensated to a maximum bridge balance value of 20 MΩ. In case series resistance exceeded this value, recordings were not included in signal analysis.

For photostimulation, we used a customized laser control system (UGA-40 with a 473 nm laser; Rapp OptoElectric) coupled to a microscope (Olympus BX51WI) equipped with a water-immersion objective [40×, 0.8 numerical aperture (NA); Olympus] and controlled by the recording software. This configuration resulted in a beam diameter of ~5 μm and power adjustable up to 650 μW at the specimen (scattering in the tissue was not taken into account). Stimuli were arranged in a rectangular 8×6 grid with 20 μm spacing, positioned over the recorded cluster avoiding interference from the recording pipettes. The stimulus duration was 2 ms, delivered to each point of the grid in a pseudorandom order with 250 ms interval. The stimulation pattern was repeated 30 times. Voltage deflections were cut at a threshold of 10 SDs beyond the average variation of the membrane potential before being identified as a response. The voltage responses obtained from stimulation of each unique location in the grid were averaged to produce a normalized mean response for each point. Voltage deflections that did not reach the threshold were not included in the average. Only grid locations with eight or more identified responses were included in subsequent analysis. From the averaged responses, onset times and amplitudes were determined for each location. In several slices, we blocked action potentials (APs) by adding tetrodotoxin (TTX; 5 μM; Sigma), a neurotoxin that binds to voltage-gated Na^+ channels (Narahashi et al., 1964). The drug was diluted in ACSF and perfused into the chamber after control recordings. After 1 min incubation, stimulation was repeated 30 times. Data analysis was done offline using Igor and MATLAB (WaveMetrics) software.

Immunohistochemistry. Immediately after each recording session, the slices were placed in 4% paraformaldehyde (PFA) overnight and subsequently permeabilized by washing seven times with 0.1 M phosphate buffer (PB) containing 1% Triton X-100 (PBT-1%), blocked for 3 h with PBT-1% with 5% normal goat serum (NGS; X0907; Dako), and then incubated for 72 h with a monoclonal anti-mCherry antibody (1:500 in PBT-1% and 5% NGS; Clontech) in 4°C. Slices were then washed three times in PB and incubated for 12 h with the mixture of Alexa Fluor (AF) 568-conjugated anti-mouse secondary antibody (1:350; Invitrogen) and AF488-conjugated streptavidin (1:350; Invitrogen) in PBT-1% and 5% NGS in 4°C. After washing in PB, the sections were incubated with the NeuroTrace deep red fluorescent Nissl stain (1:200; Invitrogen) for 30 min. After staining, the slices were washed in PB, dehydrated in increasing ethanol concentrations (30, 50, 70, 90, and twice in 100%, 10 min each) and then in a 1:1 mixture of ethanol/methylsalicylate, and finally cleared and mounted in methylsalicylate.

Electron microscopy

After 9–14 d of survival, rats with BDA injections in caudal A29b, A29c, and A30 received an overdose of Equithesin (11 mg/kg bodyweight, i.p.; Sanofi Sante). They were subsequently transcardially perfused with a fresh filtrated Ringer's solution (in mM: 145 mM NaCl, 3 mM KCl, and 2 mM $NaHCO_3$ at 4°C, brought to pH 6.9 with O_2). Next, the perfusion fluid was changed to 4% freshly filtered depolymerized PFA (Merck) with 0.1% glutaraldehyde (Merck) in 125 mM PB at 4°C. After completion of the perfusion, the brains were removed from the skull and postfixed overnight at 4°C in the same fixative. Brains were washed in 125 mM PB and cut horizontally with a vibrating microtome (Leica VT1000S; bath fluid, 125 mM PB, 4°C) at 50 μm, and all sections were collected into six equally spaced series. The sections were collected in vials containing PB at 4°C. The series were then processed in three different ways. One series was transferred to 2% dimethylsulfoxide (DMSO; Merck) in 125 mM PB and 20% glycerine (Merck) and stored at −20°C for later use, one series was processed for fluorescent microscopy, and the remaining series were processed for electron microscopy (EM).

Processing for fluorescent microscopy. Sections were rinsed three times for 10 min in PB and then three times for 10 min in Tris-buffered saline (TBS; 50 mM Tris and 153 mM NaCl) with 2% Triton X-100 (TBS-Tx; Merck), pH 8.0. The sections were incubated in AF546-conjugated streptavidin (Invitrogen) in a 1:200 solution with TBS-Tx overnight at 4°C. Next, the sections were rinsed two times for 5 min in Tris/HCl (50 mM Tris), pH 7.6, and subsequently mounted on glass slides from a 0.2% gelatin solution in Tris/HCl. After overnight drying, they were cleared in toluene and coverslipped with Entellan (Merck). Sections were inspected with dark-field and fluorescent illumination at the appropriate excitation wavelength (Zeiss Axio Imager M2), and digital images of the anterogradely labeled plexus in MEC were obtained.

Processing for EM. The sections were rinsed for 10 min in an ascending series of 10, 15, and 20% DMSO in PB at 4°C. The sections were quickly frozen in isopentane cooled by solid carbon dioxide and subsequently recovered and thawed. This freeze and thaw procedure was repeated twice. Sections were subsequently rinsed three times for 10 min in PB at 4°C and two times for 5 min in TBS, pH 7.6, at 4°C. The sections were incubated with avidin–biotin–peroxidase complex (Vectastain ABC kit

standard, PK-4000; Vector Laboratories) in TBS for 48 h at 4°C. Next, they were rinsed for three times for 10 min in TBS and two times for 5 min in Tris/HCl, pH 7.6, and subsequently stained with filtrated diaminobenzidine tetrahydrochloride (DAB; 0.067% in Tris/HCl; Sigma-Aldrich) 4°C, to which a 30% solution of H_2O_2 had been added immediately before use. If during microscopic inspection the projection from the RSC appeared to be clearly labeled in MEC, the DAB reaction was stopped with Tris/HCl, and the sections were rinsed two times for 5 min in the same buffer. Brain sections containing the densest anterograde labeling in MEC were selected and further processed.

The EC was carefully dissected from the section and postfixed in the dark for 1 h in 2% OsO_4 (Merck) in 0.1 M PB, pH 7.4. The sections were rinsed two times for 5 min in PB and then dehydrated in ascending series of ethanol in water: 50% (10 min), 70% (10 min), 90% (10 min), and 100% (four times for 15 min). Subsequently, they were put in propylenoxyde (Merck) two times for 15 min, followed by a mixture of propylenoxyde and epoxy resin (Ladd Research), first two volume parts propylenoxyde and one volume part epoxy resin for 30 min, followed by one volume part propylenoxyde and two volume parts epoxy resin for 30 min before they were put in pure epoxy resin overnight. In all solutions including epoxy resin, 1.5% of dimethylaminomethylphenol was added (Ladd Research). The sections were then embedded in epoxy resin between polyethylene foil (3M Color Laser Transparency film, CG3710) at 60°C overnight. All sections were then inspected under a dissection microscope to determine the location of the labeled plexus in MEC. Selected plexus were carefully dissected from the sections and glued with epoxy resin on blocks of procured epoxy resin. The blocks where further cured for 24–48 h at 60°C.

After curing, series of ultrathin sections (60–70 nm) were cut with an ultramicrotome (EM UC6; Leica) equipped with a diamond knife (Diatome ultra 45°) and collected on Formvar-coated (0.5% in dichlorethan; Electron Microscopy Sciences), single-slot copper grids. Sections were stained in the dark with 4% uranyl acetate in 50% ethanol for 17–20 min and counterstained with 1% lead citrate (Electron Microscopy Sciences) in 0.1 M NaOH for 4–5 min. Material was inspected with a transmission electron microscope (JEM-1011; Jeol). Digital images were taken (Morada; Olympus), and lengths of all postsynaptic densities (PSDs) and the shortest and longest diameters of each axonal bouton were measured in iTEM (version 5.0; Olympus Soft Imaging Solutions). Serial images of selected synaptic complexes were imported to Neurolucida (MicroBrightField) to make three-dimensional (3D) reconstructions.

Quantitative analysis of synapses. Synapses were obtained from at least two different 50-μm-thick sections of each of two animals. To increase the likelihood of finding synapses, the densest part of the terminal plexus in a chosen vibratome section was isolated. The synapse type and the postsynaptic target were determined in a randomly selected reference section. All synapses in this ultrathin section were counted, and their phenotype was determined. To be included, a synapse needed to comprise a BDA-labeled axon terminal, an electron-dense synaptic membrane specialization, a morphological identifiable postsynaptic element, and a distinguishable synaptic cleft. To avoid double counting, only synapses that were not visible in a parallel lookup section were used in analyses (Gundersen, 1986). Serial sections were used to establish with certainty the properties of identified synapses.

Synapse properties in terms of presynaptic varicosities and postsynaptic targets were determined on the basis of their overall morphology, using criteria described in detail previously (Gray, 1959; Uchizono, 1965; Colonnier, 1968). Synapses with a thick PSD, round vesicles in the presynaptic element, and a wide synaptic cleft were categorized as asymmetrical synapses, whereas synapses with a thin PSD, pleomorphic vesicles, and a narrow synaptic cleft were classified as symmetrical synapses. Postsynaptic targets were classified as spines if they had a clear cytoplasm and/or a spine apparatus. Postsynaptic targets with mitochondria and/or visible microtubules were classified as dendritic shafts. In each animal, analysis was continued until a sample size of ~100 synapses was reached.

After categorization of the synapses and postsynaptic targets, all electron micrographs were presented blindly to an unbiased independent observer who was asked to categorize the boutons and postsynaptic target according to the same criteria described above. Boutons and postsynaptic targets on which the first and second observer did not agree were discussed together. For all synapses analyzed the type could be determined.

Confocal analysis of putative synaptic contacts

Intracellular injections. Twenty-one days after BDA and FB tracer injections, animals were anesthetized by an overdose of Equithesin and perfused transcardially with Ringer's solution, followed by ice cold 4% PFA in PBS. The brain was extracted and postfixed in 4% PFA for 2 h in 4°C. Next, 100-μm-thick horizontal slices of RSC were cut using a vibratome (VT1000S; Leica) with ice-cold 0.1 M PB as bath fluid. Cutting started at the most dorsal level of the brain, and, after reaching the level that comprised the most dorsal part of MEC, alternating 100 and 400 μm slices were obtained. The 100-μm-thick slices were stained for the presence of BDA following the protocol described above for the EM study. The slices were scanned using a slide scanner (MIRAX MIDI; Zeiss) equipped with an AxioCam digital camera (Zeiss). The single filter set #43 (Zeiss; excitation bandpass, 545/25 nm; beam splitter, 570 nm; emission bandpass, 605/70 nm) was used for RSC sections labeled with AF546. Filter sets #43 and #49 (Zeiss; excitation, 365 nm; beam splitter, 395 nm; emission bandpass, 445/50 nm) were used for scanning MEC sections containing AF546 and FB. RSC scans were analyzed to confirm the injection site. MEC scans were used to verify the overlap between RSC fibers (AF546) and retrogradely labeled MEC layer V cells (FB). Adjacent 400 μm MEC slices were then placed in a chamber under a fixed-stage upright microscope (Axio Examiner; Zeiss) equipped with PlanApo 20×, 1.0 NA water dipping lenses, micromanipulator (Luigs & Neumann), and a custom-assembled iontophoretic injection device. The sections were simultaneously imaged with IR-DIC to resolve cell details and with fluorescent filter set 75HE (Zeiss; excitation, 365 nm; beam splitter, 395 nm; emission bandpass, 445/50 nm; separated from the IR-DIC by beam splitter, 660 nm) to visualize FB and AF568. Randomly selected FB-positive cells in layer V of MEC were intracellularly injected with a solution of AF568 hydrazide (10 mM in PBS; Invitrogen) using a 70–130 Ω glass pipette. Negative current was applied to the micropipette (2 nA, 500 ms on, 500 ms off) for at least 10 min to completely fill the impaled cell and its dendrites. Immediately after filling, the slices were transferred to 4% PFA and postfixed overnight in 4°C. Subsequently, the 400 μm slices were permeabilized by washing seven times with PBT-1%, blocked for 3 h with PBT-1% containing 5% NGS, and then incubated for 24 h with AF488-conjugated streptavidin (1:300 in PBT-1% and 5% NGS) in 4°C. Slices were then washed three times in PB, dehydrated, mounted in methylsalicylate, and imaged (see below).

Staining for putative synaptic contacts. In case of four intracellularly filled MEC layer V neurons, the existence of putative synaptic contacts with BDA-labeled RSC axons was assessed with the use of confocal laser-scanning microscopy. In this material, we stained for the presence of marker molecules for both presynaptic and postsynaptic synaptic elements, i.e., synaptophysin and PSD-95, respectively. After BDA/AF568 confocal imaging (see below), the 400 μm slices were rehydrated by reversing the dehydration protocol, washed three times in PB, and incubated in cryoprotective solution (30% w/v sucrose in PB) overnight. The slices were then flattened and embedded in NEG 50 (Thermo Fisher Scientific) on a cryostat chuck and quickly frozen in −20°C. The sections were resliced at 50 μm on a Lauda 1720 cryostat (Leitz), washed three times with 0.1 M PB, permeabilized in 0.1 M PB containing 0.5% Triton X-100 (PBT-0.5%), blocked for 3 h with PBT-0.5% with 5% NGS, and subsequently incubated for 48 h with a mixture of a monoclonal anti-PSD-95 antibody (1:150, P78352; NeuroMab) and a polyclonal anti-synaptophysin antibody (1:100, ab14692; Abcam) in PBT-0.5% and 5% NGS in 4°C. Slices were washed three times in PB and incubated for 4 h with the mixture of AF514-conjugated anti-rabbit secondary antibody, AF633-conjugated anti-mouse secondary antibody, and AF488-conjugated streptavidin (1:350; all from Invitrogen) in PBT-0.5% and 5% NGS at room temperature. Finally, after three washes in PB, sections were suspended in 0.1 M Tris-HCl, mounted on Superfrost slides (WPI), dried overnight, and coverslipped in Entellan.

Confocal microscopy

All sections were imaged with a Zeiss Meta 510 confocal microscope. Unless indicated otherwise, FB was excited by ultraviolet laser (λ = 405 nm; emission bandpass, 450/60 nm), AF488 was excited by argon laser (λ = 488 nm; emission bandpass, 505–550 nm), AF568 was excited by helium/neon laser (λ = 568 nm; emission bandpass, 595/40 nm), and NeuroTrace Nissl stain was excited by helium/neon laser (λ = 633 nm; emission long pass, 655 nm; dichroic mirror, 405/488/561/633/KP725).

Imaging of putative synaptic contacts. First, an overview image was acquired to confirm the position of AF568-filled cells within MEC. An air PlanApo 10×, 0.45 NA lens was used at the resolution of 1024 × 1024 pixels, 8-bit sampling, and *z* increment of 10 μm. Next, the colocalization of AF568 and retrograde FB labeling was confirmed for each filled cell. For this, an air PlanApo 20×, 0.8 NA objective lens was used at the resolution of 1024 × 1024, 8-bit sampling, and *z* increment of 5 μm. Finally, for high-resolution 3D analysis, a detailed scan of the AF488 (RSC fibers) and AF568 (MEC layer V cells) channels was taken using a 63×, 1.40 NA oil DIC objective lens at a resolution of 1024 × 1024 pixels, 8-bit sampling, and *z* increment of 0.35 μm. The optical section thickness was set to 0.7 μm by adjusting the pinhole for each channel. After 3D reconstruction and mapping (see below), each putative contact was then imaged in detail using 64×, 1.40 NA oil DIC objective lens at a resolution of 256 × 256 pixels, zoom 6, 8-bit sampling, and *z* increment of 0.35 μm.

Imaging of synaptic markers. In case of quadruple staining of synaptic contacts, the linear unmixing of closely located fluorescence peaks was performed using the Zeiss Meta unit and ZEN software. For three of the unmixed fluorochromes (AF488, AF514, and AF568), a reference emission spectrum was acquired using the argon laser excitation ($\lambda_{excitation}$ = 514 nm; dichroic mirror, NT 80/20; $\lambda_{emission}$ = 497–583 nm; $\Delta\lambda$ = 10 nm) at 64×, 1.40 NA oil DIC objective lens at a resolution of 256 × 256 pixels, zoom 6, 8-bit sampling, and the *z* increment of 0.35 μm. The spectral scan and unmixing of the specimen was then performed and followed by scanning of the AF633 channel with the same optical pathway ($\lambda_{excitation}$ = 633 nm; dichroic mirror, NT 80/20; $\lambda_{emission}$ = 636–711 nm). Final images were obtained by combining the results of the spectral scan (AF488, AF514 and AF568 channels) and the AF633 channel.

Confocal image analysis

3D reconstruction and mapping. Dendritic reconstruction was conducted as described previously (Kononenko and Witter, 2012). We used a custom plugin, "Skeleton tool" (Schmitt et al., 2004; Evers et al., 2005), for Amira version 4.1.2 to trace the dendritic trees and positions of the spines. For the Sholl analysis (Sholl, 1953), the number of branches crossing concentric spheres of increasing radius (Δr = 10 μm) originating at the soma was counted. Spine density was expressed as the number of spines per 10 μm of dendrite length. To quantify the number of BDA-filled putative axonal boutons and their distribution along reconstructed dendrites, the dendritic surface was expressed as triangles (Evers et al., 2005). The BDA-positive pixels were identified by thresholding the AF488 channel according to the Otsu method (Otsu, 1979). The proximity of BDA-positive voxels within 300 nm from each surface element identified as a triangle was calculated and expressed as heat map on the dendritic surface. Finally, for each putative contact, the zoomed image was analyzed, and it was determined whether it adheres to previously established criteria of a presynaptic bouton (Wouterlood et al., 2008), being an axonal swelling having a diameter three times bigger than the preceding fiber.

Synaptic reconstruction. Resliced and quadruple-labeled images (presynaptic fibers, AF488; synaptophysin, AF514; postsynaptic dendrites, AF568; postsynaptic PSD-95, AF633) were loaded into FIJI software, and previously evaluated putative synaptic contacts were again identified using the AF488 and AF568 channels. The distribution of each fluorochrome along the axis connecting the center of a presynaptic bouton and the center of dendritic spine (for spine synapses) or dendritic segment (for shaft synapses) was measured. Putative contacts showing local labeling peaks for both synaptophysin (AF514) and PSD-95 (AF633) along that axis (between peaks for AF488 and AF568) were considered synaptic. Because the axial resolution of optical microscopy is relatively poor, only the synapses in the *x–y* plane were measured. 3D reconstructions of the synapses were performed in Amira version 4.1. The confocal stacks were filtered using the Gaussian filter and thresholded using Otsu's algorithm (Otsu, 1979), and surfaces for each channel were rendered and combined.

mCherry imaging and axonal tracing. First, an overview of biocytin-filled cells within layer V of MEC and trajectory of their axons was acquired using an air PlanApo 20×, 0.8 NA objective, resolution of 1024 × 1024, 8-bit sampling, and *z* increment of 2 μm. Then, a detailed scan of the AF488 (biocytin-filled cells), AF568 (AAV-expressing cells), and NeuroTrace Nissl stain was obtained (40×, 1.30 NA oil DIC objective lenses were used at resolution of 1024 × 1024 pixels, 8-bit sampling, and *z* increment of 0.5 μm). The 20× image stacks were then loaded into the Simple Neurite Tracker plugin in FIJI software, and axonal trajectories were plotted.

Statistical analyses

All numbers are reported as mean ± SEM.

Electron microscopic experiments. The relative numbers of synapse types in each hemisphere and each animal were compared with a Fisher's exact test. Significant differences were accepted at $p < 0.05$. Measured lengths of PSDs and the average of the longest and shortest diameter of the presynaptic boutons were imported into SPSS. ANOVA and *post hoc* analysis of least significant difference were used to assess different sources of variation of the morphological data. Significant differences were accepted at $p < 0.05$.

Optogenetic experiments. Patched cells were grouped as interneurons or principal neurons based on electrophysiological and morphological characteristics. The average input resistances and kinetics of APs generated in response to depolarizing current step and onset were compared with two-sample *t* tests. Differences in onset time after photostimulation of retrosplenial and entorhinal neurons were compared using two-sample *t* tests. Significant differences were accepted at $p < 0.05$.

Confocal experiments. The proportionality between the density of labeled axons and the number of synaptic contacts assessed in the confocal microscope was assessed with *F* test for linear regression. Whether the distribution of contact frequencies normalized to the plexus density was unimodal or polymodal were tested with a Kolmogorov–Smirnov test. Significant differences were accepted at $p < 0.05$.

Results

Morphological assessment of synaptic contacts in MEC

In view of the known topographical organization of the RSC projection to MEC (Shibata, 1994; Jones and Witter, 2007), we aimed to inject BDA in multiple sites in caudal RSC to obtain a dense terminal plexus in MEC (Fig. 1*A1*,*B1*). Of the 11 animals used in the experiments destined for EM, seven animals had successful injections in RSC, without involvement of deep adjacent white matter. In total, we obtained 16 injections of BDA in RSC: seven in caudal A29ab, three in caudal A29c, two in intermediate rostrocaudal A29c, and four in caudal A30. All injections in caudal RSC resulted in a densely labeled terminal plexus in layer V of dorsal and intermediate MEC and layer III and V of dorsal presubiculum. Sparse labeling was observed in layer III of MEC. These observations are in accordance with previously published data (Shibata, 1994; Jones and Witter, 2007; Kononenko and Witter, 2012). The labeled fibers in layer V were relatively thick and had clearly visible varicosities. We subsequently selected two animals that had the densest terminal labeling after processing the tissue for EM analysis and good preservation of the ultrastructure. In animal 12901, the injections were located in layers V and VI of caudal A29ab in the right hemisphere and in layers IV and V of caudal A29c in the left hemisphere. In animal 13976, the center of the injection in the left hemisphere was located in layer II–IV of caudal A30, whereas in the right hemisphere, it involved all layers of caudal A30. In the latter animal, BDA-filled neurons

were observed in the distal part of the septal subiculum. This is likely a result of retrograde transport of BDA along subicular axons with terminals in the area in which the injections were placed (Vogt and Miller, 1983; Köhler, 1985; Witter et al., 1990; van Groen and Wyss, 1990, 2003; Miyashita and Rockland, 2007). It cannot be ruled out that BDA is transported anterogradely from the subiculum, labeling axon collaterals also terminating in the deep layers of MEC and thereby biasing the results. However, we find this very unlikely because the number of retrogradely filled neurons was very low, we never observed BDA-filled axons leaving the subiculum, and subicular neurons rarely have divergent extrinsic axon collaterals, implying that retrogradely labeled cells that project to RSC do not likely project to MEC as well (Naber and Witter, 1998).

Quantification of synapses and postsynaptic targets

In the ultrathin sections of MEC layer V, obtained from either of the two animals, labeled axons and axon terminals could easily be identified by the presence of clear DAB deposits. We observed both asymmetrical and symmetrical synapses. The first were characterized by having a thick PSD (more than twice the thickness of the PSD) and a wide synaptic cleft. Spherical vesicles could be observed in the presynaptic terminal (Figs. 2*A–D*, 3*A*). Symmetrical synapses had a postsynaptic and presynaptic density of equal thickness, a narrow synaptic cleft, and pleomorphic presynaptic vesicles were less frequently encountered (Figs. 2*E*, 3*B*; Gray, 1959; Uchizono, 1965; Colonnier, 1968). For all synapses that lacked a clear asymmetrical morphology, we analyzed consecutive serial sections of entire presynaptic and postsynaptic complexes (Fig. 3).

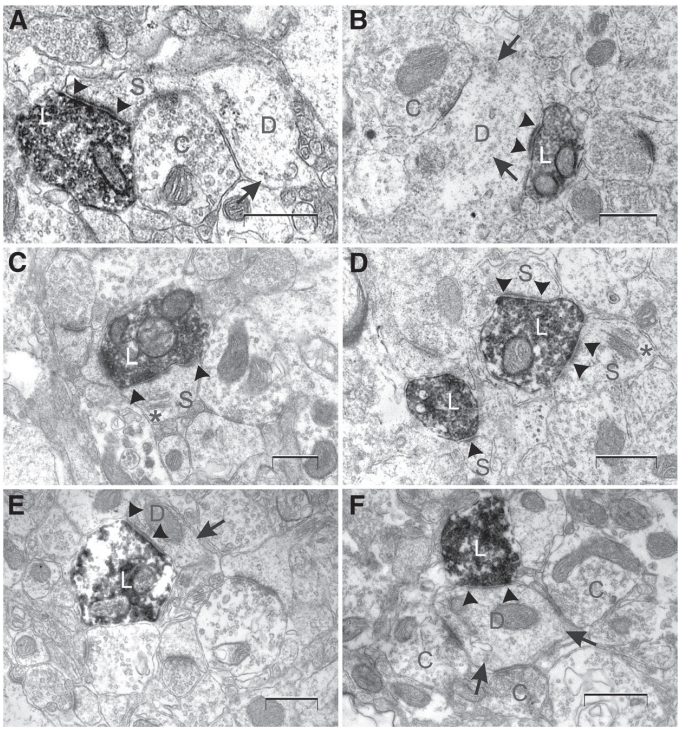

Figure 2. Electron micrographs of the main categories of labeled axon terminals in layer V of MEC. ***A***, A labeled axon terminal with round vesicles and a thick PSD forming an asymmetrical synapse with a dendritic spine emerging from a dendritic shaft. A converging unlabeled bouton (marked with C) possibly makes a synaptic contact with the spine neck. The synaptic complex is sampled from animal 12901. ***B***, A labeled axon terminal with round vesicles and a thick PSD forming an asymmetrical synapse with a dendritic shaft. A converging unlabeled bouton is making a symmetrical contact with the same dendritic shaft. The synaptic complex is sampled from animal 13976. ***C***, A labeled axon terminal with round vesicles and a thick perforated PSD making an asymmetrical synapse with a dendritic spine. A spine apparatus is evident. The synaptic complex is sampled from animal 12901. ***D***, A MSB and a SSB, sampled from animal 13976, are making in total three synapses with dendritic spines. The PSDs are thick, the synaptic clefts are wide, and the vesicles are round. ***E***, A labeled axon terminal making a symmetrical synapse with a dendritic shaft. The PSD is thin, and the synaptic cleft is relatively narrow. The synaptic complex is sampled from animal 12901. ***F***, A labeled axon terminal making a synapse on a dendritic shaft. Three converging unlabeled boutons are making synapses on the same shaft. The total synaptic complex, sampled from animal 12901, is reconstructed in Figure 4*A*. Synaptic specializations are indicated with arrowheads and microtubuli with arrows. L, Labeled axon terminal; D, dendrite; C, converging unlabeled axon terminal; S, spine; *, spine apparatus. Scale bars, 500 nm.

Postsynaptic targets were either dendritic shafts characterized by microtubules or mitochondria in the cytoplasm, or dendritic spines characterized by their overall dimensions, the presence of clear cytoplasm, and/or the presence of a spine apparatus (Gray, 1959). No axo-axonic or axo-somatic synapses were observed. PSDs were commonly continuous (Figs. 2*A*,*B*,*D–F*, 3), although perforated synapses were observed as well (Figs. 2*C*, 4*B*). In general, presynaptic elements formed synapses with only one postsynaptic element, so-called single synaptic boutons (SSBs), although multiple synaptic boutons (MSBs) were regularly observed as well (Figs. 2*D*, 4).

In total, 262 boutons, forming 301 synapses on identified postsynaptic targets, were characterized in both hemispheres of two animals (Table 1). Analyses revealed no statistically significant differences in relative numbers between the two rats or their four hemispheres. In both animals, 98% ($n = 296$) of the labeled terminals in layer V of MEC were characterized as part of asymmetrical synapses, whereas 2% ($n = 5$) of the synapses were classified as symmetrical. Dendritic spines represented 91% ($n = 273$) of the postsynaptic targets, whereas 9% ($n = 28$) were dendritic shafts. In 36% ($n = 10$) of the synapses onto dendritic shafts, these shafts showed additional multiple unlabeled synaptic contacts showing a circular arrangement around the shaft (Figs. 2*F*, 3*A*, 4*A*).

The majority of the asymmetrical synapses (92%, $n = 271$) contacted dendritic spines, whereas a small fraction (8%, $n = 25$) contacted shafts. In contrast, symmetrical synapses showed no clear preference for dendritic spines or shafts (two symmetrical synapses on dendritic spines and three on dendritic shafts). We observed that, of the asymmetrical synapses, 13% ($n = 34$) were of the MSB type. These boutons made synapses with two to four postsynaptic elements. The MSBs contacted either only dendritic spines ($n = 29$; Fig. 4*B*) or both dendritic spines and dendritic shafts ($n = 5$; Fig. 4*A*). Furthermore, 22% ($n = 59$) of the asymmetrical synapses were of the perforated type, and they contacted dendritic spines ($n = 56$) or dendritic shafts ($n = 3$).

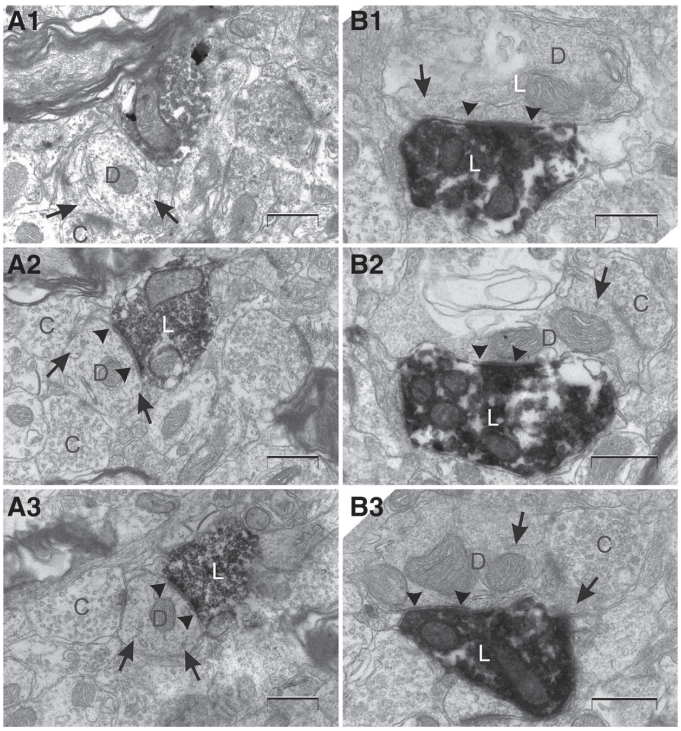

Figure 3. Representative electron micrographs taken from a series of ultrathin sections. Series of sections through an asymmetrical (***A1–A3***) and a symmetrical synapse (***B1–B3***) between a labeled axon terminal and a dendritic shaft in layer V of MEC of animal 12901. The asymmetrical synapse (***A1–A3***) has a thick PSD (not developed in ***A1*** and conspicuous in ***A2***), round vesicles, and a wide synaptic cleft. The shaft is sectioned approximately perpendicular to its long axis. The symmetrical synapse (***B1–B3***) has a thin PSD (consistent throughout the series), pleomorphic vesicles, and a narrow synaptic cleft. The shaft is sectioned approximately parallel to its long axis. Converging inputs from unlabeled axon terminals to both shafts are evident. Synaptic specializations are indicated with arrowheads, and microtubuli are marked with arrows. L, Labeled axon terminal; D, dendrite; C, converging unlabeled axon terminal. Scale bars, 500 nm.

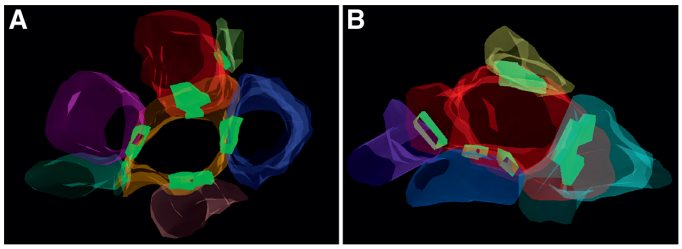

Figure 4. 3D reconstructions of representative synaptic complexes. ***A***, A labeled bouton (red), sampled from animal 12901, forming a synapse with a dendritic shaft (orange) and a dendritic spine (yellow). Four unlabeled boutons (blue, pink, turquoise, and purple) are making additional converging synaptic contacts with the same shaft. Synaptic clefts and specializations are color coded as light green. The reconstructions are based on serial sections of the synaptic complex demonstrated in Figure 2*F*. ***B***, A labeled MSB (red), sampled from animal 13976, forming a synapse with four separate dendritic spines (yellow, turquoise, blue, and purple). The synapses made with the purple and blue spines are perforated. Synaptic clefts and specializations are color coded as light green.

The average diameter of all boutons was 860 ± 17 nm. Boutons with an asymmetrical synapse had an average diameter of 859 ± 17 nm, whereas boutons with a symmetrical synapse had an average diameter of 897 ± 76 nm. SSBs had an average diameter of 1025 ± 49 nm, whereas MSBs had an average diameter of 835 ± 18 nm. Boutons with nonperforated synapses had a significantly smaller average diameter (805 ± 17 nm) compared with boutons with a perforated synapse (1050 ± 39 nm; $F_{(1,252)} = 14.385$, $p < 0.0005$; three-way ANOVA). The categorization of the synapse as symmetrical or asymmetrical or the categorization as MSB or SSB had no significant correlation with the average diameter ($F_{(3,252)} = 0.755$, $p = 0.52$; $F_{(1,252)} = 0.407$, $p = 0.52$).

The average length of the PSDs was 352 ± 8 nm. Asymmetrical synapses on spines had an average PSD length of 347 ± 8 nm, asymmetrical synapses on shafts 402 ± 33 nm, and symmetrical synapses on spines 92 ± 65 nm, and symmetrical synapses on shafts had an average PSD length of 419 ± 66 nm. Synapses belonging to SSBs had an average length of 350 ± 9 nm, whereas synapses belonging to MSBs had an average length of 357 ± 17 nm. Nonperforated synapses had a shorter average PSD length (317 ± 7 nm) compared with perforated synapses (495 ± 18 nm). Three-way ANOVA revealed that perforated synapses and synapse type had a significant correlation with the PSD length ($F_{(1,292)} = 39.356$, $p < 0.0005$; $F_{(3,292)} = 3.048$, $p = 0.029$), whereas the classification as MSB or SSB was not significantly correlated with PSD length ($F_{(1,292)} = 0.041$, $p = 0.84$). *Post hoc* analysis revealed that asymmetrical synapses on shafts had significantly larger PSD compared with asymmetrical synapses on spines ($p = 0.027$) and symmetrical synapses on shafts ($p = 0.047$).

Functional assessment of synapses in MEC

The morphological quantification of the majority of RSC synapses in MEC as asymmetrical onto spines indicated the presence of a direct, primarily excitatory input from RSC into spiny neurons in layer V of MEC (Gray, 1959; Eccles, 1964; Uchizono, 1965; Colonnier, 1968). To functionally validate this morphologically based inference, we applied an optogenetic *in vitro* approach (Petreanu et al., 2007). We expressed the ChR variant ChIEF in neurons of RSC by injecting rAAV vector expressing the fusion of ChIEF and the reporter protein mCherry under the αCaMKII promoter into caudal A29b and A29c (for details, see Materials and Methods). After 6 weeks, expression of mCherry was visible in all layers of RSC. Expression of the marker was only detected in the RSC cells and their projecting axons (Figs. 1*A2*,*B2*, 5); no ChIEF expression was observed in MEC neurons. Consistent with previous studies using anterograde tracers, strongly labeled projections from RSC to both deep and superficial layers of presubiculum, deep layers of parasubiculum, and deep layers of MEC were observed (Fig. 1*B2*).

Table 1. Distribution of asymmetrical and symmetrical synapses and their postsynaptic targets

			Asymmetrical		Symmetrical	
Animal	Boutons (*n*)	Synapses (*n*)	Spines	Shafts	Spines	Shafts
12901 R	95	104	85%	13%	0%	2%
12901 L	71	81	91%	7%	1%	0%
13976 R	40	48	94%	6%	0%	0%
13976 L	56	68	94%	3%	1%	1%
Total	262	301	90%	8%	1%	1%

Distribution of asymmetrical and symmetrical synapses and their postsynaptic targets in each of the two hemispheres of each of the two animals used for ultrastructural assessment. R, Right; L, left.

We first characterized the direct voltage responses of ChIEF-positive RSC cells to laser-scanning photostimulation. The stimulation grid (8 × 6, 20 μm spacing) was positioned over the recorded RSC layer V neurons (Fig. 5*A*). At high light intensity levels (>230 μW; Fig. 5*A*, black traces), illumination of each point on the grid evoked an AP in the recorded cell. In some cases, a brief burst of APs was recorded. With the decrease of laser power, stimulation at some grid points evoked subthreshold membrane depolarizations. At 23 μW (Fig. 5*A*, red traces), only direct somatic stimulation evoked an AP. The average onset of the responses was 11.67 ± 2.7 ms from the software trigger (n = 288; Fig. 5*C*).

Previous studies showed that ChR-positive axons can survive *in vitro* after separating from the soma and that these axons respond to photostimulation with an AP and subsequent synaptic release (Petreanu et al., 2007). In 400-μm-thick horizontal slices of EC, we observed mCherry-labeled terminal fibers originating in RSC (Fig. 5*B*). In MEC, layer V neurons within the plexus were initially identified in the live IR-DIC image based on the appearance of their soma. The selected cells were patched, and main electrophysiological properties in response to ±100 nA current steps were determined (Fig. 5*B*). The vast majority of the cells (n = 66, 94% of total) were classified as layer V principal excitatory cells (Canto and Witter, 2012). Their average input resistance was 157 ± 49 MΩ, the average width at half peak of AP generated at threshold was 1.8 ± 0.4 ms, and their dendrites showed spiny morphology (Fig. 5*B*). *Post hoc* morphological analysis confirmed that these neurons were indeed pyramidal cells (Canto and Witter, 2012). In some instances (n = 5), the patched cells were identified as inhibitory layer V fast-spiking cells (FSCs). Their average input resistance was 132 ± 40 MΩ, which was not statistically different from the excitatory cells (p = 0.12). However, the AP generated in response to depolarizing current step had different kinetics from those seen in case of principal cells (average width at half peak was 0.6 ± 0.1 ms, $p < 0.001$, t test). Moreover, the dendrites of these FSCs were spineless (Fig. 5*D*).

We performed recordings from putative postsynaptic layer V cells while photostimulating the presynaptic ChIEF-positive fibers. The stimulation grid was positioned above the basal dendrites of the recorded cells in layer V. The postsynaptic cells responded with EPSPs after stimulation in a subset of grid locations (Fig. 5*B*,*D*,*E*). The amplitude of the responses reached up to 10 mV (with average response of 1.91 ± 0.05 mV). The average onset time was 18.09 ± 3.36 ms (n = 732). The onset was significantly slower than in the case of direct optical stimulation of ChIEF-positive cells in RSC (Fig. 5*B*; $p < 0.001$), suggesting that the EPSPs in MEC were synaptic (Petreanu et al., 2007). To test whether the optically induced responses in MEC were mediated by presynaptic activation, we blocked the generation of APs by perfusing the slices with ACSF containing 5 μM TTX. This treatment completely abolished responses in all recorded cells (n = 8; Fig. 5*E*).

Principal cells of MEC layer V have been shown to display two main patterns of projection (Canto and Witter, 2012). Their axons can travel via the angular bundle, likely toward extrahippocampal targets, or they can project to superficial layers of MEC. We reconstructed and analyzed the axonal trajectories of 22 principal cells after the optogenetic experiments to determine which of the two types received the RSC input. We observed both axonal trajectories in the analyzed population. All reconstructed cells had axons projecting toward angular bundle. In a substantial fraction of neurons (n = 11), axonal collaterals were present in superficial layers (Fig. 6).

Morphological analysis of putative synaptic contacts

In the next series of experiments, we aimed to describe the target neurons of the RSC input to MEC layer V in more detail. Particularly, we wanted to identify cells in layer V that project to superficial layers II and III in MEC (Canto and Witter 2012) and to assess the overall distribution of RSC inputs onto the dendrites of these cells. In fixed slices containing anterogradely labeled RSC axons, we identified retrogradely labeled superficially projecting layer V neurons and filled them intracellularly with AF568 (Fig. 1*A3*,*B3*). A total of 27 cells were successfully filled, and it was possible to reconstruct their basal dendritic tree for additional analysis. All reconstructed cells displayed dendritic morphology typical for layer V pyramidal cells (Hamam et al., 2000; Canto and Witter, 2012). Consistent with the earlier studies, the majority of the cells were multidirectional pyramidal cells (n = 22), although several horizontal cells were included (n = 5), characterized by having the majority of basal dendrites parallel and confined to the layer. The horizontal cells did not differ in any other aspect from the pyramidal cells, and both types were pooled together for additional analysis. A typical cell showed four to nine basal dendrites originating at the soma (Fig. 7*A*). Branching peaked at a distance of 60 μm from the soma and continued up to 200 μm (Fig. 7*B*). The basal dendritic tree extended up to 300 μm in each direction. The proximal branches were almost devoid of spines, beyond 20 μm (usually after first bifurcation). The spine density reached ~10 spines/10 μm and then peaked at 14 spines/10 μm, 80 μm from the soma (Fig. 7*C*,*D*). This spine density of reconstructed neurons was consistent with previous observations for layer V pyramidal neurons in MEC (Lingenhöhl and Finch, 1991).

After neuron reconstruction, the proximity of the BDA-positive fibers labeled with AF488 was mapped onto the rendered dendritic surface (Fig. 7*E*,*F*; Schmitt et al., 2004; Evers et al., 2005). Axons positioned within one voxel from the surface (300 nm in horizontal plane) were represented as a heat map according to their fluorescence intensity (Fig. 7*F*,*H*). Each individual putative contact between presynaptic and postsynaptic label was then verified for the presence of a presynaptic bouton. Axonal swellings were classified as boutons if the diameter of the swelling was at least three times bigger than the preceding fiber (Fig. 7*I*,*J*; Wouterlood et al., 2008). We verified whether the number of RSC synaptic contacts on each MEC layer V cell was proportional to the density of incoming fibers, as predicted by Peters' rule (Peters and Payne, 1993). Indeed, the density of labeled axons showed a linear correlation with the frequency of contacts for each cell (R^2 = 0.74; Fig. 7*G*), and the distribution of contact frequencies normalized to the plexus density was unimodal (p = 0.67). Of these putative presynaptic terminals, 84% (580 of 692) contacted spines, whereas the remaining 16% (112 of 692) terminated on

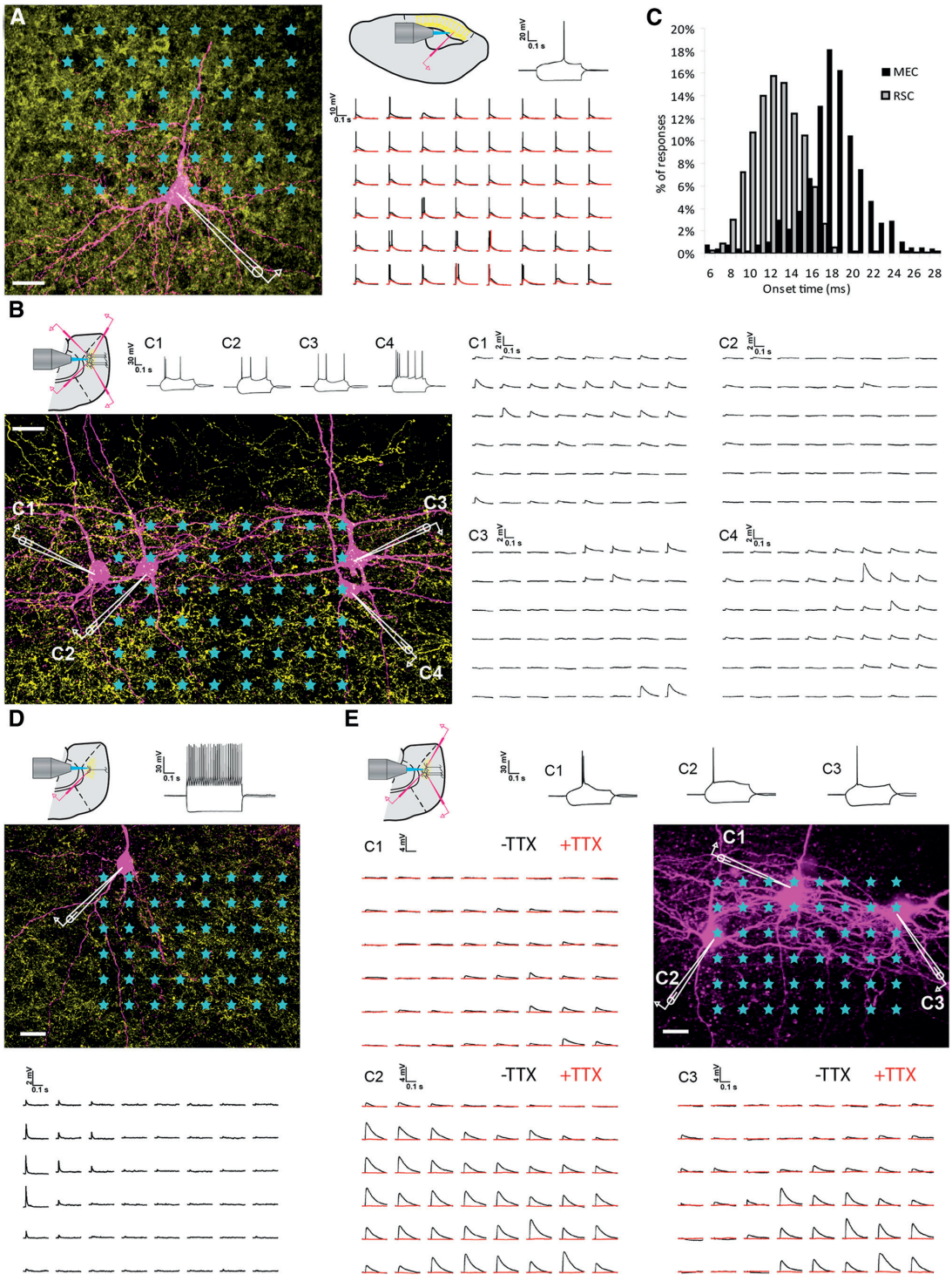

Figure 5. Optogenetic activation of ChIEF-expressing RSC cells and their projection fibers in MEC. Laser stimulation of the grid pattern was applied as indicated by asterisks. Scale bars, 20 μm. Pulse duration was 2 ms with 250 ms intervals, delivered via a 40× water-immersion lens. Grid size was 8 × 6 with 20 μm spacing between nodes. Order of activation (*Figure legend continues.*)

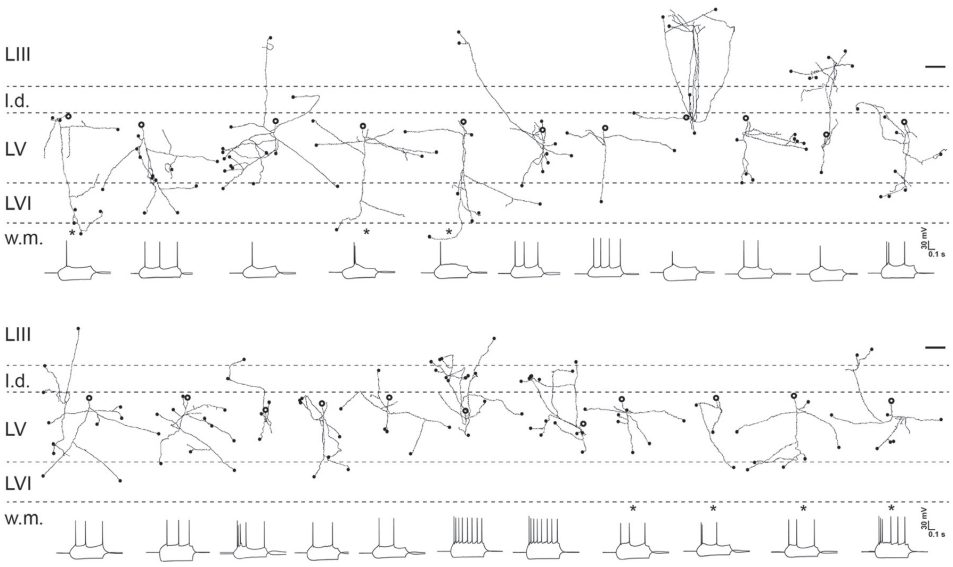

Figure 6. Individual axonal reconstructions of 22 pyramidal cells recorded in horizontal slices through MEC. The one interneuron (Fig. 5*D*) is not included. The position of the soma in layer V is indicated with the bold open circle (size of the soma is not to scale). Axons that appeared to be cut at the surface of the slice are indicated by filled circles (scale bar, 200 μm). Below each neuron is the characteristic electrophysiological test response to current steps of $\pm$100 pA (calibration: 0.1 s, 30 mV). The cells indicated with an asterisk are those for which the dendritic morphology is shown in Figure 5, *B* (4 cells in the bottom row) and ***E*** (3 cells in the top row). l.d., Lamina dissecans; L, layer; w.m., white matter.

shafts. The proximity of a presynaptic swelling and a dendritic shaft or spine does not automatically imply the presence of a synaptic contact (Peters and Palay, 1996; Wouterlood et al., 2003; Mishchenko et al., 2010). To substantiate our observations, we performed additional immunostaining of marker proteins for presynaptic terminals (synaptophysin) and for PSDs (PSD-95) and reconstructed 88 previously imaged putative contacts from four neurons. Of these, 68 contacted spines and 20 contacted shafts. In 78% of the putative spine contacts ($n = 53$ of 68) and in 55% of the putative shaft contacts ($n = 11$ of 20), both presynaptic and postsynaptic markers were found, and these contacts could therefore be confirmed as synaptic (Fig. 7*K*). Extrapolating these percentages to the entire pool of putative synaptic contacts implies that 88% ($n = 452$ of 514) of the axon terminals originating in RSC contacted spines, whereas 12% ($n = 62$ of 514) contacted shafts.

←

(*Figure legend continued.*) was pseudorandom, and subsequent illumination of adjacent points of the grid was avoided. Pipettes positions are indicated in white. Yellow, mCherry-positive neurons and fibers; magenta, biocytin-filled cells. Each trace in ***A***, ***B***, ***D***, and ***E*** represents response to stimulation at the corresponding point of the array. ***A***, Direct response of a ChIEF-expressing cell in RSC to patterned laser stimulation. Laser power was first tuned to 230 μW (black traces), and stimulation of each point evoked a single AP or a train of APs. Decrease in light intensity to 25 μW resulted in elimination of AP events (red traces). Calibration: 0.1 s, 10 mV. Insets, Schematic diagram of recording configuration and test response of the RSC layer V cell to current steps of $\pm$100 pA. Calibration: 0.2 s, 20 mV. ***B***, Somatic EPSP responses of MEC layer V cells to patterned laser stimulation of RSC terminals expressing ChIEF. Each trace represents response to stimulation at the corresponding point of the array presented in ***A*** for one of the four simultaneously recorded cells (***C1–C4***). Laser power at the specimen was 650 μW. Insets, Schematic diagram of recording configuration and test response to current steps of $\pm$100 pA for cells ***C1–C4***. ***C***, Histogram showing the distribution of onset times for optically induced responses in RSC (gray bars) and MEC (black bars). Average onset time in RSC was 11.76 $\pm$ 2.8 ms, whereas in MEC it was significantly higher (18.46 $\pm$ 2.8 ms, *t* test, $p < 0.001$). ***D***, FSC in MEC layer V showing EPSPs after stimulation of presynaptic RSC fibers. Calibration: 0.1 s, 2 mV. Insets, Schematic diagram of recording configuration and test response to current pulse of $\pm$100 pA. Calibration: 0.2 s, 30 mV. ***E***, EPSPs evoked by RSC fiber stimulation in MEC layer V require presynaptic APs. Responses shown for three cells ***C1–C3***. Insets, Schematic diagram of recording configuration and test response to current steps of $\pm$100 pA for cells ***C1–C3***. First, control responses were obtained by stimulating the presynaptic fibers with the grid pattern (30 repeats). Then the Na^+ channel blocker TTX (5 μM) was infused for 2 min, and the grid stimulation was repeated in the presence of the toxin. Control traces (black lines) show typical responses. Blocking of Na^+ channels diminished the postsynaptic response to the level of baseline (red traces) in all observed cases. Calibration: 0.1 s, 4 mV. Inset, Configuration of a typical experiment and test response to current pulse of $\pm$100 pA. Calibration: 0.2 s, 30 mV.

Discussion

Projections of the RSC to layer V of MEC are among the strongest cortical afferents to MEC (Burwell and Amaral, 1998). To study their potential impact on MEC, we used the anterograde transport of BDA and ChR-expressing rAAV to identify axons and terminals in layer V of MEC originating in RSC. Our findings that caudal RSC projects densely to layer V, with very few fibers targeting layer III of MEC, are in line with previously reported observations (Shibata, 1994; Jones and Witter, 2007). The quantitative ultrastructural assessment of the morphology of the labeled presynaptic elements and their postsynaptic targets in layer V of MEC showed that the majority of the synapses is asymmetrical, indicating that these are excitatory. Less than 2% of the terminals are symmetrical, possibly representing a small inhibitory, likely GABAergic, projection (Gray, 1959; Eccles, 1964; Uchizono, 1965; Colonnier, 1968) that at least in part targets local inhibitory neurons (Caputi et al., 2013). This interpretation is strongly supported by our functional findings that laser stimulation of ChR-positive RSC axons in layer V of MEC exclusively resulted in excitatory responses in all postsynaptic cells studied. Therefore, we conclude that RSC provides a major excitatory drive to neurons in layer V and that inhibition plays only a minor role in this connection.

We further identified the layer V postsynaptic targets of RSC input. The electron microscopic data show a striking dominance of spines as targets for RSC inputs. Previous morphological stud-

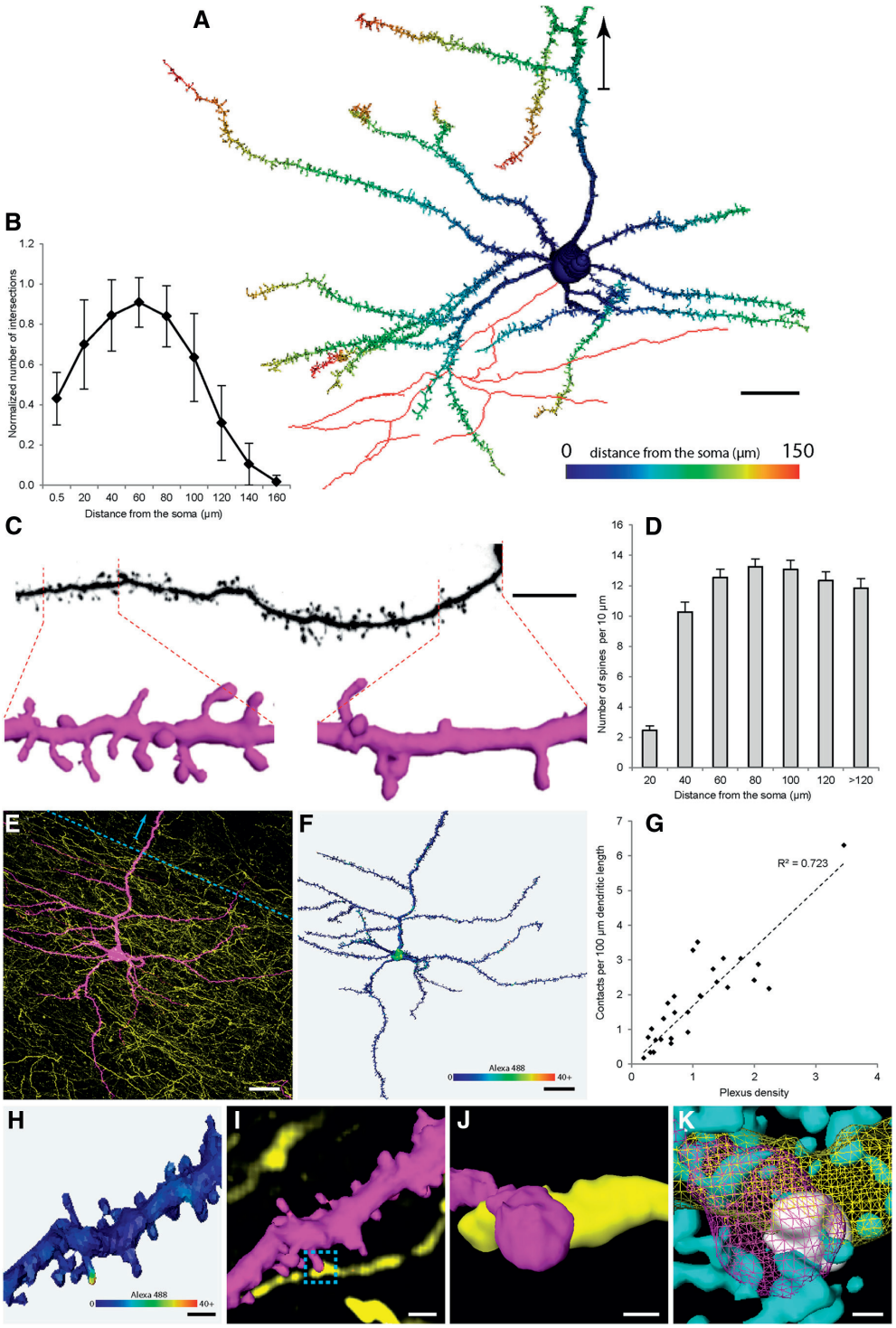

Figure 7. ***A–D***, Morphological properties of MEC layer V neurons that receive RSC input and project into layer II/III. ***E–K***, Identification and quantification of putative RSC synaptic contacts on MEC layer V neurons. ***A***, 2D projection of a typical reconstructed layer V cell showing the complexity of basal dendrites. Distance from the soma is color coded. Part of the axon reconstructed in red. Arrowhead points toward the pial surface. Scale bar, 20 μm. ***B***, Sholl analysis showing changes in dendritic branching pattern of reconstructed layer V neurons as a function (*Figure legend continues.*)

ies have shown that principal neurons in MEC are commonly spiny (Wouterlood et al., 1995; Canto and Witter, 2012), and our observations thus indicate that principal neurons in layer V of MEC form a main target of RSC projections. Only a small percentage of the labeled axon terminals made synapses with smooth dendritic shafts, likely belonging to either interneurons (Wouterlood et al., 1995; Canto et al., 2008) or to spineless parts of dendrites of principal neurons as shown by our confocal results. The notion that the shafts at least in part represent interneuron dendrites is supported by the observations that a number of the postsynaptic shafts had multiple afferents from unlabeled axon terminals showing a circular arrangement. This phenomenon is commonly accepted to be a feature of interneurons (Kisvárday et al., 1985; Johnson and Burkhalter, 1996).

These morphologically based inferences are strongly supported by the optogenetic electrophysiological results that both spiny pyramidal neurons and smooth inhibitory FSCs in MEC layer V responded to optogenetic stimulation of RSC fibers with equal latencies. The existence of postsynaptic inhibitory neurons suggests the presence of an inhibitory feedforward loop within MEC layer V that would be triggered by RSC input. The presence of a disinhibitory projection, formed by GABAergic RSC neurons targeting MEC interneurons (Caputi et al., 2013), could not be confirmed with our optogenetic experiments, likely because of the limited sampling of interneurons.

Layer V principal cells project to a number of cortical and subcortical areas (Insausti et al., 1997), issue local axon collaterals confined to layer V (Hamam et al., 2000; Canto and Witter, 2012), and project intrinsically to superficial layers (Kloosterman et al., 2003b; van Haeften et al., 2003; Quilichini et al., 2010; Canto and Witter, 2012). Our data are in accordance with previously published accounts indicating that at least two populations exist: (1) one that projects both superficially and extrinsically; and (2) one that projects extrinsically with only local collaterals in layer V (Quilichini et al., 2010; Canto and Witter, 2012). Most importantly, our data lead us to conclude that both types of layer V pyramidal cells receive excitatory RSC input.

We should point out that our experimental data only address the projection originating from a restricted, caudal part of the RSC, projecting preferentially to the dorsal half of MEC. In view of dorsoventral differences in grid-cell properties in MEC (Hafting et al., 2005; Stensola et al., 2012), it might be of interest to compare very dorsal with very ventral innervation patterns, but our current data do not allow to address this issue. However, based on the overall similar connectivity patterns for the projections from rostral and caudal RSC to MEC (Jones and Witter, 2007), and because we did not observe any striking differences between experimental data obtained within the dorsal half of MEC, we expect that our conclusions can be generalized to hold along the MEC dorsoventral axis.

The role of RSC input in HF-MEC circuitry

Principal neurons in layer V of MEC possess key anatomical and physiological features to serve an important role in integrating multiple external inputs (Canto et al., 2008). The dendritic trees of the principal cells in layer V span the total depths of MEC, receiving inputs that terminate in different layers. This has been shown for inputs to layers I–III (Medinilla et al., 2013), including those from the parasubiculum and presubiculum (Canto et al., 2012). Here we show that layer V principal neurons receive inputs from RSC. It is well established that layer V principal cells receive hippocampal output (van Haeften et al., 1995). Comparable with our results with respect to RSC input, among the hippocampal-receiving neurons are those that project superficially (Kloosterman et al., 2003b). Interestingly, the neurons that receive inputs from the parasubiculum and presubiculum also include those that send axon collaterals to superficial layers (Canto et al., 2012). These data thus indicate that layer V principal cells indeed integrate multiple inputs and subsequently forward this signal to superficial layers II and III.

The neuronal network of MEC has been implicated as a key component in brain systems mediating navigation (Moser and Moser, 2008). A striking cell type in superficial layer II of MEC is the grid cell (Hafting et al., 2005). Grid cells in MEC represent multiple positions in space, firing in a regularly patterned structure when the animal is moving in the environment. Moreover, grid cells universally code for all environments (Hafting et al., 2005). Directional information has been postulated as relevant for the emergence of stable grid-cell properties (Fuhs and Touretzky, 2006; McNaughton et al., 2006; Burgess et al., 2007) and for anchoring grid cells to distal cues (Knierim and Hamilton, 2011). This type of information is likely not generated within MEC but enters by way of the head-directional system. The head-direction signal originates in the recurrent network of the dorsal tegmental nucleus and the lateral mammillary nucleus and is relayed to multiple brain regions by way of the anterior dorsal nucleus of the thalamus (Taube, 2007). Although the presubiculum has been the main focus of research for head directionality, this type of information is also expressed in the firing patterns of neurons in RSC (Cho and Sharp, 2001). The relevance of RSC in spatial information processing is yet unclear, but it has been suggested that RSC integrates different spatial representations: (1) one based on path integration and (2) another based on external sensory information (Vann et al., 2009). We propose that the strong excitatory effect that RSC inputs exert on MEC layer V neurons is among the essential inputs for the parahippocampal–hippocampal navigational system. This assumption is supported by findings that RSC lesions affect a wide range of tasks testing different navigational strategies (Vann et al., 2009). The most severe deficits were reported when the animal needed to change

←

(*Figure legend continued.*) of distance from the soma ($n = 27$ from 8 animals). The Sholl values were normalized to the number of first-order dendrites to account for a different number of basal dendritic branches preserved during slice preparation. Sholl sphere diameter, 20 μm. ***C***, Comparison of spine density between proximal (0–20 μm from the soma) and distal (100–120 μm) segment of basal dendrite. Scale bar, 30 μm. ***D***, Histogram summarizing the changes in spine density of MEC layer V cells ($n = 27$ from 8 animals). Bin size, 20 μm. Error bars indicate SEM. ***E***, Maximum projection of confocal image stack of BDA-labeled RSC fibers (AF488, yellow) and intracellularly filled postsynaptic cells in MEC layer V (AF568, magenta). Scale bar, 20 μm. Arrowhead points toward the pia surface. ***F***, Surface rendering and RSC input mapping of cell imaged in ***E***. Staining intensity of BDA within 300 μm of the reconstructed surface is mapped and color coded. Scale bar, 20 μm. ***G***, Scatter plot showing the correlation between contact density and the number of RSC fibers present within the volume covered by dendritic tree (Peters' rule). The correlation was linear ($R^2 = 0.72$), and the distribution of contact frequencies normalized to the plexus density was unimodal ($p = 0.67$, Kolmogorov–Smirnov test). For computation of the plexus density index, see Materials and Methods. ***H***, Surface rendering of a dendritic fragment with RSC input mapping. Staining intensity of BDA within 300 μm of the reconstructed surface is mapped and color coded. Scale bar, 5 μm. ***I***, Surface reconstruction of area shown in ***H***, overlaid with volume rendering of putative afferent RSC fibers (dendrite: AF568, magenta; axon: AF488, yellow). Dashed box shows the area magnified in ***J***. Scale bar, 5 μm. ***J***, Surface reconstruction of synaptic contact targeted for immunostaining (marked by dashed box). Scale bar, 1 μm. ***K***, 3D reconstruction of the synaptic contact shown in ***H–K***. Slices containing AF568-filled cells and BDA-labeled RSC fibers were additionally immunostained with anti-synaptophysin and anti-PSD-95 antibodies. Bouton (yellow) and spine (magenta) reconstructed as mesh surface. Synaptophysin (white) and PSD-95 (cyan) reconstructed as solid surfaces.

navigational strategies or integrate spatial information of different kinds (Vann et al., 2003; Pothuizen et al., 2008). Furthermore, during RSC inactivation, the firing of place cells in the hippocampus is less specific (Cooper and Mizumori, 2001). Because RSC does not project directly to the hippocampus, except for the subiculum (Sugar et al., 2011), we propose that this change in place-cell properties in addition to the behavioral deficits seen after RSC lesions reflect the disruption of RSC activity, indirectly influencing neurons in superficial layers of MEC, by way of the pathway shown in the present study.

References

Brun VH, Leutgeb S, Wu HQ, Schwarcz R, Witter MP, Moser EI, Moser MB (2008) Impaired spatial representation in CA1 after lesion of direct input from entorhinal cortex. Neuron 57:290–302. CrossRef Medline

Burgess N, Barry C, O'Keefe J (2007) An oscillatory interference model of grid cell firing. Hippocampus 17:801–812. CrossRef Medline

Burwell RD, Amaral DG (1998) Cortical afferents of the perirhinal, postrhinal, and entorhinal cortices of the rat. J Comp Neurol 398:179–205. CrossRef Medline

Buzsáki G (1996) The hippocampo-neocortical dialogue. Cereb Cortex 6:81–92. CrossRef Medline

Canto CB, Witter MP (2012) Cellular properties of principal neurons in the rat entorhinal cortex. II. The medial entorhinal cortex. Hippocampus 22:1277–1299. CrossRef Medline

Canto CB, Wouterlood FG, Witter MP (2008) What does the anatomical organization of the entorhinal cortex tell us? Neural Plast 2008:381243. CrossRef Medline

Canto CB, Koganezawa N, Beed P, Moser EI, Witter MP (2012) All layers of medial entorhinal cortex receive presubicular and parasubicular inputs. J Neurosci 32:17620–17631. CrossRef Medline

Caputi A, Melzer S, Michael M, Monyer H (2013) The long and short of GABAergic neurons. Curr Opin Neurobiol 23:179–186. CrossRef Medline

Cho J, Sharp PE (2001) Head direction, place, and movement correlates for cells in the rat retrosplenial cortex. Behav Neurosci 115:3–25. CrossRef Medline

Chrobak JJ, Buzsáki G (1994) Selective activation of deep layer (V-VI) retrohippocampal cortical neurons during hippocampal sharp waves in the behaving rat. J Neurosci 14:6160–6170. Medline

Colonnier M (1968) Synaptic patterns on different cell types in the different laminae of the cat visual cortex. An electron microscope study. Brain Res 9:268–287. CrossRef Medline

Cooper BG, Mizumori SJ (2001) Temporary inactivation of the retrosplenial cortex causes a transient reorganization of spatial coding in the hippocampus. J Neurosci 21:3986–4001. Medline

Couey JJ, Witoelar A, Zhang SJ, Zheng K, Ye J, Dunn B, Czajkowski R, Moser MB, Moser EI, Roudi Y, Witter MP (2013) Recurrent inhibitory circuitry as a mechanism for grid formation. Nat Neurosci 16:318–324. CrossRef Medline

Eccles JC (1964) The physiology of synapses. Berlin: Springer Verlag.

Eichenbaum H, Lipton PA (2008) Towards a functional organization of the medial temporal lobe memory system: role of the parahippocampal and medial entorhinal cortical areas. Hippocampus 18:1314–1324. CrossRef Medline

Epstein RA, Parker WE, Feiler AM (2007) Where am I now? Distinct roles for parahippocampal and retrosplenial cortices in place recognition. J Neurosci 27:6141–6149. CrossRef Medline

Evers JF, Schmitt S, Sibila M, Duch C (2005) Progress in functional neuroanatomy: precise automatic geometric reconstruction of neuronal morphology from confocal image stacks. J Neurophysiol 93:2331–2342. Medline

Fuhs MC, Touretzky DS (2006) A spin glass model of path integration in rat medial entorhinal cortex. J Neurosci 26:4266–4276. CrossRef Medline

Gray EG (1959) Electron microscopy of synaptic contacts on dendrite spines of the cerebral cortex. Nature 183:1592–1593. CrossRef Medline

Gundersen HJ (1986) Stereology of arbitrary particles. A review of unbiased number and size estimators and the presentation of some new ones, in memory of William R. Thompson. J Microsc 143:3–45. CrossRef Medline

Hafting T, Fyhn M, Molden S, Moser MB, Moser EI (2005) Microstructure of a spatial map in the entorhinal cortex. Nature 436:801–806. CrossRef Medline

Hamam BN, Kennedy TE, Alonso A, Amaral DG (2000) Morphological and electrophysiological characteristics of layer V neurons of the rat medial entorhinal cortex. J Comp Neurol 418:457–472. CrossRef Medline

Insausti R, Herrero MT, Witter MP (1997) Entorhinal cortex of the rat: cytoarchitectonic subdivisions and the origin and distribution of cortical efferents. Hippocampus 7:146–183. CrossRef Medline

Ito HT, Schuman EM (2012) Functional division of hippocampal area CA1 via modulatory gating of entorhinal cortical inputs. Hippocampus 22:372–387. CrossRef Medline

Johnson RR, Burkhalter A (1996) Microcircuitry of forward and feedback connections within rat visual cortex. J Comp Neurol 368:383–398. CrossRef Medline

Jones BF, Witter MP (2007) Cingulate cortex projections to the parahippocampal region and hippocampal formation in the rat. Hippocampus 17:957–976. CrossRef Medline

Kisvárday ZF, Martin KA, Whitteridge D, Somogyi P (1985) Synaptic connections of intracellularly filled clutch cells: a type of small basket cell in the visual cortex of the cat. J Comp Neurol 241:111–137. CrossRef Medline

Kloosterman F, Van Haeften T, Lopes Silva FH (2000) Functional characterization of hippocampal output to the entorhinal cortex in the rat. Ann N Y Acad Sci 911:459–461. CrossRef Medline

Kloosterman F, Witter MP, Van Haeften T (2003a) Topographical and laminar organization of subicular projections to the parahippocampal region of the rat. J Comp Neurol 455:156–171. CrossRef Medline

Kloosterman F, Van Haeften T, Witter MP, Lopes Da Silva FH (2003b) Electrophysiological characterization of interlaminar entorhinal connections: an essential link for re-entrance in the hippocampal-entorhinal system. Eur J Neurosci 18:3037–3052. CrossRef Medline

Knierim JJ, Hamilton DA (2011) Framing spatial cognition: neural representations of proximal and distal frames of reference and their roles in navigation. Physiol Rev 91:1245–1279. CrossRef Medline

Köhler C (1985) Intrinsic projections of the retrohippocampal region in the rat brain. I. The subicular complex. J Comp Neurol 236:504–522. CrossRef Medline

Kononenko NL, Witter MP (2012) Presubiculum layer III conveys retrosplenial input to the medial entorhinal cortex. Hippocampus 22:881–895. CrossRef Medline

Lin JY, Lin MZ, Steinbach P, Tsien RY (2009) Characterization of engineered channelrhodopsin variants with improved properties and kinetics. Biophys J 96:1803–1814. CrossRef Medline

Lingenhöhl K, Finch DM (1991) Morphological characterization of rat entorhinal neurons in vivo: soma-dendritic structure and axonal domains. Exp Brain Res 84:57–74. Medline

Maguire EA (2001) The retrosplenial contribution to human navigation: a review of lesion and neuroimaging findings. Scand J Psychol 42:225–238. CrossRef Medline

McNaughton BL, Battaglia FP, Jensen O, Moser EI, Moser MB (2006) Path integration and the neural basis of the "cognitive map." Nat Rev Neurosci 7:663–678. CrossRef

Medinilla V, Johnson O, Gasparini S (2013) Features of proximal and distal excitatory synaptic inputs to layer V neurons of the rat medial entorhinal cortex. J Physiol 591:169–183. CrossRef Medline

Mishchenko Y, Hu T, Spacek J, Mendenhall J, Harris KM, Chklovskii DB (2010) Ultrastructural analysis of hippocampal neuropil from the connectomics perspective. Neuron 67:1009–1020. CrossRef Medline

Miyashita T, Rockland KS (2007) GABAergic projections from the hippocampus to the retrosplenial cortex in the rat. Eur J Neurosci 26:1193–1204. CrossRef Medline

Moser EI, Moser MB (2008) A metric for space. Hippocampus 18:1142–1156. CrossRef Medline

Naber PA, Witter MP (1998) Subicular efferents are organized mostly as parallel projections: a double-labeling, retrograde-tracing study in the rat. J Comp Neurol 393:284–297. CrossRef Medline

Narahashi T, Moore JW, Scott WR (1964) Tetrodotoxin blockage of sodium conductance increase in lobster giant axons. J Gen Physiol 47:965–974. CrossRef Medline

O'Keefe J, Dostrovsky J (1971) The hippocampus as a spatial map. Preliminary evidence from unit activity in the freely-moving rat. Brain Res 34:171–175. CrossRef Medline

O'Keefe J, Nadel L (1978) The hippocampus as a cognitive map. Oxford: Clarendon.
Otsu N (1979) Threshold selection method from gray-level histograms. IEEE Trans Syst Man Cybern 9:62–66. CrossRef
Paxinos G, Watson C (2007) The rat brain in stereotaxic coordinates, Ed 6. Amsterdam: Academic/Elsevier.
Peters A, Palay SL (1996) The morphology of synapses. J Neurocytol 25: 687–700. CrossRef Medline
Peters A, Payne BR (1993) Numerical relationships between geniculocortical afferents and pyramidal cell modules in cat primary visual cortex. Cereb Cortex 3:69–78. CrossRef Medline
Petreanu L, Huber D, Sobczyk A, Svoboda K (2007) Channelrhodopsin-2-assisted circuit mapping of long-range callosal projections. Nat Neurosci 10:663–668. CrossRef Medline
Pothuizen HH, Aggleton JP, Vann SD (2008) Do rats with retrosplenial cortex lesions lack direction? Eur J Neurosci 28:2486–2498. CrossRef Medline
Quilichini P, Sirota A, Buzsáki G (2010) Intrinsic circuit organization and theta-gamma oscillation dynamics in the entorhinal cortex of the rat. J Neurosci 30:11128–11142. CrossRef Medline
Remondes M, Schuman EM (2004) Role for a cortical input to hippocampal area CA1 in the consolidation of a long-term memory. Nature 431:699–703. CrossRef Medline
Sargolini F, Fyhn M, Hafting T, McNaughton BL, Witter MP, Moser MB, Moser EI (2006) Conjunctive representation of position, direction, and velocity in entorhinal cortex. Science 312:758–762. CrossRef Medline
Schmitt S, Evers JF, Duch C, Scholz M, Obermayer K (2004) New methods for the computer-assisted 3-D reconstruction of neurons from confocal image stacks. Neuroimage 23:1283–1298. CrossRef Medline
Shibata H (1994) Terminal distribution of projections from the retrosplenial area to the retrohippocampal region in the rat, as studied by anterograde transport of biotinylated dextran amine. Neurosci Res 20: 331–336. Medline
Sholl DA (1953) Dendritic organization in the neurons of the visual and motor cortices of the cat. J Anat 87:387–406. Medline
Solstad T, Boccara CN, Kropff E, Moser MB, Moser EI (2008) Representation of geometric borders in the entorhinal cortex. Science 322:1865–1868. CrossRef Medline
Spiers HJ, Maguire EA (2006) Thoughts, behaviour, and brain dynamics during navigation in the real world. Neuroimage 31:1826–1840. CrossRef Medline
Stensola H, Stensola T, Solstad T, Frøland K, Moser MB, Moser EI (2012) The entorhinal grid map is discretized. Nature 492:72–78. CrossRef Medline
Sugar J, Witter MP, van Strien NM, Cappaert NL (2011) The retrosplenial cortex: intrinsic connectivity and connections with the (para)hippocampal region in the rat. An interactive connectome. Front Neuroinform 5:7. CrossRef Medline
Taube JS (2007) The head direction signal: origins and sensory-motor integration. Annu Rev Neurosci 30:181–207. CrossRef Medline
Uchizono K (1965) Characteristics of excitatory and inhibitory synapses in the central nervous system of the cat. Nature 207:642–643. CrossRef Medline
Van Cauter T, Poucet B, Save E (2008) Unstable CA1 place cell representation in rats with entorhinal cortex lesions. Eur J Neurosci 27:1933–1946. CrossRef Medline
van Groen T, Wyss JM (1990) Connections of the retrosplenial granular a cortex in the rat. J Comp Neurol 300:593–606. CrossRef Medline
Van Groen T, Wyss JM (2003) Connections of the retrosplenial granular b cortex in the rat. J Comp Neurol 463:249–263. CrossRef Medline
van Haeften T, Jorritsma-Byham B, Witter MP (1995) Quantitative morphological analysis of subicular terminals in the rat entorhinal cortex. Hippocampus 5:452–459. CrossRef Medline
van Haeften T, Baks-te-Bulte LT, Goede PH, Wouterlood FG, Witter MP (2003) Morphological and numerical analysis of synaptic interactions between neurons in deep and superficial layers of the entorhinal cortex of the rat. Hippocampus 13:943–952. CrossRef Medline
van Strien NM, Cappaert NL, Witter MP (2009) The anatomy of memory: an interactive overview of the parahippocampal-hippocampal network. Nat Rev Neurosci 10:272–282. CrossRef Medline
Vann SD, Aggleton JP (2002) Extensive cytotoxic lesions of the rat retrosplenial cortex reveal consistent deficits on tasks that tax allocentric spatial memory. Behav Neurosci 116:85–94. CrossRef Medline
Vann SD, Kristina Wilton LA, Muir JL, Aggleton JP (2003) Testing the importance of the caudal retrosplenial cortex for spatial memory in rats. Behav Brain Res 140:107–118. CrossRef Medline
Vann SD, Aggleton JP, Maguire EA (2009) What does the retrosplenial cortex do? Nat Rev Neurosci 10:792–802. CrossRef Medline
Vogt BA, Miller MW (1983) Cortical connections between rat cingulate cortex and visual, motor, and postsubicular cortices. J Comp Neurol 216: 192–210. CrossRef Medline
Wesierska M, Adamska I, Malinowska M (2009) Retrosplenial cortex lesion affected segregation of spatial information in place avoidance task in the rat. Neurobiol Learn Mem 91:41–49. CrossRef Medline
Witter MP, Ostendorf RH, Groenewegen HJ (1990) Heterogeneity in the dorsal subiculum of the rat. Distinct neuronal zones project to different cortical and subcortical targets. Eur J Neurosci 2:718–725. CrossRef Medline
Wouterlood FG, Härtig W, Brückner G, Witter MP (1995) Parvalbumin-immunoreactive neurons in the entorhinal cortex of the rat: localization, morphology, connectivity and ultrastructure. J Neurocytol 24:135–153. CrossRef Medline
Wouterlood FG, Böckers T, Witter MP (2003) Synaptic contacts between identified neurons visualized in the confocal laser scanning microscope. Neuroanatomical tracing combined with immunofluorescence detection of post-synaptic density proteins and target neuron-markers. J Neurosci Methods 128:129–142. CrossRef Medline
Wouterlood FG, Boekel AJ, Kajiwara R, Beliën JA (2008) Counting contacts between neurons in 3D in confocal laser scanning images. J Neurosci Methods 171:296–308. CrossRef Medline
Zhang SJ, Ye J, Miao C, Tsao A, Cerniauskas I, Ledergerber D, Moser MB, Moser EI (2013) Optogenetic dissection of entorhinal-hippocampal functional connectivity. Science 340:1232627. CrossRef Medline

eLIFE elifesciences.org

RESEARCH ARTICLE

Postnatal development of retrosplenial projections to the parahippocampal region of the rat

Jørgen Sugar, Menno P Witter*

Kavli Institute for Systems Neuroscience and Centre for Neural Computation, Norwegian University for Science and Technology, Trondheim, Norway

Abstract The rat parahippocampal region (PHR) and retrosplenial cortex (RSC) are cortical areas important for spatial cognition. In PHR, head-direction cells are present before eye-opening, earliest detected in postnatal day (P)11 animals. Border cells have been recorded around eye-opening (P16), while grid cells do not obtain adult-like features until the fourth postnatal week. In view of these developmental time-lines, we aimed to explore when afferents originating in RSC arrive in PHR. To this end, we injected rats aged P0-P28 with anterograde tracers into RSC. First, we characterized the organization of RSC-PHR projections in postnatal rats and compared these results with data obtained in the adult. Second, we described the morphological development of axonal plexus in PHR. We conclude that the first arriving RSC-axons in PHR, present from P1 onwards, already show a topographical organization similar to that seen in adults, although the labeled plexus does not obtain adult-like densities until P12.
DOI: 10.7554/eLife.13925.001

***For correspondence:** menno.witter@ntnu.no

Competing interests: MPW: Member of the board of the Kavli Centre, and of the scientific advisory board of the Center for Behavioral Brain Sciences, Otto von Guericke University, Magdeburg, FDR. The other author declares that no competing interests exist.

Funding: See page 26

Received: 18 December 2015
Accepted: 23 March 2016
Published: 23 March 2016

Reviewing editor: Howard Eichenbaum, Boston University, United States

Introduction

The parahippocampal region (PHR) is important for learning and memory. It consists of two functionally different networks, one of which, involved in spatial functions, comprises the presubiculum (PrS), parasubiculum (PaS), medial entorhinal cortex (MEC) and postrhinal cortex (POR). The other important for object representation and processing of contextual information, comprising lateral entorhinal cortex (LEC) and perirhinal cortex (PER; ***Eichenbaum et al., 2007***; ***Canto et al., 2008***; ***Ranganath and Ritchey, 2012***; ***Knierim et al., 2014***; ***Witter et al., 2014***). PrS, PaS, and MEC harbor cells representing an animal's position (grid cells), direction (head direction cells), borders in the environment (border cells) and speed of the animal (speed cells; ***Fyhn et al., 2004***; ***Solstad et al., 2008***; ***Boccara et al., 2010***; ***Kropff et al., 2015***). Even though a complete mechanistic understanding on how these spatial codes emerge is still lacking, it is believed that both intrinsic connectivity and extrinsic afferents are necessary to produce the receptive fields observed (***Brandon et al., 2011***; ***Koenig et al., 2011***; ***Bonnevie et al., 2013***; ***Couey et al., 2013***; ***Newman et al., 2014***). One approach applied to identify the critical elements underlying the functioning of these cell types, has been to study the developmental aspects of PHR networks. The different spatially modulated neuron types in PHR emerge at different periods during development. Border cells and head-direction cells can both be observed at the end of the second- and beginning of the third postnatal week (***Bjerknes et al., 2014***; ***Bjerknes et al., 2015***; ***Tan et al., 2015***). In contrast, adult-like grid cells in layer II of MEC first appear during the fourth postnatal week (***Langston et al., 2010***; ***Wills et al., 2010***). The early presence of head-direction cells is apparently paralleled by a similarly early developed shared connectivity (***Bjerknes et al., 2015***), while the late development of grid cells is paralleled by a corresponding late development of the relevant intrinsic connectivity in MEC (***Langston et al., 2010***; ***Couey et al., 2013***). Regarding main inputs, sparse connections between

eLife digest Our ability to navigate critically depends on part of the brain called the parahippocampal region. Within this region, there are several different types of brain cells (or neurons) whose activity "codes" different aspects of navigation, such as position, direction and speed.

To understand how parahippocampal neurons are able to form these activity patterns, we need to understand how they develop connections with neurons from other brain regions that are important for navigation, such as the retrosplenial cortex. If inputs from retrosplenial neurons are important for generating the activity patterns observed in the parahippocampal region, the connections between the two groups of neurons should be fully mature before the activity patterns emerge. In rats, this should occur around 11–16 days after birth.

Sugar and Witter have now assessed how the retrosplenial inputs are organized in the parahippocampal region of rats. This revealed that, when the rats are born, there are very few retrosplenial inputs present in the parahippocampal region. However, the few inputs that are present are organized similarly to how they eventually will be organized in adults. After birth, the number of inputs gradually increases until the rats are approximately 12 days old, at which point the pattern of connections is indistinguishable from what we observe in adults. Thus it appears that retrosplenial inputs are fully mature before activity patterns emerge in the parahippocampal region.

In the future, Sugar and Witter would like to investigate how inputs to the parahippocampal region are able to organize themselves during early development. The importance of retrosplenial inputs could also be investigated by manipulating them during development and adulthood.

DOI: 10.7554/eLife.13925.002

the hippocampal formation (HF) and PHR are present from birth, reaching adult-like morphological features during the second postnatal week (***Deng et al., 2007***; ***O'Reilly et al., 2013***; ***O'Reilly et al., 2015***). A similar developmental timeline has also been reported for functional connections from PrS/PaS to MEC (***Canto et al., 2011***). However, the timeline of development of cortical afferents to HF and PHR is still unknown.

One of the most prominent cortical inputs to PHR originates in the retrosplenial cortex (RSC) and spatially modulated cells have been found also in the latter cortical domain (***Cho and Sharp, 2001***; ***Sugar et al., 2011***; ***Alexander and Nitz, 2015***). Lesions of RSC result in impairments in navigational tasks (***Vann et al., 2009***). In addition, RSC in rodents is necessary for fear conditioning, both when context or complex multimodal stimuli are used as conditional stimuli (***Keene and Bucci, 2008a***; ***2008b***; ***Corcoran et al., 2011***; ***Cowansage et al., 2014***; ***Robinson et al., 2014***) and in rabbits RSC neurons are responsive to auditory cues when used as a CS in a memory task (***Gabriel et al., 1991***), suggesting that RSC has a general role in memory processes. The effect of lesioning RSC on navigation and memory performance is surprisingly similar to that seen after lesions that inflict the HF-PHR. It has thus been postulated that interactions between RSC and HF-PHR are crucial for spatial processing. In the adult, RSC projections target preferentially POR, PrS, PaS, and MEC (***Jones and Witter, 2007***; ***Sugar et al., 2011***; ***Kononenko and Witter, 2012***; ***Czajkowski et al., 2013***). In this paper, we aimed to ascertain the relevance of the RSC-PHR projection for the development of the functionally different neuron types in PHR. We hypothesized that if inputs from RSC are important for the development of head-direction- and/or border cells, these inputs should be present before eye-opening. Alternatively, if inputs from RSC are only important for the formation of stable grid cells, these inputs might develop after eye-opening, likely reaching adult-like morphology during the third and fourth week. We injected RSC of rats at different postnatal ages, ranging from postnatal day 0 to 28 (P0-P28), with anterograde tracers. Using retrograde tracing, we identified RSC neurons originating the developing PHR projections. The anterograde experimental material was used to analyze the organization of RSC-PHR projections in postnatal rats and to compare these results with data previously obtained in the adult. We further analyzed the development of axon morphology and densities of axonal plexus in PHR.

Results

Nomenclature

Several nomenclatures have been used to describe subdivisions of RSC. These nomenclatures mainly follow the same cytoarchitectonic- and histochemical criteria and are therefore directly comparable. For a summary and direct comparison of the different nomenclatures, we refer to a recent review on the RSC-HF-PHR connectivity (***Sugar et al., 2011***). In the current manuscript, we chose to use the nomenclature of ***Vogt (2004)***. We defined the border between area (A)29 and A30 as the area where layer II changes from being very condensed in A29, to less condensed in A30. The rostral border of RSC, towards the anterior cingulate cortex (ACC) was defined as the area where layer II/III widens and where layer IV shifts from being clearly demarcated in RSC towards being more diffusely organized in ACC. The ventral border of RSC with PHR, more specifically with PrS, was defined by the appearance of a cell free lamina dissecans in PrS, not present in RSC. In adult rats, A29 can be further subdivided into three different cytoarchitectonic subdivisions; A29a, b and c, which are involved in different cognitive functions (***van Groen et al., 2004***). However, in the immature cortex, these cytoarchitectonic areas are not apparent. We therefore chose to define a continuous measure of the dorsoventral positions within RSC (see methods for details). This measure is indirectly related to the classical cytoarchitectonic subdivision since the classical borders of A29a, b and c follow approximately our continuous definition of the dorsoventral axis of RSC.

Injection sites

To investigate the development of RSC projection patterns in PHR we aimed to inject anterograde tracers in different locations within RSC of differently aged pups. Of the 82 animals used in this study, 20 animals either did not survive surgery or no injection sites were observed in RSC. In the remaining 62 animals we obtained 113 injections in RSC. Eight of these injections only involved layers I and/or layers II-III and did not result in any labeled fibers in HF-PHR. These experiments were therefore excluded from further analyses. The remaining 105 injections all covered at least parts of layer V of RSC and involved different parts of RSC. We obtained one (n=21), two (n=31), three (n=6) or four (n=1) ipsilateral injections in RSC of each brain (***Figure 1***). In our analyses, we regarded each of these injections as independent experiments. Most of the experiments (n=93) were performed in animals aged P15 or younger since other comparable corticocortical projections are developed before eye-opening and the functional cell types are present in HF-PHR at this age (***Langston et al., 2010***; ***O'Reilly et al., 2013***; ***Bjerknes et al., 2014***; ***O'Reilly et al., 2014***). However, we also obtained injections in older pups (n=12) with a maximum age of P28.

To compare the location of injections in brains of different ages, we age-normalized the position of the injections by the use of a 3D-atlas brain (see methods and ***Figure 1A***, ***Video 1*** and ***2***). This was achieved by identifying atlas-sections containing landmarks and cytoarchitectonic borders present in the histological section containing the center of each injection. In the atlas-section, we recorded the coordinate of the center of each injection. Since the caudal RSC cortex is curved both along the dorsoventral and rostrocaudal axis we divided the pial surface of RSC in the atlas brain into triangles and used these triangles to calculate normalized rostrocaudal and dorsoventral coordinates of the each injection (***Figure 1B and C***). For visualization, we plotted the normalized injection coordinates into a schematic representation of RSC (***Figure 1D***).

General projection patterns

We analyzed the anterograde labeling resulting from all 105 injections. In some (n=44), we observed a few retrogradely labeled neurons within the dorsal half of subiculum (SUB). This potentially may lead to false positive labeling, which will be addressed in the detailed descriptions below. In accordance with previous studies in adults, we observed anterogradely labeled fibers in the striatum, anterior nuclei of the thalamus, anterior cingulate cortex, parietal cortex and visual cortices and in the brainstem (***van Groen and Wyss, 1990***; ***1992***; ***2003***; ***Jones et al., 2005***). However, a detailed assessment of these projections is outside the scope of this paper and here we will detail the projections to PHR. We observed anterogradely labeled fibers in layers I, III and V-VI of PrS (in all of the experiments included in the analyses, n=105), layers V-VI of PaS (n=90), layers V-VI of MEC (n=90), layers V-VI of medial LEC (n=14) and in all layers of posterior POR (n=75). In some cases, we also

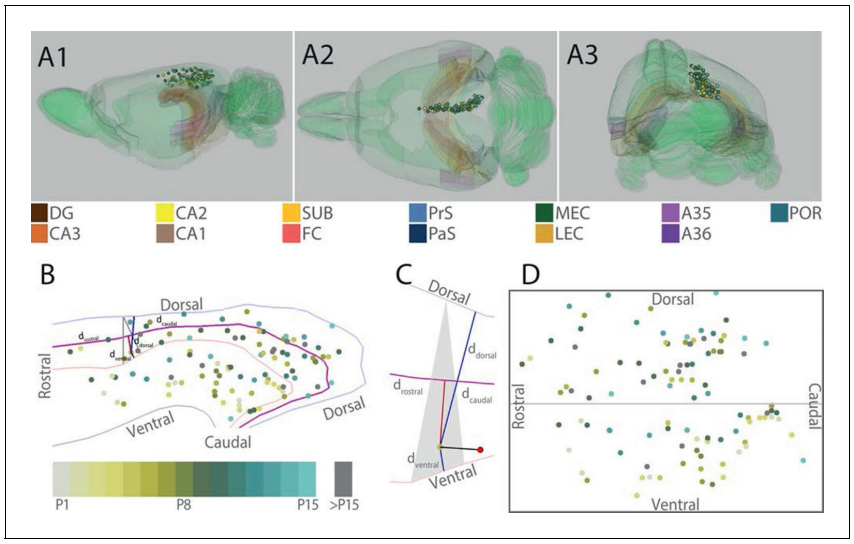

Figure 1. Location of the center of injections. (**A**) The location of the center of each injection was normalized to a standard 3D atlas of the rat brain (Waxholm space; ***Papp et al., 2014***; See ***video 1*** and ***2***). Lateral (A1), dorsal (A2) and para-caudal view (A3) of the 3D atlas brain with the center of each injection (colored spheres). The injections are color-coded according to age (see color code bottom left). Injections were performed in either the left or right hemisphere but to ease visualization, all injections were plotted in the right hemisphere. Dentate gyrus (DG), CA3-1, subiculum (SUB), fasciola cinereum (FC), pre- and parasubiculum (PrS and PaS), medial- and lateral entorhinal cortex (MEC and LEC), A35-36 and postrhinal cortex (POR) are color coded, while the rest of the brain is colored green. (**B**) Midsagital view of the center of the injections projected to the pial surface. The laminar position is disregarded to allow the injections to be plotted in 2D. Light blue, light red and grey line depict respectively the dorsal border of A30, the border between A29 and A30 and the ventral border of A29. Injections are color coded according to age. Triangle explained in C. (**C**) One example, as shown in B, of the algorithm used for calculating normalized 2D coordinates of the injections. The pial surface area of A29 and A30 was divided into triangles (grey area). The shortest vector (black line) between the injection (red sphere) and the cortical surface was calculated. Thereafter, we calculated the coordinate of the intersection of the vector and the plane within the triangle (yellow dot) which represented the 'transposed' location of the injection. The normalized dorsoventral coordinate of each injection was defined by calculating the shortest vector from the transposed injection to dorsal (d_{dorsal}) and ventral border of A29 or A30 ($d_{ventral}$). The normalized rostrocaudal coordinate was obtained by first calculating a line along the rostrocaudal extend of A29 and A30, positioned equally distant from the dorsal and ventral borders (magenta line). Next, we calculated the shortest vector between the injection and this line (red line) and found the intersection between the two. The rostrocaudal coordinate was obtained by calculating the cumulative distance from the cross section to the rostral ($d_{rostral}$) and caudal end of RSC (d_{caudal}). (**D**) Normalized flatmap of the injections. The 3D RSC is converted to a 2D normalized flatmap to obtain relative rostrocaudal and dorsoventral positions of the injections. The figure is oriented with rostral RSC (left), caudal RSC (right), dorsal RSC (top) ventral RSC (bottom) to each of the sides of the rectangle. Grey line depicts the border between A29 and A30 in RSC. In all figures, each injection is color coded according to the bottom left color scheme; light grey colored injections represent injections in pups aged P1, green colored injections represent injections in pups aged P8 while cyan colored injections represent injections in pups aged close to P15. Grey injections represent injections in pups older than P15.

DOI: 10.7554/eLife.13925.003

observed single fibers in layers I and/or III of MEC (n=34). Additionally, we observed few fibers (if present typically one or two fibers in an experiment) in the dorsal half of SUB (n=41) and/or in the dorsal CA fields (n=16). In contrast to previously published data (***Burwell and Amaral, 1998b***), we did not observe any labeled fibers in PER in any of our experiments. This includes the oldest aged pups (P27-28) and the adult cases, suggesting that this lack of perirhinal projections is not a developmental feature. It is thus obvious that all experiments shared RSC-PHR projection patterns, but there

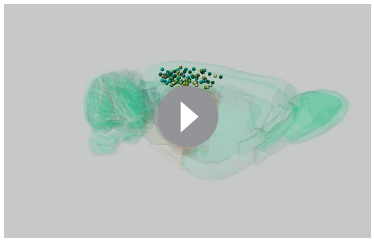

Video 1. Representation of all injection sites in RSC represented in a 3D rendering of the rat brain (Waxholm space; ***Papp et al., 2014***; ***2015***). The injection sites are color coded for age (for code see ***Figure 1***)
DOI: 10.7554/eLife.13925.004

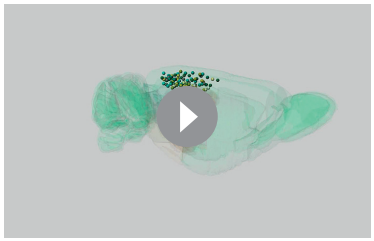

Video 2. Representation of all injection sites in RSC represented in a 3D rendering of the rat brain (Waxholm space; ***Papp et al., 2014***; ***2015***). The injection sites are color coded for age (for code see ***Figure 1***)
DOI: 10.7554/eLife.13925.005

were also marked differences from case to case depending on the location of injection within RSC. This will be systematically described in the next sections.

Injections in rostral A30

Injections in the rostral half of A30 (n=23) all resulted in comparable patterns of labeling in PHR. Labeled fibers were present in layers I, III and V-VI of the dorsal one-third of PrS. In layers I and III of PrS, labeled fibers were predominantly located in distal PrS and the densest plexus was generally observed in the dorsal extreme of PrS. Moderate numbers of labeled fibers were present in layers V-VI of dorsal PaS and layers V-VI of dorsomedial MEC. Among the injections in the rostral half of A30, the most caudal ones usually resulted in more widespread labeling in MEC. In none of the cases did we observe labeled fibers in the ventral two-thirds of PHR. We observed single labeled fibers in layer III of MEC in some of the experiments (n=3), in POR (n=16) and in HF (n=5).

In a representative animal (18433; P13), DA-A488 was injected in layers I-V in rostral A30 (***Figure 2A–D***, magenta). From the injection site, fibers continued caudally in layer VI of RSC and in the cingular bundle towards PHR. At the dorsal pole of PHR, fibers entered into the superficial layers and branched extensively in layer I and superficial layer III of intermediate proximodistal parts of the dorsal pole of PrS. At this dorsal level, labeled fibers were also present in layers V-VI of PrS. Single fibers continued into deep layers of dorsal PaS and deep layers of posterior POR and deep layers of dorsomedial MEC. No fibers were observed in more ventral levels of PHR, such that the ventral 75% of PHR did not show any labeled fibers.

Injections in rostral A30 thus resulted in labeling in the dorsal third of PHR, particularly in posterior POR, distal PrS, the complete transverse extent of PaS, and medial parts of MEC.

Injections in caudal A30

We analyzed 32 injections in caudal A30. Overall, injections in caudal A30 resulted in comparable projection patterns. Labeled axons were observed in layers I, III and V-VI in distal parts of PrS, layers V-VI of PaS and in layers V-VI medially in MEC. Compared to the labelling observed after rostral injections, the labeling resulting from caudal injections extended more ventrally in PrS, PaS and MEC (compare magenta and green topography in ***Figure 2C***). The total extend of all plexus covered approximately the dorsal half of PrS and PaS and the ventromedial part of MEC. The area receiving the densest projections was also shifted more ventrally. The maximum density of the plexus in PrS was usually located in the dorsoventral middle of its distal part. Only in one case, labeled fibers were present in the ventral one-third of PHR. At all dorsoventral levels, labeling covered the distal part of PrS, in layers I, III and V-VI, the proximodistal extent of PaS, and medial parts of MEC. After injections in caudal A30, we observed single labeled fibers in layer III of MEC in some experiments (n=12), in POR (n=29), and in HF (n=15).

In a representative animal (18453; P13), BDA was injected in layers I-V of intermediate-caudal A30 (***Figure 2A and D-E***, cyan). From the injection site labeled fibers continued caudally and ventrally in the cortex. Arriving in PHR, fibers continued ventrally in layer I and the lamina dissecans of PrS as

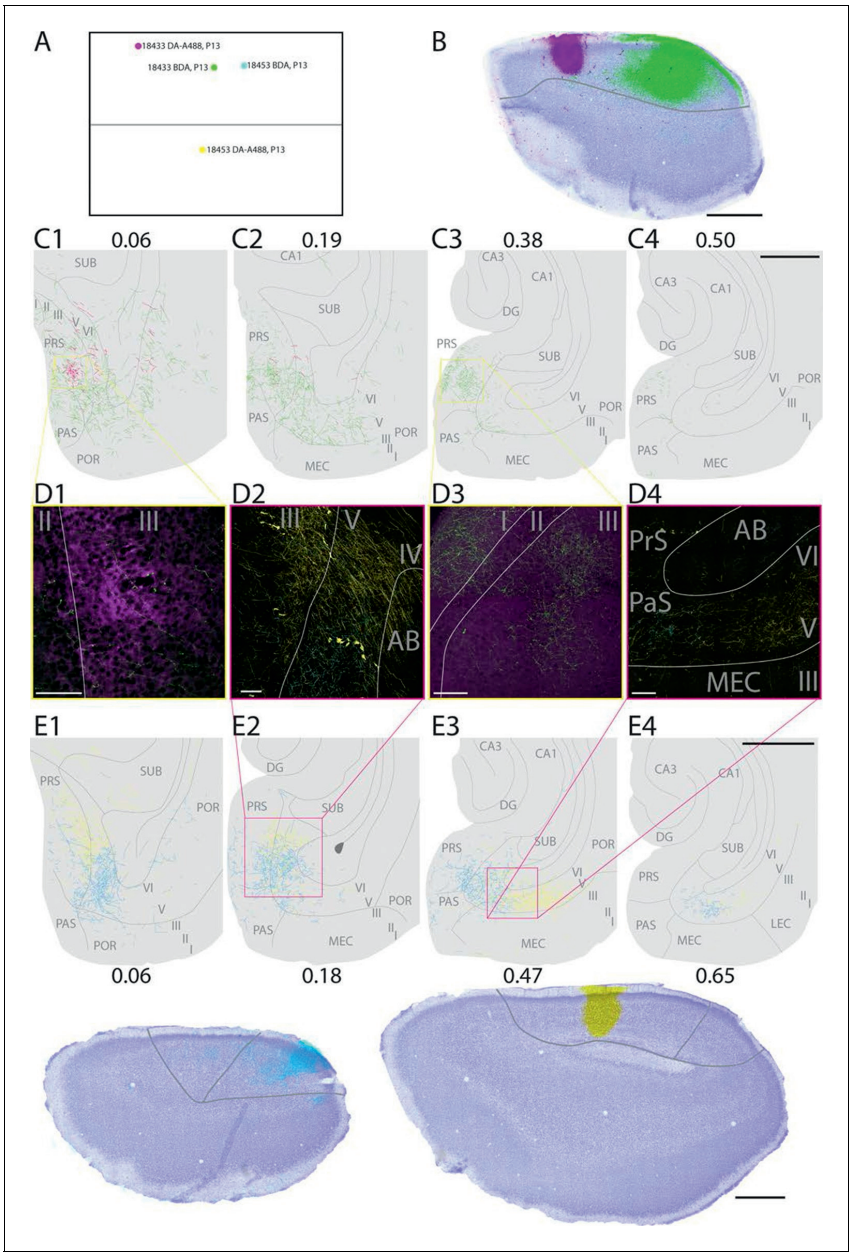

Figure 2. Representative examples of injections in RSC. (**A**) Normalized flatmap (see ***Figure 1D***) of the locations of the injections in RSC, shown in **B** and **E**. Injections are located in the rostral A30 (magenta), intermediate rostral A30 (green), intermediate caudal A30 (cyan) and the intermediate rostral quarter of A29 (yellow). (**B**) Horizontally cut and Nissl stained section at the level of the injections overlaid with a neighboring fluorescent section containing the center of an injection in rostral A30 (magenta) and intermediate-rostral A30 (green) within the same animal. Grey line depicts delineation of A30. (**C**) The projections after the two injections shown in B were traced

Figure 2 continued on next page

Figure 2 continued

and represented in a dorsoventral series of drawings of horizontal sections through the PHR. After injections in rostral A30 (magenta) labeled fibers were mostly observed in the dorsal PrS layers I and III (C1, D1). After injections in intermediate-caudal A30 (green) the densest plexus was located more ventrally in PHR and in addition to labeled fibers in layers I, III and V-VI of PrS, labeled fibers also extended into layers V-VI of PaS, POR and MEC (C2-3 and D3). Numbers above sections indicate the dorsoventral position of the section relative to the total dorsoventral extent of PHR. The yellow boxes in C1 and C3 indicate the position of high power digital images obtained from the actual sections (D1 and D3). Grey lines depict borders between the HF-PHR subdivisions, the border between cortex and white matter and lamina dissecans. (**D**) High power images of plexus depicted in the sections shown in **C** and **E**. Roman numbers indicate cortical layers. Grey lines depict borders between layers. (D1) Labeled fibers in superficial layer III of PrS after injections in rostral A30 (magenta). Additionally a few fibers are seen originating in the intermediate-caudal quarter of RSC (green). (D2) Labeled fibers in proximal PrS deep layer III and layers V-VI after injection in intermediate-rostral A29 (yellow) and labeled fibers in distal PrS deep layer III and layers V-VI after injection in intermediate-caudal A30 (cyan). (D3) Labeled fibers in layers I and III after injection in intermediate-caudal A30 (green). No fibers originating in the rostral A30 were observed. (D4) After injection in intermediate-caudal A30 labeled fibers were observed in medial MEC (cyan), while after injection in intermediate-rostral A29 labeled fibers were observed in lateral MEC (yellow). (**E**) Top: the projections after two injections (bottom) were traced and represented in a dorsoventral series of drawings of horizontal sections through the PHR. After injections in intermediate-caudal A30 (cyan) labeled fibers were observed in distal PrS dorsally (E1-3). At more ventral levels fibers also extended into deep layers of PaS and medial MEC (E3-4). After injections in intermediate-rostral A29 (yellow) the densest plexus was located in proximal parts of PrS dorsally (E1-2). At more ventral levels the plexus in PrS layers I and III disappeared while in the deep layers the plexus shifted to lateral parts of EC at successively more ventral levels (E3-4). Numbers below sections indicate the dorsoventral position of the section relative to the total dorsoventral extent of PHR. The magenta boxes in E2 and E3 indicate the position of high power digital images obtained from the actual sections (D2 and D4). Grey lines depict borders between the HF-PHR subdivisions, the border between cortex and white matter and lamina dissecans. Bottom: Horizontally cut and Nissl stained sections at the level of the injection overlaid with neighboring fluorescent sections containing the center of an injection in intermediate-caudal A30 (cyan) and intermediate-rostral A29 (yellow) within the same animal. Gray line depicts delineation of A29 and A30. Scale bars equal 100 μm (high power images) and 1000 μm (low power images).

DOI: 10.7554/eLife.13925.006

well as in deep white matter. At the dorsal pole of PrS, labeled fibers occasionally entered into layer III. A dense plexus was labeled in layers V-VI of the dorsal one-third of distal PrS, in layers V-VI of PaS and deep layers of medial POR. At more ventral levels, labeled fibers also extended into layers V-VI of MEC. In ventral parts of MEC, only a few labeled fibers were observed. No labeled fibers were observed in the most ventral one-third of PHR.

Injections in caudal A30 thus resulted in a labeling pattern in PHR comparable to that seen in case of rostral A30 injections, but extending to more ventral parts of PHR.

Injections in rostral A29

Injections in the rostral half of A29 (n=15) resulted in a comparable pattern of labeling in PHR. Labeled fibers were present in the dorsal half of PrS layers I, III and V-VI, in layers V-VI of the dorsal half of PaS and in layers V-VI of MEC. One injection also resulted in labeled fibers in dorsal LEC. In PrS, the fibers tended to be located more proximally compared to the projections originating from A30 at the same rostrocaudal level (compare cyan and yellow fibers in ***Figure 2E1–2***). Among the injections in rostral half of A29, the most caudal injections usually resulted in more extensive labeling of axons in MEC. In those cases, the plexus in MEC was located at intermediate mediolateral levels, more lateral compared to the MEC plexus seen after A30 injections (compare cyan and yellow fibers in ***Figure 2E3–4***). In some cases, we also observed single labeled fibers in layer III of MEC (n=6), in POR (n=8) and in HF (n=9).

In a representative animal (18453; P13), DA-A488 was injected in layers I-VI of intermediate-rostral A29 (***Figure 2A and D–E***, yellow). From the injection site, labeled fibers ran caudally and ventrally in the cingular bundle and in layer VI of RSC. At the dorsal pole of PrS, labeled axons continued ventrally in layer I, lamina dissecans, and in the deep white matter. At this level, labeled fibers entered PrS and branched in layers I, III and V-VI of proximal PrS. Single fibers extended into deep layers of PaS and POR. At approximately the dorsoventral middle of PHR, the density of

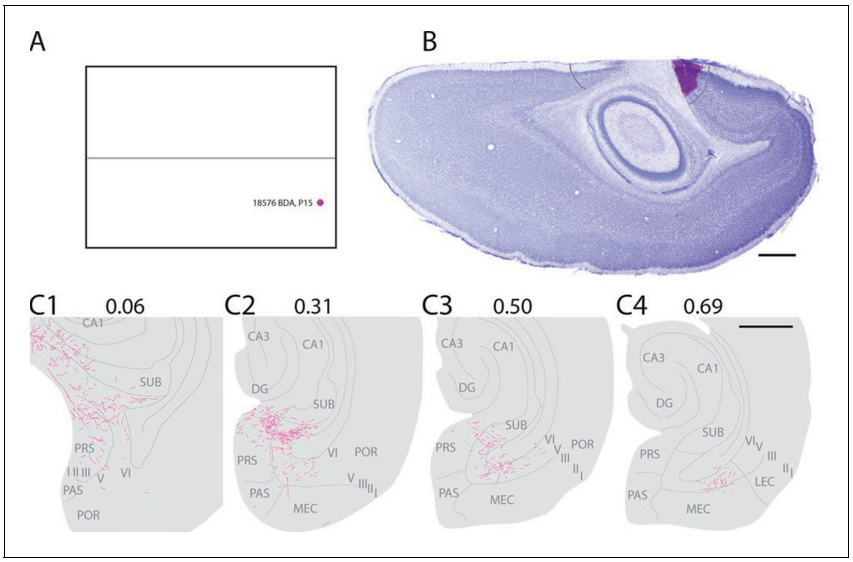

Figure 3. Representative example of an injection in caudal A29. (**A**) Normalized flatmap with location of an injection in caudal A29 (magenta). (**B**) Horizontally cut and Nissl stained section at the level of the injection overlaid with an adjacent section containing the center of the fluorescent tracer injection in caudal A29 (magenta). Grey lines depict delineation of A29 and A30. (**C**) The projections after the injection were traced and represented in a dorsoventral series of drawings of horizontal sections through the PHR. Labeled fibers are located in more proximal parts of layers I, III and V-VI of PrS compared to after projections in A30 (compare C1-3 and ***Figure 2***). At successively more ventral levels, fibers also extended into increasingly more lateral parts of layers V-VI of MEC compared with injections in A30 (compare C2-4 and ***Figure 2***). Grey lines depict borders between the HF-PHR subdivisions, the border between cortex and white matter and lamina dissecans. Scale bars equal 1000 µm.
DOI: 10.7554/eLife.13925.007

labeled fibers in proximal PrS layers I and III gradually decreased, while in the deep layers, labeled fibers gradually shifted position at successively more ventral levels. More specifically, moving from dorsal to ventral levels of PHR, labeled fibers occupied proximal PrS at dorsal levels, and distal PrS, PaS, medial MEC, lateral MEC and finally LEC at successively more ventral levels.

It is thus apparent that injections in rostral A29 resulted in labeling mainly in the dorsal third of PHR, including posterior POR and the transverse extent of PaS, similar to what was observed following injections in rostral A30. The distribution in PrS and MEC however differed from that resulting from injections in rostral A30 in that labeling was present in proximal PrS and more lateral parts of MEC.

Injections in caudal A29

Caudal A29-injections (n=35) resulted in comparable projection patterns in PHR. Labeled fibers were mostly located in the dorsal half of PrS, and the dorsal two-thirds of layers V-VI of PaS and MEC. However, in some experiments labeled fibers were also observed in ventral MEC and dorsal LEC. Compared to injections in caudal A30, injections in caudal A29 resulted in labeling also in more proximal parts of dorsal PrS. Additionally, after injections in caudal A29, very few fibers were observed in deep layers of PaS, while a dense patch of fibers was usually observed in MEC. The densest projection to PHR usually targeted the deep layers of dorsal PrS and intermediate dorsoventral MEC. We further observed in some cases single labeled fibers in layer III of MEC (n=13), in POR (n=22) and in HF (n=13).

In a representative animal (18576; P15) BDA was injected in layers I-VI of caudal A29 (***Figure 3***). Labeled fibers left the injection site and traveled through layer VI caudally and ventrally towards the RSC-PrS border. Single fibers penetrated the lamina dissecans and branched in layers I and III of

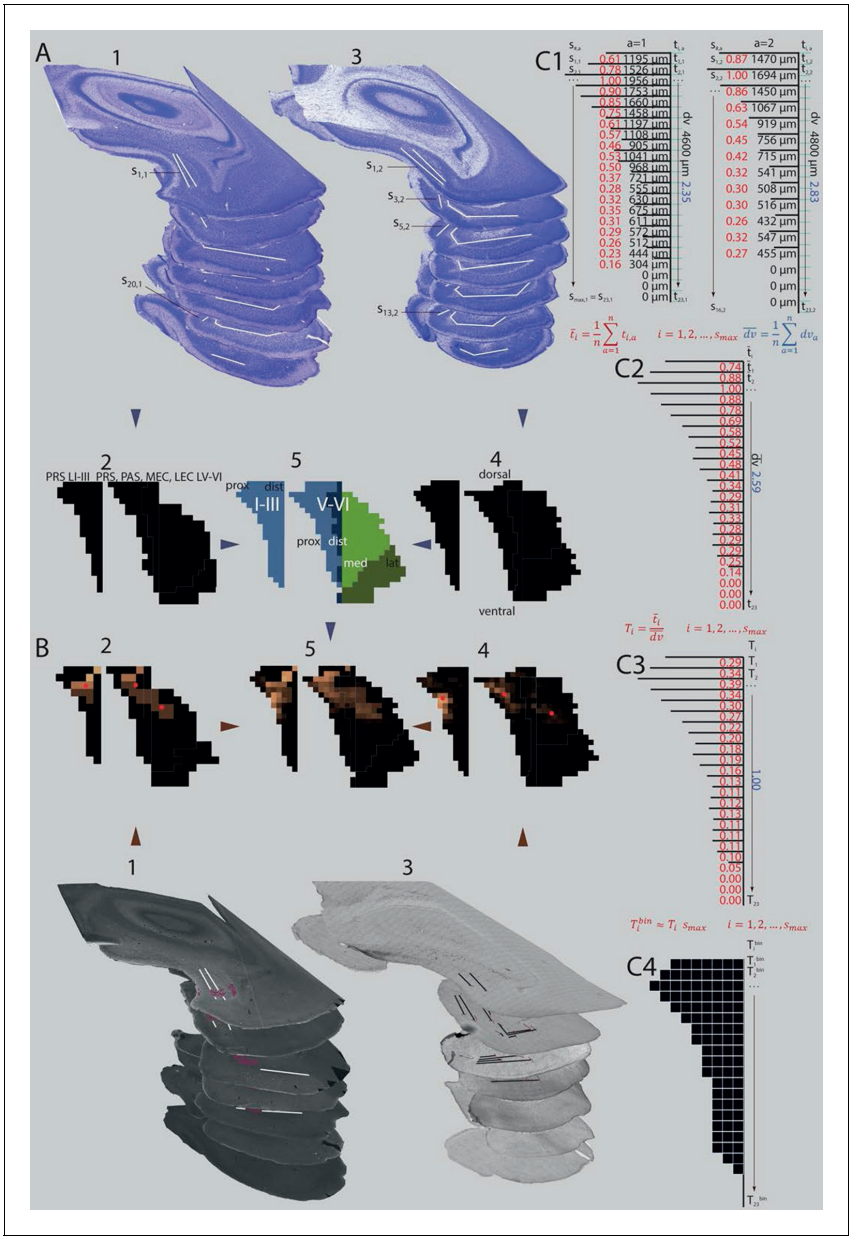

Figure 4. Standardized representation of location of labeled axons in PHR. (**A**) Extents of PrS, deep layers of PaS and deep layers of EC were measured in the horizontal plane (**1;** Nissl stained sections from case 18427, **3;** Nissl stained sections from case 18589). In every section, the extents of PrS, PaS, MEC and LEC along the transverse axis were measured. Based on the measurements of all sections in all brains (2 and 4) we binned the PHR along the dorsoventral and transverse axis and made an average representation of PHR (5; left: layers I and III of PrS (light blue), right: layers V-VI of PrS (light blue), PaS (dark blue), MEC (light green) and LEC (dark green). Dorsal, ventral, proximal (prox), distal (dist), medial (med), lateral (lat) indicates dorsoventral and transverse axis of the

Figure 4 continued on next page

Figure 4 continued

flatmaps. $s_{\#,a}$ refers to individual measurements of layers I and III of PrS in C1. (**B**) Locations of labeled fibers were obtained by measuring the distance between the plexus and the borders of the field in which the plexus was located (1; case 18427, note that we inserted magenta labeled structures to illustrate labeled fibers and their respective positions on the flatmaps). The measurements were performed in every section containing a plexus. The bins between the boundaries of each plexus were given a value ranging from 1 to 3 reflecting weak to dense labeling respectively (color coded in 2, 1 = brown; 2 = orange; 3 = bright yellow). Bins outside the plexus boundaries were given the value 0 (black, no plexus). In experiments in which we observed single labeled axons or a sparse plexus, we measured the distance from each labeled axon to one of the borders of the field in which the plexus was located (3; case 18589; repeating patterns in top sections are artefacts due to stitching of digitized images). We inserted magenta labeled fibers and their respective positions on the flatmaps). We gave each bin in the flatmap a value corresponding to the number of labeled single axons (4; bins not containing any labeled fibers: black; bins with the highest number of labeled axons: bright yellow). For all flatmaps, the centers of mass for layers I and III in PrS, layers V-VI of PrS and PaS combined and layers V-VI of MEC and LEC combined were calculated (red dots). To compare groups of injections, flatmaps of individual injections were normalized to the highest valued bin, transformed to the average flatmap and added together (5; see methods for further details). (**C**) Binning of layers I and III of PrS along the dorsoventral and along the transverse axis. The example is based on animals 18427 (left) and 18589 (right; both shown ***Figure 4A and B***). All subdivisions are binned according to the same algorithm. First the transverse measurements ($s_{\#,a}$, visualized by black lines in C1) and the dorsoventral measurement (dv_a) in all sections in all animals were normalized to the longest measurement of the respective subdivision in the particular animal (red (transverse) and blue (dorsoventral) numbers in C1). Next, we binned the dorsoventral axis of each PHR subdivision (represented by turquois lines in C1) in the same amounts of bins as the maximum number of sections containing PHR in a single series (s_{max}; 23 in the example) and calculated the transverse extends of each row of bins in each animal ($t_{i,a}$, numbers not shown). Thereafter, we calculated the means of the normalized transverse measurements across all animals for each bin ($\overline{ti}$, red numbers in C2), and the mean across all animals of the normalized dorsoventral extend of PHR ($\overline{dv}$; blue number in C2). The ratio of the mean transverse extends and the mean dorsoventral extend was calculated such that each dorsoventral level was expressed as a value relative to the dorsoventral extent of PHR (T_i; red numbers in C3). Finally, the number of bins along the transverse axis for each dorsoventral level (T_i^{bin}) was calculated (C4).

DOI: 10.7554/eLife.13925.008

dorsal PrS. Single fibers continued into deep layers of PaS and into all layers of POR close to the PaS border. A few fibers were also present in layer III of PaS. The density of labeled fibers increased at more ventral levels and reached its maximum in the middle of the dorsal half of PHR where proximal PrS layers I-III, layers V-VI of PrS were covered by labeled fibers. A few fibers were also labeled in layers V-VI of dorsomedial MEC. Single fibers invaded SUB, layer III of PaS and layer III of MEC. We observed a change in the density and position of labeled fibers along the dorsoventral extent of dorsal PHR. The density of labeling in PHR decreased at successively more ventral levels, while the position of labeled fibers in deep layers shifted from PrS and PaS at dorsal levels towards MEC at intermediate dorsoventral levels. In the ventral third of MEC labeling was only located in lateral parts of MEC. A few labeled fibers were observed in LEC.

All injections in caudal A29 thus resulted in labeling in PHR, comparable to what was seen in case of injections in rostral A29. However, the labeling from caudal A29 extended more ventrally in PHR.

Specific projection patterns from different parts of RSC

The different labeling patterns in PHR, observed after injections in different parts of RSC indicate that RSC is heterogeneous with respect to the terminal distribution of PHR projections. To systematically analyze this, we measured, in each experiment, the location of the labeled plexus in PHR. Thereafter, we produced normalized flatmaps of the location of the labeled plexus in each experiment (see methods for details). These flatmaps consisted of multiple bins spanning the dorsoventral and transverse axis of PHR (***Figure 4A***). Each bin was assigned a value between 0 (black) and 1 (yellow) reflecting the density of labeled fibers in PHR (***Figure 4B***). This approach allowed us to compare flatmaps across animals of different ages and pool flatmaps of groups of interest. For statistical analysis, we calculated the center of mass of the labeled fields and tested the relationships between this measure and the coordinates of the injection and the age of the animal.

We first performed a cluster analysis to investigate whether the patterns of labeling in PHR were clustered dependent on the location of the injection site or the age of the animal. Using the

distribution patterns as represented in the flatmaps (see methods for details), we identified five clusters. However, the injection sites in RSC associated with each of the clusters were not clustered in RSC such that several of the injections associated with one cluster of distribution patterns partly overlapped with injection sites associated with other labeling clusters in PHR. None of the clusters of labeling in PHR was associated with distinct age groups of animals. We therefore concluded that RSC does not contain regions having distinct projection patterns to PHR, but more likely has a continuous topographical organization of projections to PHR. Therefore, we next assessed whether the labeling patterns in PHC changed systematically in relationship to the rostrocaudal and/or the dorsoventral position of the injections in RSC. For the analysis of the projection patterns, we initially subdivided the injections into two groups depending on whether the injections were located in A29 (n=50) or A30 (n=55). We also subdivided each of the two areas into four equally sized rostrocaudal regions; the rostral quarter of RSC (n=16), intermediate-rostral quarter of RSC (n=22), intermediate-caudal quarter of RSC (n=48) and caudal quarter of RSC (n=19).

To evaluate the projection patterns we analyzed the data in two different ways. First, we pooled the projection patterns of all experiments in each of the eight injection groups described above. We subsequently analyzed the 'mean' projection pattern of each group, as represented on flatmaps of PHR (***Figure 5—figure supplement 1A***). However, the pooled flatmaps are sensitive to the number of bins covered by the labeled axons in each experiment. Experiments in young animals with single labeled fibers in PHR or experiments with small injections resulting in few labeled axons in PHR will contribute fewer 'labeled bins' to the pooled flatmaps, and the pooled flatmaps might therefore be biased towards the experiments with many bins containing labeled axons. Therefore, we also calculated, for each experiment, the center of mass of the projections to respectively layers I and III of PrS, layers V-VI of PrS and PaS combined, and layers V-VI of MEC and LEC combined. The centers of mass served as a quantifiable measure of the location of the labeled axons in PHR, which is independent of the number of fibers labeled in each experiment.

After injections in the rostral part of A29 and A30, labeled fibers were only seen in the dorsal one-third of PHR. Labeling was mainly present in superficial and deep layers of PrS with approximately equal densities, while only a moderate number of labeled fibers was observed in deep layers of PaS and dorsomedial MEC (***Figure 5—figure supplement 1A***). Injections in the three more caudal subdivisions of A29 and A30 resulted in labeling in PHR at successively more ventral levels. Labeling was seen in layers I, III and V-VI of the dorsal half of PrS, in layers V-VI of the dorsal half of PaS and of the medial part of MEC (***Figure 5—figure supplement 1A***). When comparing injections in A29 and A30, we did not see a systematic relationship between the placement of the injection and the dorsoventral distribution of the labeling (***Figure 5—figure supplement 1A***). The results thus suggest that the rostrocaudal placement of injection in RSC is related to the dorsoventral location of the labeled plexus in PrS, PaS, and MEC.

Multiple regressions confirmed a relationship between the rostrocaudal placement of the injection and the dorsoventral location of the center of mass of the labeled axon terminals. More rostrally placed injections resulted in centers of mass of the labeled plexus that were located more dorsally in layers I and III of PrS (***Figure 5A*** and ***Figure 5—figure supplement 1B***, $\beta=-0.201$, 95% confidence interval (CI) [−0.290, −0.111], $t_{99}=-4.452$, $p<0.001$). The dorsoventral placement of injections was not significantly related to the dorsoventral location of the centers of mass of the projections ($\beta=-0.052$, 95% CI [−0.144, 0.040], $t_{99}=-1.120$, $p=0.265$). There was no significant interaction effect of rostrocaudal-by-dorsoventral placement of the injection on the resulting patterns of anterograde labeling in PHR.

Regarding terminal labeling in layers V-VI of PrS and PaS, more rostrally placed injections in RSC resulted in terminal centers of mass located more dorsally in layers V-VI of PrS and PaS (***Figure 5A*** and ***Figure 5—figure supplement 1D***, $\beta=-0.133$, 95% CI [−0.203, −0.063], $t_{99}=-3.784$, $p<0.001$). The dorsoventral placement of the injection showed no significant relationship with the dorsoventral location of the centers of mass of the labeling ($\beta=0.020$, 95% CI [−0.052, 0.091], $t_{99}=0.547$, $p=0.585$). There was no significant interaction effect of rostrocaudal-by-dorsoventral placement of the injection.

In layers V-VI of MEC and LEC, more rostrally placed injections resulted in terminal centers of mass located more dorsally in layers V-VI of MEC and LEC (***Figure 5A***, ***Figure 5—figure supplement 1F***, $\beta=-0.186$, 95% CI [−0.269, −0.104], $t_{85}=-4.498$, $p<0.001$). The dorsoventral placement of the injection showed a weaker, but significant relationship with the dorsoventral location of the centers

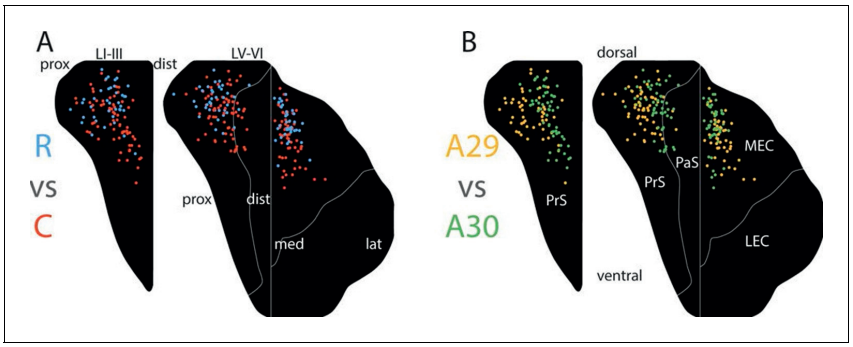

Figure 5. Topographical organization of projections. The position of the centers of mass of labelling in layers I and III of PrS, layers V-VI of PrS and PaS and layers V-VI of MEC and LEC is plotted. Each dot is color coded with respect to the rostrocaudal (**A**) or dorsoventral position (**B**) of the injections in RSC (rostral half; blue, caudal half; red, A29; yellow, A30; green). In layers I and III of PrS more caudally placed injections result in projections located more ventral compared to rostrally placed injections (**A**; $p<0.001$), while ventrally placed injections result in projections located more proximal compared to dorsally placed injections (**B**; $p<0.001$). In layers V-VI of PrS and PaS caudally placed injections result in projections located more ventral compared with rostrally placed injections (**A**; $p<0.001$), while ventral and rostrally placed injections result in projections located significantly more proximal compared with dorsally and caudally placed injections (**B**; ventral: $p<0.001$, caudal: $p=0.033$). In MEC and LEC layers V-VI, caudal and ventrally placed injections result in projections located significantly more ventral compared to rostral and dorsally placed injections (**A**; caudal: $p<0.001$, ventral: $p=0.032$), while ventrally placed injections result in projections located significantly more lateral compared to dorsally placed injections (**B**; $p=0.020$). Multiple regression was used for all statistical tests (***Figure 5—source data 1–12***). For flatmaps of the projection patterns see ***Figure 5—figure supplement 1***.

DOI: 10.7554/eLife.13925.009

The following source data and figure supplement are available for figure 5:

Source data 1. Datapoints used in multiple regressions.
DOI: 10.7554/eLife.13925.010
Source data 2. Datapoints used in multiple regressions.
DOI: 10.7554/eLife.13925.011
Source data 3. Datapoints used in multiple regressions.
DOI: 10.7554/eLife.13925.012
Source data 4. Datapoints used in multiple regressions.
DOI: 10.7554/eLife.13925.013
Source data 5. Datapoints used in multiple regressions.
DOI: 10.7554/eLife.13925.014
Source data 6. Datapoints used in multiple regressions.
DOI: 10.7554/eLife.13925.015
Source data 7. Datapoints used in multiple regressions.
DOI: 10.7554/eLife.13925.016
Source data 8. Datapoints used in multiple regressions.
DOI: 10.7554/eLife.13925.017
Source data 9. Datapoints used in multiple regressions.
DOI: 10.7554/eLife.13925.018
Source data 10. Datapoints used in multiple regressions.
DOI: 10.7554/eLife.13925.019
Source data 11. Datapoints used in multiple regressions.
DOI: 10.7554/eLife.13925.020
Source data 12. Datapoints used in multiple regressions.
DOI: 10.7554/eLife.13925.021
Figure supplement 1. Topographical organization of RSC-PHR projections in pups.
DOI: 10.7554/eLife.13925.022

of mass of the labeling since more ventrally placed injections in RSC had centers of mass located more ventral in PHR (***Figure 5B***, ***Figure 5—figure supplement 1F***, β=0.089, 95% CI [0.008, 0.171], t_{85}=2.181, p=0.032). There were no significant interaction effects of rostrocaudal-by-dorsoventral placement of the injection. Based on these data we conclude that the rostrocaudal position of injections in RSC determined the dorsoventral location of the labeled plexus in PrS, PaS and MEC.

We subsequently analyzed whether the location of the injection site influenced the transverse position of the labeled axons in the identified PHR subdivisions. A visual analysis of the plotted centers of mass and the pooled flatmaps showed that in layers I and III of PrS the labeling was generally located distally in case of injections in A30 (***Figure 5B***, ***Figure 5—figure supplement 1A***). After injections in A29, proximal PrS was also covered by labeled fibers. This suggested that the dorsoventral position of the injection in RSC is related to the transverse position of the labeled fibers in PHR. This suggestion was substantiated through multiple regression analysis, showing that following ventral injections, the centers of mass of the labeled plexus in layers I and III of PrS were significantly more proximal compared to those following injections in dorsal RSC (***Figure 5B*** and ***Figure 5—figure supplement 1C***; β=0.392, 95% CI [0.267, 0.518], t_{99}=6.200, p<0.001). The dorsoventral placement of the injections showed no significant relationship with the dorsoventral location of the centers of mass of the labeling (β=0.117, 95% CI [-0.005, 0.239], t_{99}=1.902, p=0.060). There was no significant interaction effect of rostrocaudal-by-dorsoventral placement of the injection.

In layers V-VI of PrS and PaS, the centers of mass were located significantly more proximal after injections in ventral RSC compared to injections in dorsal (***Figure 5B*** and ***Figure 5—figure supplement 1E***; β=0.292, 95% CI [0.192, 0.392], t_{99}=5.780, p<0.001). The rostrocaudal placement of the injection did show a weaker, but significant relationship with the proximodistal location of the labeled fibers (***Figure 5A*** and ***Figure 5—figure supplement 1E***, (β=0.107, 95% CI [0.009, 0.205], t_{99}=2.164, p=0.033); injections in caudal RSC had centers of mass located more distal in PrS layers V-VI, compared to what was seen following injections in rostral RSC. Additionally, we observed a significant rostrocaudal-by-dorsoventral placement of injection interaction effect, since injections located more dorsal and more caudal had centers of mass in significantly more distal parts of layers V and VI of PrS and PaS (β=1.039, 95% CI [0.529, 1.548], t_{99}=4.049, p<0.001).

The dense and extensive labeling in layers V-VI of MEC was clearly seen in case of injections in A29, while a more restricted area, medially in MEC, was covered after injections in A30 (***Figure 5—figure supplement 1A***). Multiple regression analysis confirmed that the centers of mass of the terminating axons were located more lateral after injections in ventral RSC compared to after injections in dorsal RSC (***Figure 5B*** and ***Figure 5—figure supplement 1G***; β=−0.121, 95% CI [−0.222, −0.020], t_{85}=−2.378, p=0.020). However, the rostrocaudal placement of the injection had no significant relationship with the mediolateral location of the labeled fibers (β=−0.048, 95% CI [−0.150, 0.054], t=−0.937, p=0.351). There was no significant interaction effect of rostrocaudal-by-dorsoventral placement of the injection.

The overall analysis thus supported the conclusion that the dorsoventral position of the injection in RSC determines the transverse position of the labeled fibers in PrS, PaS, and MEC. By plotting each of the transverse coordinates of the centers of mass against the dorsoventral coordinate of the injection we did not observe any discrete 'jumps' (data not shown). This suggests that the topographical organization of projections from RSC to PHR is not organized into discrete projection patterns from each of A30 or A29 or its subdivisions a, b or c, but rather is organized as a continuous dorsoventral gradient, similar to what has been reported for the adult situation.

Projection patterns in different age groups

Next, we aimed to investigate how the topographical organization of the projections developed during the postnatal period. We binned the experiments in three age groups, aged P1-P6 (n=33), P7-P13 (n=52), and injections in animals older than P14 (n=20). The labelling patterns from all experiments in each of these age groups were in general similar (***Figure 6—figure supplement 1***, All areas). In all age groups, layers I, III and V-VI of dorsal PrS, layers V-VI of dorsal PaS, and layers V-VI of medial MEC were labeled following injections in RSC. Additionally, for all age groups, the dorsal PrS was the most commonly labeled part of PHR. The distribution of labeling was comparable between all age groups.

We subsequently refined this analysis to study differences between rostral and caudal RSC with respect to labeling patterns in PHR. We plotted the centers of mass of the labeled projections

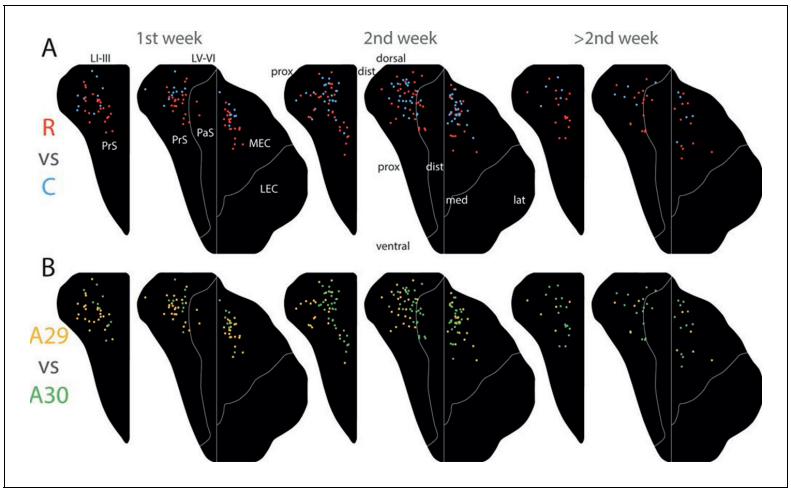

Figure 6. Development of topographies. The position of the centers of mass of the labelling in layers I and III of PrS, layers V-VI of PrS and PaS and layers V-VI of MEC and LEC is plotted (see also ***Figure 6—figure supplement 2***). Each dot is color coded with respect to the rostrocaudal (**A**) or dorsoventral position (**B**) of the injections in RSC (rostral half; blue, caudal half; red, A29; yellow, A30; green). Left column; animals aged P1-6, middle column; animals aged P7-13, right column; animals aged P14-28. Age is not related to the dorsoventral position of the plexus (PrS LI-III: p=0.876; PRS and PaS LV-VI; p=0.187; EC LV-VI: p=0.198) or the transverse position of the plexus (PrS LI-III: p=0.641; PrS and PaS LV-VI; p=0.325; EC LV-VI: p=0.402). Multiple regression was used for all statistical tests (***Figure 5—source data 1–12***). For flatmaps of the projection patterns see ***Figure 6—figure supplement 1***.
DOI: 10.7554/eLife.13925.023
The following figure supplements are available for figure 6:

Figure supplement 1. Flatmaps of projection patterns of different age groups.
DOI: 10.7554/eLife.13925.024
Figure supplement 2. Development of topographies.
DOI: 10.7554/eLife.13925.025

observed after injections in the rostral half (n=10, 1st week; n=32, 2nd week; n=5, 3rd week and older) and caudal half of RSC (n=23 1st week, n=30 2nd week, n=15 3rd week and older; ***Figure 6A***). The overall patterns across the age groups were similar and resembled the data including all injections in each subgroup. After injections in the rostral half of RSC, the labeling patterns in all age groups were limited to layers I, III and V-VI of dorsal PrS, layers V-VI of dorsal PaS and layers V-VI of MEC (***Figure 6—figure supplement 1*** R). However, in MEC, animals aged younger than a week had a tendency to only display labeled fibers in the most dorsomedial part while older animals also displayed labeled fibers in more lateral and ventral parts of MEC.

Next, we split each age group in two different subgroups with respect to the location of the injection in A29 or A30, combining data on rostral and caudal RSC. We plotted the centers of mass of the labeling after injections in A30 (n=9 1st week, n=31 2nd week, n=15 3rd week and older) and A29 (n=24 1st week, n=21 2nd week, n=5 3rd week and older, ***Figure 6B***). Following injections in A30 in all age groups, the labeled plexus were located in layers I, III and V-VI (***Figure 6—figure supplement 1*** A30). In animals aged younger than a week, a tendency for less dense labeling was seen in ventral PHR compared to the older age groups. After injections in A29, all age groups showed comparable labeling patterns. In PrS layers I, III, and V-VI, the terminating axons in all age groups were located more proximally compared to the projection patterns seen after injections in A30 (***Figure 6—figure supplement 1*** A29). Similar to injections in A30, in animals aged younger than a week, A29 injections resulted in less labeling in ventral levels of PHR. This effect was most obvious in MEC.

After injections in caudal A29 and A30, the labeling patterns were in general similar across all age groups (***Figure 6—figure supplement 1C***). Injections in caudal RSC resulted in preferred labeling in more ventral parts of PHR compared to injections in rostral RSC.

A descriptive assessment of the projection patterns thus suggested that the different age groups had comparable patterns of labeling. The topography along the transverse axis of PrS and PaS seen after A29 and A30 injections was observed already during the first postnatal week. In addition, in all age groups, caudal injections resulted in more extensive labeling in ventral PHR compared to rostral injections. However, injections in younger animals tended to have less labeled fibers in ventral PHR. To investigate this phenomenon more carefully, we plotted the coordinates of the centers of mass of the axonal labeling as a function of age and the location of the injection (***Figure 6*** and ***Figure 6—figure supplement 2***). This analysis indicated that already from the earliest postnatal ages, the position of the centers of mass are organized as described above. Already at the earliest ages, we observed that different rostrocaudal levels of RSC project to different dorsoventral levels of PrS and PaS. Even though we observed a tendency for the youngest animals to not display labeling more ventrally in PHR, age had no significant effect on the position of the centers of mass along the dorsoventral axis in neither layers I and III of PrS (***Figure 6—figure supplement 2A***, β=0.000, 95% CI [−0.005, 0.004], t_{99}=−0.157, p=0.876), in layers V-VI of PrS and PaS (***Figure 6—figure supplement 2B***, β=−0.002, 95% CI [−0.006, 0.001], t_{99}=−1.328, p=0.187), nor in layers V-VI of MEC and LEC in older animals (***Figure 6—figure supplement 2C***, β=−0.003, 95% CI [−0.007, 0.001], t_{85}=−1.299, p=0.198). To check if animals aged younger than a week had less labeled fibers in ventral PHR compared to older animals, we converted the continuous age variable to a discrete variable were animals aged younger and older than a week were considered as two different groups. However the age groups were not significantly related to the location of the center of mass (lowest p-value=0.221). In neither of the regression analyses, we observed any significant location-by-age interaction effects.

Already in the youngest cases, the centers of mass in layers I and III of PrS and layers V-VI of PrS and PaS after injections in A29 were located more proximal compared to those resulting from injections in A30 (***Figure 6B*** and ***Figure 6—figure supplement 2D and E***). Age did not predict the location of the centers of mass along the transverse axis for neither layers I and III of PrS (***Figure 6—figure supplement 2D***, β=0.001, 95% CI [-0.005, 0.008], t_{99}=0.468, p=0.641), layers V-VI of PrS and PaS (***Figure 6—figure supplement 2E***, β=0.002, 95% CI [-0.002, 0.007], t_{99}=0.990, p=0.325), nor layers V-VI of MEC and LEC (***Figure 6—figure supplement 2F***, β=0.002, 95% CI [-0.003, 0.008], t_{85}=0.843, p=0.402). However, for layers V-VI of PrS and PaS there was a significant interaction of rostrocaudal placement of injection-by-age (β=-0.033, 95% CI [-0.056, -0.11], t_{99}=-2.995, p=0.004), indicating that at older ages, respectively more rostral injections resulted in labeling in more distal parts of layers V-VI PrS and PaS.

Based on these results we conclude that the heterogeneous projection patterns observed in later postnatal stages is also present in the first postnatal stages.

Projection patterns in adolescents and adults

We next asked whether the projection patterns in PHR, observed in young animals, are also present in adult animals (approximately 3 months). To this end, we reanalyzed a dataset described in earlier publications from our lab (***Jones et al., 2005***; ***Jones and Witter, 2007***). Analyses of the cases individually, suggested that the organization of the projection pattern as we described in young animals was also present in adult animals. After injections in A30, a dense fiber plexus was observed distally in layers I and III of dorsal PrS (***Figure 7A***). Additional labeled fibers were observed in layers V-VI of distal PrS, PaS and medially in MEC, comparable to the projection pattern we observed after injections in A30 of pups (***Figure 5—figure supplement 1A*** and ***Figure 6—figure supplement 1***). Compared to injections in A30, injections in A29 resulted in labeled fibers more proximally in PrS and more laterally in MEC (***Figure 7B***). This topographical organization seems to be graded, since the injection located at the border between A29 and A30 displayed labeled fibers in a mediolateral position between the dorsally- and ventrally injected cases (compare ***Figure 7C*** with A and B respectively). Compared to rostrally placed injections (***Figure 7A and B***), we observed that caudally placed injections displayed more labeled axons in ventral PrS and MEC, and the area receiving the densest projection in both PrS and MEC was shifted more ventrally (***Figure 7C***). Taken together, these findings suggest that the RSC to PHR projections in the postnatal brain are similarly organized to the adult ones.

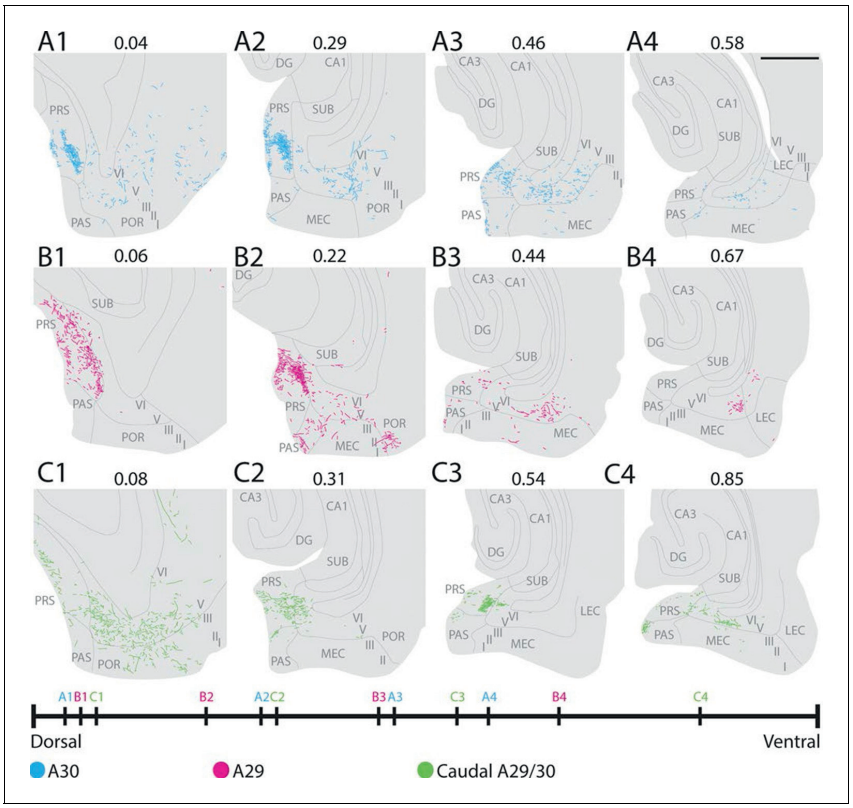

Figure 7. Labelling patterns in the adult. (**A**) An injection in intermediate rostrocaudal A30 resulted in dense labelling in layers I and III of distal PrS and a few fibers in deep PrS, PaS and POR (A1). More ventrally, fibers also invaded the MEC with the most fibers located medially in MEC (A3). (**B**) An injection in intermediate rostrocaudal A29 resulted in a dense fiber plexus in layers I and III of proximal PrS and POR (B2). At this dorsoventral level a few fibers also invaded PaS. More ventrally, a fiber plexus was present in lateral MEC. (**C**) An injection at the border of A29 and A30 in caudal RSC resulted in fibers located in layer I of PrS and deep PaS and POR dorsally (C1). More ventrally, a dense projection to layers I and III of PrS (C2 and 3) and a moderate projection to intermediate mediolateral MEC was present (C4). In A-C numbers above each section depict normalized dorsoventral position of the section and the line at the bottom of the figure represents the relative dorsoventral position of each section. Scale bar equals 1000 μm.

DOI: 10.7554/eLife.13925.026

Development of density of projection

We aimed to investigate whether there was a chronological development of the number of RSC-axons which could be traced within PHR. In the first postnatal week, very few fibers were labeled in PHR. At P1-P3 we only observed single unbranched fibers in PHR (***Figure 8A–D***). Along the fibers, axonal growth cone-like swellings were observed, independent of whether the fibers were located in the cortex or in the white matter. At P3, we observed the first branching fibers in PHR, although these fibers typically branched only once or twice in each section. After P3, the plexus gradually increased in density and complexity. However, we did not observe an adult-like plexus until P12 (***Figure 8F***). At this age, we observed dense plexus, with fibers displaying numerous branching points and each fiber containing fine extensions and protrusions, similar to what was seen in older animals and adults (***Figure 8G***). Based on these observations we concluded that the number of RSC fibers in PHR increase gradually from single fibers at P1 to adult-like densities around P12.

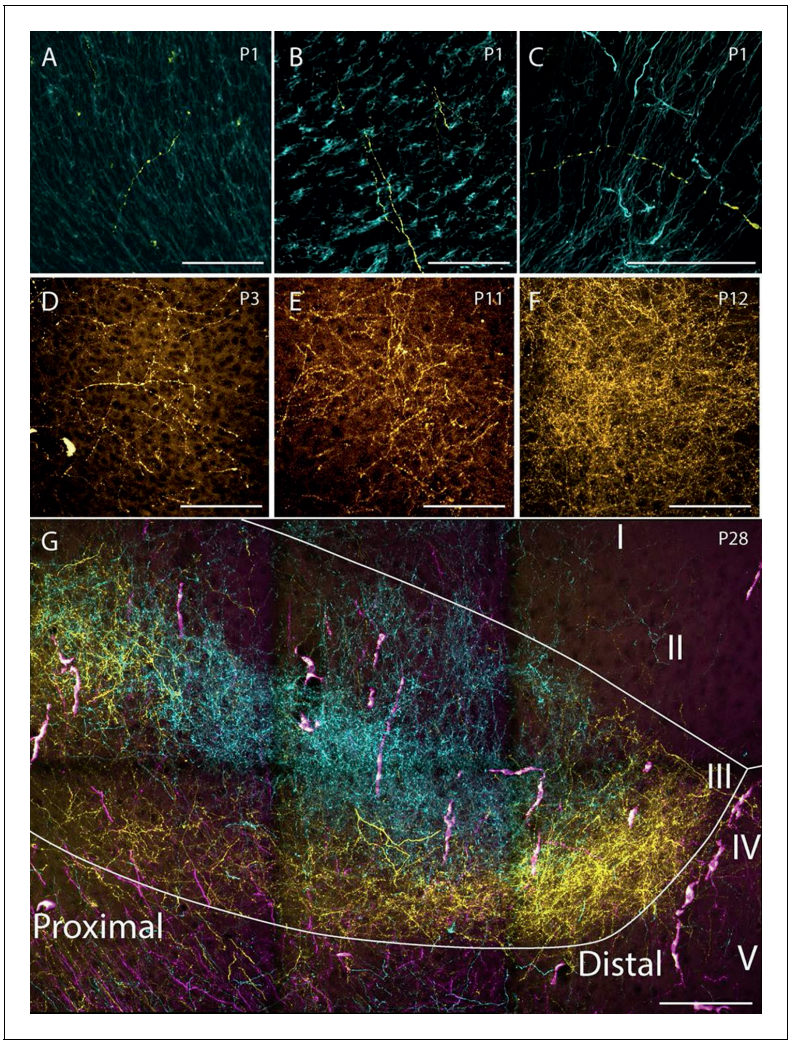

Figure 8. Examples of the densest fiber plexus observed in PHR at different ages. At birth, single unbranching fibers were present in superficial layers of PrS (**A**), deep layers of PrS (**B**) and deep layers of MEC (**C**). At P3, some branching fibers were observed (**D**, PrS). These fibers typically branched only once or twice. At P11 (**E**, PrS) the complexity of the fiber plexus increased as fibers have multiple branching points and thin fibers are seen within the plexus. At P12 (**F**, PrS) the first plexus which was comparable to plexus in adolescent animals (**G**, PrS) and adults (data not shown) was observed. In the experiment shown in **G**, the terminal distribution of three differentially labeled projections is illustrated. A plexus resulting from an injection in intermediate-rostral A29 (yellow) terminated throughout layer III of PrS, while the plexus observed after an injection in intermediate-rostral A30 terminated in the center of layer III of PrS (cyan). Fibers originating from a third injections in intermediate-caudal RSC (magenta) are observed, however the densest fiber plexus is located in a section at more ventral levels of PrS. The large, overlapping magenta and yellow structures are endothelium which take up alexa-preconjugated dextran amines. White line depicts the deep and superficial borders of layer III. Scale bars equal 100 μm.
DOI: 10.7554/eLife.13925.027

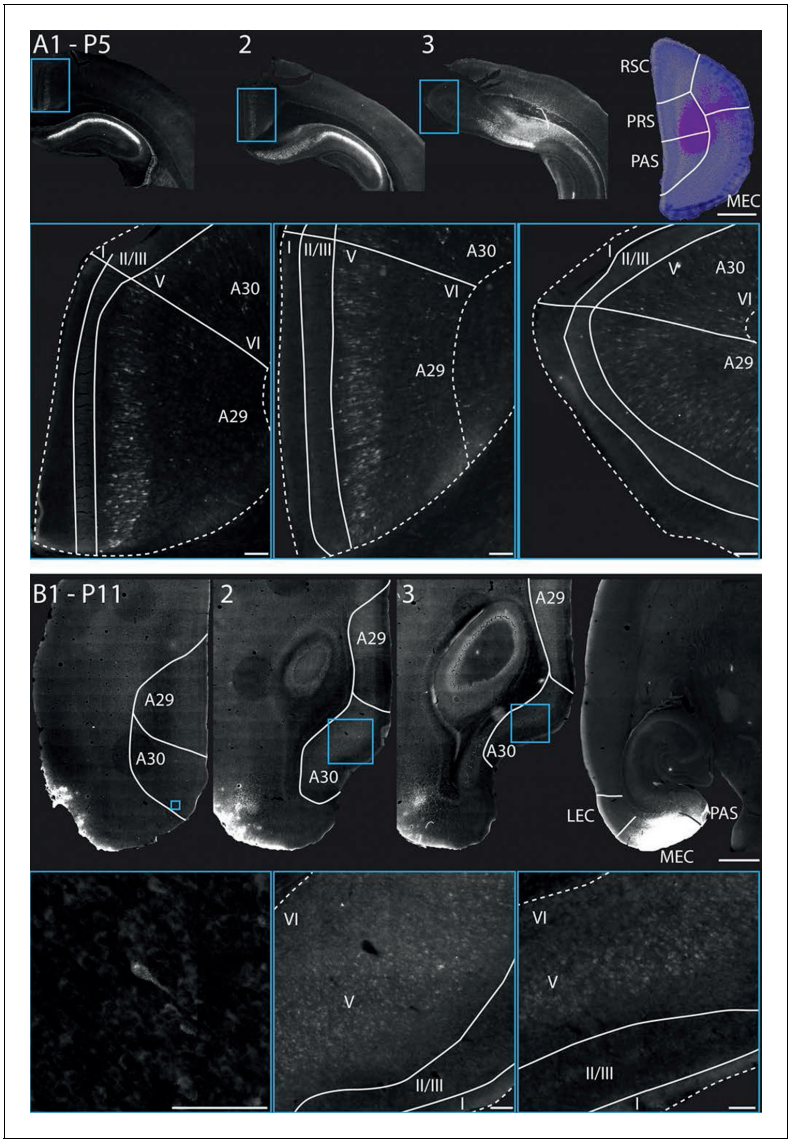

Figure 9. RSC projections to PHR arise from neurons in layer V. (**A**) A FB injection in deep layers of mainly PrS and PaS (top right; P5, coronal section) resulted in retrograde labeling of neurons in CA1, SUB and RSC (top row). Coronal sections shown are from intermediate-rostral RSC (1), intermediate-caudal RSC (2) and caudal RSC (3). Cyan squares depict size and position of high-power images in the bottom row. Bottom row: High power images of retrogradely labeled neurons in superficial layer V of RSC. Dashed lines depict the pia and the border between cortex, white matter and the corpus callosum. Solid lines depict borders between layer I, layers II-III and layer V and border between A29 and A30. Scale bars equal 100 μm (high power images) and 1000 μm (low power images). (**B**) FB was injected in an intermediate dorsoventral level in MEC and PaS (top right; P11, horizontal sections) and resulted in retrogradely labeled neurons in superficial layer V of caudal RSC (top row). Horizontal sections are organized from dorsal (1) to ventral (3). Cyan squares depict location of high-power images in the bottom row. White lines depicts borders of RSC and border between A29 and A30. Bottom row: High power

Figure 9 continued on next page

Figure 9 continued

images of retrogradely labeled neurons in superficial layer V of RSC. Dashed lines depict the pia and the border between cortex and white matter. Solid lines depict borders between layer I, layers II-III and layer V. Scale bars equal 100 μm (high power images) and 1000 μm (low power images).

DOI: 10.7554/eLife.13925.028

RSC neurons projecting to PHR

Since most of the RSC-PHR projections seemed to be fully developed very early during postnatal development, we aimed to investigate whether the PHR projecting neurons in RSC were located in layer V, similar to adults (***Burwell and Amaral, 1998a***). After fast blue injections in PHR of pups we identified labeled neurons in RSC in superficial layer V at P5 (***Figure 9A***) and P11 (***Figure 9B***), which suggested that the RSC-PHR projections are adult-like with respect to the layer in which the neurons are located already during the first postnatal week of development. These observations are in line with our anterograde material in which we observed that all injections that did not cover parts of layer V (n=8) did not result in any labeled axons in PHR.

Discussion

To study the development of RSC projections to HF-PHR, we injected anterograde tracers in RSC of rats aged P0-28. We conclude that the postnatal RSC projects densely to all layers of PrS and posterior POR and deep layers of PaS and MEC and weakly to deep layers of LEC and to SUB. Our retrograde experiments showed that the origin of these projections were neurons located in superficial parts of layer V of RSC. These findings are in accordance with previous work in the adult (***Wyss and Van Groen, 1992***; ***Shibata, 1994***; ***Burwell and Amaral, 1998a***; ***Jones and Witter, 2007***). Additionally, we report that the RSC projections to PrS, PaS and EC are topographically organized similarly already in the youngest postnatal rats and in adult rats (***Figure 10***). The notion that rostral RSC only projects to dorsal PHR, while caudal RSC projects to additional more ventral parts of PHR is in accordance with previous work in the adult (***Wyss and Van Groen, 1992***; ***Shibata, 1994***; ***Jones and Witter, 2007***). Second, dorsal RSC (A30) projects preferentially to distal PrS, PaS and medial MEC, while more ventral parts of RSC (A29) project significantly more to proximal PrS and more lateral parts of MEC. To our knowledge, such topographies have not been reported in earlier studies.

The observation that A30 is preferentially connected to distal PrS, PaS and medial MEC, while A29 is preferentially connected to proximal PrS and more lateral parts of MEC, but not PaS is in line with other connectional and functional differences. The PrS to MEC projection is topographically organized such that distal PrS projects to medial MEC, while proximal PrS projects to more lateral parts of MEC (***Shipley, 1975***; ***Honda and Ishizuka, 2004***). Furthermore, these partner domains in PrS and MEC are selectively innervated by different areas of SUB along its transverse axis such that distal SUB projects to distal PrS and medial MEC, while more proximal parts of SUB, with the exclusion of the very proximal part, project to proximal PrS and more lateral MEC (***Witter, 2006***; ***O'Reilly et al., 2013***). This indicates the existence of a connectional route linking A30, medial MEC, distal SUB and distal PrS to each other. A parallel route links A29 with more lateral MEC, more proximal SUB and proximal PrS. Although no clear transverse gradients in spatial modulation have been reported in MEC, electrophysiological properties of neurons show a transverse gradient, indicative that more medially positioned grid cells might be more precisely spatially tuned (***Canto and Witter, 2012***). Furthermore, neurons in distal SUB are more spatially modulated compared to those in proximal SUB (***Sharp and Green, 1994***). All observations thus point to a differentiation of A29 and A30 where A30 is connected preferentially to more spatially modulated neurons in medial MEC and distal SUB compared to A29 which is more connected to neurons in lateral MEC and more proximal SUB.

Additional cortical and subcortical connections are in line with this proposed differentiation between both areas of RSC. The projections to anterior cingulate cortex are differentially organized for A29 and A30 and while A30 is connected to visual area A17 and A18b, A29 is only connected to A18b. With respect to thalamic connections, A29 is connected to the anterodorsal and anteroventral nuclei while A30 preferentially connects with the anteromedial nucleus (***van Groen and Wyss, 1990***, ***1992***; ***Shibata, 1998***; ***van Groen and Wyss, 2003***; ***Jones et al., 2005***). Taken together, these connectional differences are in line with reported functional differences between the two areas

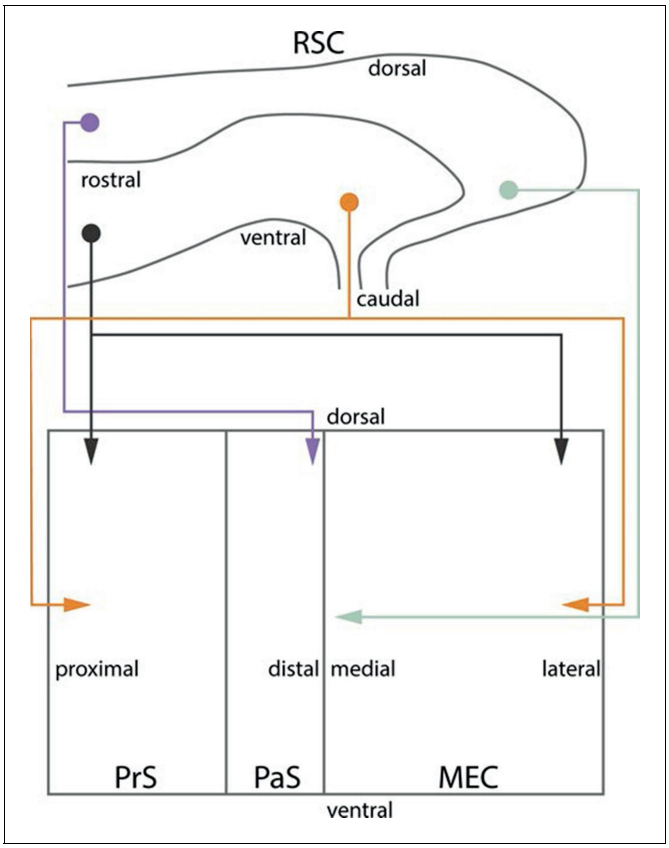

Figure 10. Summary of topographical organization of projections from RSC to PHR in the developing and adult brain. Schematic representation of the organization of the projections from RSC (top) to PHR (bottom). Projections from RSC to PHR terminate mainly in PrS, PaS and MEC. Projections originating from rostral RSC (purple and black) terminate in dorsal PHR, while projections originating from caudal RSC (yellow and grey) terminate in more ventral parts of PHR. Projections originating from ventral RSC (black and yellow) terminate in proximal PrS and in lateral parts of MEC, while projections originating from dorsal RSC (purple and grey) terminate in distal PrS and in medial parts of MEC.

DOI: 10.7554/eLife.13925.029

(***van Groen et al., 2004***; ***Vann and Aggleton, 2005***; ***Pothuizen et al., 2009***; ***Pothuizen et al., 2010***). Such a functional differentiation between A29 and A30 could thus possibly result in functional differences along the transverse axes of PrS, PaS and MEC.

During the postnatal period we observed an overall increase in the density of labeled axonal branches in all PHR subregions. Even though we did not perform a formal quantification of the number of labeled fibers in PHR, we only observed single unbranching fibers in animals aged P1-2. During the first postnatal week, the number of axons generally increased, and the fibers displayed several branching points towards the end of the first postnatal week. The first terminal plexus with adult-like densities were observed in P12 animals. Even though several other factors, such as tracer type and the number of layer V RSC neurons involved in the injection also had an impact on the number of fibers observed in each experiment, we are confident that the most important predictor of labeled fiber density was the age of the animal. Interestingly, the time window of increased density of RSC afferents in PHR is paralleled by several anatomical and physiological changes in PHR. EC

afferents originating in PaS and PrS become functional from P8 and mature gradually until they are fully adult-like around P14 (**Canto et al., 2011**). Similar developmental timescales have also been reported for the functional development of intralaminar projections within EC (**O'Reilly et al., 2010**).

Our temporal analysis revealed that RSC axons destined for PHR migrate directly into their area of termination and thereafter keeps their position constant while the number of axonal branches and the total axonal spread increases gradually until they reach adult-like plexus features. This observation is supported by our center of mass analyses of the early perinatal RSC to PHR projections, showing that projections originating in different parts of RSC show a striking terminal topography already during the first postnatal week.

Head-direction cells and border cells are all present in PHR when electrodes are lowered into the brain during the second postnatal week (**Bjerknes et al., 2014**; **Bjerknes et al., 2015**), while grid cells mature during the third and fourth postnatal week (**Langston et al., 2010**; **Wills et al., 2010**). Even though no published experiments have investigated whether border cells and head-direction cells are present before the second postnatal week, our data indicate that the topographical organization of RSC terminals in PHR is present before spatially modulated neurons are present in PHR and that adult-like axonal densities can be observed approximately at the same time-point as the first border cells and head-direction cells are observed in PHR. This conclusion is comparable to what has been observed for intrinsic HF-PHR connectivity which is also topographically organized already at early postnatal periods, demonstrating increased plexus densities for intrinsic HF-PHR projections during ongoing development (**Fricke and Cowan, 1977**; **Borrell et al., 1999**; **O'Reilly et al., 2013**; **O'Reilly et al., 2014**). It is also comparable to what has been reported in several other developing brain systems. For instance, for thalamocortical projections in the visual system of both monkeys, cats and ferrets, the first arriving axons in the visual cortex already show a topographical organization into ocular dominance columns (**Horton and Hocking, 1996**; **Crowley and Katz, 2000**; **Crair et al., 2001**). Similarly, the rat ventral posterior thalamic nucleus issue projections to the somatosensory cortex in which the first arriving axons target distinct areas later forming a defined barrel (**Catalano et al., 1996**). Sensory inputs to the olfactory bulb are present long before neurons display a receptive field. Moreover, the development of these inputs is independent of activity in sensory receptors, which suggests that the development of topographies in the olfactory bulb is experience independent (**Lin et al., 2000**). The same conclusion apparently holds for the projections from RSC to PHR, These findings are different from what has been reported for the retinogeniculate projection in several species. In this projection, there is an overshoot of axonal terminals, which are initially diffuse and later pruned into an adult-like topography (**Rakic, 1976**; **Linden et al., 1981**; **Shatz, 1983**; **Godement et al., 1984**). These differences might imply that distinct molecular- or activity based principles governs the axonal termination patterns in different neural projections.

The results presented in this study thus lead us to conclude that the topographical organization of PHR connectivity is present when the first RSC axons arrive in PHR. The densities of the terminal plexus appear to develop gradually without any clear signs of pruning, though it remains to be determined whether connectional reorganization occurs at the synaptic level during development. The first plexus with adult-like densities can be observed around P12 which is around the time when the first spatially modulated neurons in PHR have been observed (P11), but before eye-opening and before the animals starts to navigate (around P15) and thus before adult like grid cells are observed in PHR (after P25; **Langston et al., 2010**; **Wills et al., 2010**; **Bjerknes et al., 2014**; **Bjerknes et al., 2015**). These findings suggest that RSC afferents might be important for the development of head-direction and border cells.

Materials and methods

Surgeries and perfusion

Eighty two female and male Long Evans rats aged between P0 and P28 were used in this study. Additionally, we reanalyzed anterograde injections performed in approximately 3 months old adult Wistar rats (**Jones et al., 2005**; **Jones and Witter, 2007**) and retrograde injections performed in Long Evans pups (**O'Reilly et al., 2014**). We refer to these original publications for a detailed description of the experimental protocols.

The pups were bred in-house and housed in enriched cages together with their parents and littermates. Cages were checked every morning and evening for pups and the day pups were observed was considered P0. We use the day of perfusion designating the age of the animal. To avoid unnecessary stress for the animals, litters with more than ten pups were culled to ten pups at P0 or P1. At P21, the pups were separated from their parents and moved to cages together with littermates of the same sex. The animals lived in a controlled environment (22 ± 1˚C; humidity 60%; lights on from 8:00 P.M. to 8:00 A.M.). Food and water were available *ad libitum*. The experimental protocols followed the European Communities Council Directive and the Norwegian Experiments on Animals Act and local directives of the responsible veterinarian at the Norwegian University of Science and Technology.

All surgeries were conducted under isoflurane gas anesthesia. Animals were placed in an induction chamber and fully anesthetized before they were moved to a stereotaxic frame. The head was fixed using a neonatal mask and mouthpiece (model 973-B; Kopf, Tujunga, CA) and zygoma ear cups (model 921; Kopf). Animals older than P18 were mounted in a small-sized adult mask and the head was fixed with blunted ear bars. Before incision, the skin was disinfected with 2% iodine in 65% ethanol, and a local analgesic bupivacain (0.2 ml per 100 g bodyweight of a 0.5 mg/ml solution; Marcain, Astra Zeneca, London, UK) was injected subcutaneously at the place of incision. The skin was opened with a small-sized and sharp tipped scissor. After incision, the mouthpiece and ear cups were adjusted so that bregma and lambda were aligned horizontally. Before injecting, bone over the place of injection and over the posterior extreme of the sagittal sinus was removed. The exact place of injection was measured using the junction of the transverse- and sagittal sinus as a reference for the anteroposterior coordinate, the lateral edge of the midsagital sinus as a reference for the mediolateral coordinate and the level of the dura as a reference for the dorsoventral coordinate. Before injection, the dura was punctured, and glass micropipettes with an outer diameter of 20–25 µm were lowered into the brain (30–0044, Harvard Apparatus, Holliston, MA; pulled with a PP-830 puller, Narishige, Japan). The anterograde tracers biotinylated dextran amine (BDA; 5% in phosphate buffer (PB; 0.125M in H_20; pH 7.4), 10000 MW, D1956, Invitrogen, Eugene, OR) or preconjugated dextran amines (all 5% in PB, 10 000 MW; Alexa-488 DA, D22910; Alexa-546 DA, D22911; Alexa-647 DA, D22914; Invitrogen) were iontophoretically injected through the micropipettes into RSC (4–6 µA, alternating currents, 6 s on/6 s off, for 5–15 min, 51595; Stoelting, Wood Dale, IL). Throughout the surgery, appropriate amounts of sterile saline (room temperature) were administered subcutaneously to avoid dehydration. Animals were also administered carprofen during surgery as a post-surgery analgesic (1 ml per 100 g bodyweight of a 0.5 mg/ml solution; Rimadyl, Pfizer, New York, NY). After surgery, the incision was sutured and the pups were allowed to recover under a heating lamp. When fully awake, the animals were returned to maternal care until the time of sacrifice.

We euthanized the animals 18–30 hr after surgery under a terminal anesthesia with isoflurane. The thorax was opened and cold Ringer's solution (8.5 g NaCl, 0.25 g KCl and 0.2 g $NaHCO_3$ per liter of H_2O, pH 6.9) was transcardially perfused through the body. When the liver turned pale the perfusion solution was changed to a 4% solution of freshly depolymerized paraformaldehyde in PB (pH 7.4). In case of P0-P2 animals, 0.1% glutaraldehyde was added to the fixative. The brain was removed from the skull and postfixed overnight at 4˚C in the same fixative. Twenty-four hours after perfusion, the brains were transferred to PB containing 2% dimethyl sulfoxide (DMSO; VWR, Radnor, PA) and 20% glycerol (VWR).

Tissue processing

Brains were cut with a freezing microtome (HM-430 Thermo Scientific, Waltham, MA) in 40 or 50 µm thick horizontal sections. Depending on the age of the animal sections were collected in four to six equally spaced series. One of the series was mounted directly on superfrost slides (10149870, Thermo Scientific). The remaining series of sections were collected in vials containing 2% DMSO and 20% glycerol in PB and stored at -20˚C until further usage. The mounted series was Nissl-stained by first dehydrating the sections in increasing ethanol solutions (50%, 70%, 80%, 90%, 100%, 100%, 100%) followed by two minutes in xylene (VWR) to clear the sections. Thereafter, the sections were rehydrated in decreasing ethanol solutions (opposite order as the dehydration protocol) and placed in cresyl violet solution for two to six minutes. Subsequently, the sections were rinsed quickly in water and placed in 50% ethanol containing acetic acid to differentiate the staining. The

sections were dehydrated in ethanol, cleared in xylene and finally coverslipped with Entellan (107961, Merck, Darmstadt, Germany).

Visualization of anterograde tracers

In case of brains with BDA injections, one series of sections was rinsed three times for 10 min in PB and then three times for 10 min in tris(hydroxymethyl)aminomethane (Tris)-buffered saline (50 mM Tris (Merck) and 150 mM NaCl in H_2O) containing 2% Triton X-100 (TBS-Tx; Merck, pH 8.0). In experiments were multiple tracers were injected, the sections were incubated with Alexa-conjugated streptavidin (Alexa-405 S32351, Alexa-488, S11223; Alexa-546, S11225; Alexa-633, S21375, Invitrogen) in a 1:200 solution with TBS-Tx overnight at 4˚C. In experiments were BDA was the only tracer injected in the brain, sections were incubated for 90 min in TBS-Tx with avidin-biotin-peroxidase (Vectastain Standard PK-4000 ABC kit; Vector, Burlingame, CA) according to the manufacturer's instructions. Subsequently, sections were rinsed three times for 10 min in TBS-Tx and two times for 5 min in Tris-HCl (50 mM Tris in H_2O, pH adjusted to 7.6 by adding HCl) and incubated for approximately 15 min in a diaminobenzidine tetrahydrochloride (DAB)–peroxidase solution containing 5 mg DAB (D5905, Sigma-Aldrich, St. Louis, MO) and 3.3 µl H_2O_2 (H1009, Sigma-Aldrich) in 10 ml Tris-HCl. Irrespective of whether the incubations were carried out with Alexa-conjugated streptavidin or DAB, the sections were rinsed two times for 5 min in Tris-HCl, and subsequently mounted on glass slides from a 0.2% gelatin solution in Tris-HCl. After overnight drying, they were cleared in toluene and coverslipped with Entellan (Merck).

Sections were inspected with fluorescence illumination at the appropriate excitation wavelength or conventional brightfield illumination (Zeiss Axio Imager M1/2). Digital images of successful injections and anterogradely labeled plexus in HF-PHR were obtained using a slide scanner equipped for either brightfield or fluorescent imaging (Zeiss Mirax Midi; objective 20X; NA 0.8). For illustrative purposes, images of labeled cells and Nissl stained tissue were exported using Panoramic Viewer software (3DHistech, Budapest, Hungary) and processed in Adobe Photoshop and Illustrator (CS6, Adobe Systems, San Jose, CA).

Assessments of experiments

After the sections were digitized, we aimed to obtain, for each experiment, realistic estimates of the location of the anterogradely labeled axons in PHR and of the locations of the injections in RSC. To achieve this, we first produced an average flatmap of PHR based on measurements of each PHR subdivision in all animals (***Figure 4A***). Second, we measured the location of labeled fibers within PHR and represented the position of the labeled fibers on the average flatmap (***Figure 4B***). Third, we plotted the injections in a reference atlas brain (***Figure 1***).

In order to create an average flatmap, we produced individual flatmaps of all animals. To this end, we delineated all subdivisions within PHR using cytoarchitectonic differences between the different subdivisions (***Boccara et al., 2015***). Borders were established in fluorescent- or DAB-stained sections overlaid with the neighboring Nissl-stained section. In all sections, we measured (using Panoramic Viewer software, 3DHistech, Budapest, Hungary) the extent, along the transverse axis, of subdivisions containing labeled RSC axons, i.e. superficial layers of PrS, deep layers of PrS, deep layers of PaS, deep layers of MEC and deep layers of LEC (***Figure 4A1–4***). The transverse measurements where obtained from all sections of all brains, stored in excel files and the data were further processed using MatLab software (R2015b, MathWorks, Natick, MA).

We next aimed to make one average flatmap, constituting of square bins, representing the mean 'shape' of PHR across all brains. Since brains of animals of different ages have different sizes, we first converted the absolute measurements into normalized values. For this, we divided each measurement by the maximum measured extent of the respective subdivision for the particular animal (***Figure 4C1***). Next, we binned the dorsoventral axis of each PHR subdivision in 29 equally sized bins, since the maximum number of sections containing PHR in a single series was 29. Subsequently, we calculated the mean of the normalized transverse measurements, across all animals, for each of the 29 dorsoventral levels (***Figure 4C2***). This procedure was repeated for each subdivision. To obtain bins each representing a square area of the brain, we first calculated the ratio between the total dorsoventral extent of PHR and the maximum measured extent along the transverse axis of each animal (***Figure 4C1***). Thereafter, we calculated the mean of these ratios across all animals (***Figure 4C2***).

Next, the 29 normalized transverse measurements were divided by the mean of the dorsoventral extents (***Figure 4C3***). This procedure was repeated for each subdivision. This procedure thus resulted in, for each subdivision, 29 dorsoventral levels with different transverse extents, expressed as a value relative to the dorsoventral length of PHR. The transverse extents were subsequently turned into square bins (calculated as the average extent along the transverse axis x 29 and rounded to the nearest integer, ***Figure 4C4***) so that each subdivision could be represented as a flatmap containing 29 rows of bins with a variable amount of square bins in each row (***Figure 4A5***).

Location of labeled fibers

We represented the location of labeled axons in PHR for each experiment within the average flatmap in two ways. In experiments where a dense labeled plexus was present, the distances between the boundaries of the plexus and the borders of the respective PHR subdivisions were measured along the transverse axis (***Figure 4B1***). We did this for each section containing a labeled plexus. The density of labeling in each plexus in each section was subsequently given a value from 1–3 depending on a subjective evaluation. The densest plexus in each experiment was given a value of '3', while weaker plexus were valued '1' or '2' depending on the density relative to the densest plexus observed in the experiment. Alternatively, in experiments in which we observed only single labeled axons or a sparsely labeled plexus, the transverse measurements were obtained as follows. In PrS, the distance from each labeled axon to the proximal border of PrS was measured, while in deep layers of PaS the distance from each labeled axon to the distal border of PaS was measured. In deep layers of MEC and LEC, the distance from each labeled axon to the medial border of the respective subdivision was measured (***Figure 4B3***). In cases of missing or damaged sections, we estimated the putative projection pattern in the section by using the average projection pattern of the sections directly above and below.

To identify the bin(s) in the average flatmap representing the location of labeled fibers, their absolute position, as established above, was normalized within its respective area. In cases where we observed a dense plexus, each bin was given the value corresponding to what was described above (***Figure 4B2***). In cases where we measured the location of labeled fibers, each bin was given a value equal to the numbers of labeled axons present in the location represented by the respective bin (***Figure 4B4***). All bins not containing any labeled axons or located outside the labeled plexus were given the value 0.

To be able to directly compare or pool flatmaps representing either single fibers or dense plexus, we normalized the values of all bins in each experiment to the maximum valued bin in the respective experiment, resulting in bins in each experiment with values ranging between 0, representing no plexus or fibers, or 1, representing the bin with the densest labeling. To compare different sources of variability for the projection patterns, we organized the flatmaps into different groups of interest. For each group, we summed the values of bins representing the same location in all flatmaps (***Figure 4B5***). Finally, we normalized the 'summed' flatmap to the bin with the highest value, similar to the procedure described above. In flatmaps representing projection patterns of several subgroups, normalized flatmaps were summed, so that each subgroup had similar impact on the summed flatmap. For illustrative purposes, the flatmaps of individual experiments or groups of experiments were plotted using MatLab.

In all experiments, we calculated the coordinates for the 'center of mass' of the projections along the transverse and dorsoventral axis for respectively layers I and III of PrS, layers V-VI of PrS and PaS combined and for the combined layers V-VI of MEC and LEC. The center of mass-values of the axonal plexus were used for statistical analyses. In scatter plots of center of mass-values, we defined the extremes of the color scale as ± 2 standard deviations from the mean value. All values between these extremes were plotted using a linear color scale while more extreme values were thresholded to the extreme colors.

Location of injections

Since brains of different ages have different sizes, we aimed to normalize the position of the injections. In adult rats, RSC can be subdivided into four different cytoarchitectonic subdivisions A30 and A29a, b and c. In the adult brain, these four subdivisions are positioned along the dorsoventral extend of RSC. In the immature cortex, only the cytoarchitectonic border between A29 and A30 is

clearly identifiable. We therefore chose to define the dorsoventral location of the injections in A29 and A30 as a continuous coordinate. This measure is thus indirectly related to the classical discrete cytoarchitectonic subdivisions. We used the recently released reference 3D-atlas brain (***Papp et al., 2014***; ***2015***) to map all injections in a standardized space, irrespective of age. First, we identified coordinates of the dorsal, ventral, rostral and caudal border of respectively A29 and A30 in the atlas brain. The lines between the respective coordinates were smoothed using local regression. Next, we calculated the cutting angles of our experimental brains relative to the atlas brain and made sections of the standard atlas brain with the same cutting angles. We identified atlas-sections containing landmarks and cytoarchitectonic borders present in the section containing the center of each injection. The atlas coordinate of the center of each injection was recorded and served as an age-normalized 3D point-measure of the injection location within RSC. For illustrative purposes, the coordinates of all injections were plotted within the 3D volume (***Figure 1A***, ITK-SNAP, NIH).

Since the caudal RSC cortex is curved both along the dorsoventral and rostrocaudal axis we flattened RSC and transposed each injection onto a 2D plane. This was done by dividing the surface area of A29 and A30 in the atlas brain into multiple triangles (***Figure 1B***). The coordinates of the dorsal and ventral borders of A29 and A30 determined the coordinates of each triangle. For each injection, we calculated the shortest vector between the injection and the cortical surface within any of the triangles (***Figure 1C***). Thereafter, we calculated the intersection of the vector and the plane within the triangle. This coordinate represented the "transposed" location onto the cortical surface of each injection (***Figure 1B and C***). The normalized 2D coordinate of each injection was defined as follows (***Figure 1C***); the dorsoventral coordinate was defined as , $\frac{d_v}{d_v+d_d}$,where d_v and d_d represent the distance from the transposed injection to the ventral and dorsal border respectively. The rostrocaudal coordinate was obtained by first calculating a line along the rostrocaudal extend of A29 and A30, positioned equally distant from their respective dorsal and ventral borders. Next, we calculated the shortest vector between the transposed injection and the line and found the intersection between the two. The rostrocaudal coordinate was defined as $\frac{d_r}{d_r+d_c}$, where d_r and d_c is the cumulative distance from the cross section to the rostral and caudal end of RSC. This resulted in the normalized map of the positions of all injection sites analyzed in this study (***Figure 1D***).

Statistical analyses

For cluster analyses, we smoothed each flatmap by applying a Gaussian filter of 5 x 5 bins with a standard deviation of 1.5. Thereafter we calculated pairwise correlations between each possible pair of flatmaps. The correlation matrix was subsequently clustered by using the k-means clustering algorithm in MatLab. The number of clusters was subjectively decided by evaluating the ratio between within- and between cluster variance. The number of clusters was fixed when adding more clusters would not result in a substantial decrease in the within- to between cluster variance ratio.

Our dataset contained experiments in animals of all ages between P1 and P19 and injections in animals aged P27 and P28. Since we did not have samples between P19 and P27 we only included experiments in animals aged P19 or younger in the statistical analyses. Experiments that did not result in labeled axons in any of the areas of PHC where not included in the analyses. The dorsoventral and transverse coordinates of centers of mass were thereafter analyzed independently. For each of the coordinates, we fitted a linear multiple regression model to the data using age and the normalized location of the injection as predictors. A model including the main predictors and two-way interactions was fitted to the data using SPSS (version 20, IBM, Armonk, NY). We subsequently removed from the model the two-way interaction with the lowest standardized β-value and were insignificantly different from zero (t-test), and a new model was fitted. This procedure was repeated until the model only consisted of the main effects and significant two-way interaction terms. In the regression models, the center of mass coordinates ranged from 0 (ventral) to 1 (dorsal) and from 0 (proximal and medial) to 1 (distal and lateral), the coordinates of the injection cite ranged from 0 (rostral) and 1 (caudal) and from 0 (ventral) and 1 (dorsal) and the age of the animal was measured in postnatal age in days. Regression coefficients are reported unstandardized with 95% confidence intervals.

To assess whether the data met the assumption of linear relationships, we visually assessed scatter plots in which each of the independent variables were plotted versus each of the center of mass coordinates. Additionally, we evaluated the standardized predictor values plotted against the

standardized regression residuals to assess whether the assumptions of linearity, homoscedasticity, independent residuals and normally distributed residuals were met. We additionally tested whether the residuals were normally distributed by visually inspecting frequency histograms and normal probability plots. Next, we tested multicollinearity of the independent variables by correlating each of the independent variables. No multicollinearity was assumed if the Pearson's correlations were between -0.70 and 0.70. In addition, we assessed the variance inflation factor (VIF) of each model. The highest calculated VIF was 1.197, which is well below recommended cutoffs. Statistical significance of regression coefficients was determined using two sided *t*-test with $p<0.05$ as criterion.

Acknowledgements

We thank Bruno Monterotti and Paulo Giraõ for technical assistance with experiments. We would also like to thank Kally O'Reilly for sharing the retrograde experiments shown in ***Figure 9***. The adult anterograde experiments were performed by Bethany Jones, as part of her PhD-work with MPW who owns all rights to the material.

Additional information

Competing interests

MPW: Member of the board of the Kavli Centre, and of the scientific advisory board of the Center for Behavioral Brain Sciences, Otto von Guericke University, Magdeburg, FDR. The other author declares that no competing interests exist.

Funding

Funder	Grant reference number	Author
Norges Forskningsråd	145993	Menno P Witter
Norges Forskningsråd	181676	Menno P Witter
Norges Forskningsråd	Centre of Excellence grant	Menno P Witter
Kavli Foundation		Menno P Witter

The funders had no role in study design, data collection and interpretation, or the decision to submit the work for publication.

Author contributions

JS, Conception and design, Acquisition of data, Analysis and interpretation of data, Drafting or revising the article; MPW, Conception and design, Analysis and interpretation of data, Drafting or revising the article

Author ORCIDs

Menno P Witter, http://orcid.org/0000-0003-0285-1637

Ethics

Animal experimentation: The experimental protocols followed the European Communities Council Directive and the Norwegian Experiments on Animals Act and local directives of the responsible veterinarian at the Norwegian University of Science and Technology. The experimental protocols were approved by the Norwegian Food Safety Authority (#594). All surgeries were conducted under isoflurane gas anesthesia and every effort was made to minimize suffering.

References

Alexander AS, Nitz DA. 2015. Retrosplenial cortex maps the conjunction of internal and external spaces. *Nature NeurosciNeuroscience* **18**:1143–1151. doi: 10.1038/nn.4058

Bjerknes TL, Moser EI, Moser MB. 2014. Representation of geometric borders in the developing rat. *Neuron* **82**: 71–78. doi: 10.1016/j.neuron.2014.02.014

Bjerknes TL, Langston RF, Kruge IU, Moser EI, Moser MB. 2015. Coherence among head direction cells before eye opening in rat pups. *CurrCurrent Biology : CB* **25**:103–108. doi: 10.1016/j.cub.2014.11.009

Boccara CN, Sargolini F, Thoresen VH, Solstad T, Witter MP, Moser EI, Moser MB. 2010. Grid cells in pre- and parasubiculum. *NatNature NeurosciNeuroscience* **13**:987–994. doi: 10.1038/nn.2602

Boccara CN, Kjonigsen LJ, Hammer IM, Bjaalie JG, Leergaard TB, Witter MP. 2015. A three-plane architectonic atlas of the rat hippocampal region. *Hippocampus* **25**:838 857. doi: 10.1002/hipo.22407

Bonnevie T, Dunn B, Fyhn M, Hafting T, Derdikman D, Kubie JL, Roudi Y, Moser EI, Moser MB. 2013. Grid cells require excitatory drive from the hippocampus. *NatNature NeurosciNeuroscience* **16**:309–317. doi: 10.1038/nn.3311

Borrell V, Del Río JA, Alcántara S, Derer M, Martínez A, D'Arcangelo G, Nakajima K, Mikoshiba K, Derer P, Curran T, Soriano E. 1999. Reelin regulates the development and synaptogenesis of the layer-specific entorhino-hippocampal connections. *The Journal of Neuroscience* **19**:1345–1358.

Brandon MP, Bogaard AR, Libby CP, Connerney MA, Gupta K, Hasselmo ME. 2011. Reduction of theta rhythm dissociates grid cell spatial periodicity from directional tuning. *Science* **332**:595–599. doi: 10.1126/science.1201652

Burwell RD, Amaral DG. 1998a. Cortical afferents of the perirhinal, postrhinal, and entorhinal cortices of the rat. *JThe CompJournal of Comparative Neurology* **398**:179–205. doi: 10.1002/(SICI)1096-9861(19980824)398:2<179::AID-CNE3>3.0.CO;2-Y

Burwell RD, Amaral DG. 1998b. Cortical afferents of the perirhinal, postrhinal, and entorhinal cortices of the rat. *JThe CompJournal of Comparative Neurology* **398**:179–205. doi: 10.1002/(SICI)1096-9861(19980824)398:2<179::AID-CNE3>3.0.CO;2-Y

Canto CB, Wouterlood FG, Witter MP. 2008. What Does the Anatomical Organization of the Entorhinal Cortex Tell Us? *Neural Plasticity* **2008**:1–18. doi: 10.1155/2008/381243

Canto CB, Koganezawa N, Witter MP. 2011. Development of Functional Projections from Pre- and Parasubiculum to Medial Entorhinal Cortex in the Rat. In: *Doctoral Theses: Layer Specific Integrative Properties of Entorhinal Principal Neurons*. Trondheim, Norway: Kavli Institute for Systems Neuroscience and Centre for the Biology of Memory, Norwegian University of Science and Technology181–214.

Canto CB, Witter MP. 2012. Cellular properties of principal neurons in the rat entorhinal cortex. II. the medial entorhinal cortex. *Hippocampus* **22**:1277–1299. doi: 10.1002/hipo.20993

Catalano SM, Robertson RT, Killackey HP. 1996. Individual axon morphology and thalamocortical topography in developing rat somatosensory cortex. *The Journal of Comparative Neurology* **367**:36–53. doi: 10.1002/(SICI)1096-9861(19960325)367:1<36::AID-CNE4>3.0.CO;2-K

Cho J, Sharp PE. 2001. Head direction, place, and movement correlates for cells in the rat retrosplenial cortex. *Behavioral Neuroscience* **115**:3–25 . doi: 10.1037/0735-7044.115.1.3

Corcoran KA, Donnan MD, Tronson NC, Guzmán YF, Gao C, Jovasevic V, Guedea AL, Radulovic J. 2011. NMDA receptors in retrosplenial cortex are necessary for retrieval of recent and remote context fear memory. *The Journal of Neuroscience* **31**:11655–11659. doi: 10.1523/JNEUROSCI.2107-11.2011

Couey JJ, Witoelar A, Zhang SJ, Zheng K, Ye J, Dunn B, Czajkowski R, Moser MB, Moser EI, Roudi Y, Witter MP. 2013. Recurrent inhibitory circuitry as a mechanism for grid formation. *Nature Neuroscience* **16**:318–324. doi: 10.1038/nn.3310

Cowansage KK, Shuman T, Dillingham BC, Chang A, Golshani P, Mayford M. 2014. Direct reactivation of a coherent neocortical memory of context. *Neuron* **84**:432–441. doi: 10.1016/j.neuron.2014.09.022

Crair MC, Horton JC, Antonini A, Stryker MP. 2001. Emergence of ocular dominance columns in cat visual cortex by 2 weeks of age. *The Journal of Comparative Neurology* **430**:235–249 . doi: 10.1002/1096-9861(20010205)430:2<235::aid-cne1028>3.0.co;2-p

Crowley JC, Katz LC. 2000. Early development of ocular dominance columns. *Science* **290**:1321–1324 . doi: 10.1126/science.290.5495.1321

Czajkowski R, Sugar J, Zhang SJ, Couey JJ, Ye J, Witter MP. 2013. Superficially projecting principal neurons in layer V of medial entorhinal cortex in the rat receive excitatory retrosplenial input. *The Journal of Neuroscience* **33**:15779–15792. doi: 10.1523/JNEUROSCI.2646-13.2013

Deng JB, Yu DM, Wu P, Li MS, Wu P LMS. 2007. The tracing study of developing entorhino-hippocampal pathway. *International Journal of Developmental Neuroscience* **25**:251–258. doi: 10.1016/j.ijdevneu.2007.03.002

Eichenbaum H, Yonelinas AP, Ranganath C. 2007. The medial temporal lobe and recognition memory. *Annual Review of Neuroscience* **30**:123–152. doi: 10.1146/annurev.neuro.30.051606.094328

Fricke R, Cowan WM. 1977. An autoradiographic study of the development of the entorhinal and commissural afferents to the dentate gyrus of the rat. *The Journal of Comparative Neurology* **173**:231–250. doi: 10.1002/cne.901730203

Fyhn M, Molden S, Witter MP, Moser EI, Moser MB. 2004. Spatial representation in the entorhinal cortex. *Science* **305**:1258–1264. doi: 10.1126/science.1099901

Gabriel M, Vogt BA, Kubota Y, Poremba A, Kang E. 1991. Training-stage related neuronal plasticity in limbic thalamus and cingulate cortex during learning: a possible key to mnemonic retrieval. *Behavioural Brain Research* **46**:175–185 . doi: 10.1016/s0166-4328(05)80111-1

Godement P, Salaün J, Imbert M. 1984. Prenatal and postnatal development of retinogeniculate and retinocollicular projections in the mouse. *The Journal of Comparative Neurology* **230**:552–575. doi: 10.1002/cne.902300406

Honda Y, Ishizuka N. 2004. Organization of connectivity of the rat presubiculum: I. Efferent projections to the medial entorhinal cortex. *The Journal of Comparative Neurology* **473**:463–484. doi: 10.1002/cne.20093

Horton JC, Hocking DR. 1996. An adult-like pattern of ocular dominance columns in striate cortex of newborn monkeys prior to visual experience. *The Journal of Neuroscience* **16**:1791–1807.
Jones BF, Groenewegen HJ, Witter MP. 2005. Intrinsic connections of the cingulate cortex in the rat suggest the existence of multiple functionally segregated networks. *Neuroscience* **133**:193–207. doi: 10.1016/j.neuroscience.2005.01.063
Jones BF, Witter MP. 2007. Cingulate cortex projections to the parahippocampal region and hippocampal formation in the rat. *Hippocampus* **17**:957–976. doi: 10.1002/hipo.20330
Keene CS, Bucci DJ. 2008a. Contributions of the retrosplenial and posterior parietal cortices to cue-specific and contextual fear conditioning. *Behavioral Neuroscience* **122**:89–97. doi: 10.1037/0735-7044.122.1.89
Keene CS, Bucci DJ. 2008b. Involvement of the retrosplenial cortex in processing multiple conditioned stimuli. *Behavioral Neuroscience* **122**:651–658. doi: 10.1037/0735-7044.122.3.651
Knierim JJ, Neunuebel JP, Deshmukh SS. 2014. Functional correlates of the lateral and medial entorhinal cortex: objects, path integration and local-global reference frames. *Philosophical Transactions of the Royal Society of London. Series B, Biological Sciences* **369**:20130369. doi: 10.1098/rstb.2013.0369
Koenig J, Linder AN, Leutgeb JK, Leutgeb S. 2011. The spatial periodicity of grid cells is not sustained during reduced theta oscillations. *Science* **332**:592–595. doi: 10.1126/science.1201685
Kononenko NL, Witter MP. 2012. Presubiculum layer III conveys retrosplenial input to the medial entorhinal cortex. *Hippocampus* **22**:881–895. doi: 10.1002/hipo.20949
Kropff E, Carmichael JE, Moser MB, Moser EI. 2015. Speed cells in the medial entorhinal cortex. *Nature* **523**:419–424. doi: 10.1038/nature14622
Langston RF, Ainge JA, Couey JJ, Canto CB, Bjerknes TL, Witter MP, Moser EI, Moser MB. 2010. Development of the spatial representation system in the rat. *Science* **328**:1576–1580. doi: 10.1126/science.1188210
Lin DM, Wang F, Lowe G, Gold GH, Axel R, Ngai J, Brunet L. 2000. Formation of precise connections in the olfactory bulb occurs in the absence of odorant-evoked neuronal activity. *Neuron* **26**:69–80 . doi: 10.1016/s0896-6273(00)81139-3
Linden DC, Guillery RW, Cucchiaro J. 1981. The dorsal lateral geniculate nucleus of the normal ferret and its postnatal development. *The Journal of Comparative Neurology* **203**:189–211. doi: 10.1002/cne.902030204
Newman EL, Climer JR, Hasselmo ME. 2014. Grid cell spatial tuning reduced following systemic muscarinic receptor blockade. *Hippocampus* **24**:643–655. doi: 10.1002/hipo.22253
O'Reilly KC, Koganezawa N, Kruge IU, Witter MP. 2010. Postnatal development of medial entorhinal intrinsic connectivity in the rat. In: *Poster 101.10*. San Diego: Society for Neuroscience.
O'Reilly KC, Gulden Dahl A, Ulsaker Kruge I, Witter MP. 2013. Subicular-parahippocampal projections revisited: development of a complex topography in the rat. *The Journal of Comparative Neurology* **521**:4284–4299. doi: 10.1002/cne.23417
O'Reilly KC, Flatberg A, Islam S, Olsen LC, Kruge IU, Witter MP. 2015. Identification of dorsal-ventral hippocampal differentiation in neonatal rats. *Brain Structure & Function* **220**. doi: 10.1007/s00429-014-0831-8
Papp EA, Leergaard TB, Calabrese E, Johnson GA, Bjaalie JG. 2014. Waxholm Space atlas of the Sprague Dawley rat brain. *NeuroImage* **97**:374–386. doi: 10.1016/j.neuroimage.2014.04.001
Papp EA, Leergaard TB, Calabrese E, Johnson GA, Bjaalie JG. 2015. Addendum to "Waxholm Space atlas of the Sprague Dawley rat brain" [NeuroImage 97 (2014) 374-386]. *NeuroImage* **105**:561–562 . doi: 10.1016/j.neuroimage.2014.10.017
Pothuizen HH, Davies M, Albasser MM, Aggleton JP, Vann SD. 2009. Granular and dysgranular retrosplenial cortices provide qualitatively different contributions to spatial working memory: evidence from immediate-early gene imaging in rats. *The European Journal of Neuroscience* **30**:877–888. doi: 10.1111/j.1460-9568.2009.06881.x
Pothuizen HH, Davies M, Aggleton JP, Vann SD. 2010. Effects of selective granular retrosplenial cortex lesions on spatial working memory in rats. *Behavioural Brain Research* **208**:566–575. doi: 10.1016/j.bbr.2010.01.001
Rakic P. 1976. Prenatal genesis of connections subserving ocular dominance in the rhesus monkey. *Nature* **261**:467–471 . doi: 10.1038/261467a0
Ranganath C, Ritchey M. 2012. Two cortical systems for memory-guided behaviour. *Nature Reviews. Neuroscience* **13**:713–726. doi: 10.1038/nrn3338
Robinson S, Todd TP, Pasternak AR, Luikart BW, Skelton PD, Urban DJ, Bucci DJ. 2014. Chemogenetic silencing of neurons in retrosplenial cortex disrupts sensory preconditioning. *The Journal of Neuroscience* **34**:10982–10988. doi: 10.1523/JNEUROSCI.1349-14.2014
Sharp PE, Green C. 1994. Spatial correlates of firing patterns of single cells in the subiculum of the freely moving rat. *The Journal of Neuroscience* **14**:2339–2356.
Shatz CJ. 1983. The prenatal development of the cat's retinogeniculate pathway. *The Journal of Neuroscience* **3**:482–499.
Shibata H. 1994. Terminal distribution of projections from the retrosplenial area to the retrohippocampal region in the rat, as studied by anterograde transport of biotinylated dextran amine. *Neuroscience Research* **20**:331–336 . doi: 10.1016/0168-0102(94)90055-8
Shibata H. 1998. Organization of projections of rat retrosplenial cortex to the anterior thalamic nuclei. *The European Journal of Neuroscience* **10**:3210–3219.
Shipley MT. 1975. The topographical and laminar organization of the presubiculum's projection to the ipsi- and contralateral entorhinal cortex in the guinea pig. *The Journal of Comparative Neurology* **160**:127–145. doi: 10.1002/cne.901600108

Solstad T, Boccara CN, Kropff E, Moser MB, Moser EI. 2008. Representation of geometric borders in the entorhinal cortex. *Science* **322**:1865–1868. doi: 10.1126/science.1166466

Sugar J, Witter MP, van Strien NM, Cappaert NL. 2011. The retrosplenial cortex: intrinsic connectivity and connections with the (para)hippocampal region in the rat. an interactive connectome. *Frontiers in Neuroinformatics* **5**. doi: 10.3389/fninf.2011.00007

Tan HM, Bassett JP, O'Keefe J, Cacucci F, Wills TJ. 2015. The development of the head direction system before eye opening in the rat. *Current Biology* **25**:479–483. doi: 10.1016/j.cub.2014.12.030

van Groen T, Wyss JM. 1990. Connections of the retrosplenial granular a cortex in the rat. *Journal of Comparative Neurology* **300**:593–606. doi: 10.1002/cne.903000412

van Groen T, Wyss JM. 1992. Connections of the retrosplenial dysgranular cortex in the rat. *Journal of Comparative Neurology* **315**:200–216. doi: 10.1002/cne.903150207

Van Groen T, Wyss JM. 2003. Connections of the retrosplenial granular b cortex in the rat. *The Journal of Comparative Neurology* **463**:249–263. doi: 10.1002/cne.10757

van Groen T, Kadish I, Wyss JM. 2004. Retrosplenial cortex lesions of area Rgb (but not of area Rga) impair spatial learning and memory in the rat. *Behavioural Brain Research* **154**:483–491. doi: 10.1016/j.bbr.2004.03.016

Vann SD, Aggleton JP. 2005. Selective dysgranular retrosplenial cortex lesions in rats disrupt allocentric performance of the radial-arm maze task. *Behavioral Neuroscience* **119**:1682–1686. doi: 10.1037/0735-7044.119.6.1682

Vann SD, Aggleton JP, Maguire EA. 2009. What does the retrosplenial cortex do? *Nature Reviews. Neuroscience* **10**:792–802. doi: 10.1038/nrn2733

Vogt BA, Vogt L, Farber NB. 2004. Cingulate Cortex and Disease Models. In: Paxinos G eds *The Rat Nervous System*. 3rd ed Edition San Diego, CA: Elsevier705–727. doi: 10.1016/B978-012547638-6/50023-7

Wills TJ, Cacucci F, Burgess N, O'Keefe J. 2010. Development of the hippocampal cognitive map in preweanling rats. *Science* **328**:1573–1576. doi: 10.1126/science.1188224

Witter MP. 2006. Connections of the subiculum of the rat: topography in relation to columnar and laminar organization. *Behavioural Brain Research* **174**:251–264. doi: 10.1016/j.bbr.2006.06.022

Witter MP, Canto CB, Couey JJ, Koganezawa N, O'Reilly KC. 2014. Architecture of spatial circuits in the hippocampal region. *Philosophical Transactions of the Royal Society of London. Series B, Biological Sciences* **369**:20120515. doi: 10.1098/rstb.2012.0515

Wyss JM, Van Groen T. 1992. Connections between the retrosplenial cortex and the hippocampal formation in the rat: a review. *Hippocampus* **2**:1–11. doi: 10.1002/hipo.450020102

Paper 4: Haugland, Kamilla G.; Sugar, Jørgen og Witter, Menno P. Development of projections from the (para)hippocampal region to the retrosplenial cortex in the rat.

Is not included due to copyright